NANOSUSPENSIONS AND NANOSTRUCTURED LIPID CARRIERS FOR DERMAL APPLICATION

Dissertation zur Erlangung des akademischen Grades des
Doktors der Naturwissenschaften (Dr. rer. Nat.)

eingereicht im Fachbereich Biologie, Chemie, Pharmazie
der Freien Universität Berlin

vorgelegt von

Jana Pardeike

aus Berlin

Dezember 2008

The work of this thesis was performed at the Department of Pharmaceutical Technology, Biopharmaceutics and NutriCosmetics at the Freie Universität Berlin under the supervision of Prof. Dr. Rainer H. Müller from October 2005 until December 2008.

1st Reviewer: Prof. Dr. Rainer H. Müller

2nd Reviewer: Prof. Dr. Hans H. Borchert

Date of defence: February 5th 2009

Meinen lieben Eltern mit großem Dank gewidmet

Das Fehlen einer besonderen Kennzeichnung oder eines entsprechenden Hinweises auf ein Warenzeichen, ein Gebrauchmuster oder einen Patentschutz lässt nicht den Schluss zu, dass über die in dieser Arbeit angegebenen Dinge frei verfügt werden kann.

Index

Abbreviations

ATR-FTIR	Attenuated total reflection-Fourier transformed infrared spectroscopy
BMI	Body mass index
BSA	Bovine serum albumin
CAM	Choriallantic membrane
CI	Crystallinity index
$cPLA_2$	Cytosolic phospholipase A_2
DMSO	Dimethyl sulfoxide
DSC	Differential scanning calorimetry
ECVAM	European center of the validation of alternative methods
FBM	Fibroblasts basal medium
FDA	Food and drug administration
FGM	Fibroblasts growth medium
GRAS	Generally recognized as save
HET-CAM	Hen's egg test on the choriallantic membrane
HPLC	High pressure liquid chromatography
$iPLA_2$	Ca^{2+}-independent phospholipase A_2
KBM	Keratinocytes basal medium
KGM	Keratinocytes growth medium
LD	Laser diffractometry
LOD	Limit of detection
LOQ	Limit of quantification
MS	Mass spectroscopy
MTT	3-(4,5-dimethylthiazol-2yl)-2,5-diphenyl-tetrazolium bromide
NLC	Nanostructured lipid carriers
NMR	Nuclear magnetic resonance
PAF	Platelet activating factor
PBS	Phosphate buffered saline
PCS	Photon correlation spectroscopy
PI	Polydispersity index
PL	Phospholipase
PLA_2	Phospholipase A_2

PNBDI	p-Nitrobenzyl-N,N'-diisopropylisourea
ppm	Parts per million
RI	Refractive index
rpm	Rounds per minute
RSD	Relative standard deviation
SD	Standard deviation
SDS	Sodiumdodecyl sulfate
SEM	Scanning electron microscopy
SLN	Solid lipid nanoparticles
SOP	Standrad operation procedure
$sPLA_2$	Secreted phospholipase A_2
TG	Thermogravimetry
TMS	Tetramethylsilane
UV	Ultra violet

1 Introduction

1.1 Morphology and function of the skin

The skin is with a surface area of 1.5-1.8 m^2 and a weight of 8-12% of the body weight the largest human organ [1]. It forms the outer surface of the body and provides therefore a border between the environment and the inner milieu with various essential functions. The skin acts as a barrier in two directions, controlling the loss of water, electrolytes and other body constitutes, while preventing the entry of harmful or unwanted molecules from the external environment [2]. Furthermore, it protects the organism from mechanical damage and the entry of microorganisms. The skin with its immune defense system (e.g. Langerhans cells, macrophages, T lymphocytes) plays a role in immune monitoring. Due to the dilatation or contraction of blood vessels as well as via sweat glands the skin is involved in the thermoregulation of the body. The skin functions as sense organ via various receptors for temperature, pain, pressure and touch. Furthermore, it is involved in the metabolism of the individual such as the synthesis of vitamin D and the storage of fat and lipid soluble compounds (e.g. vitamin A, vitamin E). Against UV radiation the skin exhibits various protection mechanisms (e.g. increase in cell proliferation resulting in thickening of the epidermis, increase in melanin synthesis). The skin also has a social function via its appearance (e.g. color via turning pale, tattoo).

The skin consists of three main successive layers, the epidermis, the dermis and the subcutis (Figure 1.2.1-1). Epidermis and dermis together are called cutis. The cutis passes into the subcutis without a distinct border.

The epidermis is the outermost layer of the skin, which is mainly responsible for the barrier function and mechanical resistance. The epidermis has an average thickness of 0.1 mm. Depending on the body region the epidermal thickness is ranging from 30 µm to 4 mm. Next to the main cell type of the epidermis, the keratinocytes, melanin producing melanocytes, antigen presenting Langerhans cells and as sensor for touch functioning Merkel cells are present in this skin layer. The epidermis consists from the outside to the inside of several layers, the stratum corneum, which is formed of anucleated, dead corneocytes embedded in multilamellar lipid layers, and the viable epidermis composed of the stratum granulosum, the stratum spinosum and the stratum basale (Figure 1.2.1-1).

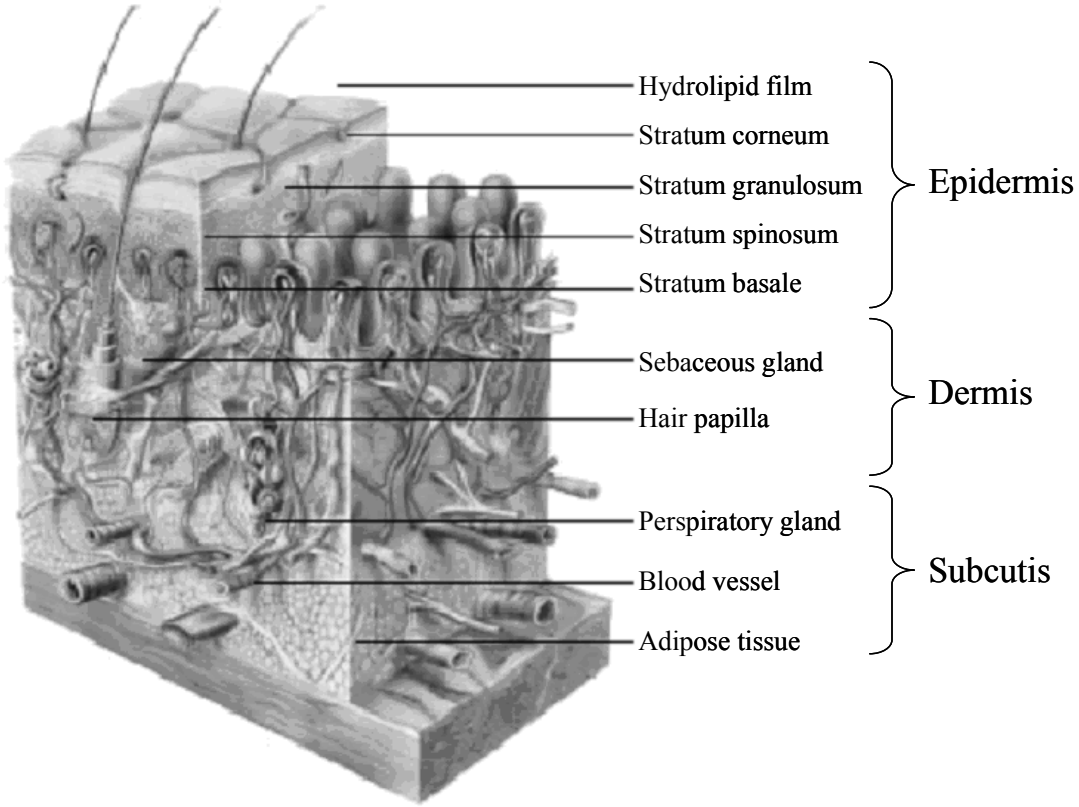

Figure 1.2.1-1: The human skin schematically (modified after [3]).

The stratum basale consists of one row of stem cells. These cells divide and half of the cells differentiate and move to the next epidermal layer to begin the maturation process whereas the other half stay in the stratum basale and divide again. Therefore, the stratum basale is responsible for the constant renewing of the epidermis. In the stratum spinosum and the stratum granulosum the cells undergo a rapid differentiation. They become flattened and lamellar granules are synthesized. These lamellar bodies migrate towards the cell periphery and are extruded to form the multilamellar lipid layers between the keratinized cells in the stratum corneum. Moreover keratohyalin is formed and the cell membrane undergoes changes, i.e. the phospholipid content is decreased whereas the ceramide content increases. At the end of this process the nucleus and cell organelle are not present anymore. Dead, keratinized cells called corneoyctes embedded in a multilamellar lipid matrix form the stratum corneum. This multilamellar lipid matrix consists mainly of free fatty acids in a mixture with their salts, triglycerides, cholesterol, cholesterol esters, cholesterol sulfate and ceramides [4, 5]. In the stratum corneum it can be distinguished between two layers, the stratum conjunctum and the stratum disjunctum, which consists of the last two to three loose-bound cell layers. It takes two to four weeks from the formation of keratinocytes in the basal layer until the cells

reach the stratum corneum. Another two weeks takes the passage of the stratum corneum until the desquamation of the corneocytes from the skin surface [6, 7]. On the surface of the skin exists a hydrolipid film, which is composed of all the components of the stratum corneum and the secretions from sebaceous and sweat glands. The pH of the skin surface is 5.4-5.9. This acidic pH contributes to the barrier function of the skin as well as to the cutaneous antimicrobial defense [8].

The connected tissue of the dermis is composed of two layers, the stratum papillare, which is located directly under the epidermis and the stratum reticulare, which passes into the subcutis. The thickness of the dermis is ranging from 3 mm to 5 mm [2]. The dermis is composed of a dense network of elastin and collagen fibers, which provide the mechanical properties of the skin. Furthermore, blood vessels, lymph vessels, nerves, cells of the immune defense system and adnexa (e.g. sweat glands, sebaceous glands, hairs) are located in the dermis and contribute to its functions (e.g. nutrition supply of the avascular epidermis, thermoregulation).

The subcutis is mainly composed of adipose tissue. Its physiological functions include insulation and storage of nutrients. The thickness of the subcutis varies depending on age, gender, nutritional status and physical conditions of the individual.

1.2 Innovative carrier systems for dermal application

By dermal application of active compounds several purposes including surface effects (e.g. cosmetics, sunscreens, insect repellents, anti-infectives), dermal effects (e.g. corticosteroids), systemic effects (e.g. nicotine patches) and effects on deeper tissues (e.g. non-steroidal anti-inflammatory drugs) may be wanted. Therefore, beside the structure of the skin, the physico-chemical characteristics of the active compound and the dosing conditions, the choice of an appropriate galenic formulation is of major importance [2, 9-12]. Several problems ranging from unwanted low uptake to unwanted systemic side effects have been reported using conventional formulations. Therefore, innovative carrier systems e.g. liposomes, niosomes, sphingosomes, microemulsions, multiple emulsions, polymeric and lipid micropraticles, nanosuspensions and lipid nanoparticles are under investigation to enhance the pemetration of active compounds and to deliver active compounds to the targeted site of action [13-17]. In the following chapters nanosuspensions and lipid nanoparticles will be described in detail as they are of major interest in this work.

1.2.1 Nanosuspension

A nanosuspension consists of drug nanocrystals, stabilizing agents, typically surfactants or polymeric stabilizers, and a liquid dispersion medium [18]. Drug nanocrystals are pure solid drug particles with a mean particle size below 1 µm, generally between 200 nm and 500 nm [19]. Although the term nanocrystals implicates a crystalline structure, the particles can be crystalline, partially crystalline or completely amorphous. The dispersion medium can be water, mixtures of water with other non-aqueous media or non-aqueous media.

Nanosuspensions can be produced by bottom up or top down technologies. Using bottom up technologies dissolved molecules are precipitated by reducing the solvent quality. Examples for bottom up technologies are hydrosols (Novartis) and NanoMorph™ (Soliqs/Abbott) [18, 20, 21]. With top down technologies nanosuspensions are produced via size reduction methods. Using the NanoCrystal® technology (élan drug technology) nanosuspensions are produced by pearl milling [22]. Applying high pressure homogenization for particle size reduction in aqueous media is called DissoCubes® technology (SkyePharma PLC/Baxter International Inc.) [23]. This process is described in details in chapter 2.4.2. Size reduction via high pressure homogenization in non-aqueous media or water content-reduced media is called Nanopure® technology (PharmaSol GmbH) [24]. Furtheremore, the production of nanosuspensions by combination technologies is possible. Applying the NANOEDGE® technology (Baxter International Inc.) the material is dissolved, precipitated and subjected to a process with energy input (e.g. high pressure homogenization) [25]. The Nanopure® XP technology (PharmaSol GmbH) summarizes production methods, where the starting material is modified via dissolution followed by an evaporation process (e.g. lyophilization, spray drying) before high pressure homogenization [26].

Nanosuspensions have several advantages, e.g. increased saturation solubility and consequently an increased dissolution velocity (for details see chapter 2.4.4). Due to the nanosize, nanosuspensions show an increased adhesion to surfaces. This results in an enhanced bioavailability of active compounds. Nanosuspensions have been under investigation for various application routes including parenteral [27], peroral [28-30], dermal [31], ocular [31] and pulmonary [32, 33]. This work focuses on dermal application.

For dermal application nanosuspensions can be incorporated into all kinds of dermally applied formulations (e.g. o/w creams, lotions) or a gel can be prepared by the addition of viscosity

enhancers to the nanosuspension. Dermal application of nanosuspensions containing products can increase the penetration into the skin. The increased saturation solubility leads to an increased concentration gradient which promotes passive diffusion. Due to the nanosize a close contact with the stratum corneum and an increased residence time on the skin due to the adhesive properties contribute to an increased penetration. Furthermore, a follicular uptake by the hair follicles, which has been reported for particulate systems, is possible for nanocrystals [34].

Five pharmaceutical oral products containing drug nanocrystals have been introduced to the market. Table 1.2.1-1 provides an overview of these products. Nanocrystals also entered the cosmetic market. For instance rutin nanocrystals are an ingredient of JUVEDICAL Age-Decoder Face Fluid and JUVEDICAL DNA skin optimizer cream by Juvena, Zürich, Switzerland as well as of Edelweiss Wrinkle Fighter Eye Lift Fluid by Audorasan, Regensburg, Germany.

Table 1.2.1-1: Marketed pharmaceutical products containing nanocrystals.

Product	Drug	Dosage form	Producer	Market introduction
Rapamune®	Sirolimus	Tablet	Weyth Pharma	August 2000
Emed®	Aprepitant	Capsule	Merck	March 2003
TriCor®	Fenofibrat	Capsule	Abbott	December 2004
Megace® ES	Megestrol	Suspension	Par Pharmaceutical Companies Inc.	July 2005
Triglide®	Fenofibrat	Tablet	SkyePharma PLC	July 2005

1.2.2 Lipid nanoparticles

It is distinguishable between two kinds of lipid nanoparticles, the first generation of lipid nanoparticles called solid lipid nanoparticles (SLN) and the second generation of lipid nanoparticles called nanostructured lipid carriers (NLC). SLN were developed at the beginning of the 1990s. They are produced by replacing the liquid lipid (oil) of an o/w emulsion by a solid lipid or a blend of solid lipids, i.e. the lipid particle matrix being solid at both room and body temperature [35]. SLN are composed of 0.1% (w/w) to 30% (w/w) solid lipid dispersed in an aqueous medium and if necessary stabilized with preferably 0.5% (w/w) to 5% (w/w) surfactant. The incorporation of cosmetic and pharmaceutical actives is feasible. The mean particle size of SLN is in the submicron rage, ranging from about 40 nm to 1000 nm [35]. In contast to SLN, NLC are produced using blends of solid lipids and liquid lipids (oils). To obtain the blends for the particles matrix, solid lipids are mixed with liquid lipids (oils), preferably in a ratio of 70:30 up to a ratio of 99.9:0.1. Due to the oil in these mixtures a melting point depression compared to the pure solid lipid is observed, but the blends obtained are also solid at both room and body temperature [36]. Furthermore, the overall solid content of NLC could be increased up to 95% (w/w) [37]. This second generation of submicron particles can also be loaded with cosmetic and pharmaceutical actives.

Both SLN and NLC have been investigated for various applications e.g. parenteral [38, 39], peroral [40-42], dermal [13, 43, 44], ocular [45, 46] and pulmonary [47]. In this work focus is put on the dermal application. The lipids and oils as well as the surfactants used for the production of lipid nanoparticles for dermal application are such currently used in dermal applied cosmetic and pharmaceutical products with accepted GRAS (generally recognized as safe) status. Both SLN and NLC have many features that are advantageous for a dermal application of cosmetic and pharmaceutical actives. Compared to conventional formulations modified release profiles [48-50] as well as targeting to certain layers of the skin can be achieved [51-55]. Moreover, a reduction in local as well as systemic side effects of active compounds has been reported [55-57]. The small size ensures a close contact to the stratum corneum and can thereby increase the amount of active compounds penetrated into the skin [44]. Due to the occlusive properties of lipid nanoparticles, an increase in stratum corneum hydration as well as a modified penetration of active compounds into the skin can be observed [58, 59]. Furthermore, lipid nanoparticles are able to enhance the chemical stability of

compounds sensitive to light, oxidation and hydrolysis [60-62]. However, NLC were developed to overcome some potential limitations associated with SLN. Compared to SLN, NLC show a higher loading capacity for a number of active compounds, avoid/minimize potential expulsion of active compounds during storage and may be produced with a lower water content of the particle suspension.

Topical products containing SLN or NLC can be obtained by admixing the lipid nanoparticles to existing products, addition of viscosity enhancers to the aqueous phase of the lipid nanoparticles to obtain a gel or the direct production of a final product containing only lipid nanoparticles in a one-step process. Addition of SLN or NLC to an existing product (e.g. o/w cream, lotion) is realized by replacing a part of the water phase with concentrated lipid nanoparticle dispersion. To maintain the lipid content of the original formulation, its lipid content can be reduced about the amount of incorporated lipid from the lipid nanoparticles [43]. Instabilities of lipid nanoparticles in these systems that might occur are aggregation of the lipid nanoparticles or dissolution of the lipid nanoparticles in the lipophilic phase. The presence of the solid lipid can be proven by differential scanning calorimetry (DSC) and the particle size can be determined by photon correlation spectroscopy (PCS) or laser diffractometry (LD) [63, 64]. The choice of the viscosity enhancer is crucial for the stability of lipid nanoparticles in hydrogel formulations. Due to their structure i.e. their charge, aggregation of lipid nanoparticles might occur due to a reduction of the zeta potential values of the lipid nanoparticles. However, a good physical stability has been reported for SLN and NLC in various hydrogel formulations [65, 66]. Using high lipid concentrations a final product can be produced in one step. These particle dispersions have a relatively high consistency. Depending on the lipid concentration they are cream like or almost solid. By PCS, LD and electron microscopy the existence of intact particles can be proven [67, 68].

The first cosmetic products containing lipid nanoparticles were introduced to the market in October 2005. Since then a number of cosmetic products followed. Table 1.2.2-1 provides an overview of cosmetic products containing lipid nanoparticles currently on the market. Until now no pharmaceutical lipid nanoparticle formulation was introduced to the market. The time for product development and market introduction is much shorter for cosmetic products due to the more complex regulations for the development of a pharmaceutical product. However, due to their positive features a pharmaceutical use of lipid nanoparticles seems to be possible in the future.

Table 1.2.2-1: Cosmetic products containing lipid nanoparticles (NLC) currently on the market.

Product name	Producer	Market introduction
Cutanova Cream Nano Repair Q10	Dr. Rimpler	October 2005
Intensive Serum NanoRepair Q10		
Cutanova Cream NanoVital Q10		June 2006
SURMER Crème Legere Nano-Protection	Isabelle Lancray	November 2006
SURMER Crème Riche Nano-Restructurante		
SURMER Elixir du Beauté Nano-Vitalisant		
SURMER Masque Crème Nano-Hydratant		
SURMER Crème Contour Des Yeux Nano-Remodelante		March 2008
NanoLipid Restore CLR	Chemisches	April 2006
NanoLipid Q10 CLR	Laboratorium	July 2006
NanoLipid Basic CLR	Dr. Kurt Richter	
NanoLipid Repair CLR		February 2007
IOPE SuperVital Cream	Amore Pacific	September 2006
IOPE SuperVital Serum		
IOPE SuperVital Eye cream		
IOPE SuperVital Extra moist softener		
IOPE SuperVital Extra moist emulsion		
NLC Deep Effect Eye Serum	Beate Johnen	December 2006
NLC Deep Effect Repair Cream		
NLC Deep Effect Reconstruction Cream		
NLC Deep Effect Reconstruction Serum		
Swiss Cellular White Illuminating Eye Essence	la prairie	January 2007
Swiss Cellular White Intensive Ampoules		
Regenerationscreme Intensiv	Scholl	June 2007
Olivenöl Anti Falten Pflegekonzentrat	Dr. Theiss	February 2008
Olivenöl Augenpflegebalsam		
Edelweiss Deluxe Repair Q10 Face Cream	Audorasan	September 2008
Edelweiss Body lotion		
Dr. Cutanova Cream Nanosensitive forte	Dr. Rimpler	October 2008
Dr. Cutanova Emuslion Nanosensitive		

2 PLA_2 inhibitors: PX-13 and PX-18

2.1 Introduction

2.1.1 General aspects about phospholipase A_2 (PLA_2)

Phospholipases are esterases. According to the position of the ester bond, which is split hydrolytically by the phospholipases, the enzymes can be classified as acylhydrolases PLA_1, PLA_2, PLB and lysophospholipases as well as phosphodiesterases PLC and PLD [69]. PLA_2s hydrolyze fatty acids from the sn-2 position of glycerophospholipids resulting in free fatty acids such as arachidonic acid and lysophospholipids [70-72]. The superfamily of PLA_2 enzymes can be divided in five types of enzymes, the secreted PLA_2s ($sPLA_2$), the cytosolic PLA_2s ($cPLA_2$), the Ca^{2+}-independent PLA_2s ($iPLA_2$), the platelet-activating factor acetylhydrolases (PAF-AH) and the lysosomal PLA_2 [73]. Table 2.1.1-1 provides an overview of currently known groups and subgroups of PLA_2.

The $sPLA_2$s have a low molecular mass (13-19 kDa) containing five to eight disulfide bonds. This group has an active side histidine and requires µM levels of Ca^{2+} for catalysis. The $sPLA_2$s have no specificity for particular fatty acids [74]. The $cPLA_2$s are large cytosolic proteins (61-114 kDa) and have a catalytic serine. The $cPLA_2$s do not require Ca^{2+} for catalysis but for translocation of the enzyme to intracellular membranes. These enzymes preferentially hydrolyse phospholipids containing arachidonic acid in the sn-2 position [75]. The $iPLA_2$s have a molecular weight of 28 to 146 kDa. They are Ca^{2+}-independent enzymes utilizing serine for catalysis. The $iPLA_2$s are not selective for any fatty acid [75]. PAF-AH catalyses the hydrolysis of acetyl groups from the sn-2 position of PAF [73, 76]. Lysosomal PLA_2 is Ca^{2+}-independent and performs transacylases using phospholipids as acyl group donor [73].

Table 2.1.1-1: Overview of the PLA_2 superfamily.

Enzyme type	Group	Subgroup	Molecular mass [kDa]
$sPLA_2$	I	A	13-15
		B	13-15
	II	A	13-15
		B	13-15
		C	15
		D	14-15
		E	14-15
		F	16-17
	III		15-18
	V		14
	IX		14
	X		14
	XI	A	12.4
		B	12.9
	XII		19
	XIII		<10
	XIV		13-19
$cPLA_2$	IV	A	85
		B	114
		C	61
		D	92-93
		E	100
		F	96
$iPLA_2$	VI	A-1	84-85
		A-2	88-90
		B	88-91
		C	146
		D	53
		E	57
		F	28
PAF-AH	VII	A	45
		B	40
	VIII	A	26
		B	26
Lysosomal PLA_2	XV		45

By hydrolyzing cell membrane phospholipids into lysophospholipids and free fatty acid, particularly arachidonic acid, PLA$_2$ reaction is the rate-limiting step for the metabolism of arachidonic acid by one of several enzymatic pathways for the production of lipid mediators (eicosanoids) [77]. For an overview see Figure 2.1.1-1. These lipid mediators are implicated in several physiological and pathological processes including inflammation, immune responses, asthma, sleep regulation, hemostasis, parturition, maintenance of renal function, pain and fever [70, 73]. Lysophospholipids generated by the enzymatic cleavage of phospholipids are precursors of platelet activation factor, a strong mediator of inflammatory processes. Lysophospholipids activate white blood cells and increase their permeation through the endothelial cell monolayer, may induce tissue damage, such as gastric ulceration, act as growth factor and induce proliferation of cancer cells [78]. Furthermore, lyso-phosphatidylserine in particular activates histamine secretion from mast cells [79].

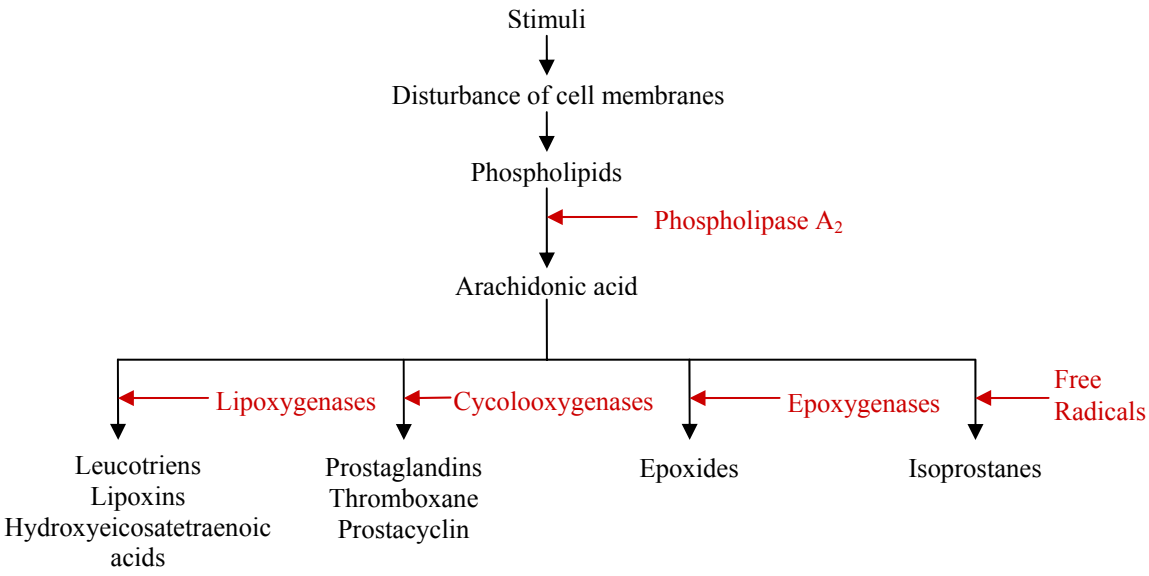

Figure 2.1.1-1: Pathway of mediators released from arachidonic acid.

The PLA$_2$ enzymes considered to regulate the generation of eicosanoids are cPLA$_2$ and sPLA$_2$ in particular group IIA, V and X [70], whereas iPLA$_2$ is believed to play a role in membrane remodelling [79]. It seems that under activated/inflammatory conditions sPLA$_2$ is the major contributor of arachidonic acid and subsequent production of eicosanoids, although cPLA$_2$ is specific to arachidonic acid [79]. Generation of arachidonic acid mediated by sPLA$_2$ occurs through different mechanisms, the direct hydrolysis of outer cell membrane phospholipids, the internalization and transfer of sPLA$_2$ to intracellular pools of phospholipids enriched in arachidonic acid and the activation of cPLA$_2$ [80]. sPLA$_2$-IIA implicates in a variety of

inflammatory processes and has been considered to be an acute phase protein. Increased levels of sPLA$_2$-IIA were reported for example in pancreatitis [81], septic shock [82], patients with burns [83], rheumatoid arthritis [84, 85], respiratory stress syndrome [86], inflammatory bowel disease [87], central nervous system inflammation [88, 89], hyperalgesia [90], psoriasis [91] and arteriosclerosis [69, 92]. A protective function of sPLA$_2$-IIA is also indicated. The enzyme was found to have bactericidal properties against Gram-positive bacteria [79].

2.1.2 PLA$_2$ in psoriasis

Psoriasis is a common, chronic, inflammatory skin disorder affecting approximately 2% of the population [93]. It is characterized by hyperplasia of epidermal keratinocytes, defective keratinisation, fibroblast activation, alteration of eicosanoid metabolism, leukocyte infiltration and inflammatory changes in both epidermis and dermis [91]. Scaly, erythematous plaques on the skin are caused by epidermal hyperproliferation and excessive angiogenesis of dermal vascular capillaries. Accumulation of inflammatory cells, particularly T lymphocytes, but also monocytes and neutrophils are characteristic for psoriasis [94]. The cause of psoriasis is still unknown till now, but activated T lymphocytes, increased levels of cytokines and other growth factors suggest that immunologic mechanisms play an important role in the pathogenesis. A number of phenomena observed in psoriasis can be explained, at least in part, by the action of eicosanoids. In human skin eicosanoids can be generated and exert proinflammatory and immunoregulatory actions through their effects on blood vessels and inflammatory cells. Eicosanoids are also involved in the regulation of growth and differentiation of the epidermis cells [95]. Activation of PLA$_2$ in response to cytokines secreted from immunological activated cells might be a link between immunologic and inflammatory mechanisms in psoriasis [91].

In healthy human skin limited amounts of sPLA$_2$-IIA are expressed in cells of the basal and spinous layers as well as in the uppermost cornified layer of the epidermis. Therefore, sPLA$_2$ activity is likely to play a role in epidermal barrier homeostasis due to the conversion of polar lipids of the upper epidermal layers into fatty acids, which together with ceramides play a key role in the permeability barrier function of the epidermis [96]. Furthermore, sPLA$_2$ expression in the most differentiated keratinocytes suggests a role of sPLA$_2$ in host protection, as the enzyme is mobilized in response to injury agents [91]. An increased expression of sPLA$_2$, especially sPLA$_2$-IIA, in psoriatic epidermis and dermis was reported in the literature. Andersen et al. found higher levels of sPLA$_2$ in involved and uninvolved psoriatic uppermost

epidermal layers than in healthy skin. Moreover, they found significantly higher amounts of sPLA$_2$ in psoriatic dermis than in healthy dermis [97]. The authors suggested that sPLA$_2$ detected in psoriatic skin is involved in eicosanoid overexpression in psoriatic tissue and potentiating cell activation, especially of T cells [97]. Haas et al. observed an upregulation of sPLA$_2$-IIA in the basal layer of psoriatic epidermis and in cells of psoriatic dermis [96]. Johansen et al. found an overexpression of sPLA$_2$ genes in psoriatic skin compared to normal skin by an overall factor of about three [91]. They proposed that the pathologic consequence of sPLA$_2$ overexpression and secretion from dermal fibroblasts is of importance in the activation of various inflammatory cells. Rys-Sikora et al. found an upregulation of sPLA$_2$-IIA and sPLA$_2$–V in cultures of human primary keratinocytes after serum stimulation, suggesting a role of these enzymes in hyperproliferation [98]. Grass et al. could show, that transgenic mice overexpressing sPLA$_2$-IIA develop chronic epidermal hyperplasia and hyperkeratosis supporting the possibility of a pathophysiological role of the enzyme [99].
Therefore, selective inhibitors for PLA$_2$ enzymes might be useful for the therapy of various inflammatory syndromes, including epidermal hyperproliferation due to increased leukotriene production, related to eicosanoid production and cell activation, in both epidermal and dermal tissue of psoriatic skin [100].

2.1.3 PLA$_2$ inhibitors

PLA$_2$ has attracted considerable interest as a pharmacological target due to its role in lipid signalling and its involvement in a number of inflammatory conditions. The control of the arachidonic acid production by inhibiting PLA$_2$ appears to be advantageous for the treatment of phatological conditions induced by phospholipase derived mediators, because the inhibition of selective pathways of eicosanoid production, e.g. cycolooxygenases or lipoxygenases, results in an upregulation of an alternative way [78]. In contrast to that, the inhibition of PLA$_2$ results in the suppression of several important classes of pro-inflammatory lipids e.g. prostaglandins, leukotrienes and PAF. Hence, the use of PLA$_2$ inhibitors has been considered an attractive therapeutic strategy in the treatment of inflammation-related diseases and tissue injuries [101]. Table 2.1.3-1 provides an overview of compounds with PLA$_2$ inhibitory activity and the type of PLA$_2$ which they inhibit.

Table 2.1.3-1: Overview of compounds with PLA_2 inhibitory properties and the type of PLA_2 which they inhibit.

Inhibition of $sPLA_2$		**Inhibition of $cPLA_2$**		**Inhibition of $iPLA_2$**	
Indoxam	[102]	AACOCF3	[106]	AACOCF3	[106]
Me-Indoxam	[103]	MAFP	[106]	MAFP	[106]
LY311727	[104]	IS-741	[79]	BEL	[106]
LY315920	[105]	Efipladib®	[79]		
PGBx	[106]				
PX-52	[106]				
PX-18	[106]				
PX-13	[106]				
PLI α, ß, γ	[107]				
Gravidin	[108]				
cis-unsaturated fatty acids	[109]				
BMS-181162	[110]				
Manoalide	[111]				
p-Bromophenacyl bromide	[112]				
Sulfasalazine	[77]				
CL42A	[77]				
1-Stearyl, 2-stearylaminodeoxy phosphatidylcholine	[113]				
Doxycycline	[114]				
Minocycline	[114]				

It has been widely discussed in the literature which PLA_2 group would be the preferable target of PLA_2 inhibitors since the specific role of the PLA_2s in inflammatory processes appears to be tissue, organ and disease specific [79, 115]. $iPLA_2$ is mainly involved in basal cell metabolism e.g. membrane remodelling [115]. Pro-inflammatory and anti-inflammatory effects of $cPLA_2$ have been reported, depending on the condition and tissue involved. Therefore, systemic non-selective inhibition of PLA_2 might result in serve adverse effects because of the essential roles of $iPLA_2$ and $cPLA_2$ in vital cellular phospholipids metabolism. However, the inhibition of $sPLA_2$ seems to be the preferable strategy due to the fact that their

induced levels are predominantly associated with pathological conditions. For the treatment of psoriasis the topical application of the sPLA$_2$ inhibitors PX-18 and PX-13, with a preference to sPLA$_2$-IIA, is suggested.

2.1.4 PX-13 and PX-18

PX-13 and PX-18 belong to a family of compounds, which are composed of at least two fatty acid moieties and contain at least one unsaturated double bond. The fatty acid moieties can be different from each other in several features, e.g. length of the hydrocarbon chain, degree of unsaturation and additional functional groups. Furthermore, the compound family has at least one acidic group or salt form thereof [116-120]. Figure 2.1.4-1 shows the chemical structure of PX-18 (2-*N,N*-Bis(oleoyloxyethyl)amino-1-ethanesulfonic acid). BES dioleate is a synonym for PX-18. This compound has a molecular weight of 742.29 g/mol and a calculated logP value of 14.98 ± 0.52 (ACD/ChemSketch Freeware version 11.0 (Advanced Chemistry Development, Inc., Toronto, ON, Cananda)).

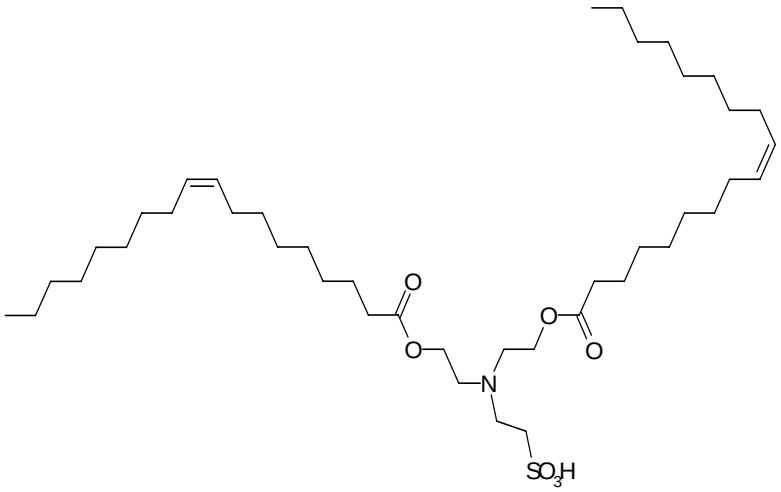

Figure 2.1.4-1: Chemical structure of PX-18 (2-*N,N*-Bis(oleoyloxyethyl)amino-1-ethanesulfonic acid).

The chemical structure of PX-13 (2-Tris(oleoyloxymethyl)methylamino)-1-ethanesulfonic acid) is shown in Figure 2.1.4-2. TES trioleate is a synonym for PX-13. The molecular weight of PX-13 is 1022.79 g/mol. A logP value of 22.86 ± 0.58 was calculated for this compound using the software ACD/ChemSketch Freeware version 11.0 (Advanced Chemistry Development, Inc., Toronto, ON, Cananda).

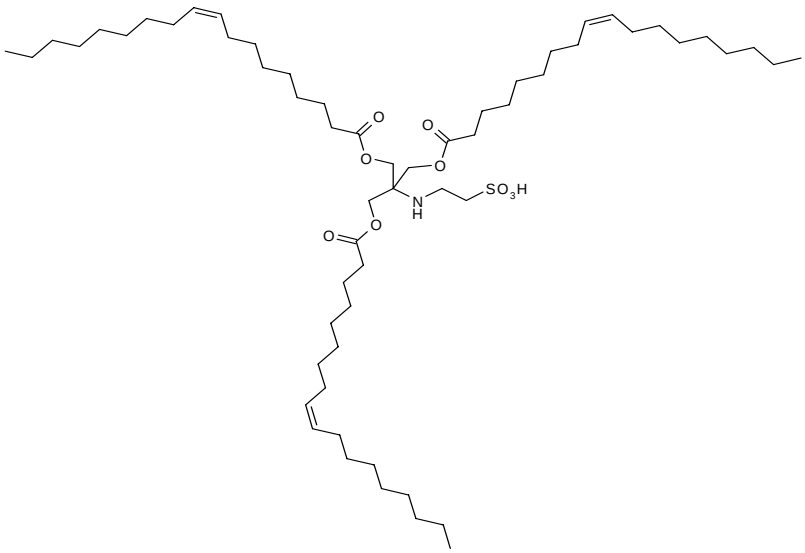

Figure 2.1.4-2: Chemical structure of PX-13 (2-Tris(oleoyloxymethyl)methylamino)-1-ethanesulfonic acid).

PX-18 and PX-13 are sPLA$_2$ inhibitors [106]. A preference of the inhibitors to sPLA$_2$-IIA was reported (personal communication, Richard Berney Associates, LLC). In a preliminary study on four psoriatic volunteers, applying a cream containing 5% (w/w) PX-13 twice daily for three weeks, a reduction in swelling, diameter and elevation of plaques was found in all four volunteers [116]. Therefore, a further investigation of PX-18 and PX-13 for a dermal application to psoriatic skin seems promising.

2.2 Purpose of the study

New chemical compounds like PX-18 and PX-13 are not commercially available. Furthermore, a detailed characterisation and a validated analytical method for the quantification are not available in the literature for new compounds. Therefore, the first part of this work is focused on the optimisation of the synthesis of PX-18 and PX-13 and the characterization of these compounds. To obtain first information about the degradation temperature, polymorphism and pseudo-polymorphism of PX-18 and PX-13 thermal investigations were performed. As quantitative analytical method for PX-18 and PX-13 a reversed-phase HPLC-UV method was developed and subsequently validated. The challenge thereby was that PX-18 and PX-13 do not exhibit a chromophore system for adequate detection sensitivity and thus a chromophore system needed to be introduced to the compounds by derivatization reaction.

It was reported, that PX-18 and PX-13 are practically insoluble in water and hard to formulate using conventional techniques due to their wax-like properties (personal communication, Richard Berney Associates, LLC). Therefore, the aim of the second part of this work was the development of physical (constant particle size distribution) and chemical (constant drug content) stable nanosuspensions applying high pressure homogenization. Additionally, the saturation solubility and the dissolution velocity of PX-18 and PX-13 bulk material was determined and compared with the ones of the according nanosuspensions.

The dermal application of the $sPLA_2$ inhibitors PX-18 and PX-13 for the treatment of psoriasis seems to be a promising approach [116]. Due to the fact, that very little/nothing was known about the dermal and ocular safety of PX-18 and PX-13, the third part of this work is focused on the evaluation of the dermal and ocular safety of PX-18 and PX-13 bulk material as well as of the according nanosuspensions. Following the principle of reducing, replacing and refining animal tests, the dermal and ocular safety was evaluated using *in vitro* test systems in particular primary human fibroblasts and keratinocytes monolayer cell cultures, the EPISKIN test, a reconstructed human epidermis model and the hen's egg test on the choriallantic membrane (HET-CAM).

2.3 Synthesis optimization, characterization and validation of an analytical method

2.3.1 Synthesis optimization and characterization of PX-13 and PX-18

2.3.1.1 Introduction

PX-13 and PX-18 are not commercially available yet. Therefore these compounds need to be synthesized for further investigations. The synthesis of the compounds is described by Franson and Ottenbrite [116, 119, 120]. However, it was found, that these methods yield compounds of low purity. Therefore, the synthesis and purification of PX-13 and PX-18 needed to be optimized. The structure and purity of the synthesized compounds were confirmed by nuclear magnetic resonance spectroscopy (^{1}H-NMR and ^{13}C-NMR), attenuated total reflection-Fourier transform infrared spectroscopy (ATR-FTIR) and mass spectroscopy (MS).

The refractive index (RI) of PX-13 and PX-18 bulk material was measured using the method established by Saveyn et al. and calculated using the Clausius-Massotti equation [121, 122]. The RI is an important property of any optical measuring system which uses refraction. In addition the RI can be used to identify compounds and their purity.

Furthermore, PX-13 and PX-18 were thermally investigated using thermogravimetry (TG) and differential scanning calorimetry (DSC) to obtain information about water associated with the compounds, the degradation temperature, the melting behavior and the polymorphism [123]. Pseudo-polymorphism, polymorphism and degradation temperature have not been previously investigated for PX-13 and PX-18.

2.3.1.2 Materials and methods

2.3.1.2.1 Materials

Acetone	Penta, Chrudim, Czech Republic
Acetonitrile, anhydrous 99.8%	Sigma Aldrich, Deisenhofen, Germany
Ethanol	Penta, Chrudim, Czech Republic
2-[(2-Hydroxy-1,1-bis(hydroxymethyl)ethyl)-amino]ethanesulfonic acid (TES)	Sigma Aldrich, Deisenhofen, Germany
N,N-Bis(2-hydroxyethyl)-2-aminoethanesulfonic acid (BES)	Sigma Aldrich, Deisenhofen, Germany
N,N-Dimethylformamide (DMF), anhydrous 99.8%	Sigma Aldrich, Deisenhofen, Germany
Oleoyl chloride	Sigma Aldrich, Deisenhofen, Germany
Pyridine	Sigma Aldrich, Deisenhofen, Germany
Triethylamine 99.5%	Sigma Aldrich, Deisenhofen, Germany

2.3.1.2.2 Methods

Nuclear magnetic resonance spectroscopy (NMR spectroscopy)

NMR spectroscopy is a method that uses the principle of nuclear magnetic resonance to study molecule structures. All nuclei that contain odd numbers of protons and/or neutrons have an intrinsic magnetic moment. The most commonly measured nuclei are hydrogen-1 (^{1}H-NMR) and carbon-13 (^{13}C-NMR). ^{1}H and ^{13}C-NMR spectra were recorded for $CDCl_3$ (Sigma Aldrich, Deisenhofen, Germany) solutions at room temperature on a Varian Mercury-Vx BB 300 spectrometer (Varian, Palo Alto, USA) operating at 300 MHz for ^{1}H and 75 MHz for ^{13}C. Chemical shifts were recorded as δ values in parts per million (ppm) and were indirectly referenced to tetramethylsilane (TMS) *via* the solvent signal (7.26 for ^{1}H and 77.0 for ^{13}C in $CDCl_3$).

Mass spectroscopy (MS)

Mass spectroscopy is an analytical technique that measures mass-to-charge ratio of charged particles [124, 125]. This technique was used to identify PX-13 and PX-18 by their mass. Low resolution mass spectra were recorded with a Finnigan LTQ XL (Thermo Scientific, San

Diego, USA). For the measurements PX-13 and PX-18 were dissolved in methanol (Riedel-deHaën, Seelze, Germany) or acetonitrile (Riedel-deHaën, Seelze, Germany).

Attenuated total reflection-Fourier transform infrared spectroscopy (ATR-FTIR)

ATR-FTIR is a common technique for material characterization [126]. The chemically specific information in the finger print region of the IR spectrum allows different materials, even in a mixture, to be distinguished as well as different polymorphic forms [127, 128]. FTIR-spectra were generated with an Excalibur 3100 FTIR spectrophotometer (Varian Inc., Palo Alto, USA). PX-13 and PX-18 were dissolved in chloroform (Merck, Dramstadt, Germany) and measured against pure chloroform. The samples were placed on a horizontal ATR accessory with a single reflection diamond crystal (Pike MIRacle, Pike Technologies, Madison, USA). 16 scans at 4 cm^{-1} resolution were averaged using Varian software (Resolution Pro 4.0).

Refractive index (RI)

The RI of a medium is defined as the ratio of the phase velocity of a wave phenomenon, such as light or sound, in a reference medium to the phase velocity in the medium itself. The RI of solid materials can be determined by measuring the RI of dilutions of the material in an appropriate solvent [121].

$$v = \frac{dn}{dc} = \lim_{c \to 0} \left(\frac{\Delta n}{c} \right)$$

$\frac{dn}{dc}$ = specific refractive index increment

c = concentration (w/v)

n = refractive index

The RI measured of known solute concentrations can be extrapolated to 100% concentration in order to calculate the RI of the bulk material by linear regression.

To determine the RI of PX-13 and PX-18 five different concentrations between 10% (w/v) and 1.25% (w/v) were prepared in chloroform (Merck, Darmstadt, Germany). A mixture of acetonitrile (Mallinckrodt Baker, Deventer, Netherlands) and N,N-dimethylformamide (Merck, Darmstadt, Germany) (1:1; v/v) was used to prepare the dilutions of PX-13 and

PX-18 at five different concentrations between 0.35% (w/v) and 0.1% (w/v). The RI of chloroform, the solvent mixture of acetonitrile and N,N-dimethylformamide, PX-13 solutions and PX-18 solutions were measured using an ATR W2plus refractometer (Schmidt and Haensch, Berlin, Germany) at 20°C. It was assumed that the solvent behaved ideal.

Another approach to gain the RI of solid materials like PX-13 and PX-18 is to use the Clausius-Mossotti equation [122]:

$$\left(\frac{4\pi}{3}\right)N_A\alpha = \left(\frac{M}{\rho}\right)(\kappa - 1)(\kappa + 2)$$

$\left(\frac{4\pi}{3}\right)N_A\alpha$ = molar refractivity

N_A = Avogadro's constant

α = molecular polarization of the molecule

M = molecular mass

ρ = density

κ = dielectric constant

For long wavelength κ can be related to the RI (n) of the material concerned. This is described in the Lorentz-Lorenz formula:

$$\left(\frac{4\pi}{3}\right)N_A\alpha = \left(\frac{M}{\rho}\right)(n^2 - 1)(n^2 + 2)$$

Based on this equation the RI of PX-13 and PX-18 was calculated using the software ACD/ChemSketch Freeware version 11.0 (Advanced Chemistry Development, Inc., Toronto, ON, Cananda).

Thermal analysis

The term thermal analysis summarizes all techniques measuring chemical or physical properties of a sample under a controlled temperature program and a controlled gas atmosphere e.g. TG and DSC [129]. Different solid phases, which may occur during crystallization or galenical processes and may be analyzed with thermal analysis are

polymorphs, amorphous phases or solvates [123]. The different solid forms of the same compound are called polymorphs or crystalline modifications. Polymorphism occurs when compounds with the same molecular structure crystallize into different molecular arrangements. Polymorphs have the same chemical composition but have unique cell parameters. Polymorphs show the same properties in the liquid and gaseous state but they behave differently in the solid state. The amorphous state is characterized by crystallisation in a non-ordered random system, related to the liquid state. The term glassy state is used for amorphous products which liquefy by undergoing a glass transition. The expression pseudo-polymorphism applies to crystals containing solvents (e.g. solvates and hydrates).

Thermogravimetry (TG)

Thermogravimetry is a technique where the weight of a sample is measured over a period of time while its temperature is changed (e.g. increased at a constant rate). This method can be used to obtain information about the thermal stability, decomposition, dehydration, oxidation and volatile content of a sample. PX-13 and PX-18 were analyzed using a Mettler TG-DTA analyzer (Mettler Toledo, Gießen, Germany). About 10-20 mg of the sample was weighed into aluminum oxide pans and heated from 30°C to 800°C with a heating rate of 10 K/min under constant purging with nitrogen at a flow rate of 80ml/min.

Differential scanning calorimetry (DSC)

DSC measures the enthalpy dependence of a sample related to a reference. Thermal events which are detectable by DSC may be endothermic (e.g. melting, vaporization, sublimation, desorption), exothermic (e.g. crystallization, condensation, adsorption) or may involve a change in heat capacity of the sample (e.g. glass transition) [130-132]. Two types of DSC instruments are available, the power compensated DSC and the heat flux DSC. Using the power compensated DSC the sample pan and the reference pan are heated from different sources. The differential temperature between the sample and the reference is maintained zero while the power to maintain the same temperature in the two pans is measured [133]. In the heat flux DSC the sample and the reference pan are heated from the same source and the differential temperature is measured [133]. For the experiments performed in this work a heat flux DSC instruments (Mettler DSC 821e, Mettler Toledo, Gießen, Germany) was used. The samples, weighing 2-3 mg, were analyzed in sealed and pin-holed standard 40 µl aluminum pans. With a heating rate of 5 K/min the samples were twice heated from -20°C to 200°C and

cooled down to -20°C. During the measurement the sample cell was continuously purged with nitrogen at a flow rate of 80 ml/min.

2.3.1.3 Results and discussion

Synthesis optimisation and characterization of PX-18

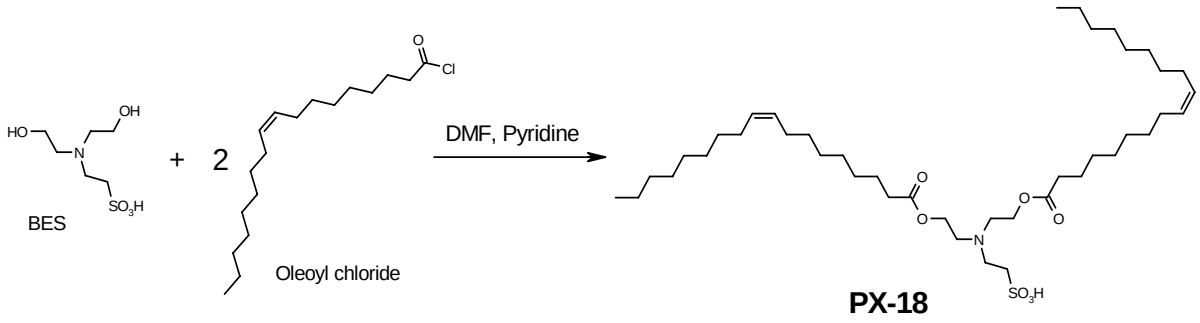

Figure 2.3.1.3-1: Reaction scheme for the synthesis of PX-18.

PX-18 was synthesized according to the reaction scheme shown in Figure 2.3.1.3-1. In a one liter round bottomed flask 16.2 g (76.0 mmol) commercially available BES was dissolved in a mixture of 60 ml dry DMF and 20.9 ml (258.3 mmol) pyridine. To the resulting solution 79.1 ml (239.3 mmol) of 85% oleoyl chloride was slowly added under argon atmosphere and constant stirring. After addition of oleoyl chloride, 300 ml of acetone was added to the suspension. The reaction mixture was stired under argon atmosphere at room temperature for 12 hrs. The precipitate was collected by filtration, washed with 300 ml acetone and 300 ml cold water. The product was dried in a vacuum to obtain PX-18 as a white solid. The yield of the reaction was 37.1 g (65.8%).

The calculated exact mass of PX-18 is 741.56 g/mol. PX-18 was identified in the mass spectrum (ESI$^+$) (*m/z*) with a peak at 742.58 (M + H). Table 2.3.1.3-1 provides an overview of the ^{1}H-NMR, ^{13}C-NMR and IR spectral data obtained for PX-18. With the help of these spectra PX-18 can be clearly identified.

Table 2.3.1.3-1: Summary of the ^{1}H-NMR, ^{13}C-NMR and IR spectral data of PX-18.

Method	Spectral data
^{1}H-NMR (300MHz, $CDCl_3$)	Δ 9.76-9.58 (br s, 1H, O**H**), 5.40-5.24 (m, 4H, 2xC**H**=C**H**), 4.53-4.39 (m, 4H, 2xC**H$_2$**O), 3.81-3.56 (m, 6H, 3xNC**H$_2$**), 3.33-3.21 (m, 2H, C**H$_2$**S), 2.40-2.29 (m, 4H, 2xCOC**H$_2$**), 2.08-1.90 (m, 8H, 2xC**H$_2$**CH=CHC**H$_2$**), 1.65-1.50 (m, 4H. 2xCOCH$_2$C**H$_2$**), 1.42-1.14 (m, 44H, 2x11xC**H$_2$**), 0.93-0.80 (m, 6H, 2xC**H$_3$**)
^{13}C-NMR (300MHz, $CDCl_3$)	Δ 173.09 (**C**=O), 130.01 (**C**=C), 129.66 (C=**C**), 57.93 (**C**H$_2$O), 53.15 (OCH$_2$**C**H$_2$N), 52.29 (SCH$_2$**C**H$_2$N), 44.73 (S**C**H$_2$CH$_2$N), 33.85, 31.89, 29.76, 29.73, 29.66, 29.52, 29.31, 29.25, 29.16, 29.11, 27.22, 27.19, 24.61, 22.67, 14.11 (**C**H$_3$)
IR (cm^{-1})	2920 s (CH_2), 2855 m (CH_2O), 1740 s (COOC), 1220 m (C-N), 1185 s (SO_2OH), 1033 s (SO_2OH).

The RI of PX-18 was determined using the method from Saveyn et al. in two different solvents [121, 134]. Furthermore, the RI of PX-18 was calculated using the Clausius-Mossotti-equation [122]. The results obtained are shown in Table 2.3.1.3-2. Using the method from Saveyn et al., identical RI in both solvents were obtained for PX-18 bulk material. The RI calculated for PX-18 using the Clausius-Mossotti-equation was of the same order of magnitude as the measured values. The RI of PX-18 is 1.496.

Table 2.3.1.3-2: Measured and calculated RI of PX-18. For the measured RI the solvent, linear regression equation (v = specific refractive index increment; c = concentration [%; (w/v)]) and the R^2 are given.

Method	Solvent	Linear regression equation	R^2	RI
Saveyn et al.	Chloroform	$v = 0.0005 \cdot c + 1.446$	>0.99	1.496
Saveyn et al.	Acetonitrile: N,N-dimethylformamide	$v = 0.0011 \cdot c + 1.386$	>0.99	1.496
Clausius-Mossotti equation				1.489 ± 0.02

A thermogravimetric curve of PX-18 is shown in Figure 2.3.1.3-2. A weight loss of 1.2% in the range of 54-74°C with a maximum weight loss at 64°C indicates the presence of free water in the sample (2 molecules of water are associated with 1 molecule of PX-18). The decomposition of PX-18 involves 76.8% weight loss in the range of 235-297°C with a maximum weight loss at 273°C and 22% weight loss in the range of 392-527°C with a maximum weight loss at 499°C. For the identification of the decomposition mechanism and products at the according temperatures e.g. thermogravimetry coupled with mass spectrometry would need to be performed [135].

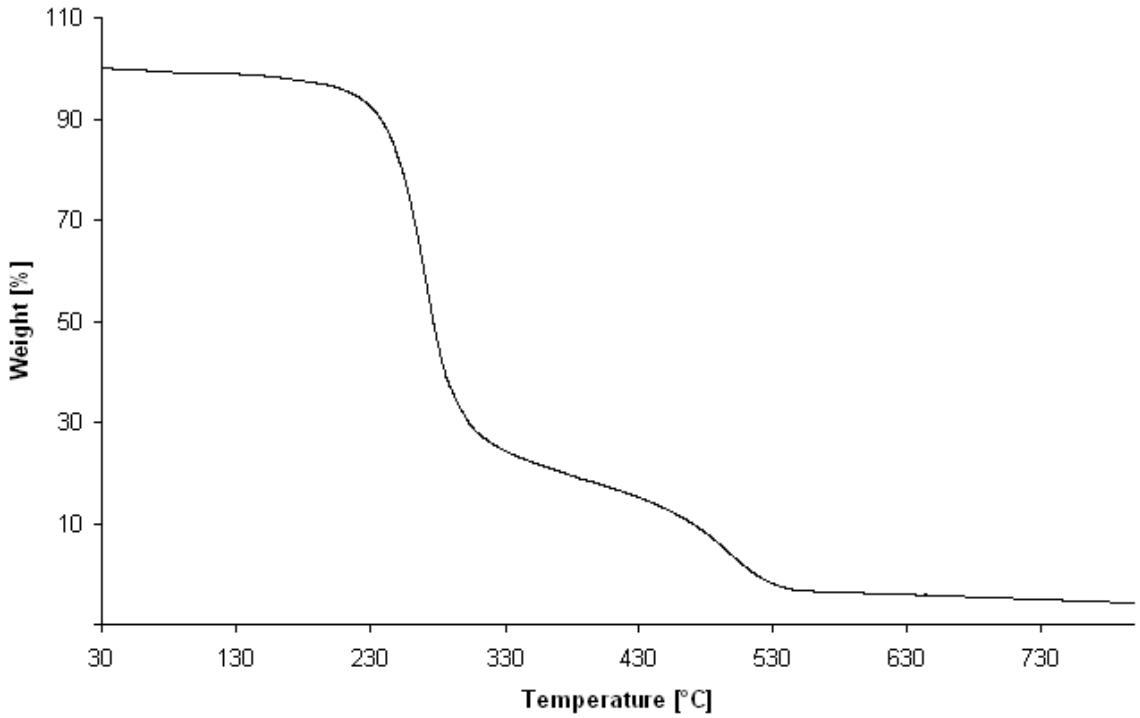

Figure 2.3.1.3-2: Thermogravimetry diagram of PX-18.

Figure 2.3.1.3-3 shows a DSC spectrum of PX-18 obtained by heating and cooling the sample twice from -20°C to 200°C and 200°C to -20°C. Table 2.3.1.3-3 provides a summary of the obtained thermal events.

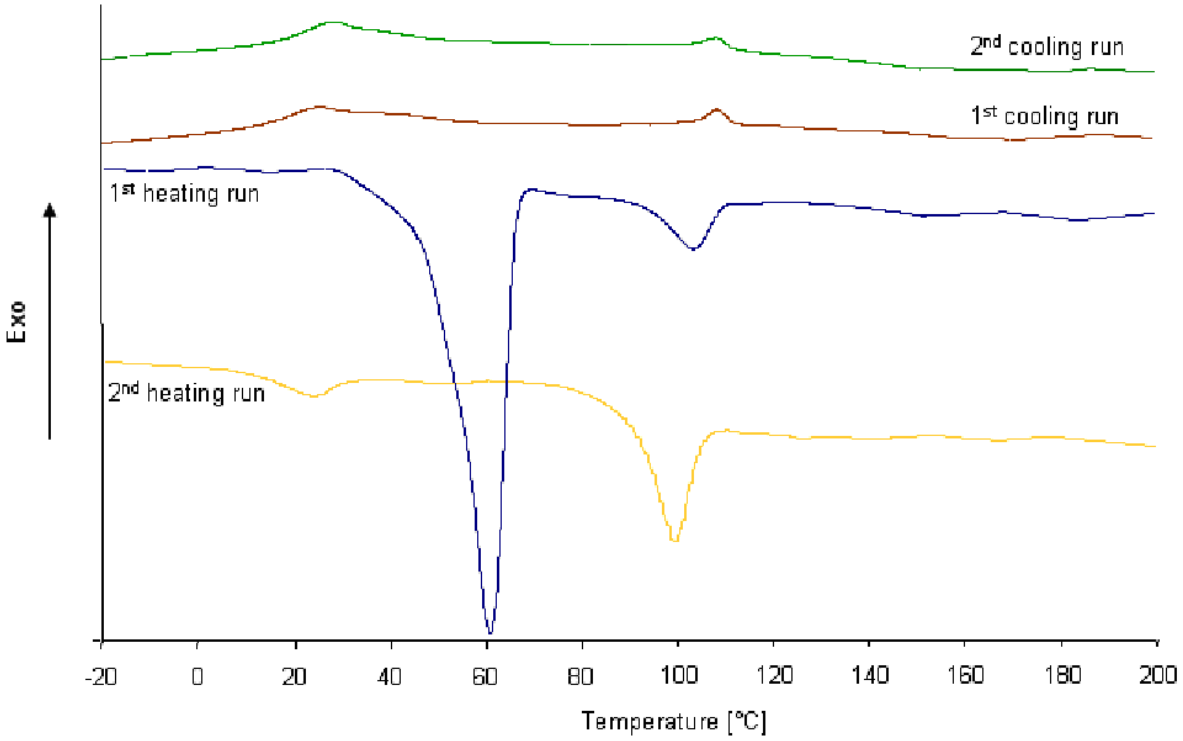

Figure 2.3.1.3-3: DSC curves of PX-18.

Table 2.3.1.3-3: Thermal events observed in DSC analyses of PX-18 shown in Figure 2.3.1.3-3.

	Thermal effect	Onset [°C]	Peak maximum [°C]
1st heating run	Endothermic	50	60
	Endothermic	95	105
1st cooling run	Exothermic	112	109
	Exothermic	32	25
2nd heating run	Endothermic	15	28
	Endothermic	92	100
2nd cooling run	Exothermic	112	110
	Exothermic	40	29

The endothermic peak with a peak maximum at 60°C, obtained in the first heating curve only, indicates the vaporization of water from the sample [130]. This finding is well in accordance with the finding of the loss of water in thermogravimetry measurements [123]. Furthermore, two polymorphs of PX-18 were found. The first modification has a melting point of 100-110°C. In the first and the second heating curve melting of this modification could be observed. In both cooling curves recrystallisation of this modification took place. The second

modification found has a melting point of 25-29°C. Crystallization of this modification could be seen in the first and second cooling curve. A melting peak for this modification was found in the second heating curve. The melting point of 133-136°C found by Franson and Ottenbrite [116, 119, 120] for PX-18 could not be observed in the present study. This can be due to the presence of another polymorph form of PX-18 which was not detectable in this study or the use of a different less accurate method than DSC by Franson and Ottenbrite (the method is not described in the patents). For a final evaluation of the polymorphism and pseudo-polymorphism of PX-18 additional experiments need to be performed e.g. by temperature resolved x-ray or temperature resolved FTIR, combining the heating of a sample with a spectroscopic measurement [123, 136, 137].

Synthesis optimization and characterization of PX-13

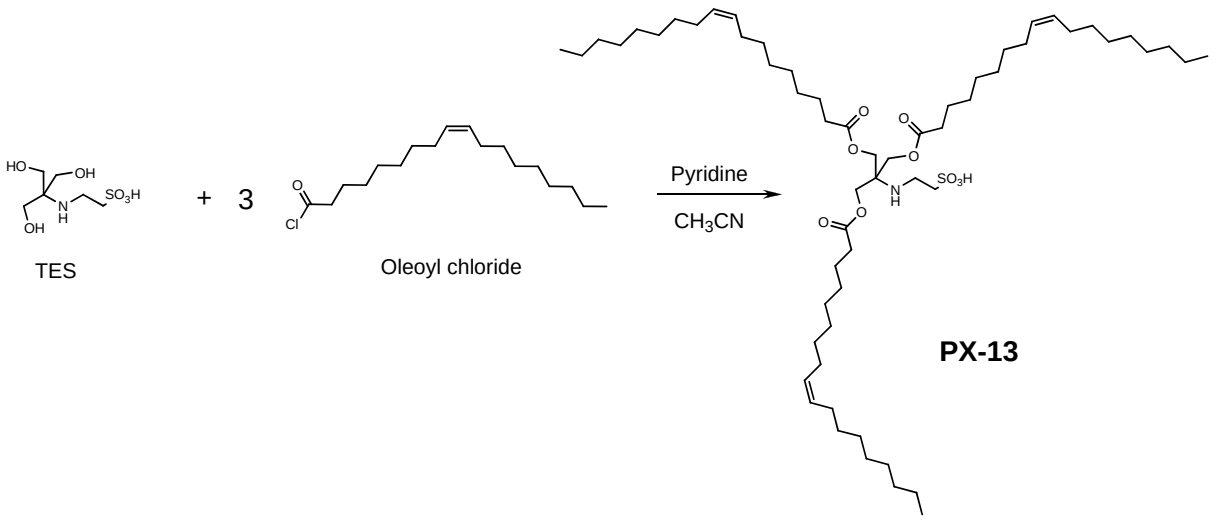

Figure 2.3.1.3-4: Reaction scheme for the synthesis of PX-13.

The procedure as described in Figure 2.3.1.3-4 is the optimized reaction to obtain pure PX-13. 19.6 g (85.5 mmol) TES was suspended in a mixture of 34.6 ml (427.50 mmol) dry pyridine and 200 ml dry acetonitrile under argon atmosphere and cooled to 0°C. Then 133.0 ml (342.0 mmol) 85% oleoyl chloride was added slowly. The resulting suspension was stirred under argon atmosphere for 20 hrs at 50°C. Then 300 ml of cold water was added to the reaction mixture and stirred for 1 hr at room temperature. The obtained white-brown suspension was filtered. The precipitate was recrystallized from approximately 4 l ethanol. The white solid was dried in a vacuum for one day. The yield of PX-13 obtained with this method was 53.6 g (61.3%).

The calculated exact mass of PX-13 is 1021.80 g/mol. PX-13 can be identified in the mass spectrum (ESI^+) (*m/z*) as a peak at 1022.81 (M + H). In Table 2.3.1.3-4 a summary of the obtained ^{1}H-NMR, ^{13}C-NMR and IR spectral data, which can be used to clearly identify PX-13, is given.

Table 2.3.1.3-4: Summary of the ^{1}H-NMR, ^{13}C-NMR and IR spectral data of PX-13.

Method	Spectral data
^{1}H-NMR (300MHz, $CDCl_3$)	δ 9.38-9.21 (br s, 2H, N**H**+O**H**), 5.43-5.27 (m, 6H, 3xC**H**=C**H**), 4.43-4.28 (m, 6H, 3xC**H_2**O), 3.66-3.52 (br s, 2H, NC**H_2**), 3.39-3.29 (br s, 2H, C**H_2**S), 2.51-2.39 (m, 6H, 3xCOC**H_2**), 2.09-1.92 (m, 12H, 3xC**H_2**CH=CHC**H_2**), 1.68-1.51 (m, 6H. 3xCOCH_2C**H_2**), 1.41-1.16 (m, 66H, 3x11xC**H_2**), 0.94-0.81 (m, 9H, 3xC**H_3**)
^{13}C-NMR (300MHz, $CDCl_3$)	δ 172.98 (**C**=O), 129.98 (**C**=C), 129.65 (C=**C**), 61.22 (**C**H_2O), 39.04 (S**C**$H_2$$CH_2$N), 33.86, 32.63, 31.90, 29.76, 29.67, 29.54, 29.33, 29.31, 29.29, 29.20, 29.12, 27.22, 24.71, 22.66, 14.11 (**C**H_3)
IR (cm^{-1})	2924 s (CH_2), 2860 m (CH_2O), 1750 s (COOC), 1465 m (CH_3), 1220 m (C-N), 1140 s (SO_2OH), 1035 s (SO_2OH)

Table 2.3.1.3-5 provides an overview of the RI of PX-13 obtained using the method from Saveyn et al. and calculated with the Clausius-Mossotti-equation. The RI obtained for PX-13 bulk material using the method from Saveyn et al. differed by 0.0002 in the two different solvents. With regard to the accuracy of the method this deviation can be neglected. The RI calculated for PX-13 using the Clausius-Mossotti-equation was of the same order of magnitude as the measured values. The RI obtained for PX-13 bulk material is 1.496. Hence, the RI of PX-13 and PX-18 are equal.

Table 2.3.1.3-5: Measured and calculated RI of PX-13. For the measured RI the solvent, linear regression equation (v = specific refractive index increment; c = concentration [%; (w/v)]) and the R^2 are given.

Method	Solvent	Linear regression equation	R^2	RI
Saveyn et al.	Chloroform	$v = 0.0005 \cdot c + 1.4459$	>0.99	1.4959
Saveyn et al.	Acetonitrile: N,N-dimethylformamide	$v = 0.0011 \cdot c + 1.3861$	>0.99	1.4961
Clausius-Mossotti equation				1.488 ± 0.02

Figure 2.3.1.3-5 shows a thermogravimetric curve of PX-13. Indicating the loss of water, a weight loss of 2.3% was found in the range of 93-159°C with maximum mass loss at 137°C [138]. This weight loss indicates that 1 molecule of PX-13 is associated with 10 molecules of water. The decomposition of PX-13 involves about 97.7% loss of mass in the ranges 245-298°C, 368-424°C and 455-582°C. PX-13 undergoes 67.4% weight loss in the range of 245-298°C with maximum weight loss at 272°C. In the range 368-424°C 13.6% loss of mass was observed with maximum weight loss at 413°C. 16.7% loss of mass of PX-13 occurs in the range of 455-582°C with a maximum weight loss at 502°C. To identify the mechanism of decomposition and the products of the decomposition at different temperatures as well as for the confirmation of the presence of PX-13 decahydrate, thermogravimetry coupled with mass spectrometry would need to be performed [135].

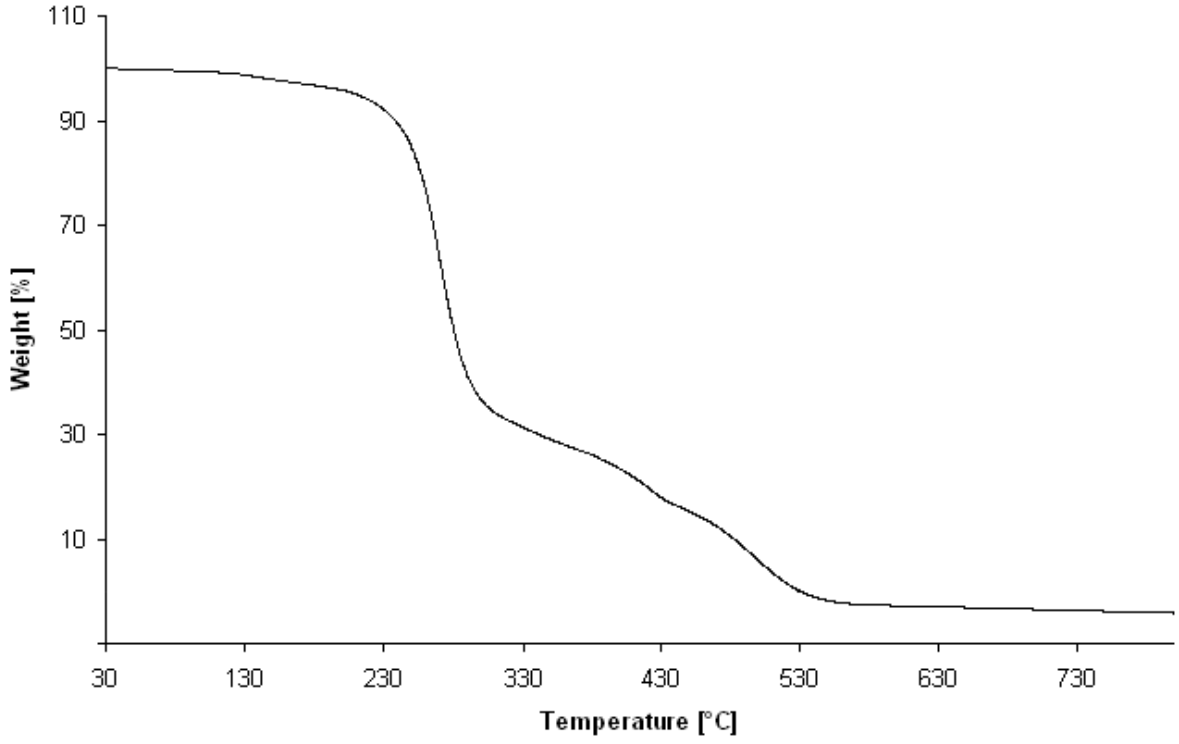

Figure 2.3.1.3-5: Thermogravimetry diagram of PX-13.

A DSC spectrum of PX-13 is depicted in Figure 2.3.1.3-6. In the first heating run from -20°C to 200°C four endothermic and one exothermic event can be observed. Table 2.3.1.3-6 provides an overview of the onset temperature and peak maximum temperature of the thermal events (A-E) in the first heating run of PX-13.

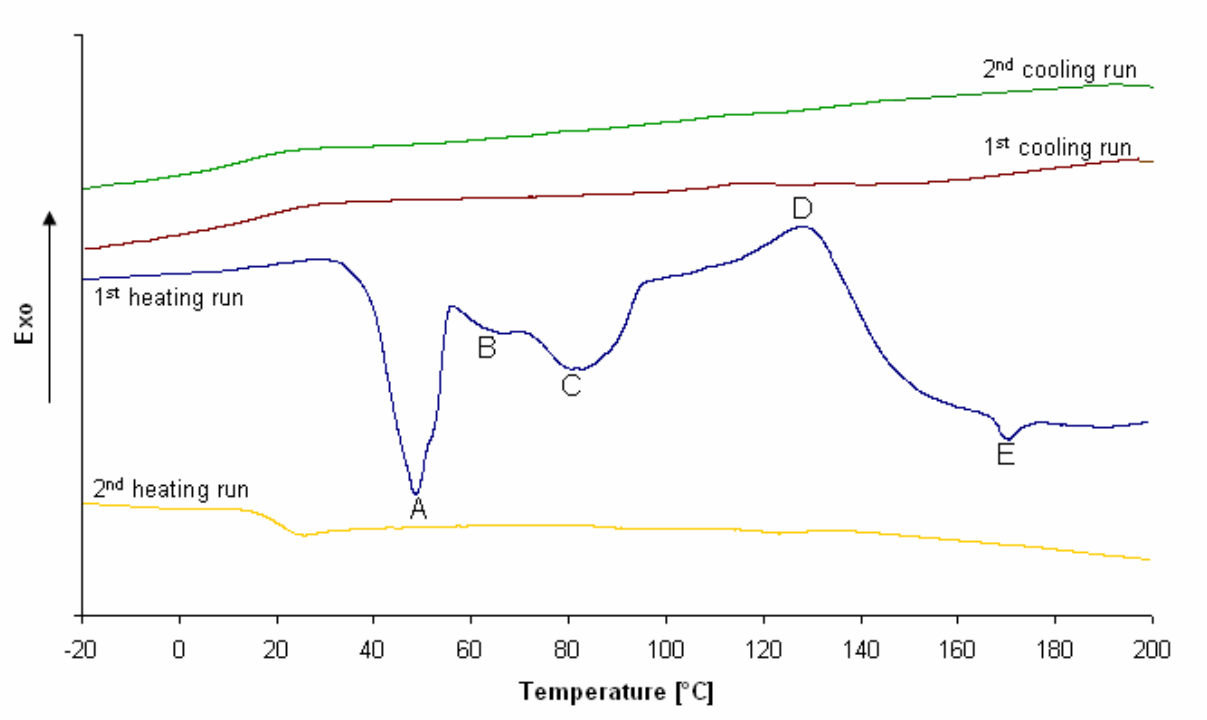

Figure 2.3.1.3-6: DSC spectrum of PX-13. In the first heating run four endothermic events (A, B, C and E) and one exothermic event (D) were observed. In the cooling runs and in the second heating run glass transition can be seen.

Table 2.3.1.3-6: Onset temperature and peak maximum of thermal events observed in the first DSC heating run of PX-13. The thermal events are labeled according to Figure 2.3.1.3-6.

Event	Thermal effect	Onset [°C]	Peak maximum [°C]
A	Endothermic	42	51
B	Endothermic	59	65
C	Endothermic	84	86
D	Exothermic	108	128
E	Endothermic	165	169

The endothermic event A indicates the melting point of the polymorph of PX-13 with the lowest melting point. The thermal event B corresponds to the melting point of PX-13 as described by Franson and Ottenbrite [116, 119, 120]. However, with thermogravimetry the presence of water in PX-13 samples was found. This indicates incongruent melting of the hydrate at 65°C [139]. The endothermic event C might be the melting point of a polymorph form of PX-13 but it is more likely that at this temperature water is removed from the sample [138]. The exothermic peak D indicates the crystallization of a higher melting polymorph form of PX-13. Event E potentially is the melting peak of the polymorph form of PX-13

formed during the exothermic event D. With a melting point of 169°C event E was the highest melting polymorph found for PX-13. Cooling PX-13 down from 200°C to -20°C does not lead to recrystallization of PX-13. Glass transition takes place at 22°C. Glass transition can also be observed in the second heating and cooling run, indicating the amorphous state of PX-13 [132, 133, 140]. For a final interpretation of the DSC thermal events and the correct evaluation of the polymorphism/pseudo-polymorphism of PX-13 additional experiments have to be performed e.g. by temperature resolved x-ray or temperature resolved FTIR, combining the heating of a sample with a spectroscopic measurement [123, 136, 137].

To sum up the results of this part it can be outlined, that the synthesis of both PX-13 and PX-18 was optimized by changing the solvent mixture for the reaction and changing the purification methods. With these new methods PX-13 and PX-18 of a high purity can be obtained, which was confirmed by ^{1}H-NMR and ^{13}C-NMR spectra. In addition the yield of PX-13 was increased by 9.3% compared to the yield from the synthesis described by Franson and Ottenbrite [116, 119, 120]. A summary of the most important spectral data (^{1}H-NMR, ^{13}C-NMR, IR and MS) is given, which helps to identify the two compounds. Furthermore, the RI of PX-13 and PX-18 is now available for the identification of the compounds and the use in optical analytical systems based on the principle of refraction e.g. laser diffractometry measurement. In this study PX-13 and PX-18 were investigated for the first time with respect to decomposition, pseudo-polymorphism and polymorphism. However, more work needs to be done to fully identify the decomposition products and all polymorphic forms.

2.3.2 Development and validation of a reversed-phase HPLC-UV method for PX-13 and PX-18

2.3.2.1 Introduction

A high pressure liquid chromatography system connected to a mass spectrometric detector (HPLC-MS) would be the best choice considering sensitivity, specificity and stability but in many laboratories HPLC-MS is not available for economic reasons. HPLC using ultraviolet detection (UV) is widely available, but has lower sensitivity and specificity compared to HPLC-MS [141, 142]. However, the UV absorbance of the functional groups present in PX-13 and PX-18 are not sufficient for adequate detection sensitivity but these functional groups are suitable for the attachment of UV absorbing moieties. To enhance the sensitivity and selectivity of detection, derivatization with a suitable choromatophore can be carried out [143]. The derivatization reaction can be performed before or after the chromatographic separation and both in on-line and off-line mode related to the chromatographic system. Pre-chromatographic off-line and post-chromatographic online modes are most commonly used for derivatization. An ideal derivatization reagent should fulfill the following criteria: complete and quantitative conversion of an analyte to a single conjugate under mild reaction conditions, performance of the reaction in either aqueous or non-aqueous solvents, minimal side reactions should occur during the reaction, the reagent as well as the conjugate should process reasonable stability at room temperature and the chromatographic separation of the reagent and the conjugate should be easy [144].

As derivatization agent p-nitrobenzyl-N,N'-diisopropylisourea (PNBDI) was chosen [145, 146]. PNBDI has an absorption maximum at 273 nm. The derivatization of PX-13 and PX-18 was carried out as a pre-chromatographic off-line derivatization. The reaction scheme for the reaction of PNBDI with sulfonic acids is shown in Figure 2.3.2.1-1.

The accuracy, precision, specificity, detection limit, quantification limit, linearity and range of the HPLC method for PX-13 and PX-18 were determined according to the International Conference of Harmonisation (ICH) guideline Q2(R1) [147]. The aim of this validation study was to establish an HPLC method, which can be used for the detection of the stability of PX-13 and PX-18 in nanosuspensions as well as for the determination of the saturation solubility and dissolution velocity of both compounds.

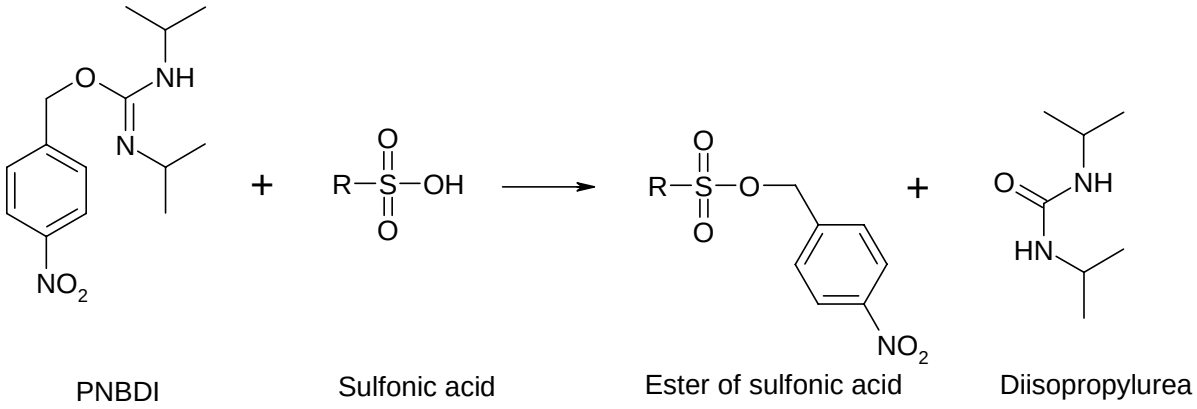

Figure 2.3.2.1-1: Reaction scheme of PNBDI with sulfuric acids.

2.3.2.2 Equipment and chromatographic conditions

The HPLC system used consisted of an auto sampler model 560, a pump system model 525 and a diode array detector model 540 (Kontron Instruments, Groß-Zimmern, Germany). This system was linked to a KromaSystem 2000 v. 1.70 data acquisition and process system, which also controlled the HPLC modules. 20 µl of the sample were injected onto a Superspher 100 RP-18 (4 µm) endcapped 250x 4 mm column with a matching pre-column (Knauer, Berlin, Germany). The column was kept at 30°C during the measurement. The mobile phase consisted of acetonitrile HPLC grade (Mallinckrodt Baker, Deventer, Netherlands) and distilled water. The mobile phase was run with a flow rate of 1 ml/min using a gradient (Table 2.3.2.2-1). The UV-spectrum was recorded at a wavelength of 273 nm.

Table 2.3.2.2-1: Gradient used for the chromatography of PX-18 and PX-13.

Time in min	Procedure	Water:Acetonitrile
0-3	maintaining	70:30
3-23	adjusting	50:50
23-32	maintaining	50:50
32-37	adjusting	70:30

2.3.2.3 Sample preparation

PNBDI (Sigma Alrich, Deisenhofem, Germany) was dissolved in HPLC grade acetonitrile (Mallinckrodt Baker, Deventer, Netherlands) to a final concentration of 5 mM. PX-13 or PX-18 powder for standard curves as well as PX-13 or PX-18 containing samples were

dissolved in a mixture of acetonitrile and N,N-dimethylformamide (Merck, Darmstadt, Germany) (1:1; v/v) without exceeding a concentration of 2.5 mM. 1 ml of the PNBDI solution was mixed with 1 ml of PX-18 or PX-13 containing dilution respectively. The derivatization reaction was carried out over 24 hrs at 75°C under constant shaking at 150 rpm using an Innova 4230 refrigerated incubator shaker (New Brunswick Scientific, New Jersey, USA).

2.3.2.4 Optimization of the derivatization reaction

2.3.2.4.1 Temperature screening

To find the optimal temperature for the derivatization reaction the reaction was performed using the same amount of PX-18 (520 µg/ml) and PX-13 (1298 µg/ml) at 6 different temperatures. The reaction time was 1 hr at all temperatures. All reactions were performed three times. The mean of the peak areas of all three reactions for PX-18 and PX-13 are shown in Table 2.3.2.4-1.

Table 2.3.2.4-1: Mean of the peak areas obtained for PX-13 and PX-18 after a reaction time of 1 hr at different temperatures (n=3).

Temperature	Mean peak area	
	PX-13	**PX-18**
30°C	0.10	-
40°C	0.38	1.01
50°C	1.285	1.08
60°C	3.55	2.49
70°C	14.31	8.78
75°C	27.72	22.25

It can be seen in Table 2.3.2.4-1 that with an increasing temperature the amount of PX-18 and PX-13 derivatised with PNBDI increases. Therefore, a temperature of 75°C was chosen for further investigations.

2.3.2.4.2 Investigations of reaction time

Using a concentration of 545 µg/ml PX-18 and a concentration of 270 µg/ml PX-13 respectively, the derivatization reaction was performed at 75°C for 1, 2, 3, 6 and 24 hrs in triplicate. The mean value of the peak areas (n=3) according to the reaction time is shown in Table 2.3.2.4-2.

Table 2.3.2.4-2: Mean of the peak areas obtained after different reaction times performing the derivatization reaction of PX-13 and PX-18 at 75°C (n=3).

Reaction time	Mean peak area	
in hrs	PX-13	PX-18
1	0.99	24.34
2	3.03	30.90
3	4.72	70.35
6	15.35	130.99
24	56.85	301.57

With an increasing reaction time the amount of PX-13 and PX-18 transferred into its UV detectable derivate increases. Therefore, for the further development of the HPLC method all derivatization reactions were carried out at 75°C over 24 hrs.

2.3.2.5 Specificity

Specificity is the ability of the method to measure the analyte response in the presence of compounds which may be present in a test sample [147]. Figure 2.3.2.5-1 shows a chromatogram of PNBDI, after exposing PNBDI to the conditions of the derivatization reaction and a chromatogram of derivatized PX-18. It can be seen, that the derivatized PX-18 can be separated from the derivatization agent and can be detected in the presencs of it. Furthermore, the product of the derivatization reactions was analyzed by ^{1}H-NMR. The ^{1}H-NMR spectrum confirms the structure of the expected product.

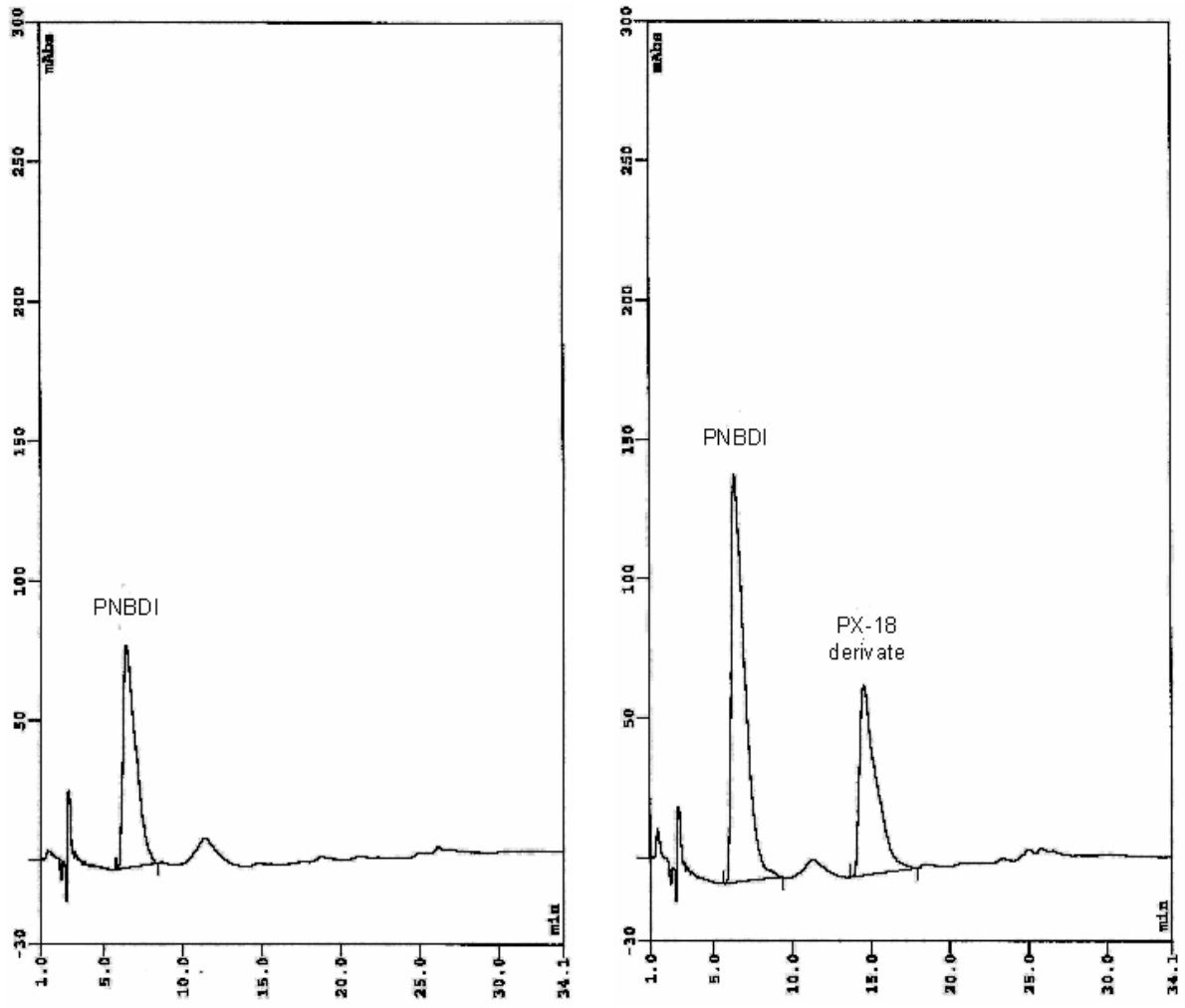

Figure 2.3.2.5-1: Chromatogram of PNBDI after exposure to the derivatization conditions (left) and a chromatogram of a PX-18 containing test sample after derivatization (right).

In Figure 2.3.2.5-2 a chromatogram of PNDBI exposed to the derivatization conditions and a chromatogram of PX-13 derivatized with PNBDI is shown. The results obtained demonstrate that the method was capable of resolving the peak of derivatized PX-13 from the peak of PNBDI. Furthermore, the product of the derivatization reactions was analyzed by ^{1}H-NMR. The ^{1}H-NMR spectrum confirms the structure of the expected product.

Possible impurities of PX-13 and PX-18 are the starting materials used in their synthesis. Therefore, BES, TES and oleic acid were exposed to the same reaction conditions as PX-13 and PX-18 as well as the mixtures of PX-13 and TES, PX-13 and oleic acid, PX-18 and BES and PX-18 and oleic acid. In case of the oleic acid no reaction between PNBDI and oleic acid took place, so this compound cannot be detected with this method. For all other combinations there were no interfering peaks of possible impurities obtained at the retention time of the analytes.

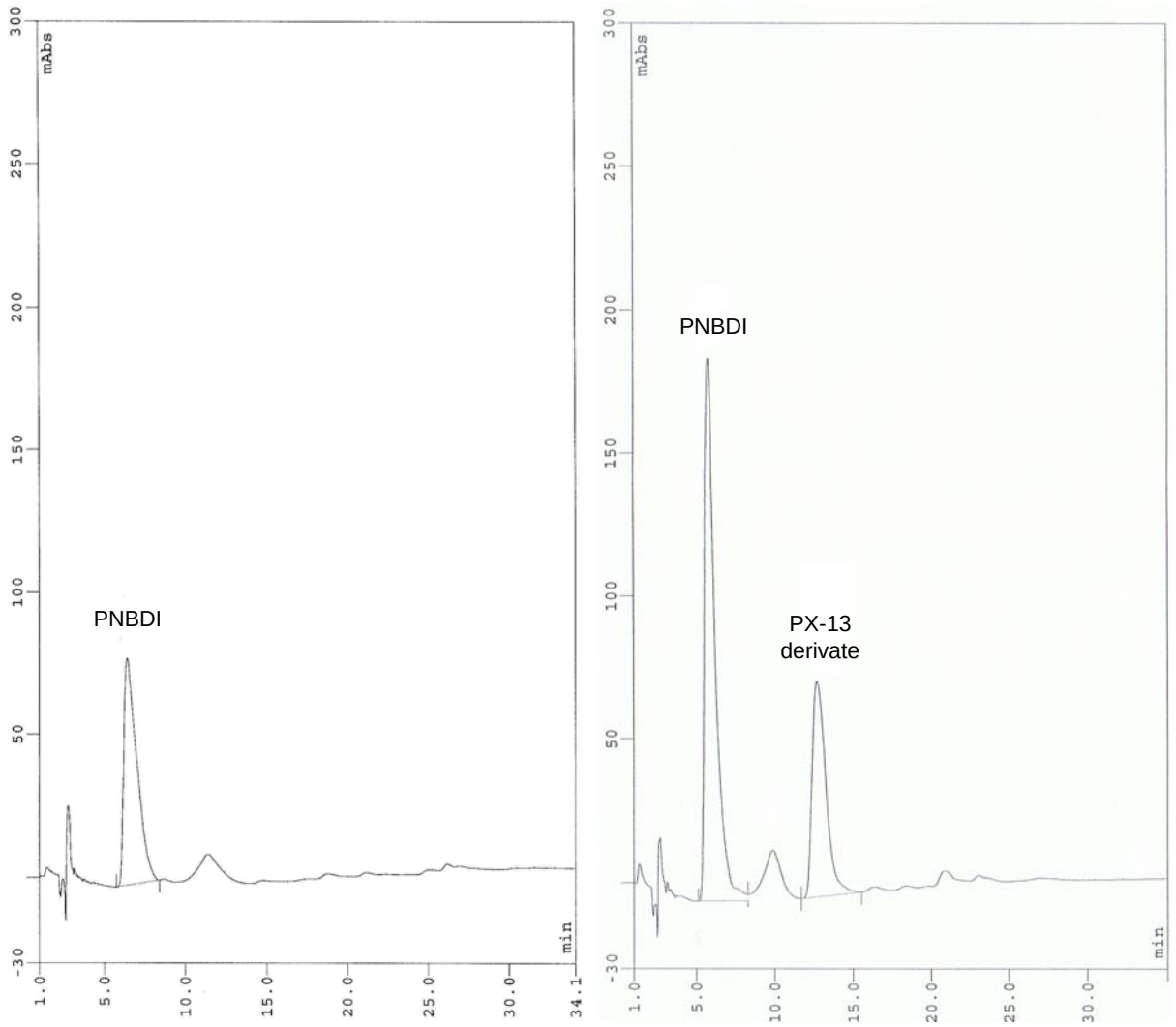

Figure 2.3.2.5-2: Chromatogram of PNBDI after exposure to the derivatization conditions (left) and a chromatogram of a PX-13 containing test sample after derivatization (right).

2.3.2.6 Limit of detection (LOD) and limit of quantification (LOQ)

The LOD is the lowest amount of an analyte in a sample which can be detected but not necessarily quantified as an exact value. The LOQ is the lowest concentration of a compound in a sample which can be quantified with a suitable precision and accuracy [147-149].

To estimate the LOD and LOQ of PX-13 and PX-18 the magnitude of the analytical background response was measured by analyzing 6 samples containing the derivatization agent PNBDI and exposing it to the derivatization conditions. From these 6 samples the standard deviation (SD) of the peak areas was calculated. With this SD and the slope of the calibration curves (m) the LOD and the LOQ can be calculated using the following equations:

$$LOD = \frac{3.3 \times SD}{m}$$

$$LOQ = \frac{10 \times SD}{m}$$

The estimated values for the LOD and the LOQ for the evaluated method were 1.3 µg/ml and 4.0 µg/ml respectively for PX-18. For PX-13 an LOD of 2.2 µg/ml and a LOQ of 6.7 µg/m was estimated with this method.

2.3.2.7 Linearity and goodness of fit

The linearity of an analytical method is its ability to obtain test results which are directly proportional to the concentration of the analyte in the sample [150]. For the linearity test 8 dilutions of different concentrations were prepared from a stock solution and assayed in triplicate. The calibration curve was obtained by plotting the peak area ratios of derivatized PX-13 or PX-18 versus their concentration (µg/ml) and performing linear regression analyses. Equations of the type $y = m \times x$ were obtained, where y is the peak area, x the concentration of PX-13/PX-18 and m the slope. For PX-18 the linearity of the method was confirmed over the tested concentration range (6.8-500 µg/ml). An example for a calibration curve obtained during the validation process is shown in Figure 2.3.2.7-1.

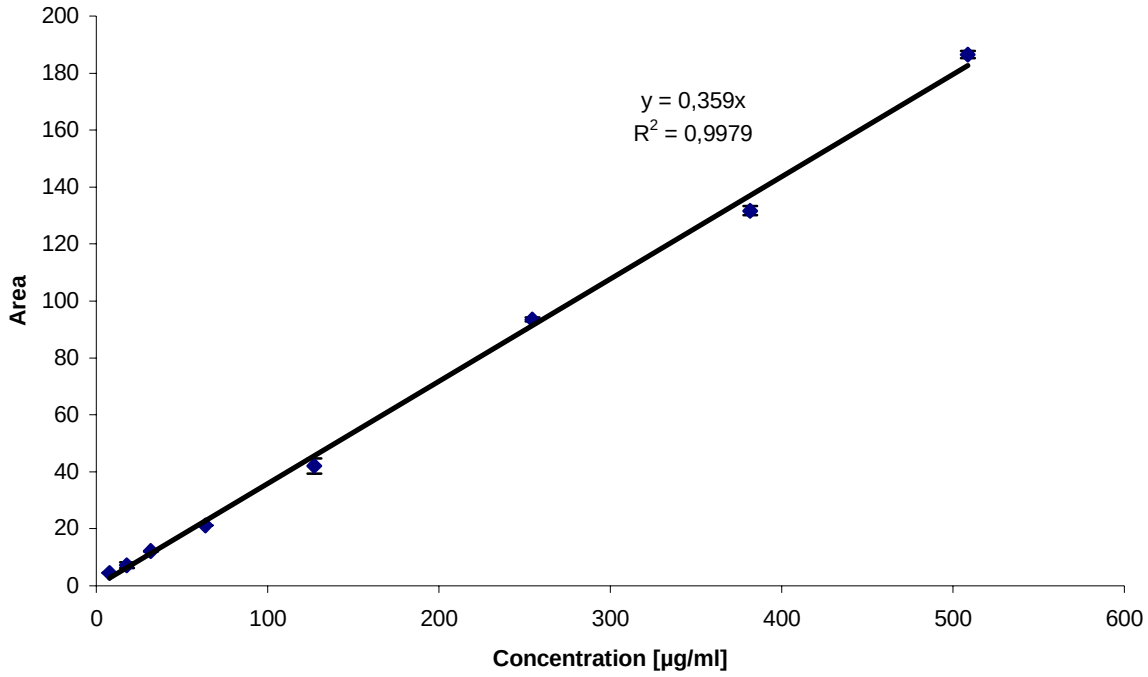

Figure 2.3.2.7-1: Linearity graph of PX-18 average peak areas response (n=3) against the concentration injected.

For PX-13 the investigated linearity range covered the concentrations from 7 µg/ml to 520 µg/ml. A typical calibration curve obtained during the validation process can be seen in Figure 2.3.2.7-2.

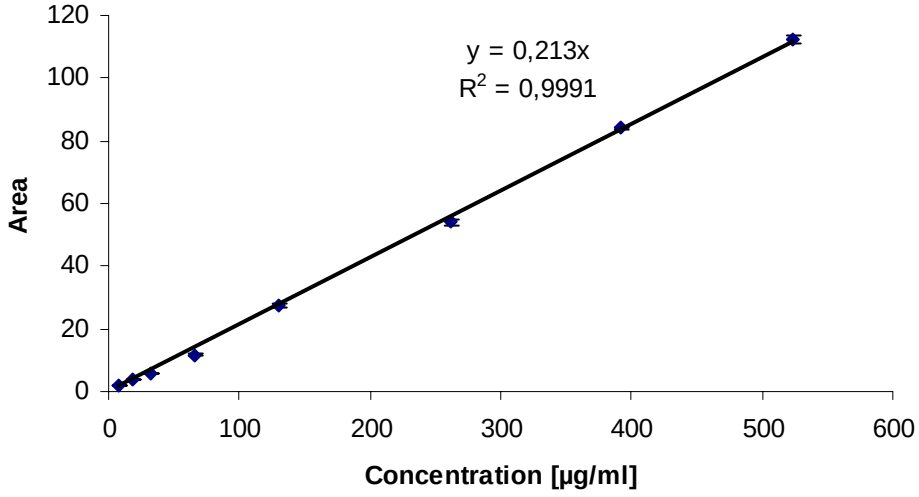

Figure 2.3.2.7-2: Linearity graph of PX-13 average peak areas response (n=3) against the concentration injected.

The results show, that a good correlation between the peak areas and the concentration of PX-13 and PX-18 exists. The goodness of fit was consistently greater than 0.99 during the course of validation. Calibration curves were established on each day of analyses.

2.3.2.8 Accuracy/ absolute recovery

The accuracy indicates the conformity of the mean of the measuring result $\bar{x}$ and the expected reference value μ. Therefore, the accuracy is equivalent to the absolute recovered amount of sample. The accuracy can be calculated using the following equation:

$$accuracy\,[\%] = \frac{\bar{x} \times 100}{\mu}$$

The results are acceptable up to a deviation of the measured value from the expected value of 15% in high and medium concentration ranges and up to 20% in the low concentration range.

2.3.2.8.1 Intra-assay accuracy

The intra-assay accuracy of the HPLC method was evaluated for both compounds PX-13 and PX-18 in triplicate at 8 concentrations covering the range of linearity. The percentage of the recovery was calculated from the slope of the calibration curve obtained. The percentage of absolute recovery of PX-18 ranged from 92.2% to 120% (Table 2.3.2.8-1). For PX-13 the experimental results showed approximate 93.3% to 102% recoveries (Table 2.3.2.8-2). Therefore, the intra-assay accuracy fulfills the requirement over the tested range for all data points. In this HPLC method, the quantification was based on the external standard that was prepared at the analytical concentration level of PX-13 and PX-18 [151]. Based on the recovery data, the assay of PX-13 and PX-18 has been demonstrated to be accurate for the intended purpose and is adequate for routine analysis.

2.3.2.8.2 Inter-assay accuracy

The inter-assay accuracy was evaluated by performing 3 independent assays at 8 different concentration levels of PX-13 and PX-18 on 3 consecutive days. The inter assay accuracy of PX-18 ranged from 85% to 104% (Table 2.3.2.9-1). For PX-13 the inter assay accuracy

ranged from 90.4% to 118.8% (Table 2.3.2.9-2). Therefore, the inter-assay accuracy is within the required limitations [152].

Table 2.3.2.8-1: Evaluation of intra-assay accuracy and precision of the HPLC method for PX-18 (n=3).

Nominal concentration (µg/ml)	Measured concentration (µg/ml; mean ± SD)	Accuracy (%)	Precision (%)
508.6	519.4 ± 3.5	102.1	0.7
381.6	366.8 ± 4.5	96.2	1.2
254.3	260.5 ± 2.1	102.4	0.8
127.2	117.2 ± 7.3	92.2	6.3
64.9	64.8 ± 0.3	99.8	0.4
32.5	30.3 ± 0.1	93.4	0.5
18.2	19.0 ± 0.1	104.6	0.3
6.8	8.3 ± 0.3	120.0	3.6

Table 2.3.2.8-2: Evaluation of intra-assay accuracy and precision of the HPLC method for PX-13 (n=3).

Nominal concentration (µg/ml)	Measured concentration (µg/ml; mean ± SD)	Accuracy (%)	Precision (%)
523.3	528.1 ± 6.3	100.9	1.2
392.5	395.5 ± 1.4	100.8	0.4
261.7	253.6 ± 3.9	96.9	1.5
130.8	127.8 ± 2.9	97.7	2.3
63.2	59.1 ± 1.8	93.6	3.1
32.2	32.1 ± 1.0	99.9	3.1
18.3	17.1 ± 0.6	93.3	3.7
7.8	8.0 ± 0.4	102.0	4.5

2.3.2.9 Precision

The precision is a measurement of the degree of reproducibility of analytical results repeating the same analytical method under the same terms and conditions. For the evaluation of the precision the relative standard deviation (RSD) can be used.

$$RSD\ [\%] = \frac{SD \times 100}{\bar{x}}$$

The precision should not vary more than 15% at high and medium concentrations and 20% at low concentrations [152].

2.3.2.9.1 Intra-assay precision

The intra-assay precision of the HPLC method was evaluated in triplicate at 8 concentrations covering the range of linearity for both compounds. The intra-assay RSD for PX-18 were within 0.3% and 6.3% (Table 2.3.2.8-1) during the assay method precision study. Table 2.3.2.8-2 shows the intra-assay precision of PX-13 with a RSD ranging from 0.4% to 4.5%. For all tested concentrations the intra-assay precision fulfilled the requirements and indicates a very good reproducibility of the method.

2.3.2.9.2 Inter-assay precision

Inter-assay precision was evaluated by performing 3 independent assays on 3 consecutive days at 8 concentration levels of PX-13 and PX-18. The inter-assay precision ranged between 2% and 14.9% for PX-18 (Table 2.3.2.9-1) and 0.5% and 15.6% for PX-13 (Table 2.3.2.9-2) respectively. The inter-assay precision of the HPLC method was for all tested concentrations within the required limitations and therefore confirms a good precision of the method.

Table 2.3.2.9-1: Evaluation of inter-assay accuracy and precision of the HPLC method for PX-18 (n=9).

Nominal concentration (µg/ml)	Measured concentration (µg/ml; mean ± SD)	Accuracy (%)	Precision (%)
459.5	478.0 ± 9.3	104.0	2.0
334.6	340.9 ± 12.7	98.9	3.7
229.8	215.4 ± 5.7	93.7	2.6
114.9	99.8 ± 6.8	86.9	6.8
57.4	48.8 ± 2.5	85.0	5.1
28.1	24.8 ± 2.9	88.2	11.8
11.3	10.1 ± 0.7	90.0	6.9
6.8	6.4 ± 1.0	94.7	14.9

Table 2.3.2.9-2: Evaluation of inter-assay accuracy and precision of the HPLC method for PX-13 (n=9).

Nominal concentration (µg/ml)	Measured concentration (µg/ml; mean ± SD)	Accuracy (%)	Precision (%)
514.4	527.6 ± 11.4	102.6	2.2
385.8	385.4 ± 2.0	99.9	0.5
257.2	256.4 ± 11.8	99.7	5.6
128.6	117.6 ± 12.3	91.4	10.5
64.3	58.1 ± 3.4	90.4	5.9
32.2	31.9 ± 2.1	99.3	6.5
18.0	18.4 ± 0.8	102.0	4.6
7.7	9.2 ± 1.4	118.8	15.6

2.3.2.10 Range

The range of an analytical method is the interval between the upper and lower concentration of the analyte for which it has been demonstrated that the analytical procedure has a suitable level of precision, accuracy and linearity [147]. Accordingly, the range of the HPLC-UV method for PX-13 and PX-18 is 7 µg/ml to 500 µg/ml.

The developed gradient reversed-phase HPLC method using UV detection was validated for the determination of PX-13 and PX-18 content in their nanosuspensions as well as for the determination of the saturation solubility and the dissolution velocity of these compounds. The method showed satisfying data for all tested validation parameters.

2.4 Preparation, characterization and stability investigations of PX-13 and PX-18 nanosuspensions

2.4.1 Screening of stabilisation agents – Contact angle measurment

2.4.1.1 Introduction

A three phase system composed of a gas phase, a liquid and a solid is creating a contact angle at the point where the three phases meet. The contact angle is a quantitative measurement of the wetting of a solid by a liquid. Knowing the contact angle is important in many technological processes e.g. tabletting, preparation of suspensions and dissolution processes [153, 154].

Depending on the affinity of the liquid to the solid, the surface tension of the liquid and the surface tension of the solid, different contact angles will be obtained. Figure 2.4.1.1-1 provides an overview of the different drop shapes and resulting from the drop shape the different contact angle, which can be obtained. Contact angles smaller than 90° indicate good wetting where as contact angles higher than 90° indicate bad wetting of the solid with the liquid. A contact angle of 0° represents complete wetting. No wetting is obtained if the contact angle equals 180°.

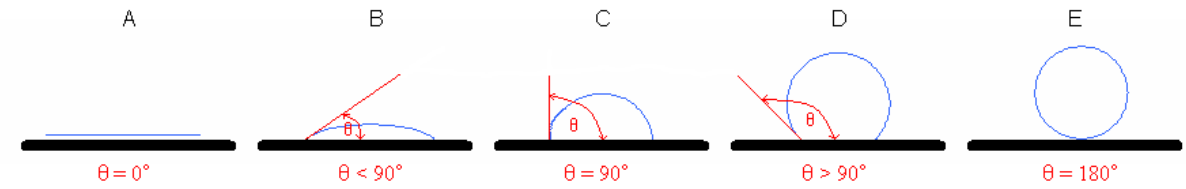

Figure 2.4.1.1-1: Contact angle θ (red) between a solid (black) and different liquids (blue) (A = complete wetting; B = good wetting; C = transition from good to bad wetting; D = bad wetting; E = no wetting).

At the point of contact between the three phases the surface tension of the solid (σ_S), the surface tension of the liquid (σ_L) and the interfacial tension between liquid and solid ($\sigma_{L/S}$) are balanced, which results in a specific contact angle (θ) for the observed system [155]. This equilibration can be described with the Young equation [156]:

$$\cos\theta = \frac{\sigma_S - \sigma_{L/S}}{\sigma_L}$$

For the stabilisation of PX-13 and PX-18 nanosuspensions the surfactant solution performing the best wetting of the powders compressed into a disc was evaluate. The different surfactant solutions will yield specific stabilites with the same drug molecule due to differences in adsorption onto the surface of the drug particles during the homogenization process.

2.4.1.2 Materials and methods

2.4.1.2.1 Materials

Brij 56	ICI Surfactants, Cleveland, Great Britain
Inutec	Nordmann, Rassmann, Hamburg, Germany
L.A.S.	Gattefossé, Saint-Priest, France
Lipoid E80	Lipoid, Ludwigshafen, Germany
Montanov 202	Kreglinger Europe, Antwerp, Belgium
Phospholipon	Nattermann, Köln, Germany
Pluronic F68 Prill	BASF, New Jersey, USA
Tagat S	Goldschmidt, Essen, Germany
Tegin M Pellets	Goldschmidt, Essen, Germany
Tego® Care 450	Goldschmidt, Essen, Germany

Plantacare® 2000

Plantacare® 2000 is a cloudy, viscous, aqueous solution of a C8-C16 fatty alcohol polyglycoside. It contains maximum 1% C6, 33-40% C8, 21-28% C10, 27-32% C12, 9-12% C14 and maximum 1% C16 fatty alcohols obtained from coconut and palm kernel oil. The glucose part of the molecule is derived from corn and potato starch. Synonyms for Plantacare® 2000 are Alkyl (8-16) Glucoside and Decyl Glucoside. Plantacare® 2000 is a non-ionic surfactant with a good dermatological compatibility. Plantacare® 2000 used in this work was obtained from Cognis (Monheim, Germany).

Tween 80

Twenn 80 is an ester, mainly oleate ester, of sorbitol and its anhydrides. One mole of sorbitol or sorbitol anhydride is copolymerized with approximately 20 moles of ethylene oxide. The chemical structure is shown in Figure 2.4.1.2-1. Polysorbate 80 and Polyoxyethylene 20 sorbitan monooleate are synonyms for Tween 80. Tween 80 is a clear, yellowish, oily liquid which is miscible with water. It is a non-ionic surfactant with an HLB value of 15. Due to its

relatively low toxicity, Tween 80 can be used in parenteral (e.g. i.v. and pulmonary) applied formulations. Tween 80 used in this work was obtained from Sigma Aldrich (Deisenhofen, Germany).

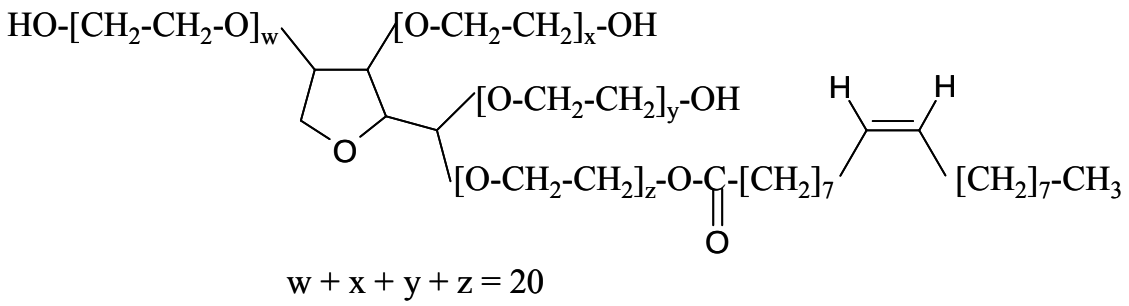

Figure 2.4.1.2-1: Chemical structure of Tween 80 (Polyoxyethylene 20 sorbitan monooleate).

2.4.1.2.2 Methods

Goniometry on a compressed disc

Goniometry is based on the analysis of the shape of a drop of a test liquid on a test solid. The contact angle is assessed directly by measuring the angle formed between the solid and the tangent to the drop. 0.1% (w/v) solutions of surfactants in purified water were prepared. 500 mg of PX-13 and PX-18 were compressed to a disc with a diameter of 1 cm using a single punch tablet machine (Emil Korsch Maschinenfabrik, Berlin, Germany). Goniometric measurement of the contact angle was performed 15 sec after application of a drop on the compressed disc using a Contact Angle Meter G1 (Krüss, Hamburg, Germany) at room temperature.

2.4.1.3 Results and discussion

The preparation of a compressed disc and the observation of a drop on the surface is the most popular approach in order to obtain indirect contact angles for powders. However, it should be taken into account, that some practical problems are associated with this method. Swelling and deformation of the disc, dynamic effects on the surface of powder compacts, which make the direct observation of the contact angle difficult and alteration on the outer surface of the disc during the compression process, which make it difficult to compare the contact angles obtained on a disc with a powder, are some of them [157]. Nevertheless, the primary focus of the contact angle study is in assessing the wetting characteristics of the solids PX-18 and

PX-13 with different surfactant solutions for the evaluation of the best wetting surfactant solution to be used as stabilizing agent in the nanosuspensions. The contact angle is commonly used as the most direct measurement of wetting [158]. The contact angles obtained with purified water and different surfactant solutions are shown in Table 2.4.1.3-1.

Table 2.4.1.3-1: Contact angles obtained for water and 0.1% (w/v) surfactant solutions on compressed discs of PX-13 and PX-18 (n=3, $\bar{x}$ ± SD).

Liquid	PX-13 [°]	PX-18 [°]
Purified water	85.3 ± 0.6	51.6 ± 0.6
Brij 56	30.3 ± 0.6	30.5 ± 1.3
Inotec	54.5 ± 0.5	32.8 ± 0.6
Lipoid E80	63 ± 1	38 ± 0
L.A.S.	26.7 ± 0.6	26 ± 1
Nontanov 202	64.8 ± 0.3	35 ± 0.6
Phospholipon	69.8 ± 0.3	37.8 ± 0.8
Plantacare® 2000	24.5 ± 1	25.6 ± 0.6
Pluronic F68	34.3 ± 1.2	28 ± 0
Tagat S	43.3 ± 0.3	29 ± 0.6
TegoAcid S40P	35.7 ± 0.6	42.3 ± 0.6
Tego® Care 450	51.7 ± 1.2	29.8 ± 0.8
Tween 80	37 ± 1	23.2 ± 0.3

Due to the fact that surfactants exhibit a lower surface tension compared to purified water, for all surfactant solutions smaller contact angles were measured on the compressed discs than for purified water. For PX-13 the best wetting was obtained with 0.1% Plantacare® 2000 solution. Compared to purified water the contact angle was reduced by 60.8°. Therefore, Plantacare® 2000 was selected as stabilizer for the production of PX-13 nanosuspensions. For PX-18 the best wetting was obtained with 0.1 % Tween 80 solution. Purified water showed a contact angle of 51.6° on the compressed PX-18 disc. With 0.1% Tween 80 solution the contact angle was reduced to 23.2°. Therefore, Tween 80 was chosen as stabilising agent for PX-18 nanosuspensions.

Knowing about the best wetting agent for PX-13 and PX-18 the production of nanosuspensions out of these materials can be optimized with regards to surfactant concentration, temperature, homogenization pressure and cycle number.

2.4.2 Formulation optimisation of PX-13 and PX-18 nanosuspensions

2.4.2.1 Introduction

High pressure homogenization was developed for the dairy industry about 100 years ago. Due to the reduction of fat droplet size and narrowing of fat droplet size distribution the creaming of the fatty phase of milk is avoided or reduced [159, 160]. Nowadays high pressure homogenisation is widely used for the production of emulsions and liposomes in food, cosmetic and pharmaceutical industry as well as for cell disruption in microbiology and biochemistry [161-165]. Furthermore, high pressure homogenization can be used for the production of SLN, NLC and nanosuspensions [166, 167].

Homogenization can be performed using a jet stream homogenizer (e.g. Microfluidizer, Microfluidics, Newton, USA) or a piston-gap homogenizer (e.g. Micron LAB 40, APV Deutschland GmbH, Unna, Germany). In jet stream homogenizers the particle containing fluid stream is accelerated and passed with a high velocity through either a "Z"-type or a "Y"-type homogenisation chamber. In the "Z"-type chamber the particle dispersion stream changes its flow direction a few times, while in the "Y"-type chamber the particle dispersion stream is divided into two streams which then collide frontally. Particle size reduction in this type of homogenizers is obtained by particle collision, sheare force and cavitaion forces [18, 19].

In piston-gap homogenizers the dispersion (e.g. suspension, emulsion) is placed in a cylinder with a piston having a relative large diameter. A pressure is applied to the piston pressing the dispersion through a narrow gap with a high streaming velocity (Figure 2.4.2.1-1). The principle of particle size reduction is based on the Bernoulli equation, which gives evidence that the sum of static pressure and dynamic pressure is constant in a system:

$$p_s + \frac{\rho v^2}{2} = constant$$

p_s = static pressure

ρ = density

v = velocity

$\frac{\rho v^2}{2}$ = dynamic pressure

In the gap the dynamic pressure dramatically increases and simultaneously the static pressure decreases. If water is used as dispersion medium, the static pressure drops below its vapor pressure at room temperature. This results in boiling of water at room temperature and the formation of gas bubbles. Leaving the gap, the static pressure increases, which leads to the implosion of the gas bubbles (= cavitation). Due to cavitaion, shock waves are formed, which lead to particle size reduction [18, 19, 168]. Furthermore, turbulent flow resulting in shear forces and collision of particles are involved in particle size reduction using piston-gap homogenizers [169, 170].

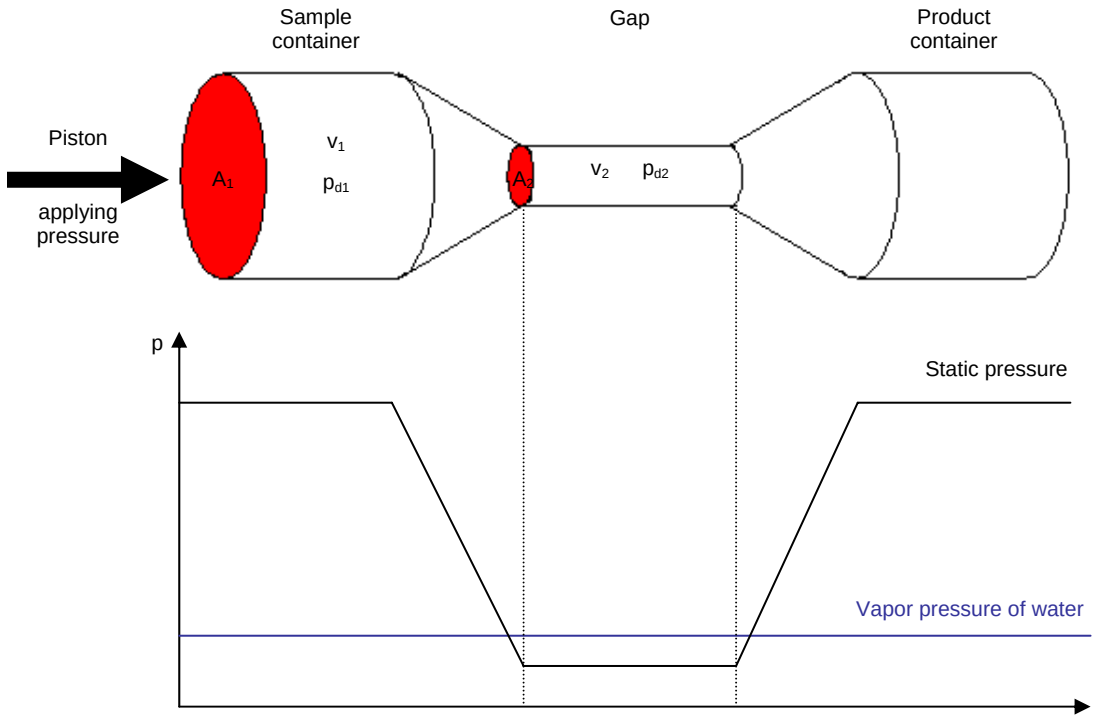

Figure 2.4.2.1-1: Schematic overview of the change in diameter (A_1>A_2), streaming velocity (v_1<v_2), dynamic pressure (p_{d1}<p_{d2}) and static pressure, if a dispersion is passed from a sample container through a gap in a piston-gap homogenizer. The static pressure as a function of the localisation in the homogenizer is shown in the lower part of the figure using water as dispersion medium. In the gap the static pressure drops below the vapor pressure of water at room temperature.

There is a correlation between the particle size achieved in drug nanosuspensions and the power density in the dispersing zone. The power density (P_V) is defined as the dissipated energy (W) in the dispersing zone of a homogenizer per time (t) and per volume unit (V_D):

$$P_V = \frac{W}{V_D\, t}$$

Therefore, the homogenization pressure, the width of the homogenization gap and the number of homogenization cycles are the main factors influencing the power density and thus the particle size obtained. Furthermore, the temperature, the fineness of the starting material and the hardness of the material affect the achievable particle size [19, 30, 166, 171, 172].

2.4.2.2 Methods

High pressure homogenization

A Micron LAB 40 (APV Systems, Unna, Germany) equipped with a water jacket for temperature control was used for the production of PX-13 and PX-18 nanosuspensions. The machine was operated discontinuously. Batches of 20 to 40 ml can be processed with this homogenizer in the discontinuous mode applying pressures between 100 and 1500 bar. PX-13 and PX-18 powder were pre-dispersed in aqueous surfactant solution using a mortar and pestle. The obtained pre-dispersion was then homogenized using the production parameters (pre-treatment, temperature, cycle number, homogenization pressure) outlined in the result and discussion part of this chapter.

Photon correlation spectroscopy (PCS)

PCS is a widely used technique for measuring the size of particles in the submicron range [173-177]. Dynamic light scattering and quasi-electric light scattering are synonyms for PCS. For PCS measurements particle dispersions are illuminated with a laser light. The dispersed particles have to exhibit random movements due to Brownian motion. This limits the particle size to a maximum, because no sedimentation or flotation of particles should occur. The particle movement is related to the particle size by calculating an autocorrelation function from the time dependent intensity fluctuation of the scattered light. Small particles have a higher diffusion velocity and therefore a higher time dependent intensity fluctuation of the scattered light, which results in a faster decay of the calculated autocorrelation function than observed for larger particles. The calculated correlation function is related to a theoretical correlation function $g(\tau)$:

$$g(\tau) = e^{-2D\tau K^2}$$

D = diffusion coefficient
K = absolute value of scattered light vector
τ = delay time

K and τ can be calculated from known parameters during the measurement:

$$\tau = n\,\Delta t \qquad K = \frac{4\,\pi\,n}{\lambda}\sin\left(\frac{\theta}{2}\right)$$

n = amount of channels
Δt = cycle time

n = refractive index of the dispersant medium
λ = wavelength of the laser light
θ = angle of scattered light

Hence, the diffusion coefficient is the only unknown parameter in the theoretical correlation function. The particle radius can be calculated using the Stokes-Einstein equation:

$$r = \frac{k\,T}{6\,\pi\,\eta\,D}$$

r = radius
k = Boltzmann constant
T = absolute temperature
η = dynamic viscosity

It should be taken into account, that the obtained diameter is the diameter of a sphere that has the same diffusion coefficient as the particle.
Beside the average particle size the polydispersity index (PI), which is a measure of the width of the particle size distribution, is obtained. The PI describes mathematically the deviation between the calculated correlation function and the fitted correlation function g(τ). The PI is a dimensionless value ranging from 0 to 1. A PI of 0.03 to 0.06 indicates a monodisperse particles size distribution. A narrow distribution is described with a PI between 0.10 and 0.20.

A broad distribution typically has a PI between 0.25 and 0.50. A PI > 0.5 indicates a broad particle size distribution with an unknown shape [173].

PCS measurements were performed using a Zetasizer Nano ZS (Malvern Instruments, Malvern, UK). This instrument is equipped with a red laser (633 nm) and non-invasive back scattering detection optics. Due to the location of the detector at an angle of 173°, particle sizes ranging between 0.6 nm to 6 µm can be detected. Before the measurement samples were diluted with bidistilled water. The average particles size and PI from 30 runs is given in this work.

Laser diffractometry (LD)

LD is a technique for measuring the particles size of nanoparticles and microparticles. Static light scattering is a synonym for LD. LD uses the fact that the pattern of diffracted light or more correctly scattered light, because light is not only diffracted but also reflected, refracted and absorbed, depends on the particle size of the sample under investigation [178]. Between the radius of the particles and the angles of diffraction exists a reverse proportionality [173]. In LD measurement a laser light is widened by an optical system for the illumination of a sample cell. In the sample cell light is scattered on the particles under investigation. With a Fourier lens the diffraction patterns are focused on the same area of the multi element detector independent of the fact where the particles are located in the sample cell. The collected information is used to calculate the particle size using a computer. In this work an LS230 (Beckmann-Coulter, Krefeld, Germany) was used. This instrument has a measuring range of 40 nm to 2000 µm due to the use of two Fourier lenses and three detectors (low-, mid- and high-angle-detector) as well as PIDS (Polarization Intensity Differential Scattering) technology. PIDS technology uses the relation between the intensity of scattered light, direction of polarized light, wavelength of the light, particle size and the angle of arriving and scattered light. The sample is illuminated with horizontal and vertical polarized light at three different wavelengths (450 nm, 600 nm and 900 nm) using a filter band, which allows only one wavelength and one direction of polarized light to pass at a time. The intensity of the scattered light is analyzed at 6 different angles (60°, 75°, 90°, 105°, 120° and 146°). For every wavelength the difference of the intensities of horizontal and vertical polarized light is evaluated.

The diffraction patterns can be analysed using Fraunhofer approximation and Mie theory. Fraunhofer approximation is only valid for particles which are at least four times larger than the wavelength of the light used [173]. The LS230 uses laser light with a wavelength of

750 nm. Therefore, the Fraunhofer approximation gives only correct results for particles larger than 3 µm. With the Mie theory also particles in the submicron range can be evaluated. Furthermore, this theory has the advantage that all phenomena which occur, if light hits a spherical particle, are described. It should be taken into account, that the Mie theory is only valid for spherical particles. For LD measurement this limitation is without influence because due to the circular location of the detector elements spherical particles are postulated anyway. The knowledge of the real and imaginary RI of the particles under investigation as well as the real RI of the measurement medium is required to calculate the particle size using the Mie theory [179].

In this work LD measurements in combination with PIDS technology were performed. The run length of one measurement was 60 sec. The obscuration was adjusted to 40-50%. All measurements were performed in triplicate. The Mie theory was used for data evaluation. Water with a RI of 1.33 was used as measurement medium. The real RI of PX-13 and PX-18 is 1.496 (see chapter 2.3.1). To evaluate the imaginary part of the RI, LD measurements were performed with 5% PX-13 and 5% PX-18 nanosuspension with a PIDS obscuration between 40% and 50%. The samples were collected after the measurement and the absorbance was measured using a UV-1700 PharmaSpec (Shimadzu Deutschland, Duisburg, Germany). Knowing the absorbance, the imaginary part of the refractive index can be calculated using the following equation [180]:

$$k = \frac{2.30\ A}{4\ \pi\ \tilde{\nu}\ z}$$

k = imaginary part of the RI
A = absorbance
$\tilde{\nu}$ = wave number
z = layer thickness

The values obtained of three samples were of the magnitude of 10^{-6}. Due to software limitations of the Beckman Coulter LS version 3.19 (Beckmann-Coulter, Krefeld, Germany) an imaginary RI of 0 was used for the evaluation of the particle size of PX-13 and PX-18 nanosuspensions. The LD data were evaluated using the diameter 50% (LD 50), 90% (LD 90) and 95% (LD 95), which means that either 50%, 90% or 95% (volume distribution) of the measured particles are below this size.

Light microscopy

A light microscope (Leitz, Wetzlar, Germany) equipped with a CMEX-1 digital camera (Euromex microscopes, Arnheim, Netherlands) connected to Image Focus software version 1.3.1.4. (Euromex microscopes, Arnheim, Netherlands) was used. Magnifications of the analysed material by 16x10-fold, 40x10-fold, 63x10-fold and 100x10-fold were possible with the equipment.

Scanning electron microscopy (SEM)

SEM is a type of electron microscopy that images the sample surface by scanning it with a high-energy beam of electrons in a raster scan pattern. This method can be used to study surfaces of solid objects directly e.g. surface topography, composition and conductivity. In this study SEM was used to obtain information about the size and shape of PX-13 and PX-18 nanoparticles produced by high pressure homogenization.

SEM studies were performed at Zentraleinrichtung Elektronenmikroskopie (Technische Universität Berlin, Berlin, Germany) using a Hitachi S-4000 (Hitachi High-Technologies, Europe, Krefeld, Germany). PX-13 and PX-18 nanosuspension were applied to carbon object holders and dried before analyses.

2.4.2.3 Results and discussion

PX-18 and PX-13 bulk material

Figure 2.4.2.3-1 shows light microscope pictures of PX-18 and PX-13 bulk material pre-dispersed in an aqueous surfactant solution using mortar and pestle. Both bulk materials have a large particle size. Furthermore, both materials exhibit an inhomogeneous particle size distribution.

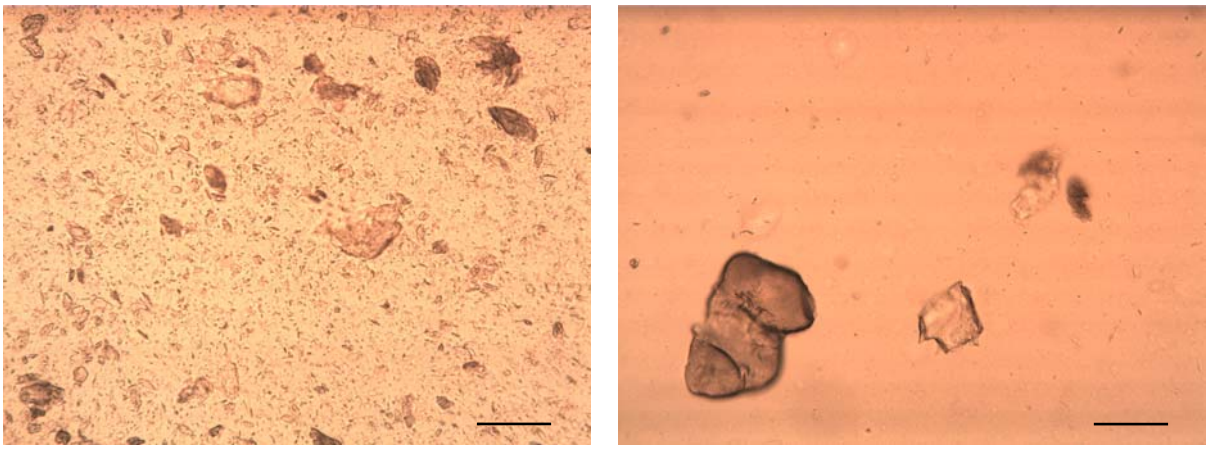

Figure 2.4.2.3-1: Light microscope pictures of PX-18 bulk material suspended in 1% (w/w) Tween 80 solution (left) and PX-13 bulk material suspended in 2% (w/w) Plantacare® 2000 solution (right) magnified 16x10-folds. The bar refers to 100 µm.

These findings were confirmed by LD measurement. Figure 2.4.2.3-2 shows the volume distribution of both bulk materials measured by LD. The particles size of the PX-13 bulk material was larger than the particles size of the PX-18 bulk material. A further disintegration of PX-13 bulk material using mortar and pestle was not possible due to the stickiness of the material.

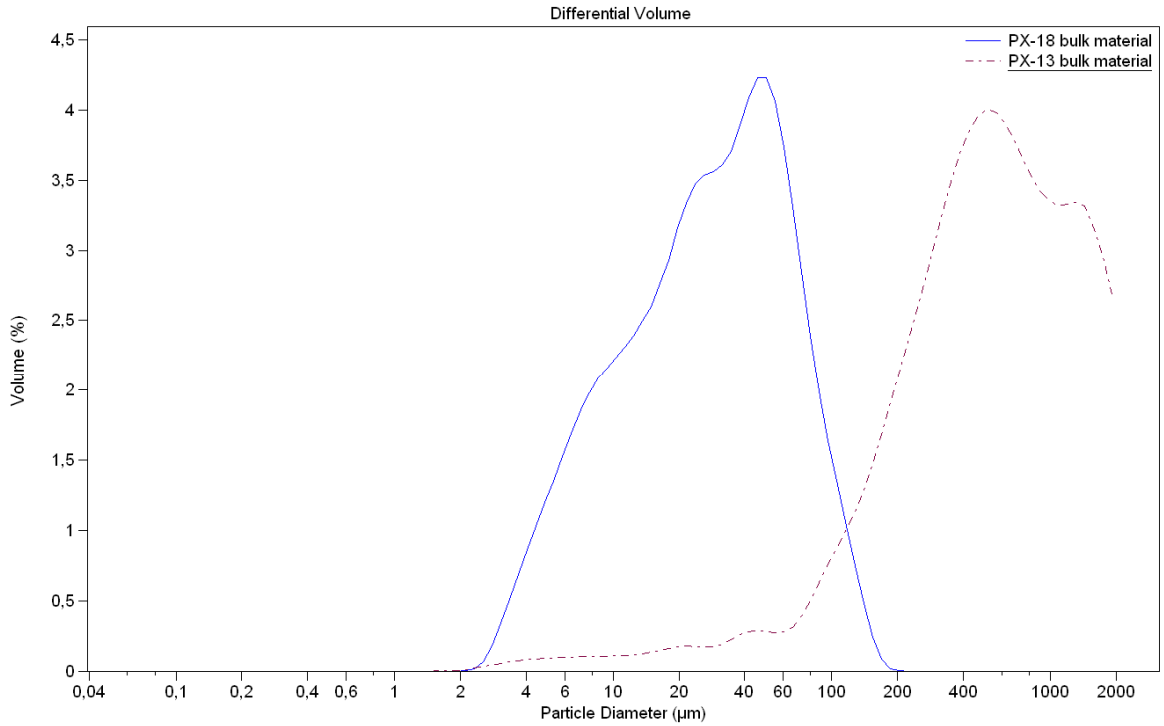

Figure 2.4.2.3-2: LD data of PX-18 and PX-13 bulk material suspended in an aqueous surfactant solution using mortar and pestle.

Formulation optimisation of PX-18 nanosuspensions

Nanosuspensions containing 1% PX-18 (w/w), 5% PX-18 (w/w) and 10% PX-18 (w/w) stabilized with 1% (w/w) Tween 80 were produced at 5°C. Due to the application of energy during the homogenization process, the temperature of the product increases. After several cycles the temperature increase might affect the quality of the product. Therefore, after each homogenization cycle the PX-18 dispersion was cooled down to 5°C. In order to have a controlled production at this temperature, the high pressure homogenizer was equipped with a water jacked and cooled down to 5°C. The PX-18 dispersion was pre-homogenized running two cycles at 150 bar followed by two cycles at 500 bar and two cycles at 1000 bar to avoid the blockage of the homogenization gap. The homogenization gap is larger at lower pressures, thus allowing larger particles to be processed. In the pre-homogenization step larger particles are reduced in number and size allowing a further processing at a higher pressure and consequently with a smaller gap [172]. The homogenization process was completed running 20 cycles at 1500 bar.

The homogenization process reduces the mean particle size and simultaneously narrows the width of the size distribution [166]. A continuous decrease in particles size with an increasing number of applied homogenization cycles at 1500 bar was observed for the 1% PX-18

nanosuspension (Figure 2.4.2.3-3). Moreover a continuous decrease in PI can be seen. The product is getting more homogeneous in size, due to the disintegration of larger particles.

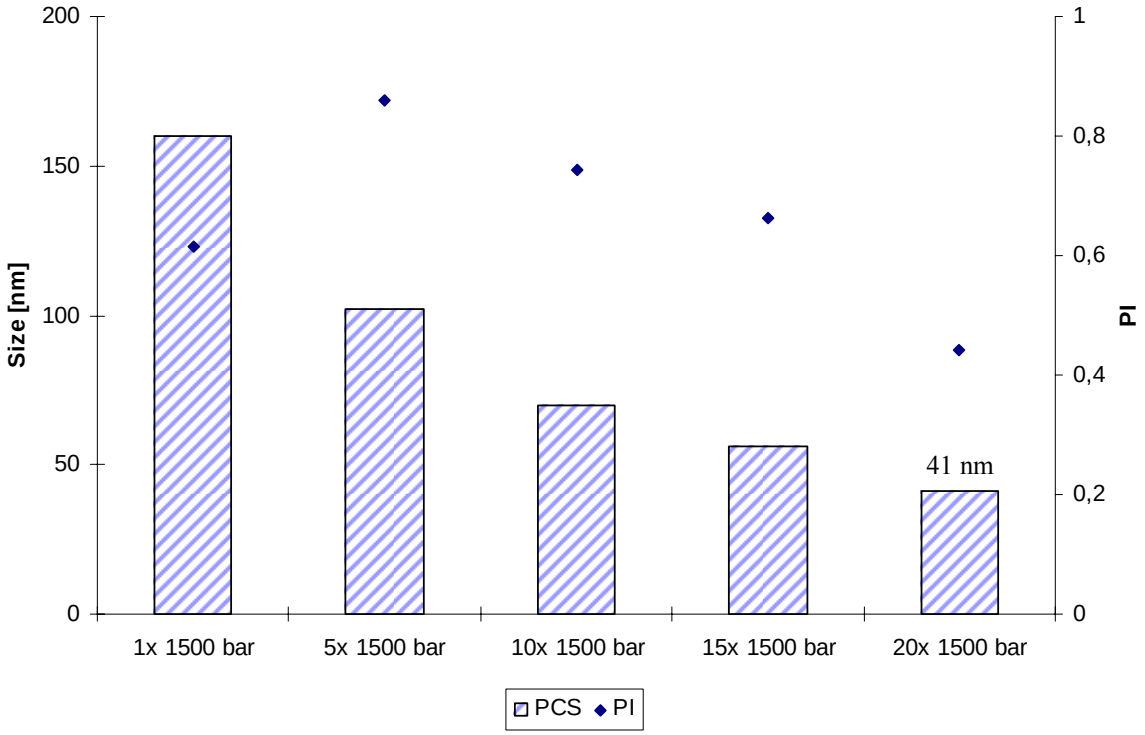

Figure 2.4.2.3-3: Average particle size and PI measured by PCS of a 1% PX-18 nanosuspension after 1, 5, 10, 15 and 20 homogenization cycles at 1500 bar at 5°C.

Figure 2.4.2.3-4 shows an SEM picture of a 1% PX-18 nanosuspension after 20 homogenization cycles at 1500 bar at 5°C. On the picture an agglomerate of PX-18 nanoparticles can be seen. Agglomeration of PX-18 nanoparticles might be caused by sample preparation for SEM. Investigating the size of the single particles of the agglomerate, the picture confirms the particle size measured by PCS.

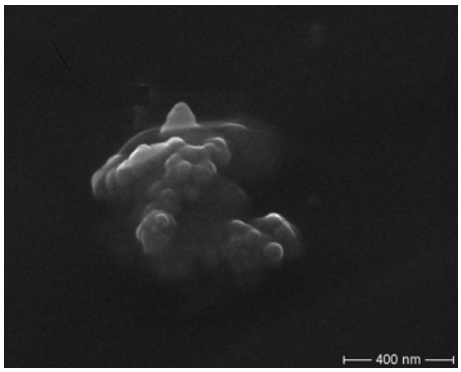

Figure 2.4.2.3-4: SEM picture of 1% PX-18 nanosuspension homogenized 20 cycles at 1500 bar at 5°C.

The decrease in particles size of a 5% PX-18 dispersion subjected to high pressure homogenization at 1500 bar in dependence on the cycle number can be seen in Figure 2.4.2.3-5 and Figure 2.4.2.3-6.

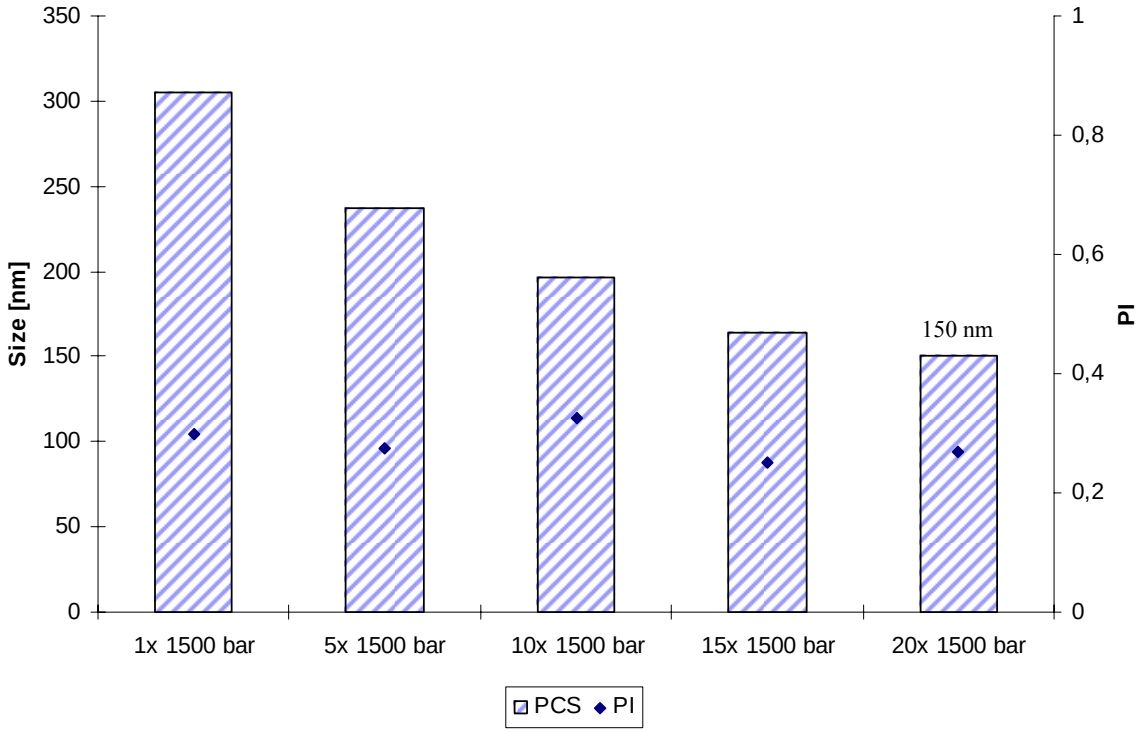

Figure 2.4.2.3-5: Average particle size and PI of a 5% PX-18 nanosuspension after 1, 5, 10, 15 and 20 homogenization cycles at 1500 bar at 5°C measured by PCS.

While the PCS mean diameter changes only about 14 nm between cycle 15 and 20, the LD 95 was reduced about 800 nm between these cycles. This is due to the fact that with an increasing cycle number a more uniform product is reached by the reduction of particles in the micrometer range. During the homogenization process particles break at imperfections of their crystal structure. With a decreasing particles size the number of imperfections is reduced. Therefore, the force required to break the particles increases with a decreasing particle size. This can be observed by a rather exponential decrease in particle size than a linear decrease in Figure 2.4.2.3-5 and Figure 2.4.2.3-6. If the forces in the homogenizer are equal to the interaction forces in the crystal, no further decrease in particle size will be observed, even when additional homogenization cycles are applied. Therefore, a decrease of the LD 95, being more sensitive to larger particles in the formulation, can be seen up to cycle number 20 while the average particles size measured by PCS stays nearly constant.

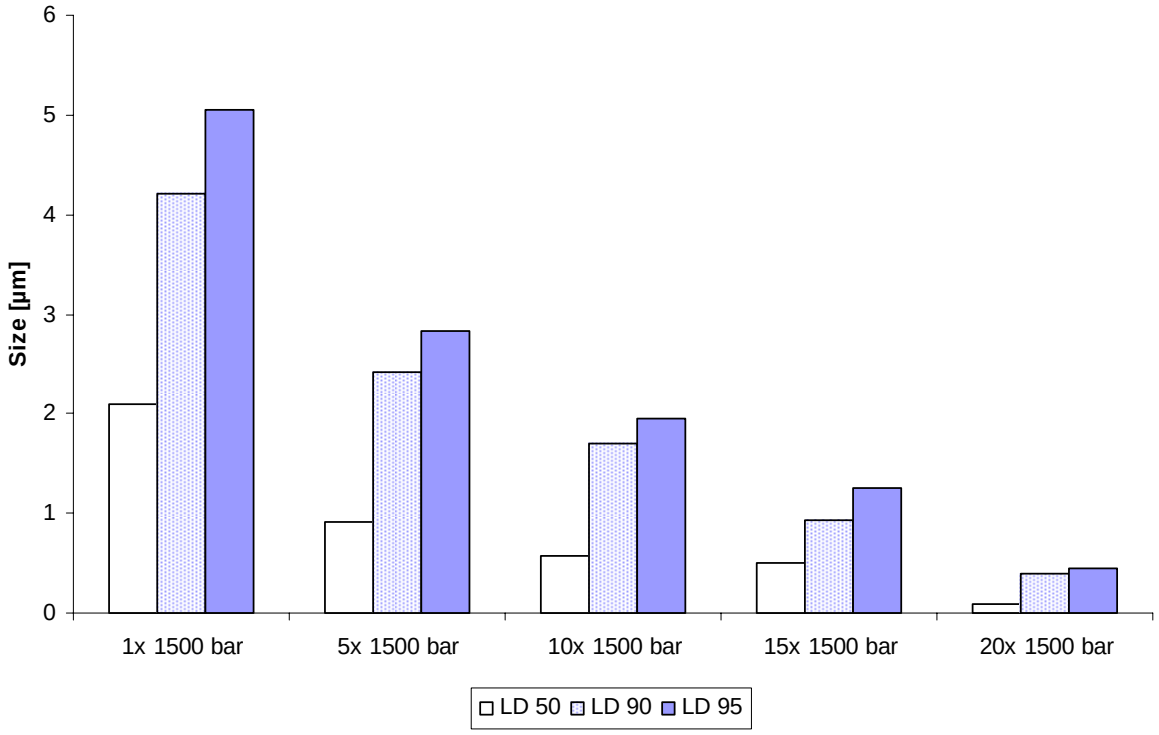

Figure 2.4.2.3-6: LD 50, LD 90 and LD 95 of a 5% PX-18 nanosuspension after 1, 5, 10, 15 and 20 homogenization cycles at 1500 bar at 5°C.

In Figure 2.4.2.3-7 an SEM picture of a 5% PX-18 nanosuspension subjected to 20 cycles at 1500 bar at 5°C is shown. It was reported previously that nanoparticles with different shapes e.g. cube-shape, rode-shape and needle-shape were obtained by high pressure homogenization [166]. PX-18 nanoparticles with a rod-shape were obtained with this procedure. The rod-shape nanoparticles were homogeneous in size. The particles had a length of approximately 140 to 180 nm and a width of approximately 60 to 100 nm. This is well in agreement with the results obtained by PCS measurement.

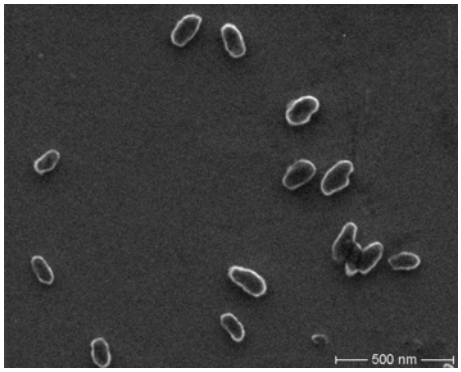

Figure 2.4.2.3-7: SEM picture of 5% PX-18 nanosuspension after 20 homogenization cycles at 1500 bar at 5°C.

Figure 2.4.2.3-8 shows the mean diameter measured by PCS during the production of 10% PX-18 nanosuspension. In Figure 2.4.2.3-9 the decrease in particles size measured by LD related to the cycle number is shown for this formulation.

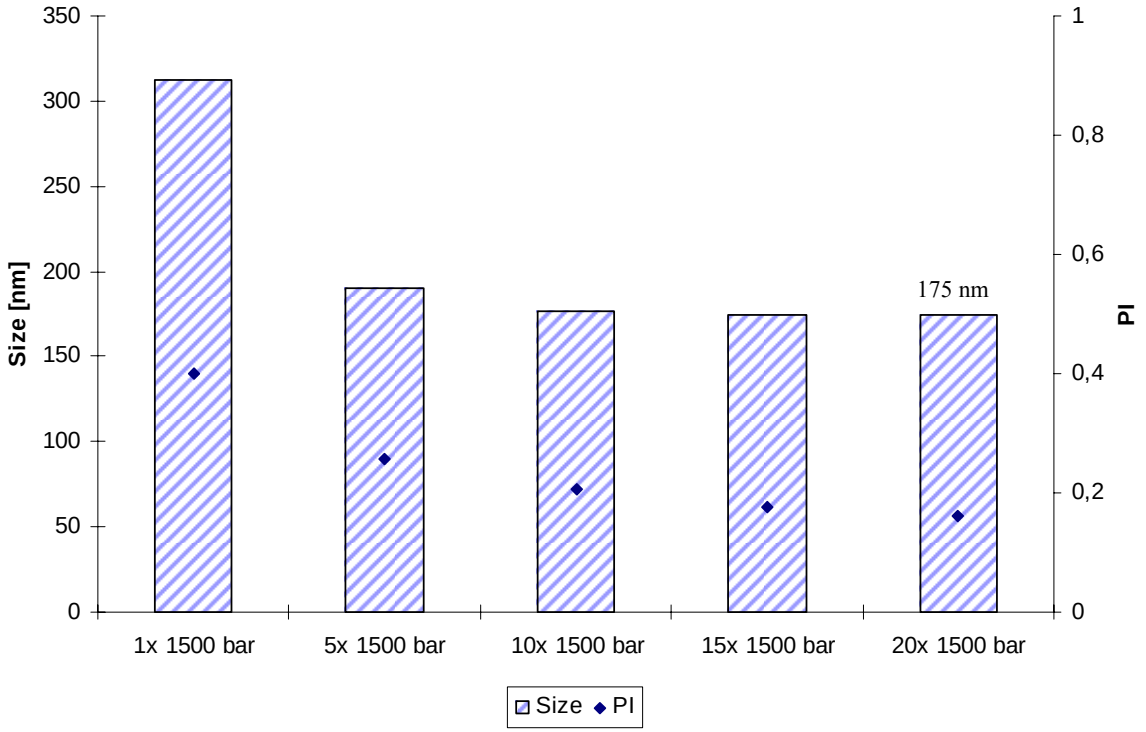

Figure 2.4.2.3-8: Average particles size and PI measured by PCS of a 10% PX-18 nanosuspension after 1, 5, 10, 15 and 20 homogenization cycles at 1500 bar at 5°C.

From cycle 10 on the mean particles size measured by PCS stays constant while a further decrease in PI up to cycle 20 was observed. Narrowing of the size distribution of 10% PX-18 nanosuspension was also shown by LD measurements. The LD 90 and LD 95 decrease with increasing cycle number to a greater extent than the LD 50. This can be explained by the fact that the structure of the PX-18 particles is getting more perfect with increasing cycle number. That means the force required to break the particles increases. This leads to the breakage of larger particles and maintains the smaller particle fraction at a constant size.

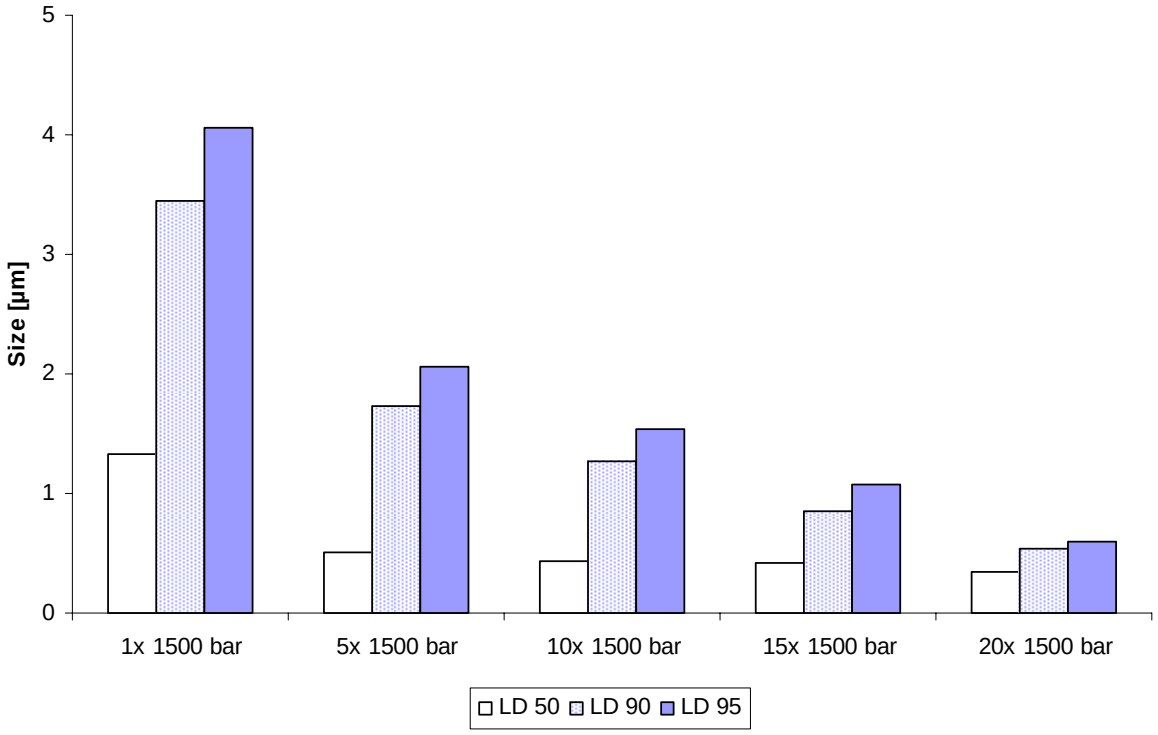

Figure 2.4.2.3-9: LD 50, LD 90 and LD 95 of a 10% PX-18 nanosuspension subjected to 1, 5, 10, 15 and 20 homogenization cycles at 1500 bar at 5°C.

Figure 2.4.2.3-10 shows an SEM picture of a 10% PX-18 nanosuspension. A single PX-18 particle with a length of approximately 980 nm and a width of approximately 520 nm can be seen in this picture. The particle size of this particle is in agreement with the particle size measured by PCS and LD. Furthermore, the rod-shape of the particles found for the 5% PX-18 nanosuspension can be confirmed for the 10% PX-18 nanosuspension.

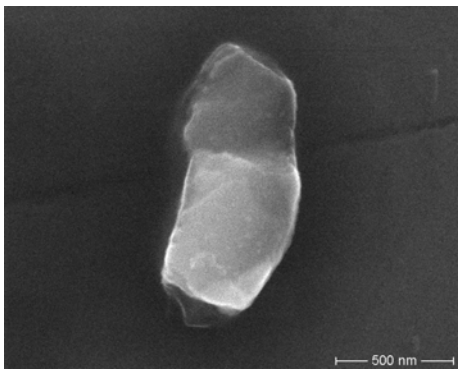

Figure 2.4.2.3-10: SEM picture of 10% PX-18 nanosuspension after 20 homogenization cycles at 1500 bar at 5°C.

To obtain a maximum physical stability, Ostwald ripening should be avoided. Therefore, the nanosuspension should be as homogeneous as possible and the amount of microparticles present in the formulation should be reduced as much as possible [31]. 1%, 5% and 10% PX-18 nanosuspensions with a particles size below 1 µm could be prepared using 20 homogenization cycles at 1500 bar at 5°C. It is well known, that the achievable particle size reduction depends on the hardness of the material subjected to the homogenization process [18, 19, 181]. In the literature average particles sizes measured by PCS of approximately 460 nm for a 1% buparvaquone nanosuspension [182], 600 nm for a 1% budesonide nanosuspension [33] and 920 nm for a 1% omeprazol nanosuspension [183] were reported after applying 20 homogenization cycles at 1500 bar. For the 1% PX-18 nanosuspension an average particle size measured by PCS <50 nm was obtained using the same production conditions. Particle sizes as small as this have been previously only been reported for nanosuspensions produced using a combination technology, where the material is lyophilized and afterwards subjected to high pressure homogenization [26]. Also at higher concentrations, i.e. 5% and 10% PX-18, relatively small particles were obtained under the applied conditions, which provide evidence that PX-18 is a soft material. In the literature an average particle size measured by PCS of approximately 760 nm for a 5% omeprazol nanosuspension [183], 940 nm for a 10% omeprazol nanosuspension [183] and 435 nm for a 10% budesonide nanosuspension [33] were reported. For some materials it was reported, that the particle size decreases with an increasing drug concentration [33]. This was explained by the higher shear forces and collision in the homogenization gap, when higher amounts of drug are present. Increasing the amount of PX-18 from 5% to 10% a smaller particle size was measured by LD after the first homogenization cycle at 1500 bar for the 10% PX-18 nanosuspension. With increasing cycle number the particle size of the 5% PX-18 nanosuspension decreased further than the particle size of the 10% PX-18 nanosuspension. The increased diameters with higher concentration of the homogenized material can be explained via the power density [184]. The production conditions were kept constant for the formulations with different concentrations, which means the energy to disintegrate the particles was identical in all three productions despite the fact that the amount of material to be disintegrated was increased.

All in all it could be shown that high pressure homogenization applying 20 cycles at 1500 bar at 5°C can be used to formulate PX-18 suspensions with particles in the nanometer range and a narrow particle size distribution. The degree of particle fineness of the PX-18 nanosuspensions was found to increase with an increasing number of homogenization cycles.

Formulation optimisation of PX-13 nanosuspensions

PX-13 nanosuspensions with an active concentration of 1% (w/w) and 5% (w/w), stabilized with an aqueous solution containing 1% (w/w) Plantacare® 2000, were produced under the same conditions as the PX-18 nanosuspensions i.e. pre-homogenization two cycles at 150 bar, two cycles at 500 bar and two cycles at 1000 bar followed by 20 cycles at 1500 bar at 5°C.

Figure 2.4.2.3-11 shows the average particle size and PI measured by PCS of a 1% PX-13 nanosuspension stabilized with an aqueous 1% (w/w) Plantacare® 2000 solution in dependence on the homogenization cycle number applied. After the 10th homogenization cycle the particle size decreased only slightly. After 20 homogenization cycles at 1500 bar an average particle size of 911 nm was obtained by PCS measurement. A PI of 1 was measured at all homogenisation cycles. No decrease of the PI was observed. This indicates a broad particle size distribution with an unknown shape.

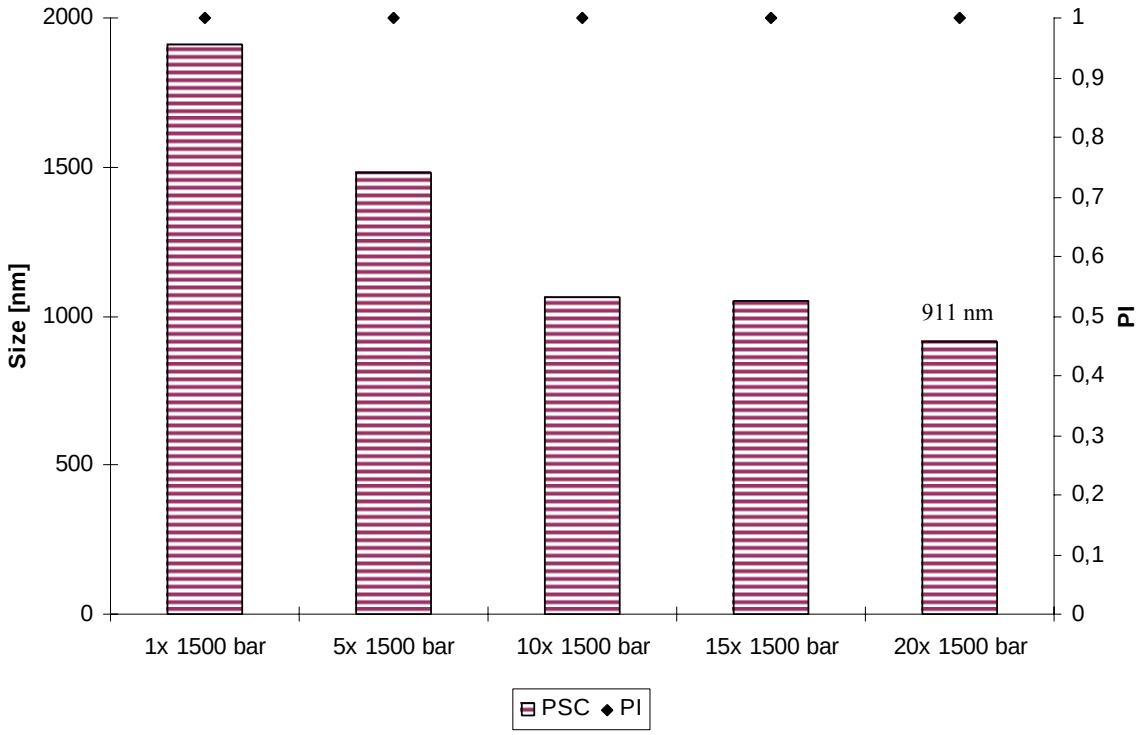

Figure 2.4.2.3-11: Average particle size and PI of a 1% PX-13 nanosuspension stabilized with 1% Plantacare® 2000 solution after 1, 5, 10, 15 and 20 cycles at 1500 bar at 5°C.

By light microscopy and LD the presence of larger particles, which cannot be detected by PCS measurement, was confirmed. Figure 2.4.2.3-12 shows a light microscopy picture and the LD values obtained after 20 homogenization cycles at 1500 bar. In the formulation a high

amount of microparticles is present. Microparticles >10 µm can be seen in the light microscope picture and were found by LD measurement. Particle growth due to Ostwald ripening, caused by different saturation solubilities in the vicinity of particles with different sizes, is pronounced if a particle fraction above 10 µm is present. Above 10 µm the intrinsic dissolution rate is much lower than for particles <<10 µm [185]. Therefore, the formulation of 1% PX-13 nanosuspension needed to be further optimized.

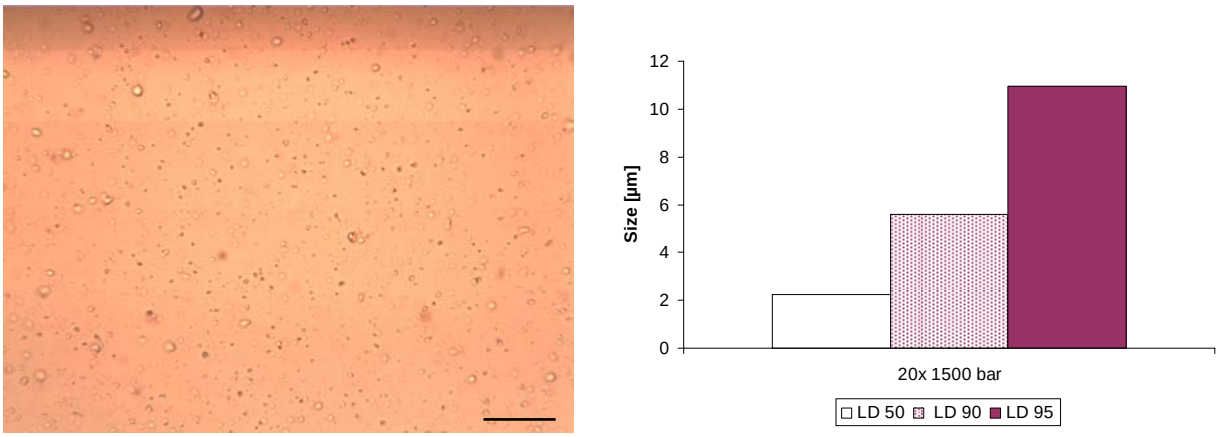

Figure 2.4.2.3-12: Light microscope picture magnified 40x10-times (bar refers to 40 µm) (left) and LD 50, LD 90 and LD 95 values (right) of a 1% PX-13 nanosuspension stabilized with 1% Plantacare® 2000 after 20 homogenization cycles at 1500 bar at 5°C.

Due to the fact that smaller particle sizes have been reported in the literature for higher drug concentrations applying the same homogenization conditions, 5% PX-13 dispersed in 1% Plantacare® 2000 solution was subjected to the same procedure as 1% PX-13 dispersion [33]. In Figure 2.4.2.3-13 and Figure 2.4.2.3-14 the particle size of a 5% PX-13 nanosuspension stabilized with 1% Plantacare® 2000 solution measured after 1, 5, 10, 15 and 20 homogenization cycles at 1500 bar and 5°C is presented.

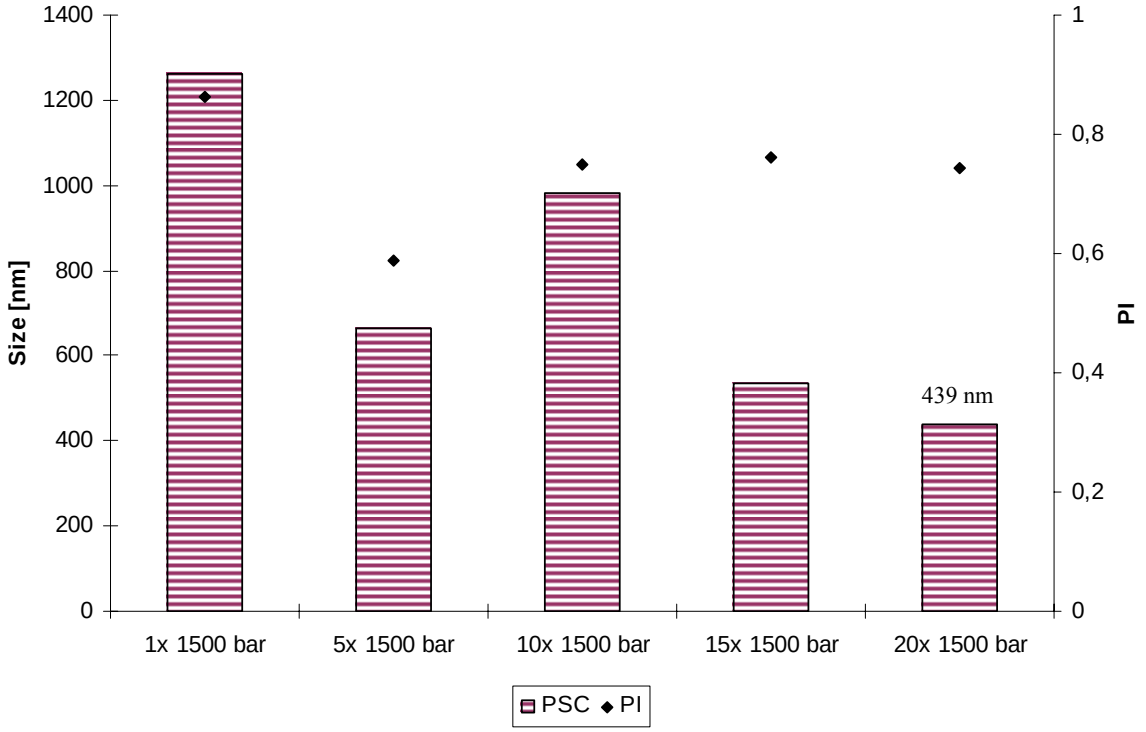

Figure 2.4.2.3-13: Average particle size and PI measured by PCS of a 5% PX-13 nanosuspension stabilized with 1% Plantacare® 2000 solution after 1, 5, 10, 15 and 20 homogenization cycles at 1500 bar at 5°C.

Within the first 5 cycles a particle size reduction was found for the 5% PX-13 nanosuspension by PCS and LD measurement. After 10 homogenization cycles at 1500 bar the particles size increased. This increase in particle size is related to agglomeration of PX-13 particles during the homogenization process. Agglomerates can form due to insufficient coverage of new generated surfaces by surfactants, during the homogenization procedure [30]. In case agglomerates form during the homogenization process they need to be dispersed again in the next homogenization cycles. This could be observed by a reduction in particle size measured by PCS and LD in the following homogenization cycles. Nevertheless agglomerates were still present after 20 homogenization cycles. This can be seen in the light microscope picture in Figure 2.4.2.3-14. Furthermore, a very high PI (0.743) was obtained for the 5% PX-13 nanosuspension after 20 homogenization cycles at 1500 bar indicating a broad particle size distribution with unknown shape.

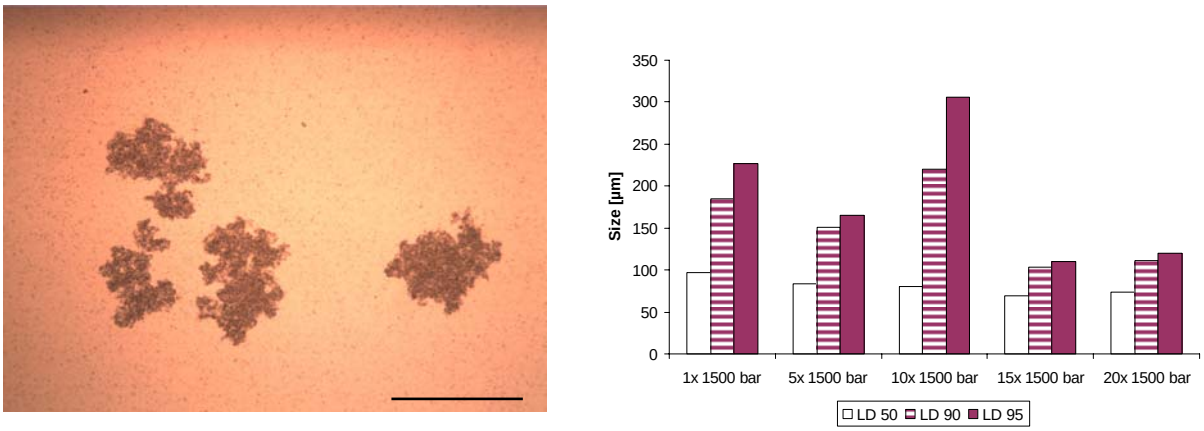

Figure 2.4.2.3-14: Light microscope picture magnified 16x10-times after 20 homogenization cycles at 1500 bar of a 5% PX-13 nanosuspension stabilized with 1% Plantacare® 2000 (bar refers to 200 µm) (left). LD 50, LD 90 and LD 95 values after 1, 5, 10, 15 and 20 homogenization cycles at 1500 bar at 5°C (right) of the same formulation.

Surfactants are used as wetting agents and for the prevention of particle agglomeration during the homogenization process. Therefore, surfactants play an important role in the production of finely dispersed and non-agglomerated nanosuspensions. Whether the production of nanoparticles is successful depends on the properties of the surfactant such as diffusion velocity and affinity to the particle surface. It was found by contact angle measurement, that Plantacare® 2000 had the best affinity to PX-13 among all surfactants tested. To avoid agglomeration and to gain a further particle size reduction the concentration of Plantacare® 2000 was increased to 2% (w/w) in the following formulations. The production parameters were kept constant.

Figure 2.4.2.3-15 shows the average particle size and PI measured by PCS of a 1% PX-13 nanosuspension stabilized with 2% Plantacare® 2000 related to the homogenization cycle number. A decrease in particle size and PI could be observed with increasing homogenization cycle number. From cycle 10 on the average particle size measured by PCS decreases about 10 nm every 5 homogenization cycles. Increasing the Plantacare® 2000 concentration from 1% to 2% in the formulation, lead to the reduction of the average particle size measured by PCS after 20 homogenization cycles at 1500 bar at 5°C from 911 nm to 250 nm. Furthermore, a reduction of the LD 50 value by approximately 800 nm could be seen. A reduction of the LD 95 by increasing the surfactant concentration could not be observed (Figure 2.4.2.3-16). Therefore, a further optimization of production parameters for 1% PX-13 nanosuspension needed to be performed.

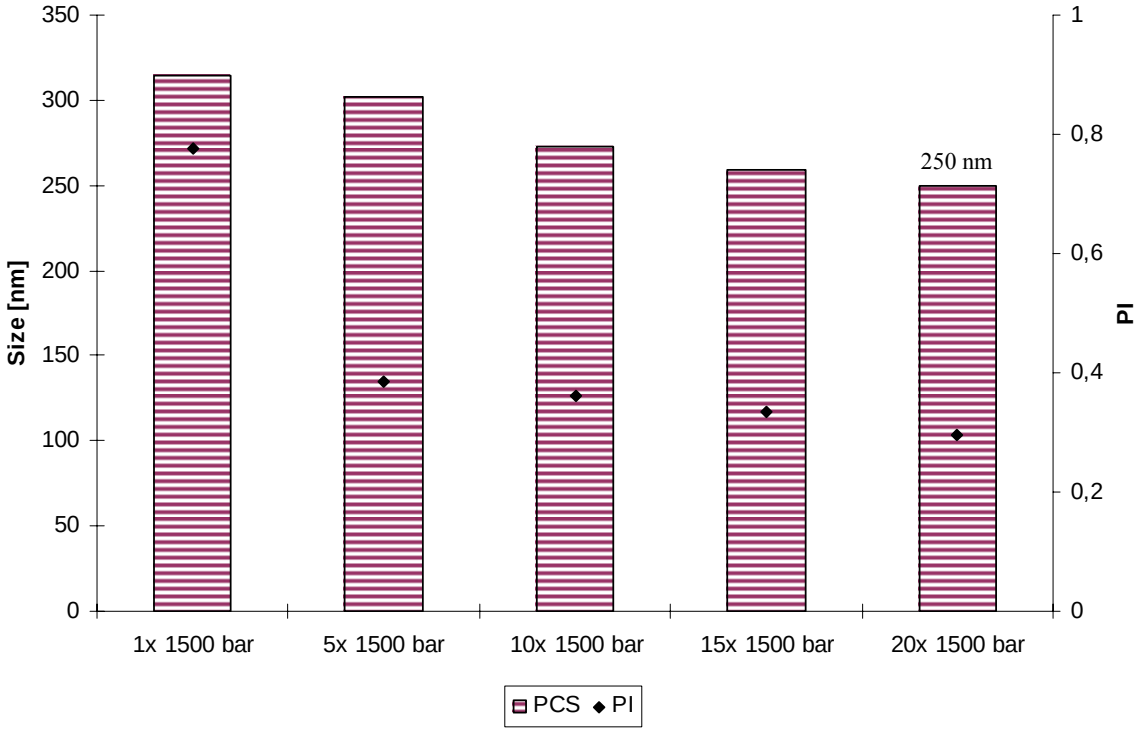

Figure 2.4.2.3-15: Average particle size and PI measured by PCS of a 1% PX-13 nanosuspension stabilized with 2% Plantacare® 2000 after 1, 5, 10, 15 and 20 homogenization cycles at 1500 bar at 5°C.

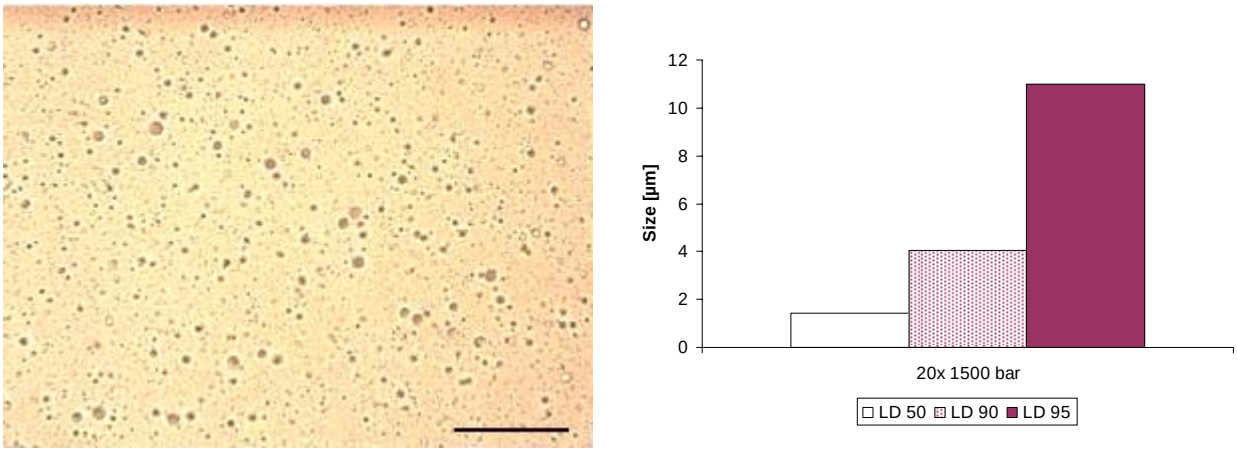

Figure 2.4.2.3-16: Light microscope picture magnified 63x10-times (bar refers to 40 µm) (left) and LD 50, LD 90 and LD 95 values (right) of a 1% PX-13 nanosuspension stabilized with 2% Plantacare® 2000 after 20 homogenization cycles at 1500 bar at 5°C.

In Figure 2.4.2.3-17 the particle size measured by PCS of the 5% PX-13 nanosuspension stabilized with 2% Plantacare® 2000 in dependence on the homogenization cycle number is shown. It was found that agglomeration of PX-13 particles during the production could be reduced but not avoided by increasing the surfactant concentration. Over the first 10 cycles a decrease in the particle size can be observed. An increase in the average particle size can be seen at cycle 15 applying 1500 bar, which is caused by agglomeration of the particles during

the production process. Within the next homogenization cycles the agglomerates are dissipated, which was evidenced by a reduction in particle size and PI up to cycles 20. Increasing the surfactant concentration from 1% to 2% reduced the average particle size after 20 homogenization cycles at 1500 bar and 5°C measured by PCS from 439 nm to 244 nm. However, an LD 50 value of approximately 600 nm was obtained after 20 homogenization cycles. Figure 2.4.2.3-18 shows a light microscope picture and the LD 50, LD 90 and LD 95 of the nanosuspension after 20 homogenization cycles. An LD 90 value >22 µm was obtained for the formulation. In the picture agglomerates as well as large particles can be seen, which is well in accordance with the results of the LD measurement. Therefore, a further optimization of the production parameters for the 5% PX-13 nanosuspension was needed.

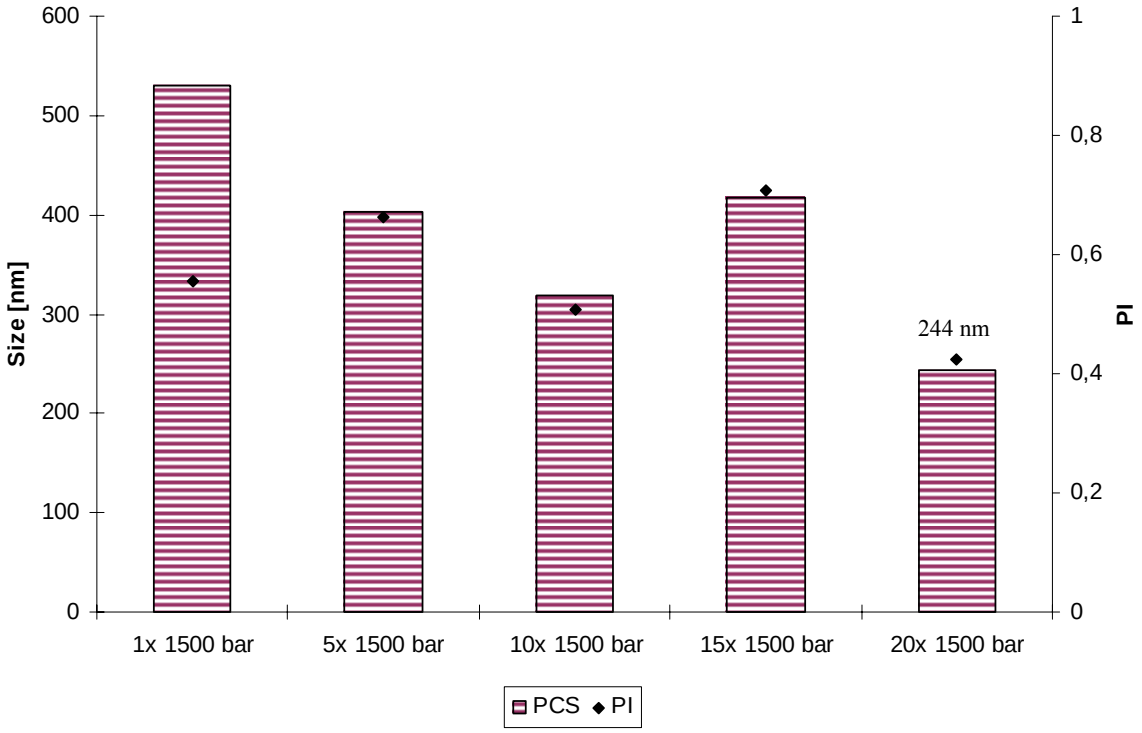

Figure 2.4.2.3-17: Average particle size and PI measured by PCS of a 5% PX-13 nanosuspension stabilized with 2% Plantacare® 2000 after 1, 5, 10, 15 and 20 homogenization cycles at 1500 bar at 5°C.

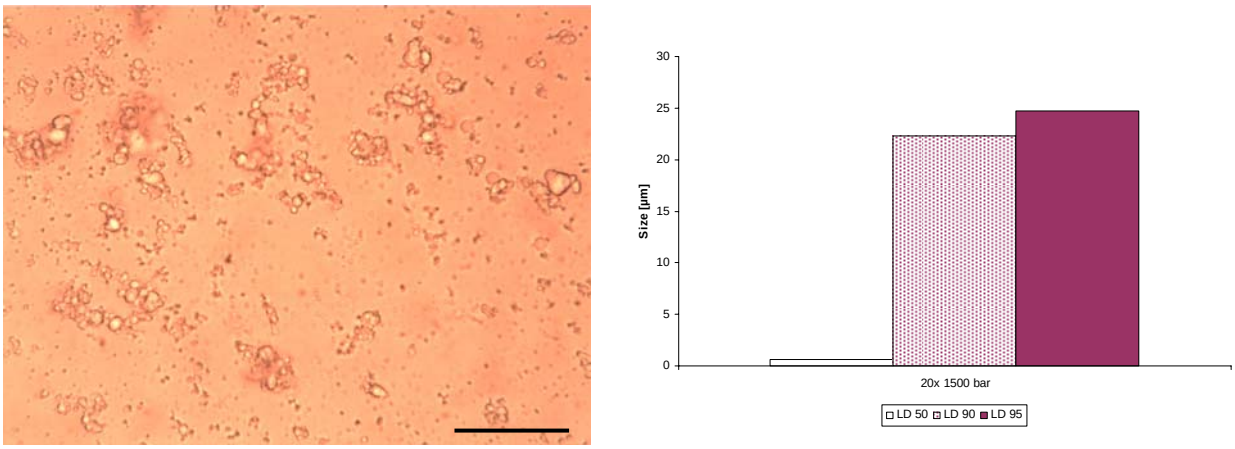

Figure 2.4.2.3-18: Light microscope picture magnified 63x10-fold (bar refers to 40 µm) (left) and LD 50, LD 90 and LD 95 values (right) of a 5% PX-13 nanosuspension stabilized with 2% Plantacare® 2000 after 20 homogenization cycles at 1500°C at 5°C.

For a further optimization of the formulation, PX-13 was suspended in 2% Plantacare® 2000 solution using mortar and pestle. The suspension was kept boiling for 30 min. Within this time PX-13 melted. The dispersion was homogenized at 95°C applying three homogenization cycles at 500 bar. After the production the dispersion was cooled down in an ice bath, allowing PX-13 to solidify.

Figure 2.4.2.3-19 shows the average particle size and the PI measured by PCS after every homogenization cycle. The average particle size measured by PCS after the first homogenization cycles at 95°C is already smaller than the average particle size obtained applying 20 homogenization cycles at 1500 bar at 5°C. The particles size of the 1% PX-13 nanodispersion stayed nearly constant over the three homogenization cycles while a further reduction in PI can be observed.

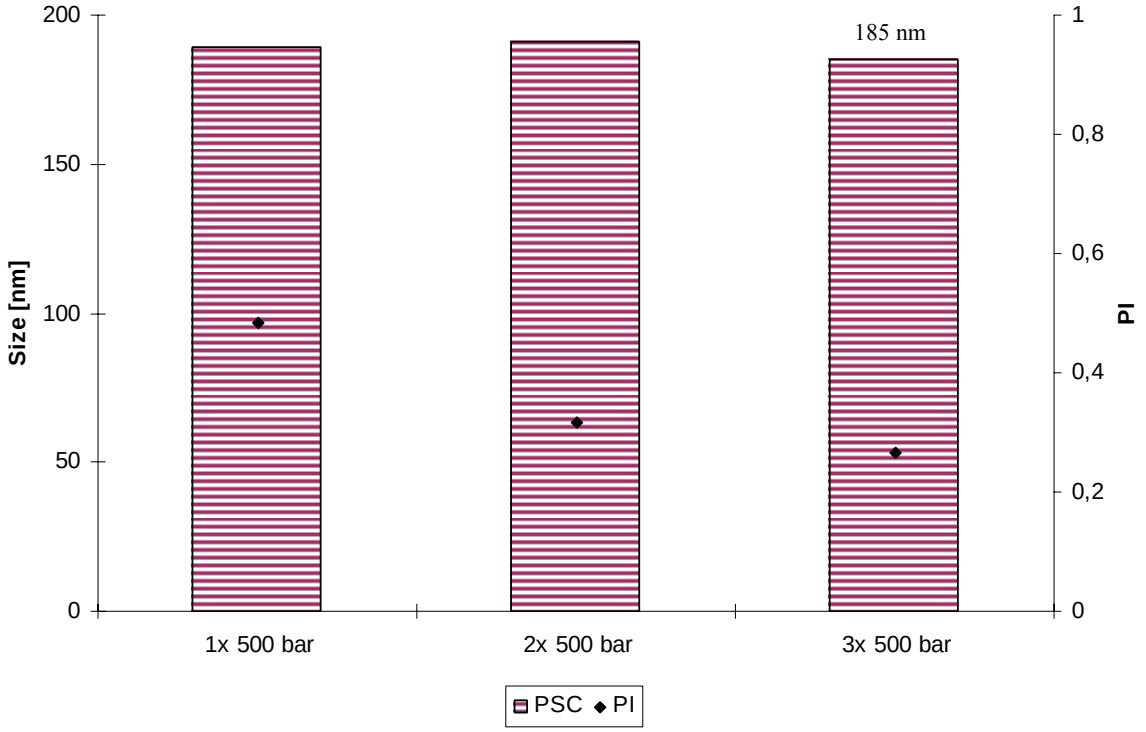

Figure 2.4.2.3-19: Average particle size and PI measured by PCS of a 1% PX-13 nanosuspenmsion stabilized with 2% Plantacare® 2000 after 1, 2 and 3 homogenization cycles at 500 bar at 95°C.

Figure 2.4.2.3-20 provides an overview of the particle size measured by LD during the production. The LD 50 and LD 90 stay nearly constant during the production while the LD 95 decreases by 265 nm from cycle one to cycle three. Comparing the LD 95 values of the 1% PX-13 nanosuspension produced using 1500 bar at 5°C and using 500 bar at 95°C, it can be seen that the LD 95 decreased by approximates 9 µm due to processing melted PX-13. For a drug particle with a given perfection of its crystal structure only a certain small size can be achieved under the given production conditions. Melting the drug destroys the crystal structure resulting in a softer, easier to break material which leads to a smaller particles size.

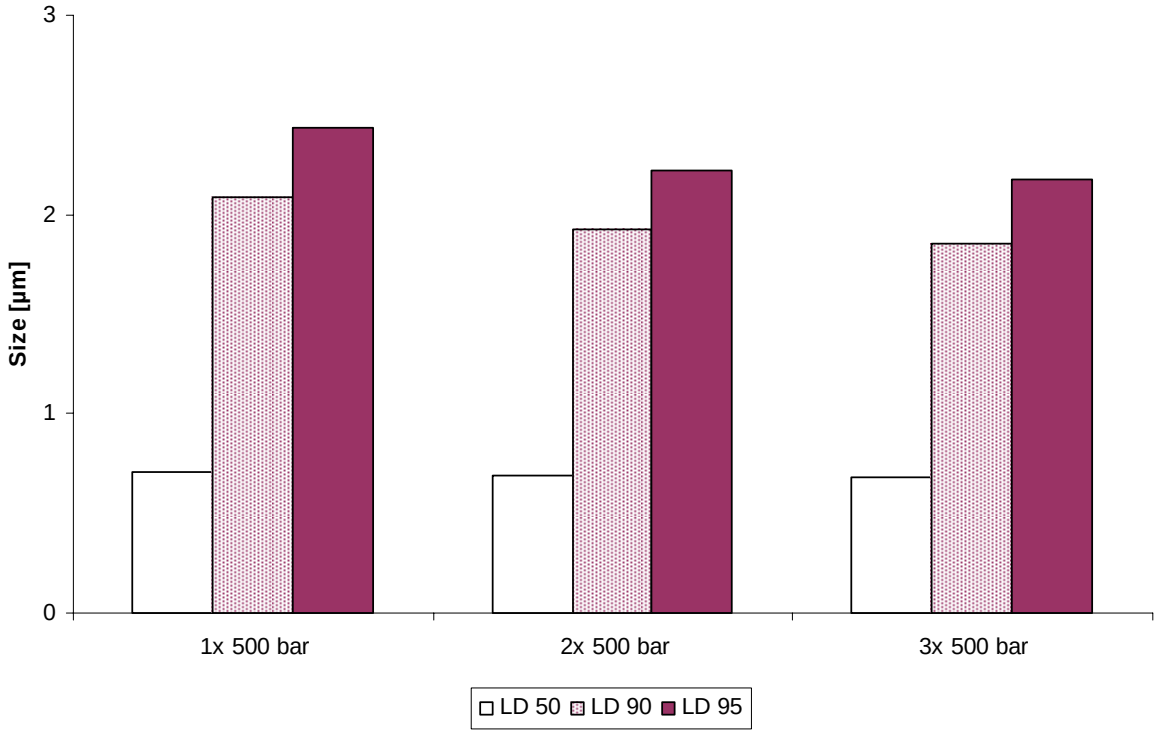

Figure 2.4.2.3-20: LD 50, LD 90 and LD 95 of a 1% PX-13 nanosuspension stabilized with 2% Plantacare® 2000 after 1, 2 and 3 homogenization cycles at 500 bar at 95°C.

In Figure 2.4.2.3-21 an SEM picture of a 1% PX-13 nanosuspension after 3 homogenization cycles at 500 bar at 95°C is shown. By investigating the particle size of the nanoparticles in the picture, a good agreement with the particle size measured by PCS and LD was found.

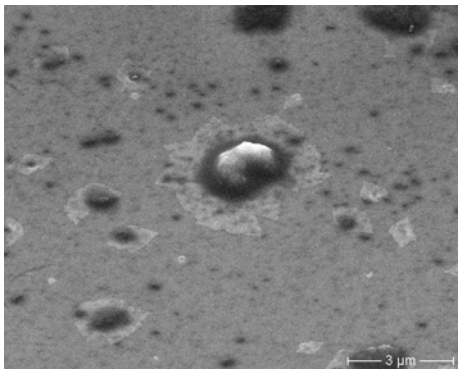

Figure 2.4.2.3-21: SEM picture of a 1% PX-13 nanosuspension homogenized 3 cycles at 500 bar at 95°C.

Figure 2.4.2.3-22 and Figure 2.4.2.3-23 show the particle size of a 5% PX-13 nanosuspension after 1, 2 and 3 homogenization cycles at 500 bar at 95°C. The particle size stays nearly constant after the first homogenization cycle. The PI was decreasing from cycle one to cycle two, staying almost constant after cycle two. Applying this production conditions

agglomeration of PX-13 nanoparticles could be avoided. Furthermore, the particle size of the largest particles in the formulation is reduced due to softening of the material by melting. Heating reduces the interfacial tension between PX-13 and water, which makes it easier to accommodate the surfactant at the interface, which helps avoiding agglomeration and facilities the production of smaller particles [170]. Increasing the production temperature decreases the viscosity of PX-13 and the aqueous phase, which results also in an easier particle size reduction [170, 186].

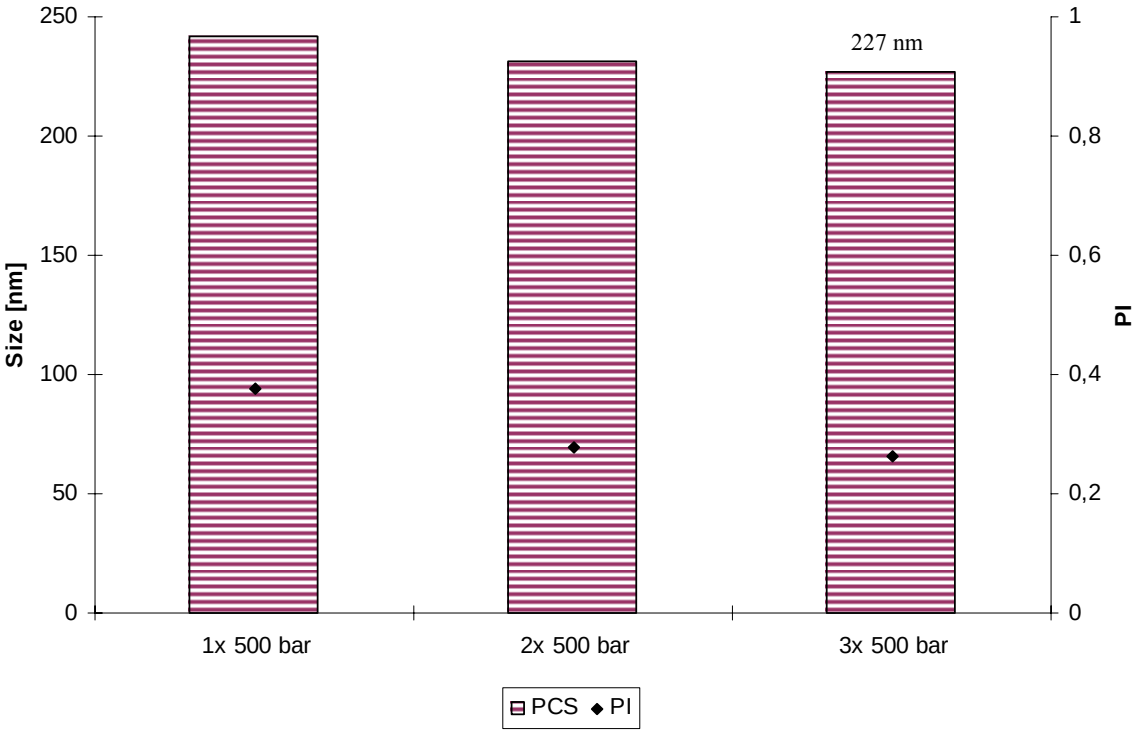

Figure 2.4.2.3-22: Average particle size and PI measured by PCS of a 5% PX-13 nanosuspension stabilized with 2% Plantacare® 2000 after 1, 2 and 3 cycles at 500 bar at 95°C.

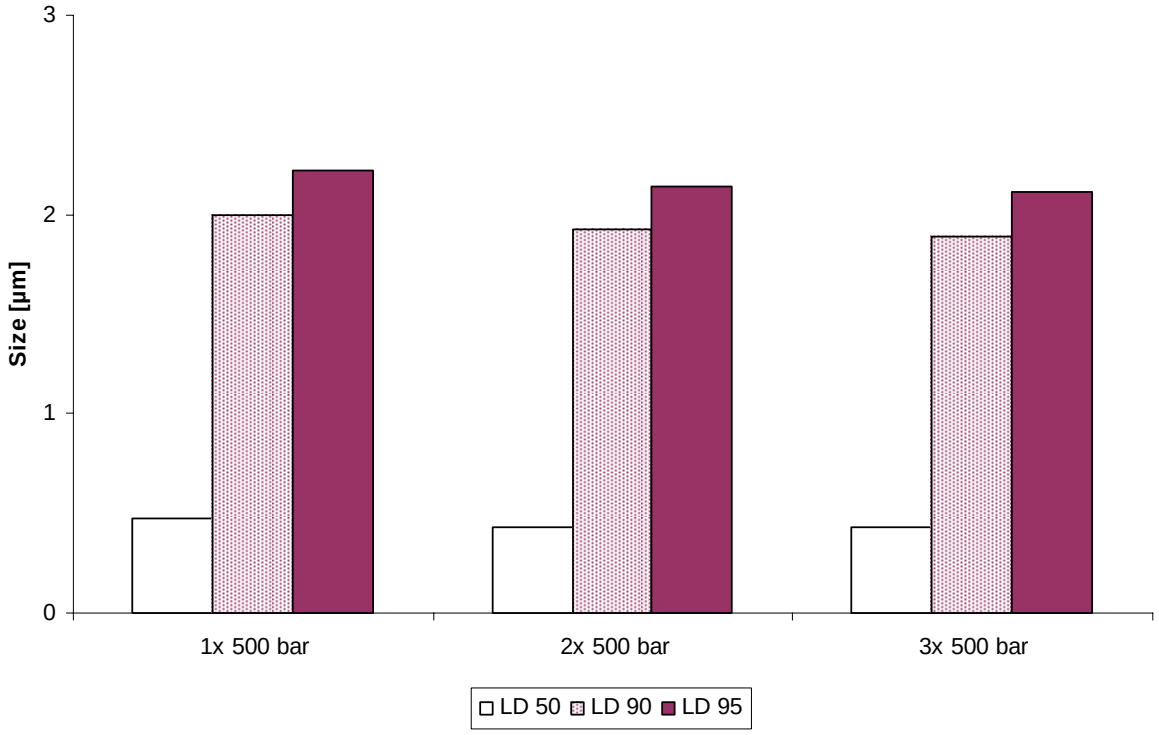

Figure 2.4.2.3-23: LD 50, LD 90 and LD 95 of a 5% PX-13 nanosuspension stabilized with 2% Plantacare® 2000 after 1, 2 and 3 homogenization cycles at 500 bar at 95°C.

In summary, it was found that it is not possible to produce PX-13 nanosuspensions with 1% Plantacare® 2000 solution as stabilizer subjecting the material to a pre-homogenization process followed by 20 cycles at 1500 bar at 5°C. Increasing the Plantacare® 2000 concentration from 1% to 2% resulted in a decrease of the average particle size measured by PCS of approximately 3.5-folds in case of the 1% PX-13 nanosuspension and about 2-folds in case of the 5% PX-13 nanosuspension. However, particles >10 µm were still present in this formulations after 20 homogenization cycles. Moreover, agglomeration of PX-13 occurred during the production using an active content of 5%. Melting PX-13 in the aqueous surfactant solution and homogenizing the obtained emulsion applying three homogenization cycles at 500 bar at 95°C led to a further reduction of particle size. For the 1% and 5% PX-13 naosuspension LD 95 values of approximately 2 µm could be obtained. Agglomeration of 5% PX-13 nanosuspension could be avoided during the production. Therefore, for further investigations PX-13 nanosuspensions were prepared by this method.

Reproducibility of PX-13 and PX-18 nanosuspensions

For the evaluation of the reproducibility of the particle size of PX-13 and PX-18 nanosuspensions three batches of each formulation were produced using the production parameters outlined above. The particle size of each batch was evaluated by PCS and LD. The mean particle size and PI obtained by PCS as well as the mean LD 50, LD 90 and LD 95 values were calculated from the three different batches. For the evaluation of the reproducibility the relative standard deviation was used. The results of this study are shown in Table 2.4.2.3-1 and Table 2.4.2.3-2.

Table 2.4.2.3-1: Average particle size and PI of three batches of 1%, 5% and 10% PX-18 nanosuspension and 1% and 5% PX-13 nanosuspension. The mean particle size and PI as well as the according relative standard deviation (RSD) of the three batches were calculated.

Formulation	Average particle size [nm]					PI				
	Batch 1	Batch 2	Batch 3	Mean	RSD [%]	Batch 1	Batch 2	Batch 3	Mean	RSD [%]
1% PX-18	41	48	44	44.3	7.9	0.443	0.424	0.441	0.436	2.4
5% PX-18	146	151	134	143.7	6.1	0.274	0.268	0.253	0.265	4.1
10% PX-18	175	202	185	187.3	7.3	0.169	0.185	0.200	0.185	8.4
1% PX-13	185	224	217	209	10.0	0.265	0.224	0.264	0.251	9.3
5% PX-13	227	245	232	235	4.2	0.264	0.303	0.274	0.249	7.2

Table 2.4.2.3-2: LD 50, LD 90 and LD 95 values of three batches of 5% and 10% PX-18 nanosuspension and 1% and 5% PX-13 nanosuspension. The mean particle size as well as the according relative standard deviation (RSD) of the three batches was calculated.

Formulation	Value	Average particle size [µm]				
		Batch 1	Batch 2	Batch 3	Mean	RSD [%]
5% PX-18	LD 50	0.095	0.093	0.110	0.099	9.7
	LD 90	0.400	0.364	0.418	0.388	9.7
	LD 95	0.45	0.404	0.487	0.447	9.3
10% PX-18	LD 50	0.347	0.353	0.375	0.358	4.1
	LD 90	0.541	0.570	0.649	0.587	9.5
	LD 95	0.604	0.643	0.704	0.650	7.8
1% PX-13	LD 50	0.681	0.670	0.684	0.678	1.1
	LD 90	1.859	1.850	1.853	1.854	0.3
	LD 95	2.172	2.170	2.162	2.168	0.2
5% PX-13	LD 50	0.423	0.354	0.365	0.381	9.7
	LD 90	1.867	1.656	1.648	1.724	7.2
	LD 95	2.113	1.932	1.983	2.009	4.6

A good reproducibility of the mean particle size in between the batches was obtained for PX-18 and PX-13 nanosuspensions at all tested concentrations. The relative standard deviation was ≤10% at all measurement points. This is well in agreement with earlier findings, where a good reproducibility of the particles size was reported for nanosuspensions produced by high pressure homogenization [187, 188].

2.4.3 Stability investigations of PX-13 and PX-18 nanosuspensions

2.4.3.1 Introduction and theoretical background

The purpose of stability tests is to provide evidence on how the quality of a formulation varies with time under the influence of a variety of environmental factors [189]. The physical and chemical stability of PX-13 and PX-18 nanosuspensions were investigated. Suspensions and nanosuspensions are considered to be physically stable if the particle size distribution is not changing or changes only within defined limits during the observation period under the storage conditions. Physical instabilities which may occur in suspensions and nanosuspensions are agglomeration, aggregation, sedimentation, flotation, caking and crystal growth [153-155].

The physical stability of dispersions is a function of stabilizing electrostatic repulsion (V_R) and destabilizing van der Waals attraction (V_A). With the theory of Derjaguin, Landau, Verwey and Overbeek (DLVO theory) the resulting total interaction energy (V_T) can be described as a function of the distance between the particles (Figure 2.4.3.1-1) [190]. With a big or medium distance between equally charged particles the electrostatic repulsion dominates because the van der Waals attraction decreases with increasing distance. The curve of the total interaction energy exhibits an energy barrier, the maximum (V_m). Aggregation of particles can be avoided, if V_m is high enough. In this case particles can get as close as H_m. If the distance between the particles is smaller than H_m, they need to overcome the electrostatic repulsion. If the particles overcome the maximum of the electrostatic repulsion (V_m), the van der Waals attraction dominates and particles tend to aggregate. Born energy (V_B) is a further repulsion energy. For a particle distance of zero in the aggregate the particles need to be dehydrated. For the dehydration of particles energy needs to be applied. Therefore, the Born energy leads to a minimum in the resulting total interaction energy curve (primary minimum). However, for the stability of suspensions the Born energy is of minor importance because in practice there is no difference if aggregated solid particles are still hydrated or not.

It is possible that with a bigger particle distance the van der Waals attraction dominates, which results in the formation of a secondary minimum. If two particles have the distance of the secondary minimum, they are fixed at that distance. They cannot get closer due to the energy barrier V_m. A displacement is not possible due to the van der Waals attraction. Agglomeration of the particles occurs.

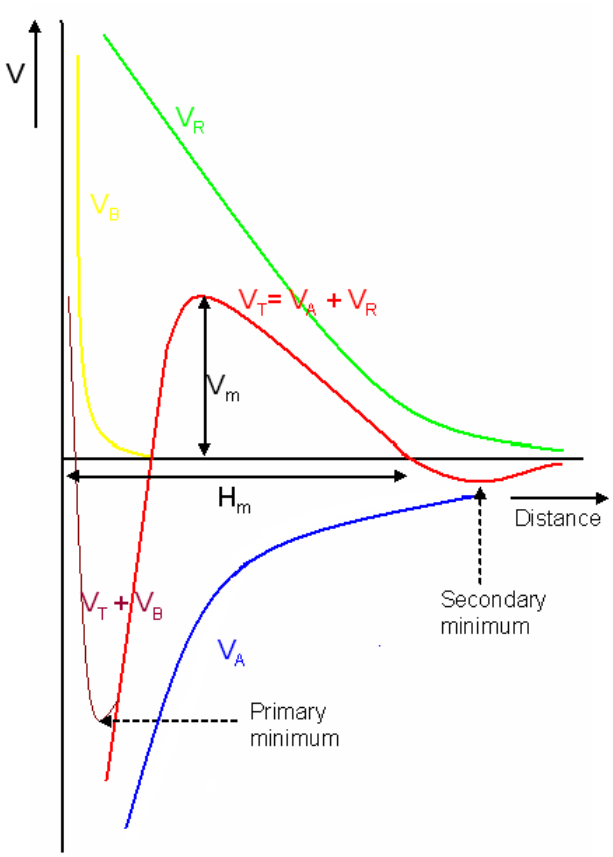

Figure 2.4.3.1-1: Electrostatic repulsion (V_R), van der Waals attraction (V_A), Born energy (V_B) and the resulting total energy (V_T) as a function of the distance between two particles according to the DLVO theory. Due to the predominance of electrostatic repulsion at a certain distance, an energy barrier (V_m) is formed, which avoids that the particles come closer than H_m. If the particles can overcome V_m aggregation of the particles occurs. A primary minimum is formed due to the interaction of van der Waals attraction and Born repulsion. In case the system exhibits a secondary minimum, agglomeration of the particles can be observed at this particle distance (modified after [190]).

The electrostatic repulsion is a function of the surface charge (Nernst potential) and the thickness of the diffuse layer. Due to the absorption of ions in the Stern layer, the Stern potential is responsible for the decay of the diffuse layer, the electrostatic repulsion (V_R) and the resulting total energy (V_T). The measurable zeta potential is smaller than the Stern potential because the hydrodynamic shear plane is located at a certain distance from the Stern layer. However, if the zeta potential is measured in a measuring medium with a very low electrolyte concentration the difference between the Stern potential and the zeta potential is very little. That means, the zeta potential can be used to predict the stability of electrostatically stabilized disperse systems.

Aggregation is only possible if the particles overcome the energy barrier (V_m). This can occur due to kinetic energy of the particles. In dispersions particles < 5 µm get kinetic energy due to Brownian motion of the molecules of the dispersant medium. The dispersant molecules hit the particles and distribute kinetic energy to the particles. Therefore, diffusion of the particles in

the dispersant medium occurs. The diffusion constant, described in the Stokes-Einstein equation, is a measure for the particle velocity. Furthermore, kinetic energy can be applied to the particles due to gravitation force. If particles >1 µm are present, sedimentation or flotation can occur due to density differences of the dispersant medium and the dispersed phase. The sedimentation or flotation velocity can be described by Stokes law.

Stokes-Einstein equation:

$$D = \frac{k\,T}{6\,\pi\,\eta\,r}$$

D = diffusion constant
r = radius
k = Boltzmann constant
T = absolute temperature
η = dynamic viscosity

Stokes law:

$$v = \frac{2\,(\rho_s - \rho_l)\,g\,r^2}{9\,\eta}$$

ρ_s = density of the solid phase
ρ_l = density of the liquid phase
g = gravitation force
r = radius
η = viscosity of the liquid phase

Crystal growth in suspensions can occur because of Ostwald ripening, which is caused by differences in the solubility and the concentration gradient between small and big particles. Small particles exhibit a higher degree of curvature and therefore a higher solubility than larger particles. Molecules from the higher concentrated solution around small particles diffuse to the vicinity of larger particles, where a lower concentration is present. This causes particle growth of the large particles due to supersaturation and drug crystallization. At the same time the concentration in vicinity of the small particles drops below their saturation solubility leading to a further dissolution of drug from small particles. This process finally leads to the disappearance of the small particles and a further growth of the larger ones [171, 191]. Furthermore, the recrystallization process can lead to caking, if particles grow together in the sediment.

2.4.3.2 Methods

Zeta potential

When the zeta potential is known, predictions about the long-term stability of dispersed systems can be made [192]. Due to the presence of ionized groups on the particle surface, particles exhibit a surface charge, which results in the creation of a surface potential (= Nernst potential) related to a far distance in the dispersant medium. Most particles exhibit a negative surface charge. Therefore, the course of the potential of a negatively charged particle in an aqueous medium containing electrolytes will be described. On the negative charged surface negative dehydrated ions are adsorbed in most of the cases (= inner Helmholtz layer). At short distances van der Waals forces are stronger than electrostatic forces, which explains the adsorption of negatively charged particles on the negatively charged particle surface. These forces are strong enough to cause the loss of the hydrate layer of the ions. After that follows the outer Helmholtz layer, which consists of hydrated, positively charged ions. These ions are fixed due to electrostatic interactions. The inner and the outer Helmholtz layer, also called Stern layer, are fixed to the particle surface and cannot be removed during the movement of the particle in an electrical field. The Stern layer is followed by the diffuse layer. In the diffuse layer freely movable, hydrated positively (= couter-ions) and negatively charged ions are present. Close to the Stern layer the concentration of positively charged particles is high due to electrostatic attraction and decreases with an increasing distance from the particle surface. Due to this, an exponential decay of the potential can be observed in the diffuse layer. If the particle is accelerated in an electrical field, parts of the diffuse layer can be removed. The boundary between the resitent part and the removed part of the diffuse layer is called hydrodynamic shear plane. The potential that is exhibited at the hydrodynamic shear plane is called zeta potential. The zeta potential is measured by Laser Doppler Anemometry applying an electrical field in which equilibrium between friction forces and particle acceleration is reached and the particles move with a constant velocity (= electrophoretic mobility). With the Helmholtz-Smoluchowski equation the zeta potential can be calculated from the electrophoretic mobility:

$$\zeta = EM \times \frac{4\,\pi\,\eta}{\varepsilon}$$

ξ = zeta potential
EM = electrophoretic mobility
η = viscosity of the dispersant medium
ε = dielectric constant

In this work a Zetasizer Nano ZS (Malvern Instruments, Malvern, UK), applying a combination of Laser Doppler Anemometry and Phase Analysis Light Scattering for zeta potential measurement, was used. The samples were diluted with distilled water adjusted with 0.9% (w/v) sodium chloride solution to a conductivity of 50 µS cm^{-1}. The pH was in the range of 5.5 to 6.0. Furthermore, the zeta potential was measured in the original medium, which was obtained by filtration of the nanosuspensions through Centrisart filters with a molecular weight cut off of 300 000 (Sartorius, Göttingen, Germany). The mean value of the zeta potential and the standard deviation of 30 measurements are given.

Stability investigations

To investigate the physical and chemical long term stability of 1%, 5% and 10% PX-18 nanosuspensions as well as of 1% and 5% PX-13 nanosuspensions, they were stored at 5°C ± 3°C, 25°C ± 2°C and 40°C ± 2°C. The particle size of the formulations was measured on day 0, 1, 7, 14, 30, 90 and 180 by PCS and LD. No LD measurements were performed for the 1% PX-13 and 1% PX-18 nanosuspension due to the high transparency of the samples. Chemical long term stability was investigated of the physically most stable formulation at the day of production (day 0) and day 180 by HPLC measurement using the method descried in chapter 2.3.2.

2.4.3.3 Results and discussion

Zeta potential

According to the DLVO theory the physical stability of a disperse system increases with increasing electrostatic repulsion energy. The electrostatic repulsion increases with increasing surface charge and increasing thickness of the diffuse layer. To investigate the surface properties of the nanosuspensions the zeta potential was measured in distilled water adjusted to a conductivity of 50 µS cm^{-1}. A minimum zeta potential of |-30 mV| is required for a good physical stability [190, 193]. All nanosuspensions under investigation showed a zeta potential higher than |-30 mV| measured in distilled water adjusted to a conductivity of 50 µS cm^{-1} (Table 2.4.3.3-1). Measuring the zeta potential in the original dispersion medium, it is an indirect measure of the thickness of the diffuse layer. In the original medium zeta potential values ranging from |-30| to |-60 mV| indicate a good stability [194]. The zeta potential of the PX-13 nanosuspensions is well in between this range (Table 2.4.3.3-1). The absolute value of the zeta potential of the PX-18 nanosuspension measured in the original medium is below |-30 mV| (Table 2.4.3.3-1). However, the zeta potential allows only predicting the electrostatic stabilization. Further stabilizing factors or destabilizing factors cannot be predicted with the zeta potential. Both, Tween 80 and Plantacare® 2000, perform an additional sterical stabilization of the nanoparticles. It has been reported, that in a combined electrostatic and sterical stabilization a zeta potential of about |-20 mV| can be sufficient for physical stability [33].

Table 2.4.3.3-1: Zeta potential values of 1%, 5% and 10% PX-18 nanosuspensions and 1% and 5% PX-13 nanosuspensions measured in distilled water adjusted to a conductivity of 50 µS cm^{-1} and the original medium (n =30, mean ± SD).

Formulation	Distilled water adjusted to 50 µS cm^{-1} [mV]	Original medium [mV]
1% PX-18	-50.6 ± 2.5	-19.8 ± 6.1
5% PX-18	-50.8 ± 5.7	-19.3 ± 4.9
10% PX-18	-56.2 ± 6.8	-19.0 ± 5.1
1% PX-13	-81.6 ± 6.4	-57.6 ± 6.2
5% PX-13	-82.0 ± 6.5	-48.7 ± 8.5

Physical stability

The particle size distribution of the PX-18 and PX-13 nanosuspensions stored refrigerated (5°C ± 3°C), at 25°C ± 2°C and at 40°C ± 2°C was monitored up to 180 days by PCS and LD. Figure 2.4.3.3-1 provides an overview of the particle size and PI measured by PCS of the 1% PX-18 nanosuspension under different storage temperatures. At all storage temperatures a reduction in the average particle diameter can be seen one day after production. This can be caused by partial dissolution of the nanoparticles due to the fact that drug nanoparticles have a higher saturation solubility compared to microparticles [185]. The 1% PX-18 nanosuspension was physically stable over the investigated period of time, when stored refrigerated (5°C ± 3°C). Under the other storage temperatures an increase of the average particle diameter measured by PCS could be seen during the storage period. An increase in particle size occurred after 90 days of storage at 25°C ± 2°C and after 14 days of storage at 40°C. Due to the extremely small particle size an increase in particle size due to energetic reasons cannot be excluded. Storing the nanosuspension at 40°C led to a complete phase separation (sedimentation) after 180 days of storage.

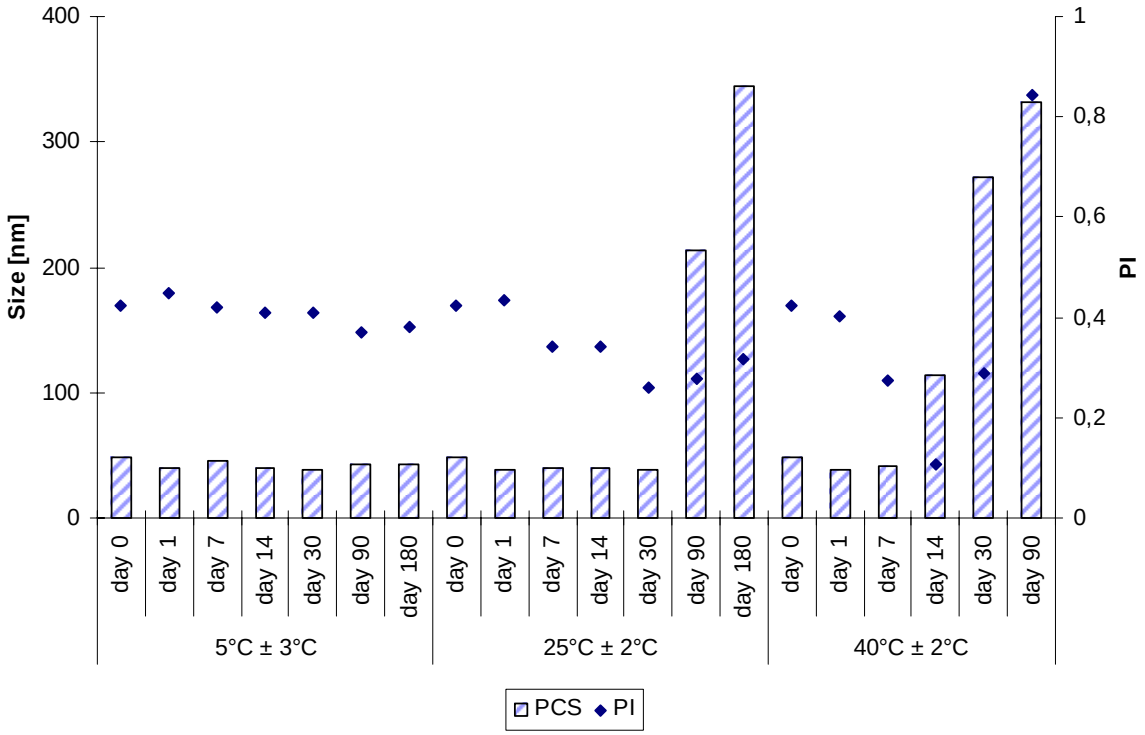

Figure 2.4.3.3-1: Particle size and PI of 1% PX-18 nanosuspension stabilized with 1% Tween 80 measured by PCS over a period of 180 days stored at 5°C ± 3°C, 25°C ± 2°C and 40°C ± 2°C.

Figure 2.4.3.3-2 and Figure 2.4.3.3-3 show the results of the particle size measurements of 5% PX-18 nanosuspension stored at different temperatures for 180 days. The 5% PX-18 nanosuspension stored refrigerated (5°C ± 3°C) was physically stable over the observation period. At the other storage temperatures physical instabilities were observed. After 14 days storing 5% PX-18 nanosuspension at 25°C ± 2°C an increase of the LD 50 and the average particle diameter measured by PCS could be seen while a decrease of the PI could be observed at the previous measurement points. This indicates dissolution of a smaller particle fraction, which narrows the particle size distribution and results consequently in an increase of the average particle size measured by PCS and an increase of the LD 50 while the LD 90 and LD 95 stay nearly constant. Recrystallisation of PX-18 and aggregation of the nanoparticles resulted in a further increase in particle size during the observation period. Particle growth and aggregation also took place in the nanosuspension stored at 40°C ± 2°C starting on day 7. After 180 days of storage complete phase separation (sedimentation) occurred at 40°C ± 2°C.

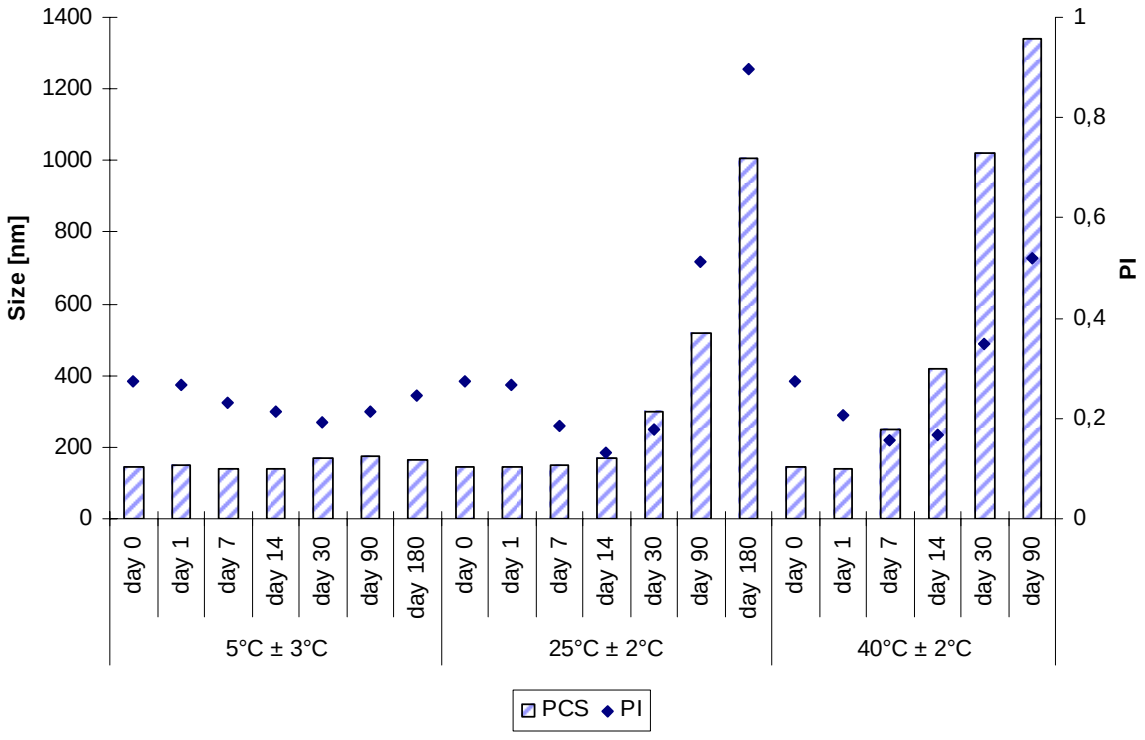

Figure 2.4.3.3-2: Particles size and PI of 5% PX-18 nanosuspension stabilized with 1% Tween 80 measured by PCS over a period of 180 days stored at 5°C ± 3°C, 25°C ± 2°C and 40°C ± 2°C.

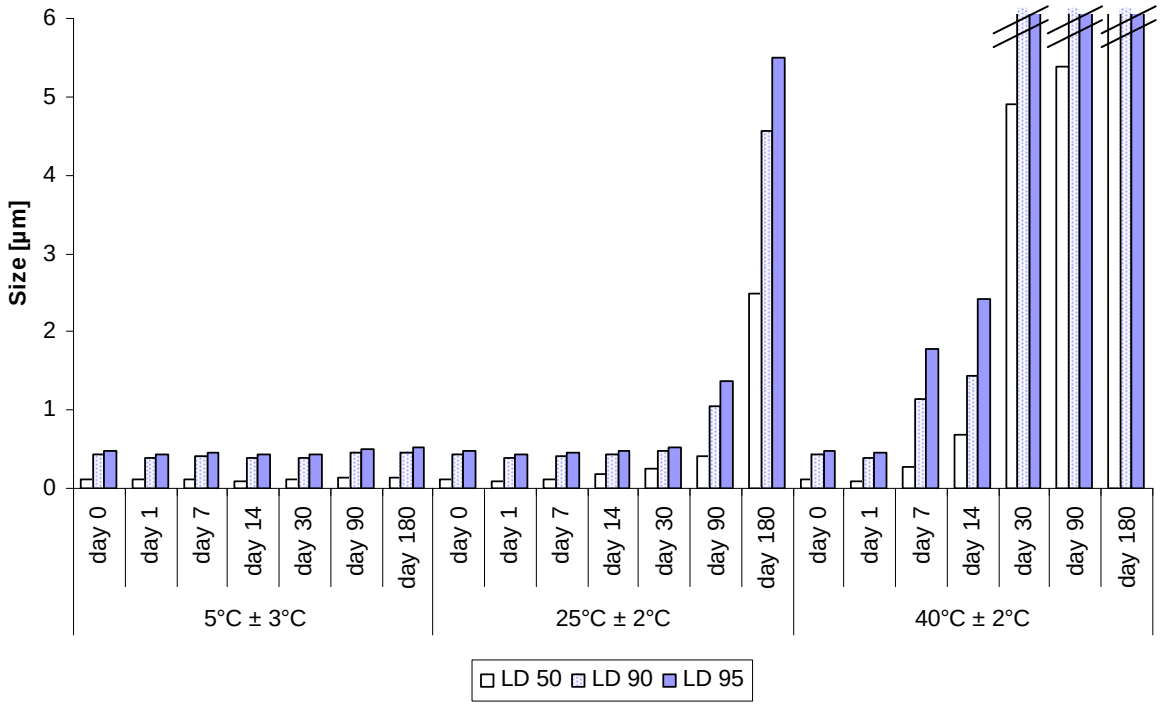

Figure 2.4.3.3-3: LD 50, LD 90 and LD 95 of 5% PX-18 nanosuspension stabilized with 1% Tween 80 measured over a period of 180 days stored at 5°C ± 3°C, 25°C ± 2°C and 40°C ± 2°C.

The particle size measured by PCS and LD of the 10% PX-18 nanosuspension stored under different temperatures for 180 days is shown in Figure 2.4.3.3-4 and Figure 2.4.3.3-5. The 10% PX-18 nanosuspension stored refrigerated (5°C ± 3°C) was physically stable over the observation period. At the other storage temperatures instabilities could be observed. After 30 days the LD 90 and LD 95 double while the LD 50 stayed nearly constant at 25°C ± 2°C. At 40°C ± 2°C the LD 90 increased about 4-folds and the LD 95 about 5.5-fold while the LD 50 increased just by 0.129 µm within 7 days of storage. This phenomenon relates to particle aggregation. Particle aggregation could be confirmed by light microscopy. Furthermore, recrystallisation processes have been involved in particle growth indicated as well by the results of the PCS measurement. Storing 10% PX-18 nanosuspension at 25°C ± 2°C led to caking after 180 days of storage. Complete phase separation (sedimentation) was observed at 40°C ± 2°C after 180 days of storage.

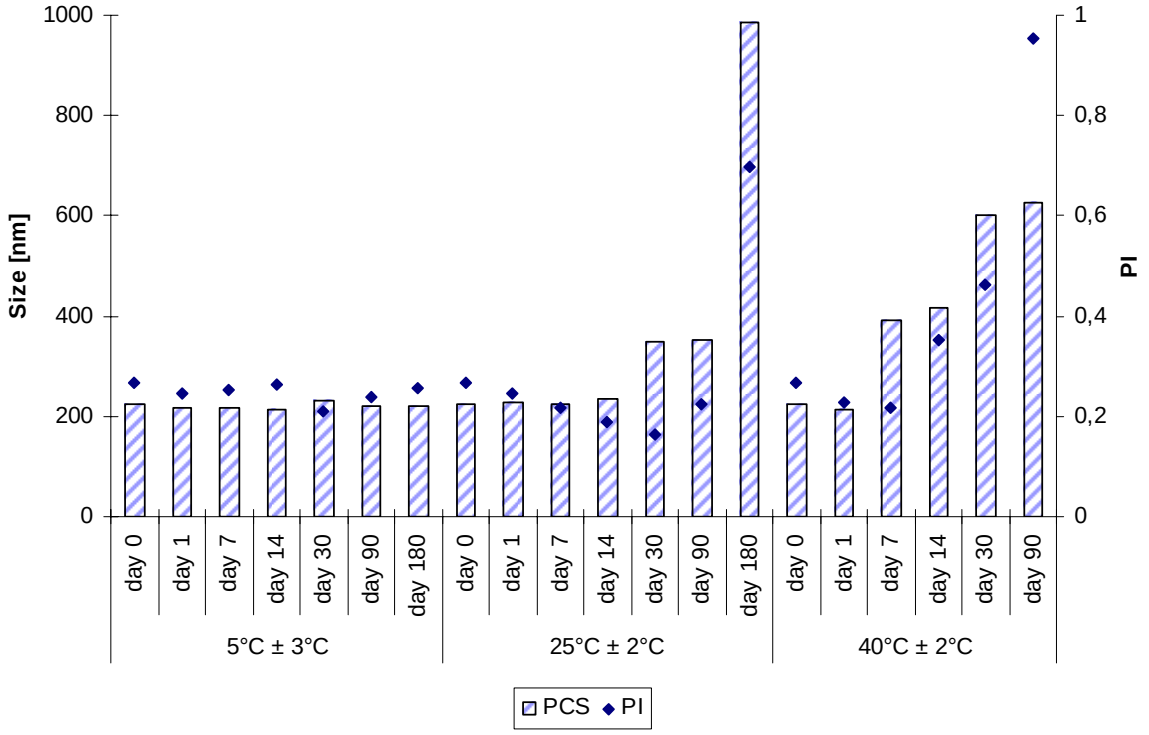

Figure 2.4.3.3-4: Particle size and PI of 10% PX-18 nanosuspension stabilized with 1% Tween 80 measured by PCS over a period of 180 days stored at 5°C ± 3°C, 25°C ± 2°C and 40°C ± 2°C.

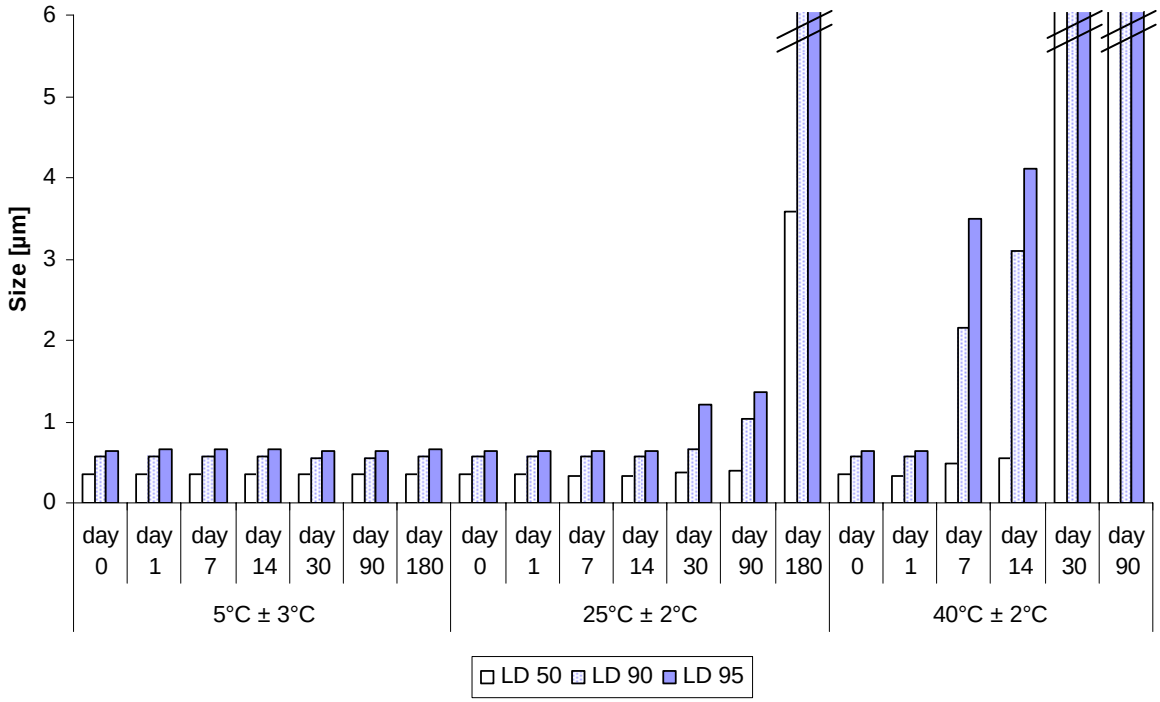

Figure 2.4.3.3-5: LD 50, LD 90 and LD 95 of 10% PX-18 nanosuspension stabilized with 1% Tween 80 measured over a period of 180 days stored at 5°C ± 3°C, 25°C ± 2°C and 40°C ± 2°C.

For all PX-18 nanosuspensions the best physical stability was found when stored refrigerated (5°C ± 3°C). Under this condition no changes in the particle size distribution occurred. Physical long term stability of nanosuspensions stored refrigerated for up to three years has previously been reported [188]. Increasing the storage temperature leads to physical instability of the PX-18 nanosuspensions. Under these conditions the low zeta potential measured in the original medium in combination with steric stabilization was not sufficient to prevent particle aggregation. Increasing the temperature leads to a decrease of the dynamic viscosity. According to the Stokes-Einstein equation an increase in temperature and a decrease in dynamic viscosity results in an increase of the diffusion constant. A higher diffusion constant leads to a faster diffusion of the particles. Having a higher kinetic energy, the electrostatic repulsion between the particles can be easier overcome, which results in particle aggregation. Furthermore, particle growth took place, if PX-18 nanosuspensions were stored at 25°C ± 2°C and at 40°C ± 2°C.

In Figure 2.4.3.3-6 the average particles diameter measured by PCS of a 1% PX-13 nanosuspension stored at three different temperatures for 180 days is shown. At 5°C ± 3°C an increase in particle size was found at day 180. The best physical stability of the 1% PX-13 nanosuspension was found when stored at 25°C ± 2°C. At 40°C ± 2°C a decrease in particle size could be observed up to day 7 indicating dissolution of the PX-13. From day 14 the average particle size increased with storage time due to recrystallisation. At day 180 complete phase separation (sedimentation) occurred.

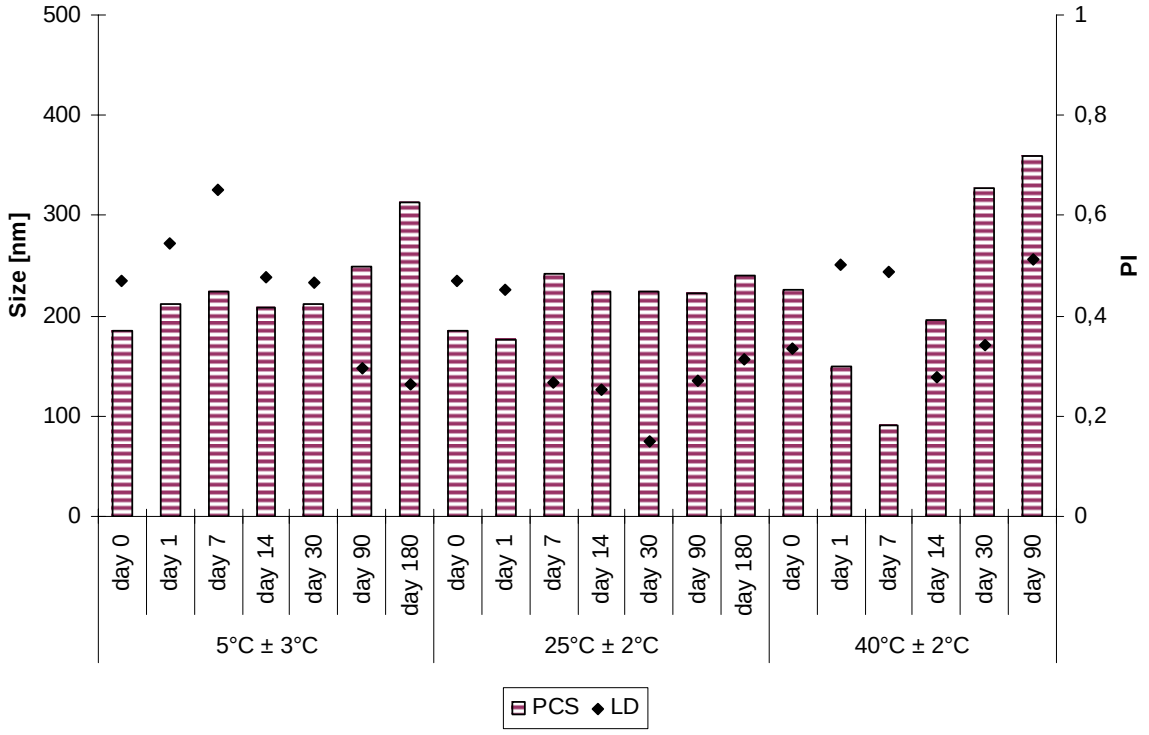

Figure 2.4.3.3-6: Particle size and PI of 1% PX-13 nanosuspension stabilized with 2% Plantacare® 2000 measured by PCS over a period of 180 days stored at 5°C ± 3°C, 25°C ± 2°C and 40°C ± 2°C.

Figure 2.4.3.3-7 and Figure 2.4.3.3-8 provide an overview of the particle size measured by PCS and LD storing a 5% PX-13 nanosuspension at 5°C ± 3°C, 25°C ± 2°C and 40°C ± 2°C for 180 days. Storing 5% PX-13 nanosuspension refrigerated (5°C ± 3°C) led already after one day to particle agglomeration. This can be seen by an increase of the LD 90 and LD 95 by 4-fold and 6.5-fold respectively, while the LD 50 and the average particle diameter measured by PCS stayed constant. The formation of agglomerates was confirmed by light microscopy. At day 30 an increase in the LD 50 value could be seen. At day 90 also the PCS average particles size increased. This indicates particles growth due to dissolution and recrystallisation process. Furthermore, sedimentation occurred at this storage temperature. At 25°C ± 2°C the

average particle size measured over a period of 180 days by PCS stayed constant indicating a good physically stability. However, at day 90 an increase in the LD 90 and LD 95 value was found. These values increased further until day 180. The LD 50 value stayed nearly constant over the observation period. The tendency to agglomerate was also found at 25°C ± 2°C. By storing the 5% PX-13 nanosuspension at 40°C ± 2°C it was found, that all LD values increase from day 1 on. Recrystallisation and agglomeration are responsible for this increase. Also an increase of the PCS average particle size was found at day 30. After 180 days of storage at 40°C ± 2°C complete phase separation (sedimentation) occurred.

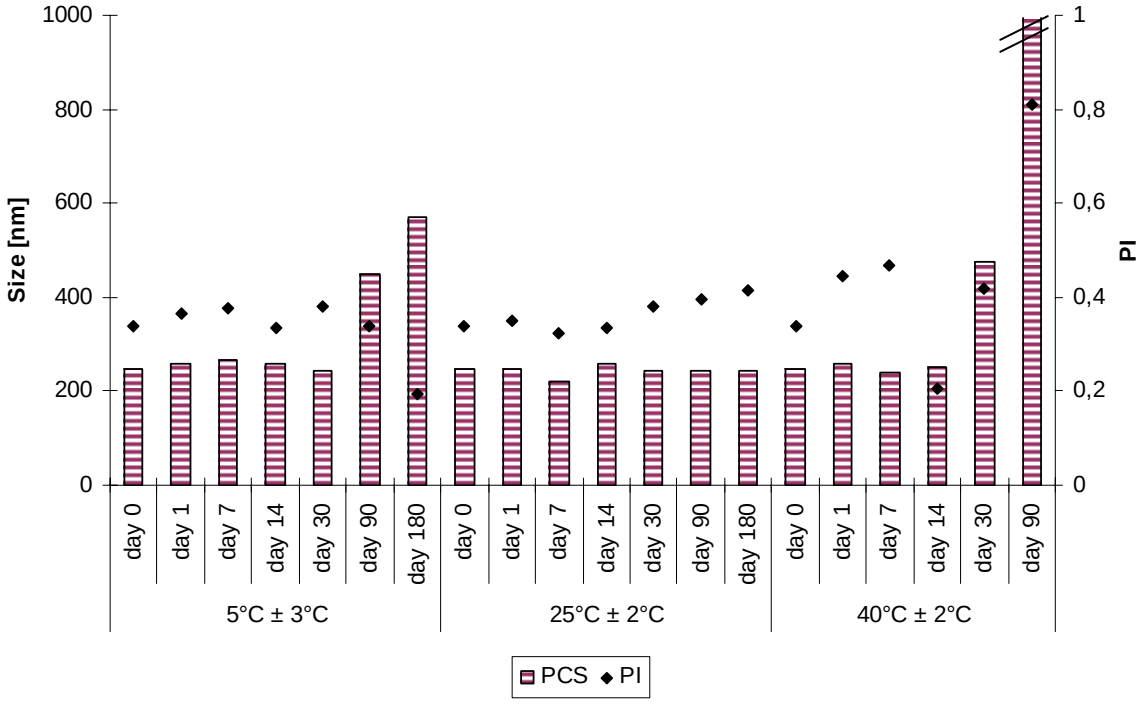

Figure 2.4.3.3-7: Particle size and PI of 5% PX-13 nanosuspension stabilized with 2% Plantacare® 2000 measured by PCS over a period of 180 days stored at 5°C ± 3°C, 25°C ± 2°C and 40°C ± 2°C.

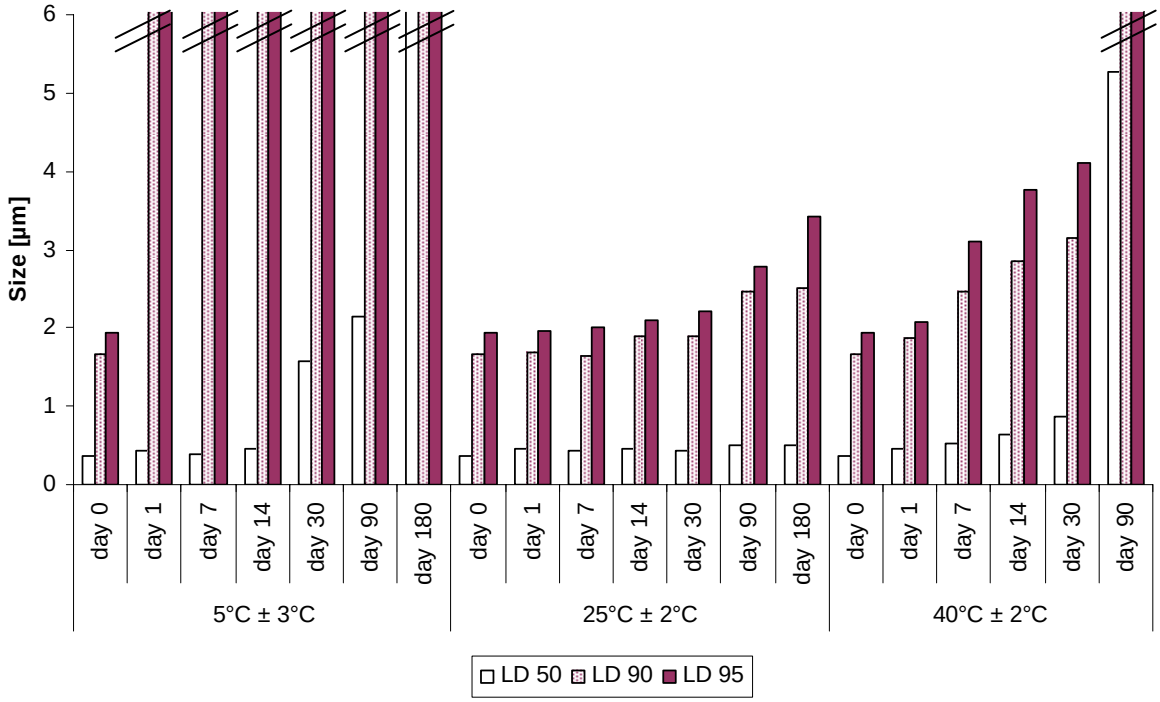

Figure 2.4.3.3-8: LD 50, LD 90 and LD 95 of 5% PX-13 nanosuspension stabilized with 2% Plantacare® 2000 measured over a period of 180 days stored at 5°C ± 3°C, 25°C ± 2°C and 40°C ± 2°C.

The best physical stability for PX-13 nanosuspensions was found at 25°C ± 2°C. However, agglomerates were found at this temperature after 90 days of storage in the nanosuspension with an active content of 5%, which was confirmed by light microscopy. This can be explained via the zeta potential. In PX-13 nanosuspensions, which exhibit a high zeta potential in both distilled water adjusted to a conductivity of 50 µS cm^{-1} and in the original medium, no aggregation was found storing the samples for 180 days. However, agglomeration of the particles was found which provides evidence that a secondary minimum is present in the resulting total energy curve of electrostatic repulsion and van der Waals attraction. With regards to a potential dermal application of PX-13 nanosuspensions, incorporation into a hydrogel would be a promising approach to increase the physical stability. Increasing the viscosity of the aqueous phase of the nanosuspensions with a gelling agent would result in a reduction of particle mobility in the system and hence prevent agglomeration of PX-13 nanoparticles. It was already reported in the literature that increasing the viscosity of the aqueous phase of nanosuspensions increases the physical stability [188, 195].

Chemical stability

Additionally to the physical stability of the PX-18 and PX-13 nanosuspensions a quantification of the drug content was performed using HPLC technique in order to detect possible chemical instabilities. The PX-18 and PX-13 content was determined at the day of production (day 0) and after 180 days of storage at 5°C ± 3°C for the PX-18 nanosuspensions stabilized with 1% Tween 80 and at 25°C ± 2°C for the PX-13 nanosuspensions stabilized with 2% Plantacare® 2000. Table 2.4.3.3-2 provides an overview of the results obtained in this study.

Table 2.4.3.3-2: Drug content in percent determined by HPLC of physically stable PX-18 and PX-13 nanosuspensions at the day of production (day 0) and after 180 days of storage at 5°C ± 3°C for the PX-18 nanosuspensions and at 25°C ± 2°C for the PX-13 nanosuspensions (n = 3, mean ± SD).

Formulation	Day 0 Concentration [%]	Day 180 Concentration [%]
1% PX-18	1.05 ± 0.08	1.14 ± 0.13
5% PX-18	5.33 ± 0.56	5.07 ± 0.09
10% PX-18	10.23 ± 0.67	10.68 ± 0.03
1% PX-13	1.05 ±0.01	1.00 ± 0.03
5% PX-13	4.62 ± 0.45	4.61 ± 0.46

All formulations with a good physical stability showed also a good chemical stability within the investigated period. The drug content of all formulations was equal at the day of production and after 180 days of storage.

2.4.4 Saturation solubility and dissolution velocity

2.4.4.1 Introduction

Generally saturation solubility is defined as the maximum quantity of a compound (solute) that can be dissolved in a certain quantity of a solvent at a specified temperature [196]. Table 2.4.4.1-1 provides an overview of the terms of solubility and their definition referred to a temperature of 15°C to 25°C according to European Pharmacopoeia. It should be taken into account that the saturation solubility also depends on the modification of polymorph compounds [123, 140] and the particle size in case particles < 2 µm are present [197].

Table 2.4.4.1-1: Terms of solubility and their definition referred to a temperature of 15°C to 25°C according to European Pharmacopoeia.

Descriptive term	Approximate volume of solvent in ml per g of solute			
Very soluble	Less than	1		
Freely soluble	From	1	to	10
Soluble	From	10	to	30
Sparingly soluble	From	30	to	100
Slightly soluble	From	100	to	1000
Very slightly soluble	From	1000	to	10 000
Practically insoluble	More than			10 000

If the particle size is reduced below 2 µm, the ratio between the surface area and the volume is increased that much, that the saturation solubility increases by an increased interaction surface between solute and solvent and the reduction of the diffusion layer [198, 199]. The principle of the increase in saturation solubility, if the particle size is reduced below 2 µm, is described in the Kelvin equation and the Ostwald-Freundlich equation. The Kelvin equation describes the vapour pressure over a curved surface of a liquid droplet in a gas phase. The vapour pressure increases with an increasing curvature caused by a decreasing particle size. This equation, describing the transition of molecules from a liquid phase to a gas phase, can also be applied to the transition of molecules from the solid phase to the liquid phase. The vapour pressure is then replaced by the dissolution pressure:

$$\ln \frac{p_r}{p_\infty} = \frac{2\,\gamma\,M}{r\,R\,T\,\rho}$$

p_r = dissolution pressure of a particle with the radius r
p_∞ = dissolution pressure of an infinitely large particle
γ = surface tention
M = molecular weight
r = radius
R = gas constant
T = absolute temperature
ρ = density of the particle

The saturation solubility is equilibrium between dissolving molecules and recrystallizing molecules. Increasing the dissolution pressure shifts the equilibrium resulting in an increase in saturation solubility.
The dependency of the saturation solubility on the particle size is described in the Ostwald-Freundlich equation:

$$(1-\alpha\, n)\frac{R\,T}{M}\ln\frac{c_{s2}}{c_{s1}} = \frac{4\,\delta}{\rho}\left(\frac{1}{d_2}-\frac{1}{d_1}\right)$$

α = dissociation grade
n = number of ions
R = gas constant
T = absolute temperature
M = molecular weight
c_{S1} = saturation concentration of population 1
c_{S2} = saturation concentration of population 2
δ = interfacial energy
ρ = density
d_1 = diameter of population 1
d_1 = diameter of population 1

Additionally this equation gives another possible explanation for the increase in saturation solubility via the creation of high energy surfaces when disrupting microparticles into nanoparticles. Lyophobic surfaces from the inner of the particle will be exposed to the

aqueous dispersion medium. According to the Ostwald-Freundlich equation the saturation solubility is a function of the interfacial energy. Differences in the interfacial energy cause differences in the saturation solubility of polymorph forms [18, 200]. The same might be valid for differences in saturation solubility from nanosuspensions to microparticulate suspensions [166].

Another feature of nanoparticles is an increase in dissolution velocity. The dissolution velocity depends on the surface area of the solid, diffusional transport of dissolved material and the saturation solubility. The Noyes-Whitney equation describes, that an increase in dissolution velocity is proportional to an increase in surface area which occurs when the particle size is reduced [201]:

$$\frac{dc_x}{dt} = \frac{D\ A}{h}\left(c_s - c_x\right)$$

$\frac{dc_x}{dt}$ = dissolution velocity

D = diffusion constant

A = surface area of the particle

h = diffusional distance

c_s = saturation solubility

c_x = concentration at the time point x

The decrease in the diffusional distance is an additional factor accelerating the dissolution velocity. According to the Prandtl equation the diffusional distance is reduced with an increasing curvature of ultrafine particles [198, 202]:

$$h = k\left(\frac{L^{\frac{1}{2}}}{V^{\frac{1}{3}}}\right)$$

h = hydrodynamic boundary layer thickness

k = constant

V = relative flow velocity of the flowing liquid against a flat surface

L = length of the surface in the direction of flow

According to the Kelvin equation, Ostwald-Freundlich equation, Noyes-Whitney equation and Prandtl equation the reduction in drug particle size to the nanometer range increases the saturation solubility as well as the dissolution velocity. In this part of the work the influence of the reduction of the particle size of PX-13 and PX-18 from the micrometer range to the nanometer range on the saturation solubility and dissolution velocity was investigated.

2.4.4.2 Methods

Saturation solubility

To determine the saturation solubility of PX-18 and PX-13 powder, the compounds were suspended in 1% Tween 80 in case of PX-18 and in 2% Plantacare® 2000 in case of PX-13 to a final active concentration of 5% using mortar and pestle. Nanosuspensions with an active content of 5% were used. 2.0 ml of each formulation were added to 20.0 ml of bidistilled water. The samples were stored at 25°C shaking with 100 rpm in an Innova 4230 refrigerated incubator shaker (New Brunswick Scientific, New Jersey, USA). After one week the samples were filtered through 0.02 µm filters (Anotop 25 Plus, Whatman, Maidstine, Great Britain). 10.0 ml of the filtrate were collected and freeze dried. The amount PX-18 and PX-13 present was analyzed using the HPLC method described in chapter 2.3.2.

Dissolution velocity

The dissolution velocity study of PX-18 and PX-13 as well as of the according nanosuspensions with an active content of 5% was carried out in glass bottles. Suspensions with an active concentration of 5% were prepared of PX-13 and PX-18 powder as described in the method for determining the saturation solubility. Bidistilled water was used as dissolution medium. 5 µg/ml of each formulation was placed in the dissolution medium. After shaking the glass bottles for 15, 30, 60, 90, 120 and 240 min at 25°C with 100 rpm using a Innova 4230 refrigerated incubator shaker (New Brunswick Scientific, New Jersey, USA) the samples were filtrated using 0.02 µm filters (Anotop 25 Plus, Whatman, Maidstine, Great Britain). 15.0 ml of the filtrate were collected and freeze dried. The amount of PX-18 and PX-13 present was analyzed using the HPLC method described in chapter 2.3.2.

2.4.4.3 Results and discussion

The saturation solubility of PX-18 and PX-13 microsuspensions as well as of the according nanosuspensions in water at 25°C is shown in Figure 2.4.4.3-1 and Figure 2.4.4.3-2. To avoid the influence of the surfactant used as stabilizers in the nanosuspensions, e.g. increased wetting of the material and solubilization, microsupensions with the same surfactant content were produced before testing. According to the European Pharmacopoeia the PX-18 microsuspension with a saturation solubility of 24.4 µg/ml and the PX-13 microsuspension with a saturation solubility of 5.0 µg/ml can be classified as practically insoluble. Decreasing the particle size of PX-18 from the micrometer range to the nanometer range, results in an increase of the saturation solubility by 46% (Figure 2.4.4.3-1).

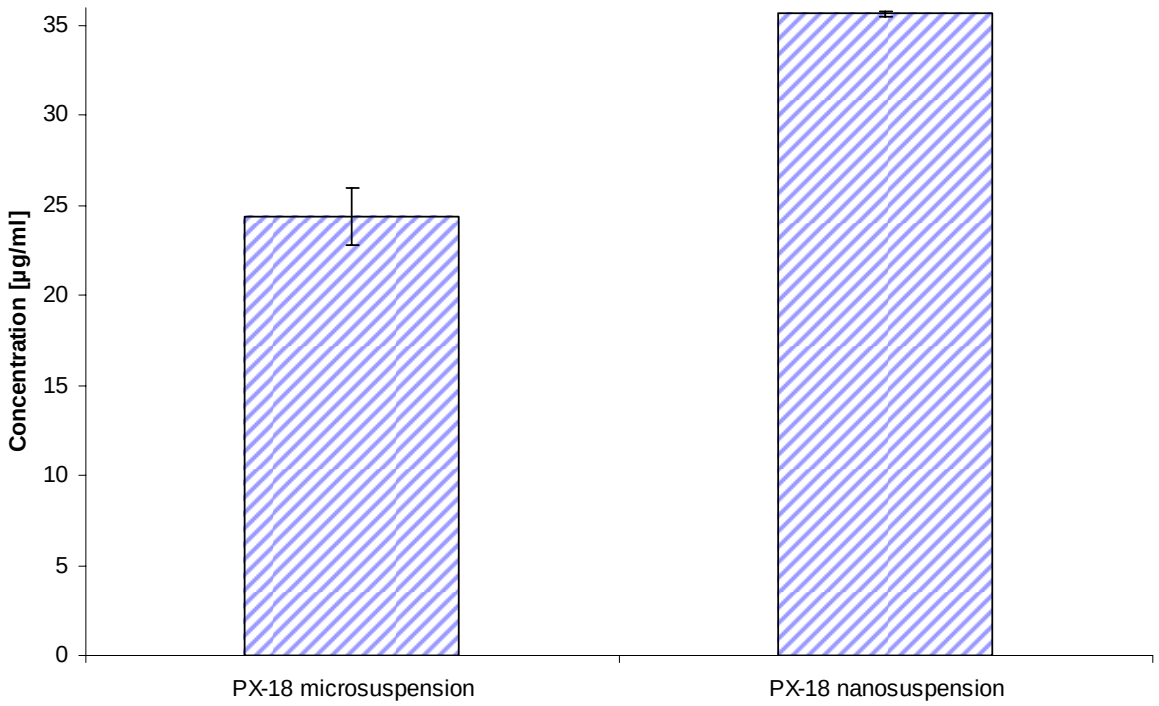

Figure 2.4.4.3-1: Saturation solubility of PX-18 microsuspension (LD 50 = 27.37 µm) and PX-18 nanosuspension (LD 50 = 0.099 µm) at 25°C in bidistilled water (n = 3; mean ± SD).

In case of PX-13 an increase of the saturation solubility by 146% could be achieved by decreasing the particles size from the micrometer range to the nanometer range (Figure 2.4.4.3-2).

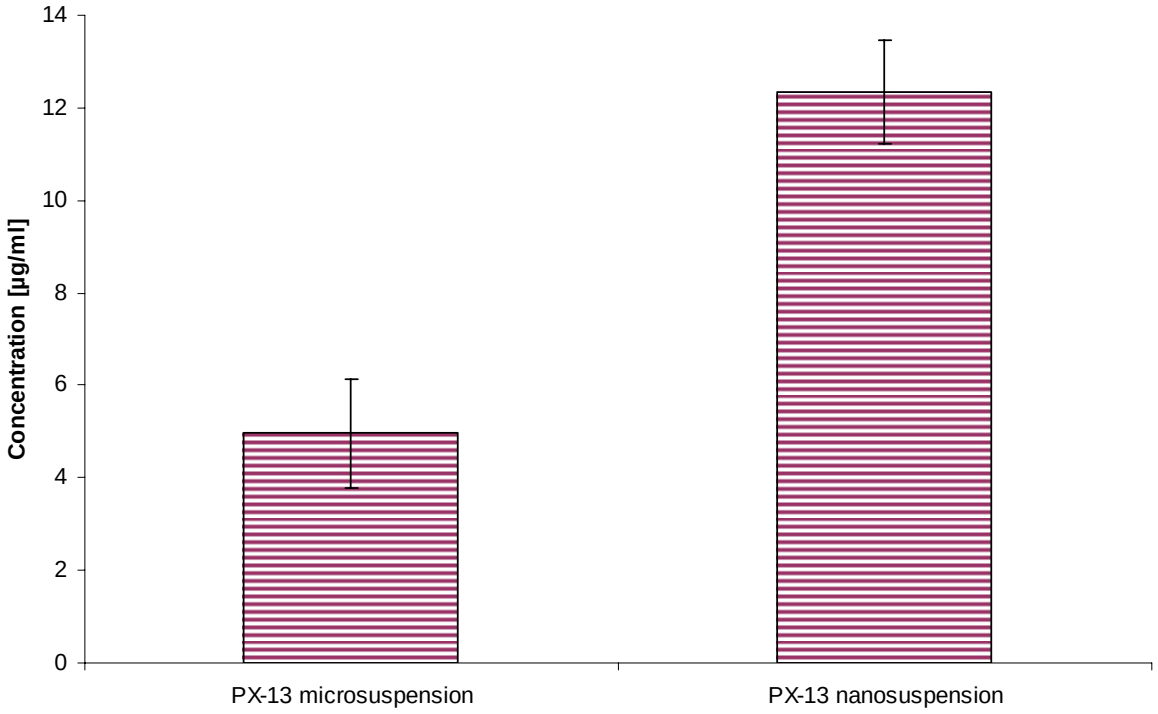

Figure 2.4.4.3-2: Saturation solubility of PX-13 microsuspension (LD 50 = 497.0 µm) and PX-13 nanosuspension (LD 50 = 0.381) at 25°C in bidistilled water (n = 3; mean ± SD).

The determination of the dissolution rate of poorly soluble compounds is very challenging. Up till now there is no general accepted validated method available [203]. Furthermore, the separation of dissolved drug from undissolved drug nanoparticles is quite challenging due to the small particle size. The dissolution profiles of PX-18 and PX-13 powder as well as of the according nanosuspensions were recorded under non-sink condition in bidistilled water. Due to the poor solubility of the compounds it was not possible to perform the test under sink conditions having still manageable volumes to filtrate without undergoing the detection limit of the analytical method. However, the chosen conditions were suitable to show the difference in the dissolution velocity of suspensions with a particle size in the micrometer range and nanosuspensions. The dissolution profiles of 5% PX-18 microsuspension and nanosuspension are shown in Figure 2.4.4.3-3. The dissolution profile of PX-18 nanosuspension was higher than the one of the according microsuspension indicating a faster dissolution of the nanosuspension. After 60 min only 13% PX-18 of the microsuspension were dissolved whereas at the same time point already 40.4% PX-18 of the nanosuspension were dissolved.

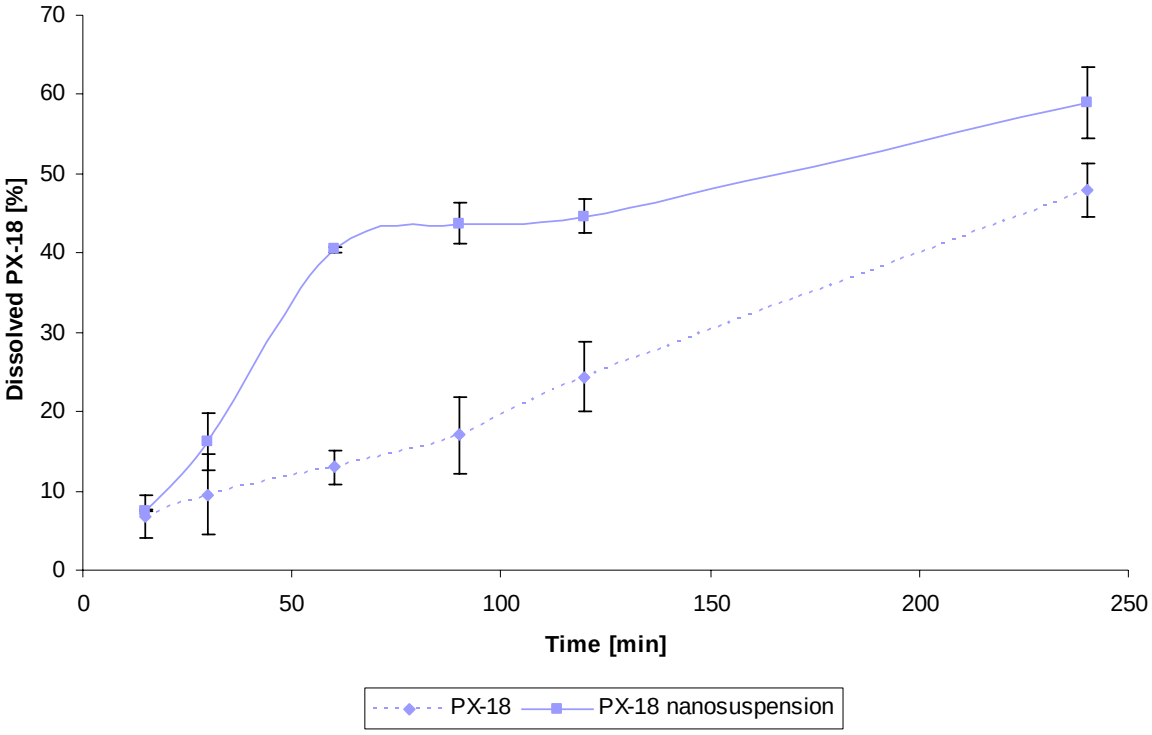

Figure 2.4.4.3-3: Dissolution profiles of 5% PX-18 microsuspension (LD 50 = 27.37 µm) and PX-18 nanosuspension (LD 50 = 0.099 µm) at 25°C in bidistilled water (n = 3; mean ± SD).

Figure 2.4.4.3-4 shows the dissolution profile of 5% PX-13 microsuspension and nanosuspension. Also for PX-13 a higher dissolution profile was obtained for the nanosuspension compared to the microsuspension. In case of the nanosuspension 20.2% of PX-13 were dissolved within 60 min whereas at the same time point only 11.5% of the according microsuspension were dissolved.

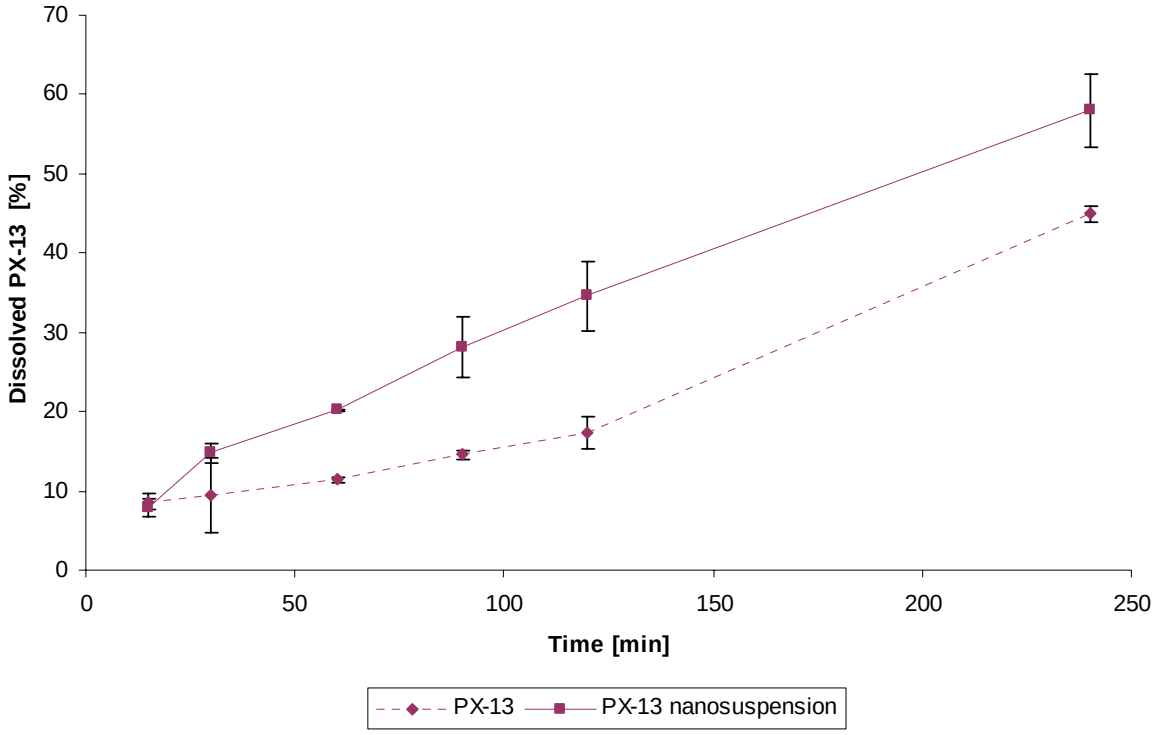

Figure 2.4.4.3-4: Dissolution profiles of 5% PX-13 microsuspension (LD 50 = 27.37 µm) and PX-13 nanosuspension (LD 50 = 0.099 µm) at 25°C in bidistilled water (n = 3; mean ± SD).

With the Kelvin equation, Ostwald-Freundlich requation, Noyes-Whitney equation and the Prandtl equation it was shown theoretically how the saturation solubility and dissolution velocity increases when decreasing the particle size from the micrometer range to the nanometer range. In the literature various examples are given for an increase in saturation solubility and dissolution velocity decreasing the particle size from the micrometer range to the nanometer range [182, 188, 195]. The results obtained with PX-18 and PX-13 were well in agreement with the theory and previously reported findings. For both compounds an increase in saturation solubility as well as in the dilution velocity could be shown by decreasing the particle size from the micrometer range to the nanometer range.

2.5 Dermal and ocular safety of PX-13 and PX-18

2.5.1 Evaluation of the cytotoxic potential using primary human fibroblasts and keratinocytes monolayer cell cultures

2.5.1.1 Introduction

In vitro cytotoxicity has generally been found to be a useful predictor of skin irritation potential [204-206]. Cell cultures using skin cells are useful for the design of safer, more efficient and more cost effective human skin irritation tests. Skin irritation is a reversible inflammatory reaction produced by the arachidonic acid cascade and cytokines in viable keratinocytes and fibroblasts of the skin. Human keratinocyte and fibroblast cultures offer an appropriate *in vitro* model for skin irritation because they are relevant to the organ and species of concern. A further advantage of using monolayer cell culture models for the evaluation of skin irritation potential is the possibility of a quick identification of toxic compounds. However, it should be taken into account, that cell cultures lack of the properties of intact skin, such as its selective barrier role or the interaction between different cell types [207].

In this study the cytotoxic potential of PX-13, PX-18 and betamethasone on primary human keratinocyte and fibroblast monolayer cell cultures was studied by two quantitative colorimetric cytotoxicity assays, the MTT assay and the Neutral red assay.

The MTT assay modified after Pagé et al. [208] was used to assess the cell viability and proliferation rate of fibroblasts and keratinocytes. With this test the activity of the mitochondrial succinate dehydrogenases of living cells is measured independent of the fact if DNA is synthesized at the moment of the test or not. The yellow colored 3-(4,5-dimethylthiazol-2-yl)-2,5-diphenyl-tetrazolium bromide (MTT) gets into the cells, where it is reduced to the dark blue colored formazan by mitochondrial succinate dehydrogenases of vital cells (Figure 2.5.1.1-1) [209, 210]. Therefore, the quantification of the formazan can be used as a measurement of the viability of the cells. The blue colored formazan is insoluble in the aqueous cell culture medium but has a good solubility in DMSO.

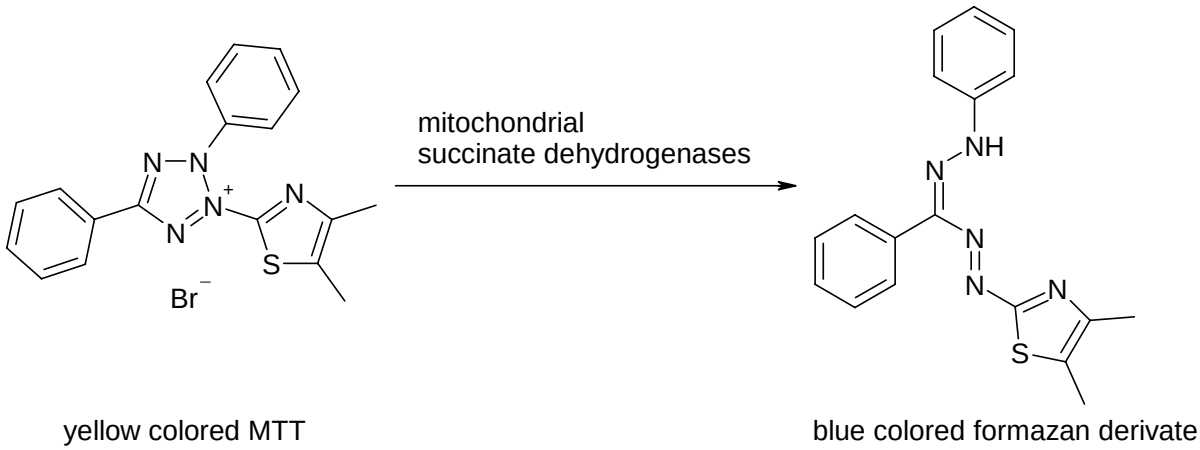

Figure 2.5.1.1-1: Reduction of yellow colored MTT to blue colored formazan derivate in viable cells due to the activity of mitochondrial succinate dehydrogenases.

The Neutral red cytotoxicity assay is a cell viability chemosensitivity assay, based on the ability of viable cells to incorporate and bind neutral red [211]. Neutral red is a weak cationic dye (Figure 2.5.1.1-2) that readily penetrates cell membranes by non-ionic diffusion, accumulating intracellularly in lyosomes, where it binds with anionic sites in the lyosomal matrix. Alterations of the cell surface or the sensitive lyosomal membrane lead to lyosomal fragility and other changes that gradually become irreversible. Such changes result in a decreased uptake and binding of Neutral red [212].

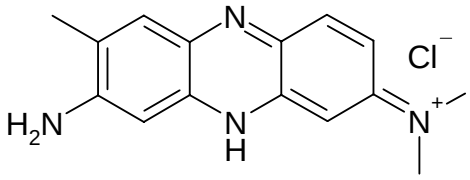

Figure 2.5.1.1-2: Chemical structure of Neutral red used in Neutral red cytotoxicity assay.

2.5.1.2 Materials and methods

2.5.1.2.1 Materials

Acetic acid	Merck, Darmstadt, Germany
BSA	Biochrom, Berlin, Germany
Cell culture flask	TPP, Trasadingen, Switzerland
Centrifuge Megafuge 1.0R	Heraeus, Hanau, Germany
Dimethyl sulfoxide (DMSO)	Merck, Darmstadt, Germany
Dulbecco's Modified Eagle's Medium Nutrient Mixture F-12 HAM	Sigma Aldrich, Deisenhofen, Germany
EDTA	Sigma Aldrich, Deisenhofen, Germany
Ethanol	Monopolverwaltung für Branntwein, Berlin, Germany
FLUOstar Optima	GMB Labtech, Offenburg, Germany
Incubator Hera cell 240	Heraeus, Hanau, Germany
KCl	Merck, Darmstadt, Germany
Keratinocytes basal medium (KBM)	Cambrex Bio Science, Verviers, Belgien
Keratinocytes growth medium (KGM) Single Quotes	Cambrex Bio Science, Verviers, Belgien
KH_2PO_4	Merck, Darmstadt, Germany
L-glutamine	PAA Laboratories, Cölbe, Germany
Minimum essential medium Eagle	Sigma Aldrich, Deisenhofen, Germany
MTT (3-(4,5-dimethylthiazole-2-yl)-2,5-diphenyl-tetrazolium bromide)	Sigma Aldrich, Deisenhofen, Germany
Na_2HPO_4	Merck, Darmstadt, Germany
NaCl	Merck, Darmstadt, Germany
Neubauer counting chamber (0.0025 mm^2/0.1 mm)	Zeiss, Jena, Germany
Neutral red (NR) (3-amino-7-dimethylamino-2-methylphenazine hydrochloride)	Merck, Darmstadt, Germany
Penicillin-Streptomycin	Sigma Aldrich, Deisenhofen, Germany
Plate shaker IKA MTS 2	Janke & Kunkel, Staufen, Germany
Tissue culture test plates 24	TPP, Trasadingen, Switzerland
Trypsin	Biochrom, Berlin, Germany

Betamethasone

Betamethasone (9-Fluoro-11β,17,21-trihydroxy-16β-methylpregna-1,4diene-3,20-dione) is a white, crystalline powder which is practically insoluble in water [213]. This compound has a molecular weight of 392.47 g/mol. The melting point of betamethasone is 231-234°C. The chemical structure of betamethasone is shown in Figure 2.5.1.2-1. Betamethasone is a glucocorticoide, derived from prednisolone. Due to the fluorine substitution in the 9α-position and the methyl group in the 16β-position the anti-inflammatory action is increased by factor 5-10 compared to prednisolone, while the mineralocorticoide action is nearly abolished. Betamethasone is widely used for the topical treatment of inflammatory, allergic and pruritic skin diseases, e.g. psoriasis, dermatitis, neurodermatitis and eczema [214]. Betamethasone used in this work was obtained from Sigma Alrich (Deisenhofem, Germany).

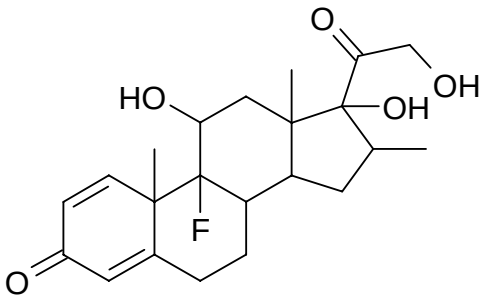

Figure 2.5.1.2-1: Chemical structure of betamethasone (9-Fluoro-11β,17,21-trihydroxy-16β-methylpregna-1,4diene-3,20-dione).

Media and solutions for cell culture experiments

The following cell culture media and solutions were used in the experiments. Preparation was done under aseptic conditions.

Medium for keratinocytes

Keratinocytes growth medium (KGM) was obtained by adding the following supplements to keratinocytes basal medium (KBM):

BPE	30 µg/ml
hEGF	0.1 ng/ml
Hydrocortisone	0.5 µg/ml
Insulin	5 µg/ml
Amphotericin B	50 ng/ml
Gentamicinsulfat	50 µg/ml

Medium for fibroblasts

Fibroblasts growth medium (FGM) was used to grow and culture the fibroblasts. FGM was prepared by adding the following supplements to Dulbecco's Modified Eeagle's Medium Nutrient Mixture F-12 HAM:

BSA	7.5%
Penicillin	10 000 units/ml
Streptomycin	10 mg/ml
L-glutamine	0.2 mM/ml

Fibroblasts basal medium (FBM) was used in the experiments. FBM was prepared by adding the following supplements to Dulbecco's Modified Eeagle's Medium Nutrient Mixture F-12 HAM:

Penicillin	10 000 units/ml
Streptomycin	10 mg/ml
L-glutamine	0.2 mM/ml

Stop medium:

BSA	10%

in Dulbecco's Modified Eeagle's Medium Nutrient Mixture F-12 HAM

Phosphate buffered saline (PBS):

KCl	0.2 g/l
NaCl	8.0 g/l
KH_2PO_4	0.2 g/l
Na_2HPO_4	1.44 g/l

in aqua bidest

Trypsin-EDTA-solution:

Trypsin	1.67 mg/ml
EDTA	0.67 mg/ml

in PBS

MTT-solution:

MTT	5 mg/ml
in PBS	

Neutral red stock solution:

Neutral red	4 mg/ml
in aqua bidest.	

Neutral red Medium for fibroblasts:

Neutral red stock solution	1 ml
FBM	79 ml

Neutral red Medium for keratinocytes:

Neutral red stock solution	1 ml
KGM	79 ml

Neutral red desorb was prepared immediately prior to use.

Acetic acid	1 g
Ethanol	50 g
Aqua bidest.	49 g

2.5.1.2.2 Methods

Isolation and cultivation of fibroblasts and keratinocytes

Primary cultures of keratinocytes and fibroblasts were obtained from human juvenile foreskin biopsies. The foreskin was incubated for 20 hrs at 4°C with Trypsin-EDTA-solution (cold trypsinization). The enzymatic reaction was stopped using the Stop medium. The keratinocytes were scraped off the tissue into ice cold PBS using forceps. The keratinocytes containing dispersion was centrifuged for 5 min at 1000 rpm at 4°C. After decantation of the supernatant and resuspending the cells in PBS it was centrifuged again under the same conditions. The keratinocytes were taken up in KGM, dispensed into cell culture flasks and incubated at 37°C and 5% CO_2.

To obtain the fibroblasts, the foreskin was afterwards trypsinized for 10 min at 37°C and 5% CO_2 (warm trypsinization). The reaction was stopped using Stop medium and the foreskin

was washed with PBS. After centrifugation for 5 min at 1000 rpm at a temperature of 4°C the supernatant was decanted and the fibroblasts taken up in FGM. The fibroblasts were cultivated in cell culture flasks at 37°C and 5% CO_2.

To eliminate specific properties of the donor, keratinocytes and fibroblasts were pooled from at least three different donors. The keratinocytes were split 1:3 if maximum 70% confluence was reached. Fibroblasts were passaged every 2^{nd} week in a relation of 1:4. Keratinocytes of the 2^{nd} to 4^{th} passage and fibroblasts of the 2^{nd} to 6^{th} passage were used for the experiments.

Preparation of test compound dilutions

A stock solution with a concentration of 10^{-3} M was prepared in pure ethanol of PX-13, PX-18 and betamethasone. The stock dilutions were diluted with pure ethanol to obtain concentrations of 10^{-4}, 10^{-5}, 10^{-6} and 10^{-7} M. The dilutions of the test substances were stored at -80°C until use (maximum of 3 months). During the MTT assay and the Neutral red assay the samples were diluted 1:100 with cell culture medium that final concentrations of 10^{-5}, 10^{-6}, 10^{-7}, 10^{-8} and 10^{-9} M were obtained.

MTT assay

For the MTT assay 20 000 fibroblasts per well were seeded to a 24-well plate. In the case of keratinocytes 40 000 cells were seeded to each well of the 24-well plate. The number of cells was quantified using a Neubauer counting chamber. After 24 hrs in case of fibroblasts the medium was changed from FGM to FBM. For keratinocytes the medium was renewed using KGM. Fibroblasts and keratinocytes were stimulated with the test substances which were diluted in ethanol. The final concentration of ethanol was 1% in each treated well. As a control the cells were stimulated with 1% ethanol. To obtain a blank value cells were placed in medium only. After 48 hrs, under exclusion of light, 50 µl of the MTT-solution were added to each well leaving out the blank. The plates were stored in darkness for 4 hrs at 37°C and 5% CO_2. The supernatant was removed and 250 µl DMSO were added for cell lyses and to dissolve the blue colored formazan derivate. The plates were allowed to shake for 5 min on a plate shaker. The absorbance of each well was measured at a wavelength of 540 nm using an plate reader. The cell viability was calculated using the following equation:

$$Viability\ [\%] = \frac{Absorbance_{Sample} - Absorbance_{Blank}}{Absorbance_{Control} - Absorbance_{Blank}} \times 100$$

Neutral red assay

To perform the Neutral red assay 20 000 fibroblasts or 40 000 keratinocytes respectively were seeded to each well of a 24-well plate. A Neubauer counting chamber was used to quantify the number of cells. After 24 hrs the cell culture medium was changed. In case of fibroblasts the medium was changed from FGM to FBM. In case of keratinocytes the KGM was renewed. The cells were stimulated with the test substances which were diluted in ethanol. The final ethanol concentration in each well was 1%. 1% ethanol in cell culture medium served as a control. The blank value was obtained by placing the cells in cell culture medium. After 48 hrs cells were washed with 500 µl PBS and 500 µl FBM containing Neutral red or KGM containing Neural red respectively were added under exclusion of light. To obtain the blank cell culture medium without Neutral red was used. The plates were incubated in darkness at 37°C and 5% CO_2 for 3 hrs. Then the cell culture medium was decanted and the cells were washed with 250 µl PBS. 250 µl Neutral red desorb were added to each well [215]. After shaking the plates using a plate shaker for 5 min, the absorbance was measured at a wavelength of 540 nm using a plate reader. The measured absorbance correlates directly with the vitality of the cells and can be calculated using the same equation as for the MTT assay.

2.5.1.3 Results and discussion

A balance between therapeutic and toxicological effects of a compound is an important parameter when evaluating its potential as a pharmaceutical drug. Cell cultures can be used to evaluate basic cytotoxicity and target organ toxicity. Biological relevant *in vitro* test systems for skin irritation are human epidermal keratinocytes and human dermal fibroblasts (Figure 2.5.1.3-1).

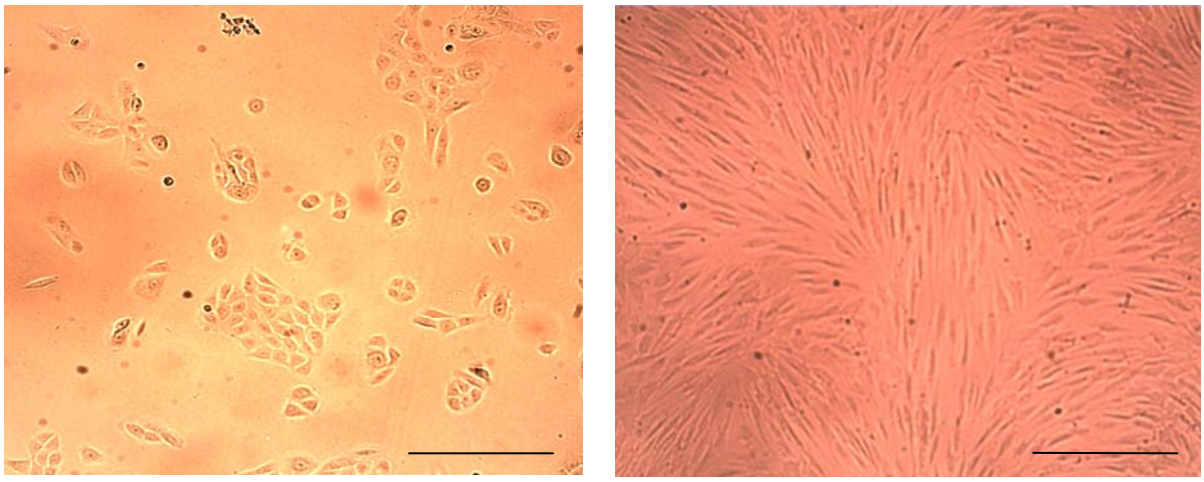

Figure 2.5.1.3-1: Light microscope pictures of human primary keratinocytes (left) and human primary fibroblasts (right) magnified 10-times (bar refers to 500 µm).

Evaluation of the cytotoxic potential on keratinocytes

A viability reduction of 30% is considered to correlate with a toxic effect on the cells [209]. Figure 2.5.1.3-2 shows the results obtained by MTT assay applying betamethasone, PX-13 and PX-18 to keratinocytes.

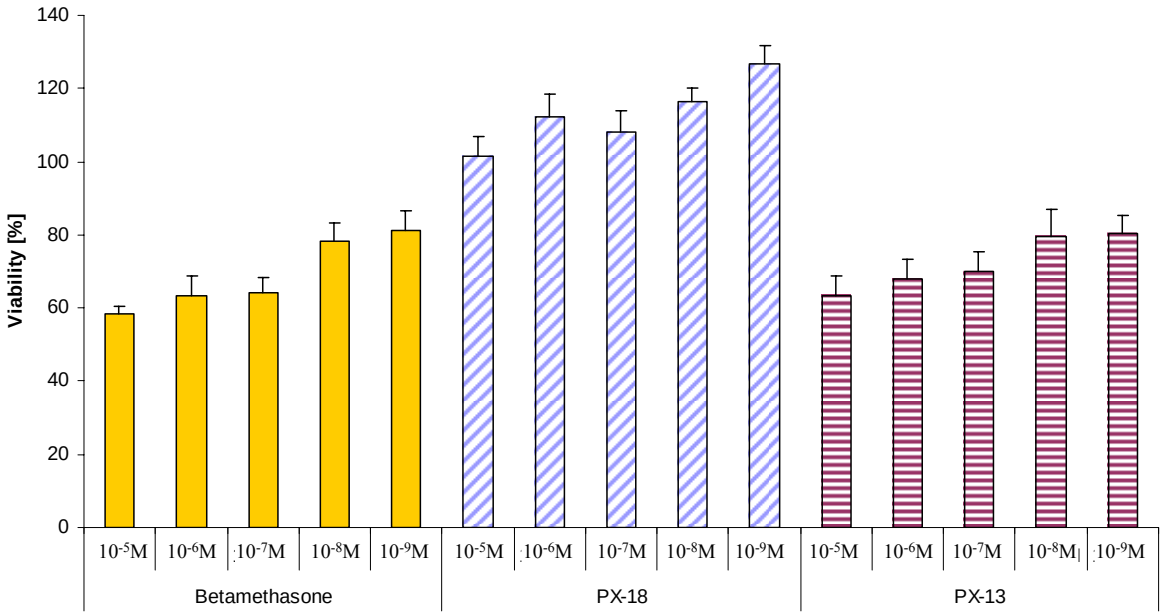

Figure 2.5.1.3-2: Viability of keratinocytes after treatment with 10^{-5}, 10^{-6}, 10^{-7}, 10^{-8} and 10^{-9} M betamethasone, PX-18 and PX-13 found with the MTT assay (n = 12; $\bar{x}$ ± RSD).

For betamethasone with concentrations of 10^{-5} M to 10^{-7} M a reduction of viability in comparison to control keratinocytes was found to be about 40%. That means betamethasone is considered to be toxic in these concentrations. No toxic effect was found for betamethasone with concentrations of 10^{-8} M and 10^{-9} M. In these concentrations the viability of keratinocytes was found to be 80%.

For PX-18 with all applied concentrations no toxic effect was found. The survival rate of keratinocytes was similar to the survival rate of the control at all tested concentrations.

A reduction of viability of keratinocytes of 37% was found in the MTT assay for 10^{-5} M PX-13. 30% reduction of viability was obtained if keratinocytes were treated with 10^{-6} M and 10^{-7} M PX-13. These concentrations are considered to be toxic for keratinocytes under the test conditions. By applying PX-13 with a concentration of 10^{-8} M and 10^{-9} M no toxic effect was found. The survival rate of keratinocytes was about 80%.

Figure 2.5.1.3-3 shows the results obtained by Neutral red assay performed on keratinocytes with betamethasone, PX-18 and PX-13.

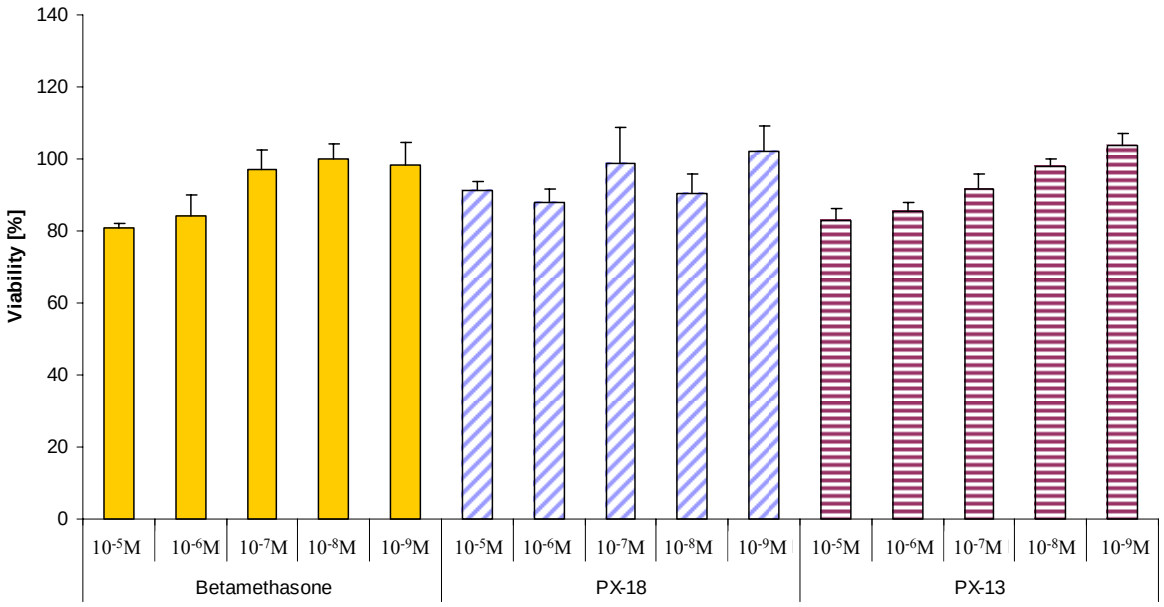

Figure 2.5.1.3-3: Viability of keratinocytes after treatment with 10^{-5}, 10^{-6}, 10^{-7}, 10^{-8} and 10^{-9} M betamethasone, PX-18 and PX-13 found with the Neutral red assay (n = 12; $\bar{x}$ ± RSD).

Betamethasone did not show any toxic effects in the Neutral red assay performed on keratinocytes. For betamethasone with a concentration of 10^{-5} M the cell viability was found to be 80%. A concentration of 10^{-6} M betamethasone applied to keratinocytes showed a cell viability of 85%. All other tested betamethasone concentrations showed a cell viability of about 100%.

No toxic effects were found for PX-18. The viability of cells was over 90% for all tested concentrations.

For PX-13 no toxic effect was found on keratinocytes with the Neutral red assay. 10^{-5} M and 10^{-6} M of PX-13 applied to keratinocytes showed a cell viability of approximately 85%. All other tested concentrations showed cell viability of about 100%.

All in all no toxic effect was found for all tested compounds on keratinocytes by Neutral red assay under the test conditions. By MTT assay performed on keratinocytes no toxic potential was found for PX-18. The toxic potential found by MTT assay of PX-13 was similar to the one of betamethasone. Betamethasone and PX-13 in concentrations of 10^{-5} to 10^{-7} M showed a reduction in cell viability of more than 30% in the MTT assay.

Evaluation of the cytotoxic potential on fibroblasts

A reduction of 30% of the viability parameters in comparison to the control is considered to correlate to a toxic effect on the cells [209]. Figure 2.5.1.3-4 provides an overview of the results obtained testing the cytotoxic potential of betamethasone, PX-18 and PX-13 with the MTT assay on human primary fibroblasts.

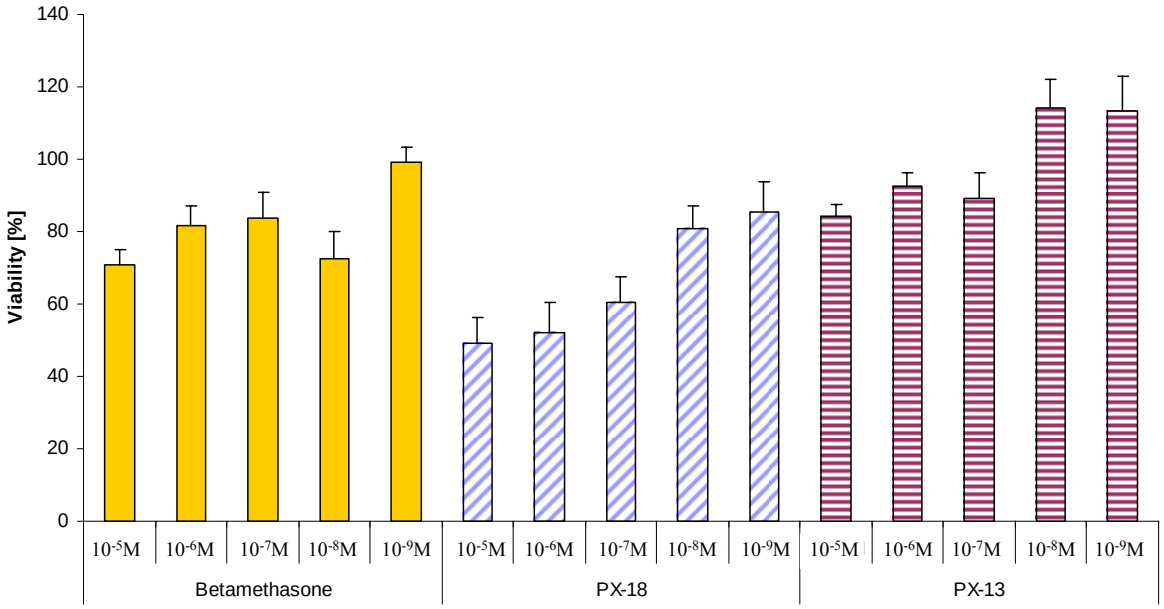

Figure 2.5.1.3-4: Viability of fibroblasts after treatment with 10^{-5}, 10^{-6}, 10^{-7}, 10^{-8} and 10^{-9} M betamethasone, PX-18 and PX-13 found with the MTT assay (n = 12; $\bar{x}$ ± RSD).

Betamethasone did not show a toxic effect under the test conditions. The cell viability in all tested concentrations is higher than 70%.

For PX-18 a toxic effect on fibroblasts was found with concentrations from 10^{-5} M to 10^{-7} M. 10^{-5} M PX-18 applied to fibroblasts under the test conditions reduced the viability by 50%. A decrease of cell viability of 48% was found for 10^{-6} M PX-18 and of 40% for 10^{-7} M PX-18 respectively. No toxic effect was found with the MTT assay after applying PX-18 to fibroblasts with a concentration of 10^{-8} M and 10^{-9} M. The cell viability at those concentrations was 80% and 85% respectively.

Testing PX-13 on fibroblasts with the MTT assay no toxic effect could be found. Cell viability for all tested concentrations was ranging between 85% and 115%.

Figure 2.5.1.3-5 shows the results of the Neutral red assay performed on fibroblasts with betamethasone, PX-18 and PX-13.

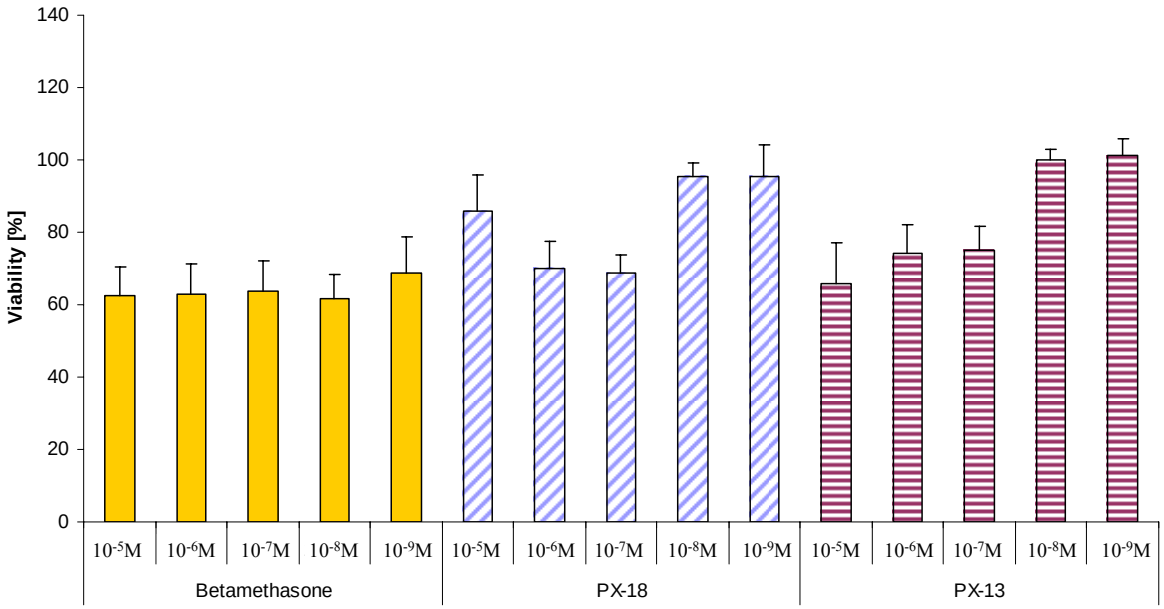

Figure 2.5.1.3-5: Viability of fibroblasts after treatment with 10^{-5}, 10^{-6}, 10^{-7}, 10^{-8} and 10^{-9} M betamethasone, PX-18 and PX-13 found with the Neutral red assay (n = 12; $\bar{x}$ ± RSD).

Toxic effects on fibroblasts were found by Neural red assay for betamethasone in all tested concentrations. The cell viability of fibroblasts after the application of betamethasone was ranging between 62% and 68% for the tested concentrations.

For PX-18 cell viability values ranging between 70 and 95% were found. Applying PX-18 in a concentration of 10^{-6} and 10^{-7} M reduced the cell viability by 30%. At a concentration of 10^{-5} M a higher viability was found. However, due to the high standard deviation there was no significatnt difference to 10^{-6} and 10^{-7} M. Concentrations of 10^{-8} and 10^{-9} M did not show toxic effects under the test conditions.

For PX-13 a toxic effect was found at a concentration of 10^{-5} M. At this concentration the cell viability was reduced by 34%. At all other concentration levels tested of PX-13 no toxic effects could be seen. The values of the cell viability were 75% for 10^{-6} and 10^{-7} M PX-13 and 100% for 10^{-8} and 10^{-9} M PX-13 respectively.

Summarizing the results of the MTT assay performed on fibroblasts, no toxic effects were found for PX-13 and betamethasone in all tested concentrations. For PX-18 toxic effects were found for 10^{-5} M to 10^{-7} M under the test conditions, while the concentrations of 10^{-8} M and 10^{-9} M did not show a toxic effect. In the Neutral red assay performed on fibroblasts a toxic effect was found for betamethasone in all tested concentrations. PX-18 and PX-13 showed a less toxic potential on fibroblasts in the Neutral red test than betamethasone. For PX-18 toxic

effects were only found at a concentration of 10^{-6} and 10^{-7} M. PX-13 showed a toxic effect on fibroblasts in the Neutral red assay after applying it in a concentration of 10^{-5} M.

The two different endpoints were used in order to obtain information about the cytotoxicity *in vitro*. The MTT reduction assesses the functional intactness of mitochondria based on the enzymatic reduction of a tetrazolium salt by the mitochondrial dehydrogenase of viable cells. The Neutral red assay is a measure of lysosomal integrity, as it reflects the capacity of viable cells to incorporate vital dye into these organelles. The use of different tests may provide some evidence of the toxicity mechanism of a compound [216]. With regards to the contradiction of the data obtained on keratinocytes and fibroblasts it seems not to be completely founded to conclude that PX-18 or PX-13 affects rather the mitochondrial succinate dehydrogenases than the lysosomal membrane.

Comparing the results obtained in keratinocytes and fibroblasts, it can be seen that keratinocytes are less sensitive than fibroblasts to irritation. This was also found in previous studies [217, 218]. However, it is preferable to use keratinocytes as well for the evaluation of the cytotoxical potential since they are the first target cell type exposed to a dermal applied compound.

In general, *in vitro* skin cultures are useful to designing safer, more efficient and more cost effective human skin irritation tests. *In vitro* cytotoxicity has been found to predict skin irritation to a large extent [204, 205, 219, 220]. For PX-13 and PX-18 it was found that the cytotoxic potential of these compounds on primary human keratinocytes and fibroblast monolayer cell cultures is similar to or even less than the cytotoxic potential of betamethasone, one of the compounds used as standard therapy for inflammatory skin diseases. Therefore, further investigations on the dermal safety of the PLA_2 inhibitors PX-13 and PX-18 seamed to be useful.

2.5.2 Evaluation of the skin irritation potential using reconstructed human epidermis

2.5.2.1 Introduction

Skin irritation is defined as a locally arising, non-immunogenic, reversible reaction, which appears shortly after stimulation [221]. In general, the physiological response to a chemical stimulus applied to the skin is irritation, which involves objective changes like local redness and oedema and subjective changes like pruritus and pain. Before humans can be exposed, the tendency of new compounds to cause skin irritation must be determined. Traditionally the skin irritation potential is evaluated by the Draize skin irritation test [222, 223]. In this test the test materials are applied to the shaved skin of rabbits for 4 hrs and the appearance of oedema and/or erythema is evaluated 1, 24, 48 and 72 hrs after application. Products can be classified according to a scoring system [224]. The Draize test has many disadvantages. The subjective nature of the visual rating system, its arguable extrapolation to humans because rabbit skin and human skin have different physiological properties and show different responses [225, 226], its costs and the fact that the animals can suffer. The effort to reduce, refine and replace animal tests led to the development of *in vitro* and human skin irritation tests [227]. Skin irritation can be evaluated on healthy volunteers in clinical trials (patch test) with medical surveillance. Nevertheless, for ethical, scientific and economic reasons, preliminary tests need to be performed. These tests are based on *in vitro* methods e.g. monolayer keratinocytes cell cultures, human tissue which can be cadaver skin, biopsy material or skin from cosmetic surgery and three-dimensional reconstructed human epidermis cultures. Three-dimensional cultures of skin epithelial cells represent an attractive *in vitro* system as alternative to *in vivo* tests because they simulate the multilayer tissue architecture present *in vivo* which provide a sufficient complexity to mimic the human skin barrier and cell viability [228]. Three-dimensional cell cultures are generated by growing keratinocytes cultures at the air-liquid interface on de-epidermized dermis, acellular or fibroblast-populated dermal substrates such as inert filters or collagen matrix. The cultures exhibit a well-stratified and cornified epidermis, with basal, spinous and granular layer along with a functional stratum corneum [229].

Reconstructed skin models possess several advantages for dermatoxicity testing. They are similar to the *in vivo* skin morphology and well standardised. They allow the measurement of quantifiable and objective endpoints relevant to *in vivo* irritation phenomena [230]. Their production in kit form makes them available for screening large amount of materials.

EPISKIN (SkinEthic laboratories, Nice, France), EpiDerm (MatTek Corporation, Ashland, USA), SkinEthic (SkinEthic laboratories, Nice, France) and Epidermal skin test 1000 (EST-1000) (CellSystems, St. Katharinen, Germany) are examples for commercially available human epidermis models. Materials can be tested regardless their physicochemical properties. There are also drawbacks of reconstructed epidermis models. Some divisions in tissue homeostasis and barrier properties in comparison to normal human epidermis still need to be optimized. All three-dimensional models show a higher permeability than human skin [231]. Furthermore, *in vitro* skin culture systems are typically composed of only one or two cell types. Many important cell types (e.g. melanocytes and Langerhans cells) and skin structures (e.g. sweat glands and hair follicles) are lacking in these systems.

The principle of the *in vitro* skin model irritation assay is based on the fact that irritant chemicals are able to penetrate the stratum corneum by diffusion and damage the cells of the underlying layers. The test chemical is applied for 15 min to the surface of the three-dimensional human epidermis model, followed by a post-treatment incubation period of 42 hrs and the subsequent assessment of their effect on cell viability by MTT assay. The reduction of cell viability in treated tissue is compared to a negative control and expressed in %. The % reduction in viability is used to predict the irritation potential according to EU classification system (R 38 or no label). If the cell viability is $\leq$ 50%, the chemical is classified as irritant (R 38). If the cell viability is > 50%, the chemical is classified as non irritant.

After an ECVAM (European Centre of the Validation of Alternative Methods) pre-validation study (1998-2000), followed by a test optimization period (2001-2004), the ECVAM Skin Irritation Validation Study has been performed (2004-2006). Initially the EPISKIN human skin model, the EpiDerm human skin model, PREDISKIN human skin (human skin from surgery), the pig ear test and the mouse skin integrity function test (SIFT) have been evaluated. From the five *in vitro* methods only the EPISKIN and the EpiDerm skin irritation test past through the whole pre-validation and validation tests. Both skin models provide a sufficient intra- and inter-laboratory reproducibility. Furthermore, the EPISKIN test has been found to be sufficiently sensitive and specific for a stand alone method that is able to fully replace the *in vivo* skin irritation test in rabbits [232]. Therefore, it was decided to use the EPISKIN test for the evaluation of the skin irritation potential of PX-18 and PX-13 as well as of the 5% PX-18 and 5% PX-13 nanosuspensions.

2.5.2.2 Materials and methods

2.5.2.2.1 Materials

Ascorbic acid	Sigma Aldrich, Deisenhofen, Germany
Biopsy punch	SkinEthic laboratories, Nice, France
EPISKIN-SM™ (0.38 cm^2)	SkinEthic laboratories, Nice, France
FLUOstar Optima	GMB Labtech, Offenburg, Germany
Incubator Hera cell 240	Heraeus, Hanau, Germany
HCl	Sigma Aldrich, Deisenhofen, Germany
Isopropanol	Sigma Aldrich, Deisenhofen, Germany
MTT (3-(4,5-dimethylthiazole-2-yl)-2,5-diphenyl-tetrazolium bromide)	Sigma Aldrich, Deisenhofen, Germany
Sodiumdodecyl sulphate (SDS)	Sigma Aldrich, Deisenhofen, Germany
Tissue culture test plates 12	TPP, Trasadingen, Switzerland

2.5.2.2.2 Methods

Test for direct MTT reduction of the test materials

To identify a possible interference between MTT and the test compounds, each test substance was checked for its ability to reduce MTT directly against references. 2 ml of 0.3 mg/ml MTT solution were filled in the wells of a 12-well plate for testing 1% Tween 80 aqueous solution, 2% Plantacare® 2000 aqueous solution, PX-18 powder, PX-13 powder, 5% PX-18 nanosuspension, 5% PX-13 nanosuspension, PBS as negative control and ascorbic acid as positive control under exclusion of light. 10 µl of liquids or 10 mg of solids respectively were added to the MTT solution and mixed. The mixture was incubated for 3 hrs at 37°C in darkness. If there is no direct reduction the MTT solution stays yellow. If in the MTT solution the formation of blue crystals can be observed, the substance interacts with MTT. It is then necessary to evaluate the non specific reduction of MTT during the EPISKIN test.

EPISKIN test

EPISKIN is a three-dimensional human epidermis model which was first developed by Tinois [233]. Adult human-derived epidermal keratinocytes are seeded on a dermal substitute consisting of collagen type I matrix coated with type IV collagen. A highly differentiated and stratified epidermis model is obtained after 13 days. The EPISKIN model consists of a basal,

supra basal, spinous and granuar layer as well as a functional stratum corneum. The EPISKIN test was performed according to the SOP of the ECVAM Skin Irritation Validation Study [234].

Day 0

The EPISKIN kit was received and parameters, which affect the quality of the assay, were checked. The epidermis units were transferred into 2 ml of pre-warmed maintenance medium and incubated for 24 hrs at 37°C and 5% CO_2.

3 mg/ml MTT stock solution in PBS buffer, 0.04 N HCl in isopropanol and 5% (w/v) SDS solution in water were prepared. The solutions were stored refrigerated and protected from light until use.

Day 1

10 µl in case of liquids and 10 mg in case of solids were applied in triplicate to the surface of the tissues. 10 µl PBS served as negative control. 10 µl of 5% SDS were used as positive control. To improve the distribution of the positive control the material was respreaded after 7 min contact time. The materials were rinsed of the tissue with 25 ml sterile PBS after a contact time of 15 min. Remaining PBS was removed from the tissue by tapping them on an absorbent paper and sweeping the surface with a cotton-bund. The tissue units were then transferred into 2 ml of fresh maintenance medium, followed by a 42 hrs post-incubation period at 37°C and 5% CO_2.

Day 4

MTT stock solution was diluted with assay medium to a final concentration of 0.3 mg/ml. The tissue units were transferred to 2 ml 0.3 mg/ml MTT solution and incubated for 3 hrs in darkness. A biopsy was done of the epidermis using a biopsy punch. The epidermis was separated from the collagen matrix and both parts placed in a micro tube. 500 µl acetic isopropanol were added. Samples were vortexed and stored for 4 hrs at room temperature. After mixing the samples 2x 200 µl of each sample were transferred to a 96-well plate and the absorbance was measured using a plate reader at 570 nm. The blank value was obtained by measuring the absorbance of acetic isopropanol. The tissue viability was calculated using the following equation:

$$Viability\ [\%] = \frac{Absorbance_{Sample} - Absorbance_{Blank}}{Absorbance_{Negative\ Control} - Absorbance_{Blank}} \times 100$$

2.5.2.3 Results and discussion

The relative conversion of MTT by the epidermal tissue is the parameter evaluated in the EPISKIN assay. A test substance may directly reduce MTT and mimic dehydrogenase activity of the cellular mitochondria. To exclude the interference of the test materials with MTT, the test for direct MTT reduction was performed. The results of this test are shown in Figure 2.5.2.3-1. Ascorbic acid, an easily oxidized compound, was used as a reference showing the reduction of MTT to the blue formazan derivate within 3 hrs incubation time. Neither Tween 80 and Plantacare® 2000 used as stabilisation agents for the nanosuspensions, nor PX-18 and PX-13 or the according nanosuspensions reduced MTT. Therefore, no interaction of the tested materials with the endpoint assessed in that EPISKIN assay is expected.

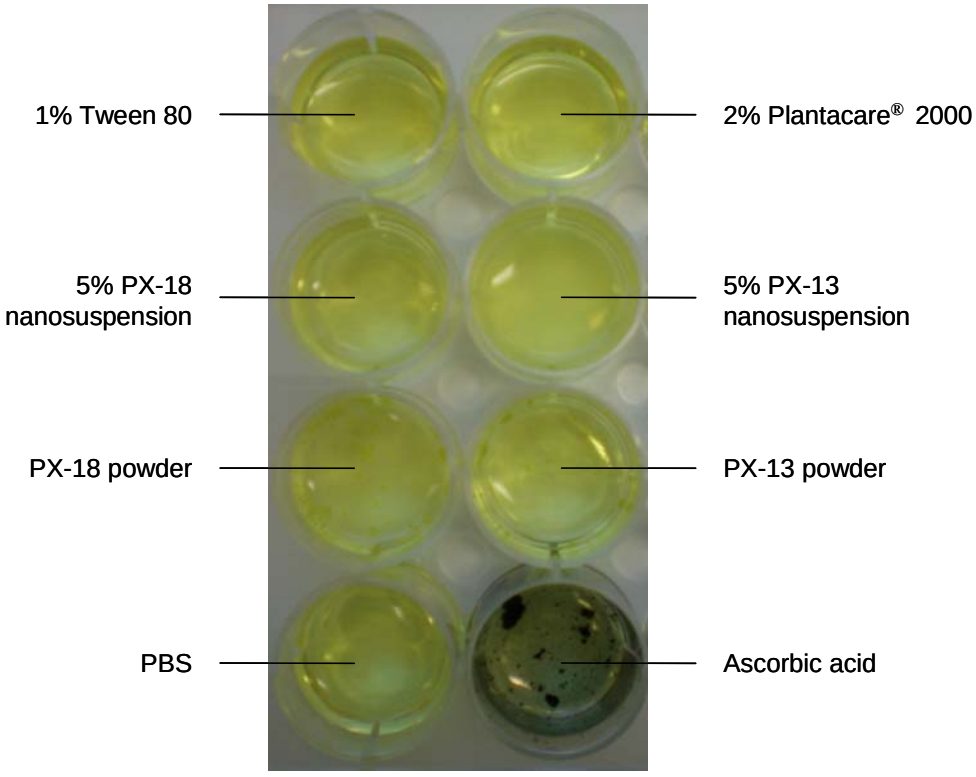

Figure 2.5.2.3-1: Results of the test for direct MTT reduction of the test compounds: MTT stays yellow after exposing it for 3 hrs under light exclusion to 1% Tween 80, 2% Plantacare® 2000, 5% PX-18 nanosuspension, 5% PX-13 nanosuspension, PX-18, PX-13 and PBS. These substances do not interact with MTT. Ascorbic acid, an easily oxidized substance, reduces MTT under the test conditions and the formation of the blue formazan derivate can be observed.

An irritation potential of a test material according to EU classification (R38 or no label) is predicted, if the mean relative tissue viability of three individual tissues exposed to the test substance is less than 50% of the mean viability of the negative control e.g. PBS [228].

Figure 2.5.2.3-2 shows the results of the EPISKIN test obtained with 5% SDS as positive control, PBS as negative control, PX-18 powder, 5% PX-18 nanosuspension, PX-13 powder and 5% PX-13 nanosuspension.

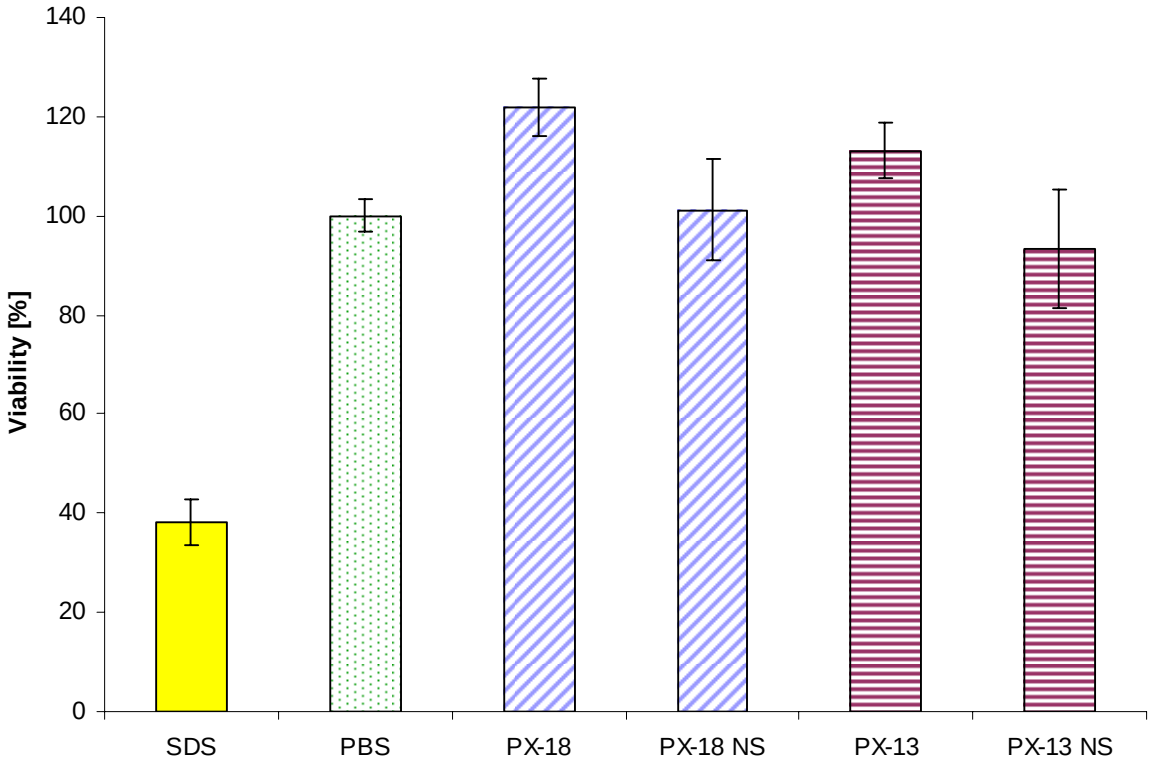

Figure 2.5.2.3-2: Percentage tissue viability (MTT reduction) obtained in the EPISKIN test with 5% SDS as positive control (SDS), PBS as negative control, PX-18 powder (PX-18), 5% PX-18 nanosuspension (PX-18 NS), PX-13 powder (PX-13) and 5% PX-13 nanosuspension (PX-13 NS).

The mean value of tissue viability (MTT reduction) of the negative control was set 100% and the corresponding percentage of tissue viability for the positive control, PX-18 powder, 5% PX-18 nanosuspension, PX-13 powder and 5% PX-13 nanosuspension were calculated. The mean viability of the tissues treated with 5% SDS was 38% ± 4.7. Therefore, the positive control fulfils the requirements (viability ≤ 40%; SD ≤ 20). The raw materials PX-18 and PX-13 showed a mean tissue viability of 122% ± 5.8 and 113% ± 5.5 respectively. 5% PX-18 nanosuspension and 5% PX-13 nanosuspension showed a tissue viability of 101% ± 10.1 and 93% ± 11.9. Therefore, PX-18 and PX-13 powder as well as both nanosuspensions can be classified as non irritant to the skin according to the EU classification system.

Human data are certainly the most informative data for the evaluation of the skin irritation potential. But they are available only for a few compounds and strongly depend on the

protocol used for their evaluation, the age, the anatomical site and the seasonal variability [235]. Biophysical properties of *in vivo* human epidermis are mimicked by *in vitro* reconstructed human epidermal tissue. However, its barrier function seems less effective compared to adult skin [236]. While this would certainly limit their use for penetration studies, it can be an advantage in skin irritation testing for test compounds which are only mild irritant. The limited barrier function leads to a higher sensitivity to the applied test samples [237]. Therefore, when no toxic effect is observed on reconstructed human epidermis, the material can be considered to cause no irritation after dermal application to humans [238]. Nevertheless, it should be kept in mind, that until now with the EPISKIN test it can only be differentiated between skin irritant and non-irritant. It is not possible to differentiate skin irritants from mild irritants from non-irritants as defined by the Global Harmonised System (GHS).

The reconstructed human epidermis models allow measuring quantifiable and objective endpoints relevant to *in vivo* irritation phenomena. The MTT assay has been well validated for the assessment of cytotoxicity of skin cells due to the exposure to test materials [239, 240]. Furthermore, *in vitro* tests using reconstructed human epidermis lead to reproducible results, which can be used for a definite classification of the tested materials [230, 241, 242]. The MTT values obtained in this study for each sample were of the same order of magnitude. The standard deviation of the obtained viability values ranged from 4.7 to 11.9. The reproducibility is therefore better than the one of the Draize test [243] and the human patch test [244].

By evaluating the skin irritation potential using the EPISKIN assay, it can be concluded, that the $sPLA_2$ inhibitors PX-18 and PX-13, as well as the according nanosuspensions with an active concentration of 5% (w/w) can be classified as non irritant to the skin according to the EU classification system. No skin irritation is expected after applying these compounds and nanosuspensions to the skin.

2.5.3 Evaluation of the eye irritation potential

2.5.3.1 General aspects

For the purpose of appropriate labeling of industrial products, in order to ensure protection of the customer as well as safety at the workplace, chemical substances need to be tested for their potential to cause irritation of/or injury to the eye. This applies especially to new formulations to be used in the household and for personal care (e.g. cosmetics) as well as medication intended to be applied topically [245]. The eye irritation potential has traditionally been scored using the Draize rabbit eye test [222]. This method has been used for more than 60 years in attempts to predict the human ocular irritancy of a wide variety of substances designed for industrial, pharmaceutical and cosmetic use. The method is based on the application of a test compound to the rabbit eye and the evaluation of the damage caused to the cornea, iris and conjunctiva. Ocular responses are scored 1, 24, 48 and 72 hrs as well as 7 days after application. The exposure of the rabbit eye to a foreign material may result in responses ranging from slight redness to severe injury with loss of the corneal epithelium, damage of the underlying stroma and loss of vision [224]. This test has a lot of disadvantages [246]. The high number of variables in the Draize rabbit eye test limits its reproducibility especially for moderate irritant compounds. Animals of the same species and strain can react in various ways to an applied test compound and different examiners can obtain different results from the same test. Furthermore, the anatomy and biochemistry of the rabbit eye is different to the one of the human eye. Rabbits have a lower tear production, a lower blink frequency and a lower surface sensitivity. It also should be taken into account that this test can be very painful to the rabbit. Due to all of these disadvantages of the Draize rabbit eye test, investigations have been done to find a suitable replacement for this test [247-249]. Tests under consideration are cell culture methods based on red blood cell haemolysis, neutral red uptake or fluorescein leakage, *ex vivo* tests on the isolated rabbit eye, on the isolated chicken eye or the bovine corneal opacity/permeability test, the hen's egg chorioallantoic membrane (HET-CAM) test as well as a physiochemical method based on protein precipitation (EYTEX^{TM}).

2.5.3.2 The hen's egg test on the choriallantic membrane (HET-CAM)

In 1985 the HET-CAM test was developed by Lüpke [250]. This test serves as a model of the mucous ocular tissue. It is assumed that the adverse effect provoked by irritating substances on the small blood vessels and proteins of the choriallantoic membrane (CAM) are similar to the response they might produce on the eye. The potential irritancy of compounds can be detected by the observation of adverse changes which occur on the CAM of an egg after exposure to test chemicals. Therefore, chemicals are placed directly onto the CAM of the hen's egg. The occurrence of vascular injury or coagulation in response to a tested compound is the basis for employing this technique as an indication of the potential of a chemical to damage mucous membranes (in particular the eye) *in vivo* [251]. Advantages of using the HET-CAM test for the evaluation of the irritant potential of a compound are its simplicity, rapidity, sensitivity, easy performance and its relative cheapness [251]. The major disadvantage of the HET-CAM test is the subjective nature of the evaluation of the results. This disadvantage can be overcome to a certain extent by the inclusion of positive standards and by the use of a comprehensive scheme for scoring the irritant effects of the tested compounds [251]. The HET-CAM test cannot be used for vasoactive test substances with a pharmacological effect on blood vessels, dyes which stain the CAM irreversible and sticky substances such as adhesives which cover the CAM [252]. A factor of consideration is whether the HET-CAM test is an animal experiment or not. For the HET-CAM test chicken eggs are used on day 9 of embryogenesis when nerve tissue and pain perception have not yet developed. At present the HET-CAM test is often looked upon as a borderline, although it is used to reduce the number of mammalians used in conventional testing (e.g. the Draize rabbit eye test) and to contribute towards a reduction in the associated suffering. In different studies it could be already shown, that with the HET-CAM test also only slightly irritant compounds can be identified reliably because of the high sensitivity of the CAM [245]. In some cases it is possible to predict the irritation potential even more reliable than with the Draize rabbit eye test [253].

2.5.3.3 Materials and methods

2.5.3.3.1 Materials

Acetic acid	Merck, Darmstadt, Germany
Eggs of the White Leghorn	Lohmann Tierzucht, Cuxhaven, Germany
NaOH	Merck, Darmstadt, Germany
SZX 12 Stereo microscope	Olympus, Hamburg, Germany
Texapone ASV 50	Henkel, Düsseldorf, Germany

2.5.3.3.2 Methods

Fresh, intact chicken eggs of the White Leghorn were used in this test. The eggs were incubated for 9 days using an incubator with automatic turning device (Brutmaschine Modell 3000/d, Butmaschinen-Janoschitz, Hammelburg, Germany) at 37.5 ± 0.5°C and a relative humidity of 62.5 ± 7.5%. Each egg was candled to ensure viability. Only eggs with an emergent embryonal vascular system were used for further testing. Eggs that have not been fertilized or have not undergone embryogenesis were rejected. The air spaces at the bunt end of the eggs were marked during candling. The egg shell was opened along the marked line. The egg membrane was moistened with a few µl of physiological saline. Immediately before application of the test substance the moistened egg membrane was carefully removed. Materials under investigation were PX-13 powder, PX-18 powder, 5% PX-13 nanosuspension, 5% PX-18 nanosuspension as well as an aqueous 2% Plantacare® 2000 solution and an aqueous 1% Tween 80 solution, to determine effects of the stabilizing surfactant used in the nanosuspension. In case of the PX powders, a quantity was applied, that covered approximately 50% of the CAM. In cases of liquids, 300 µl were applied to the CAM. Due to the fact, that PX-13 and PX-18 powder as well as the turbid nanosuspensions of the compounds were tested, the end-point assessment was performed. Therefore, each test substance was tested on 6 prepared eggs. After applying the test substance to the CAM a chronometer was started and after 3 min the test substance was rinsed off the CAM with physiological saline. Because any blood present may also be rinsed off the CAM, a weak haemorrage could be overlooked immediately after rinsing. In order to avoid this, the CAM was assessed 30 sec after rinsing. Haemorrhage, lysis and coagulation were recorded semi-quantitatively by types as follows:

0 = none

1 = weak

2 = moderate

3 = strong reaction

For the quantitative evaluation of haemorrage, lysis and coagulation the following positive standards were applied to two eggs and the reactions seen defined as references for the test [252]:

1. Haemorrhage

Haemorrhage is the bleeding out from blood vessels of the CAM.

Weak:
- only fine blood vessels are bleeding and only small amounts of blood flow out
- 0.5% Texapone ASV 50 5 min contact

Moderate:
- fine and larger blood vessels are bleeding and a distinct amount of blood is flowing out
- 1% Texapone ASV 50 5 min contact

Strong:
- nearly all blood vessels are bleeding with a considerable amount of blood flowing out
- 5% Texapone ASV 50 5 min contact

2. Lysis

Lysis is the disappearance of small blood vessels on the CAM.

Weak:
- only small blood vessels lysing
- 0.5% Texapone ASV 50 5 min contact

Moderate:
- small and larger blood vessels are lysing
- 1% Texapone ASV 50 5 min contact

Strong:
- large blood vessels and whole cords lysing
- 5% Texapone ASV 50 5 min contact

3. Coagulation

Only large and medium sized blood vessels are taken into consideration. Thrombosis as an intravascular coagulation is recognizable as dark intravascular spots. Extravascular coagulation manifests as external dark spots. The opacity of the CAM can also increase.

Weak:
- only weak intra- and/or extravascular coagulation and/or slight increase in CAM opacity is observable
- coagulation: 0.2% (w/w) NaOH 5 min contact
- opacity: 0.3% (w/w) acetic acid 5 min contact

Moderate:
- moderate extravascular coagulation and/or moderate increase in CAM opacity is observable
- coagulation: 0.3% (w/w) NaOH 5 min contact
- opacity: 3% (w/w) acetic acid 5 min contact

Strong:
- severe extravascular coagulation and/or severe increase in CAM opacity is observable
- coagulation: 0.5% (w/w) NaOH 5 min contact
- opacity: 30% (w/w) acetic acid 5 min contact

A substance can be classified as none or only slightly irritant, if the sum of all scores (haemorrhage, lysis and coagulation) is less than 12. Classification as a moderately irritant is given, if the sum of all scores is between 12 and 16. Severe *in vivo* effects are expected, if the sum of all scores is equal or greater than 16 (Table 2.5.3.3-1).

Table 2.5.3.3-1: Overview of the classification of irritants in relation to the sum of the scores of haemorrhage, lysis and coagulation from 6 eggs evaluated after an application time of 3 min.

Sum of scores after 30 sec	Non/slightly irritant	Moderate irritant	Severely irritant
≤ 12	+		
> 12 < 16		+	
≥ 16			+

2.5.3.4 Results and discussion

Before starting the test with the test compounds, all standards were tested on 2 eggs and the results were recorded. Figure 2.5.3.4-1 shows exemplary a picture of an untreated CAM as well as a picture of all references used in the test.

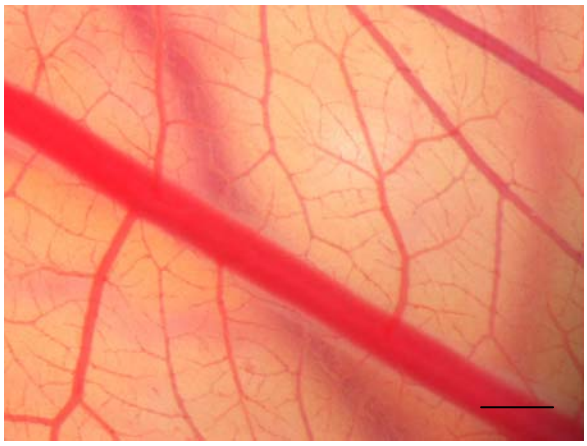

A: Picture of the CAM without treatment.

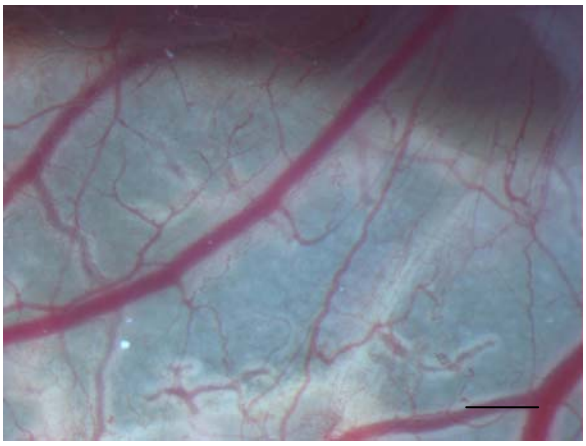

B: Weak haemorrage and lysis 5 min after applying 0.5% Texapone ASV 50 to the CAM.

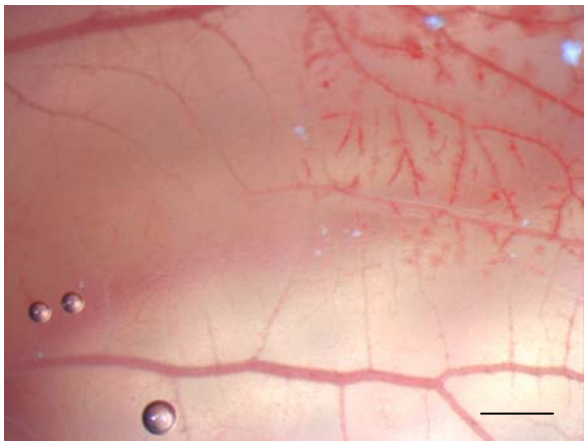

C: Moderate haemorrage and lysis 5 min after applying 1% Texapone ASV 50 to the CAM.

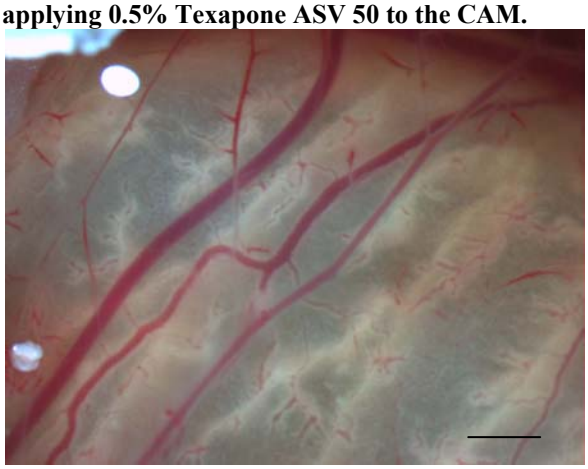

D: Strong haemorrage and lysis 5 min after applying 5% Texapone ASV 50 to the CAM.

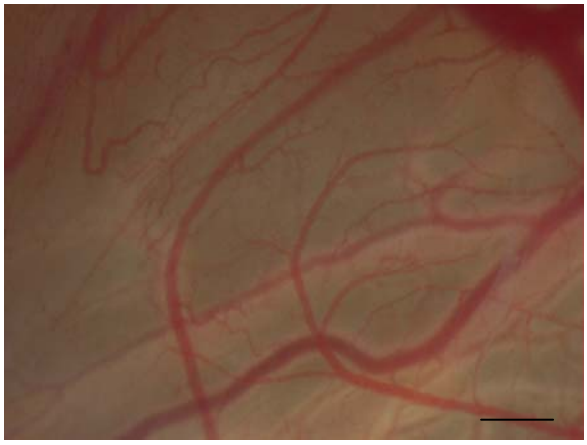

E: Weak opacity 5 min after applying 0.3% acetic acid to the CAM.

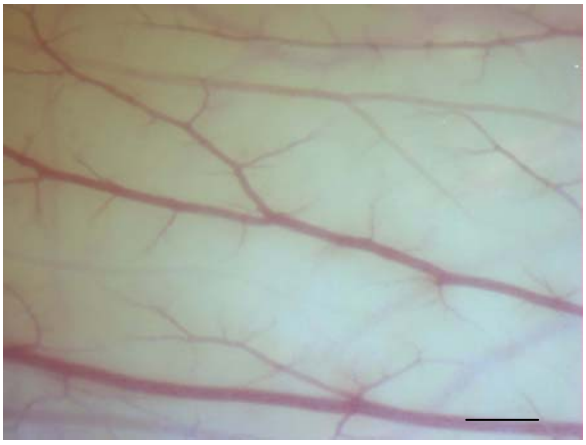

F: Moderate opacity 5 min after applying 3% acetic acid to the CAM.

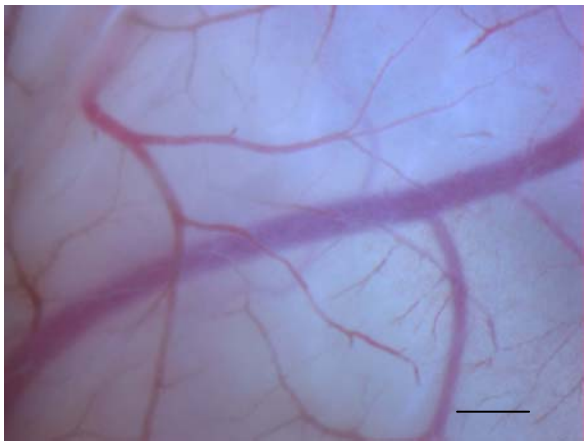

G: Strong opacity 5 min after applying 30% acetic to the CAM.

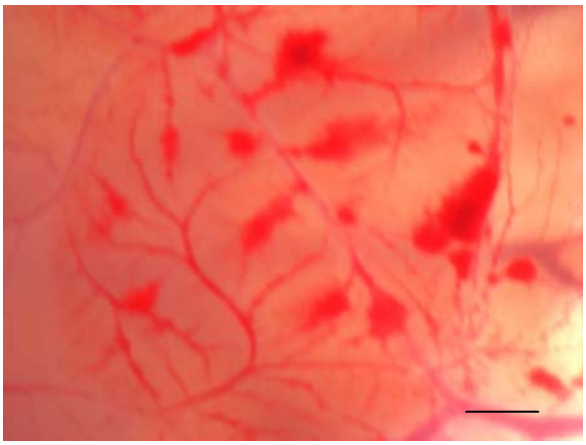

H: Weak coagulation 5 min after applying 0.2% NaOH to the CAM.

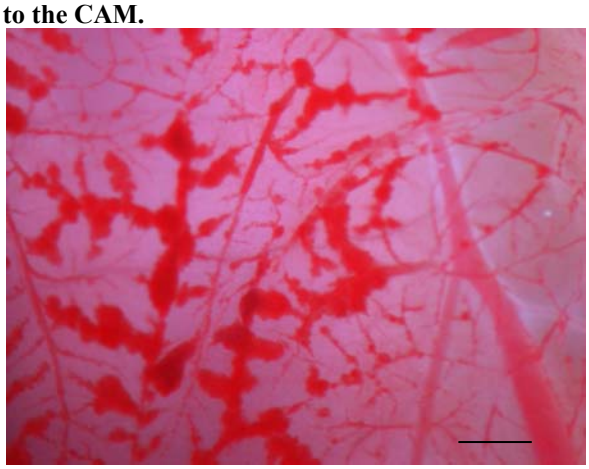

I: Moderate coagulation 5 min after applying 0.3% NaOH to the CAM.

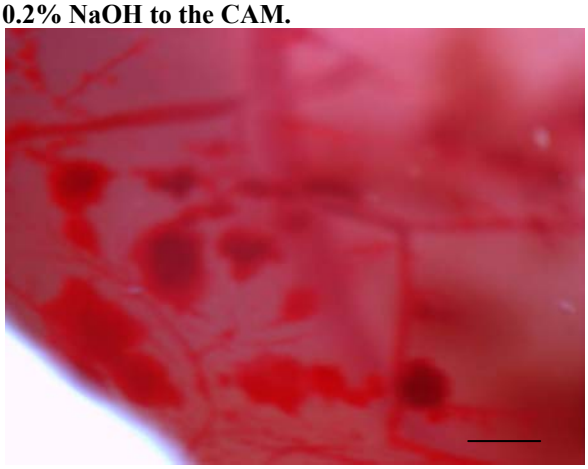

J: Strong coagulation 5 min after applying 0.5% NaOH to the CAM.

Figure 2.5.3.4-1: Reference pictures used for the evaluation of the irritation potential. The pictures A-J are magnified 63-times. The bars refer to 1 mm.

Comparing the results obtained after applying an aqueous 1% Tween 80 solution, an aqueous 2% Plantacare® 2000 solution, PX-13 powder, PX-18 powder, 5% PX-13 naosuspension and 5% PX-18 nanosuspension with the references, each egg was given scores with regards to the intensity of haemorrage, lysis and coagulation (0 = none; 1 = weak; 2 = moderate; 3 = strong reaction).

Figure 2.5.3.4-2 shows an example of a CAM before and after treatment with 1% Tween 80. It can be seen that no changes occurred on the CAM after treating it with 1% Tween 80. In Table 2.5.3.4-1 the scores given for each of the 6 egg tested are listed. For 1% Tween 80 the sum of all scores (haemorrhage, lysis and coagulation) from the 6 eggs assayed is 0. According to the test protocol applied 1% Tween 80 can be classified as non/slightly irritant.

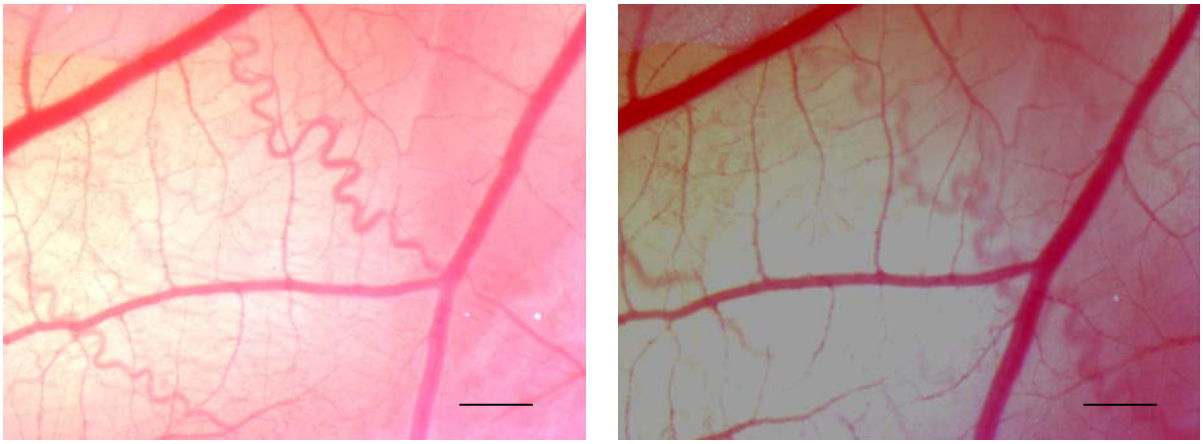

Figure 2.5.3.4-2: Picture of the CAM before treatment with 1% Tween 80 (left) and after treating with 1% Tween 80 for 3 min (right). The pictures are taken with a 63-times magnification. The bars refer to 1 mm.

Table 2.5.3.4-1: Scores given for each egg after application of 1% Tween 80 solution for 3 min.

Egg	Haemorrhage	Lysis	Coagulation	Sum of scores
1.	0	0	0	0
2.	0	0	0	0
3.	0	0	0	0
4.	0	0	0	0
5.	0	0	0	0
6.	0	0	0	0

Figure 2.5.3.4-3 shows an example picture of the CAM out of the 6 eggs tested before and after applying 2% Plantacare® 2000. A weak haemorrhage can be seen in the picture after applying 2% Plantacare® 2000 for 3 min to the CAM. Table 2.5.3.4-2 gives an overview of the scores given for each egg tested with 2% Plantacare® 2000. For 2% Plantacare® 2000 in water the sum of all scores (haemorrhage, lysis and coagulation) after 3 min is 3. Therefore, the 2% Plantacare solution can be classified as non/slightly irritant to the eye.

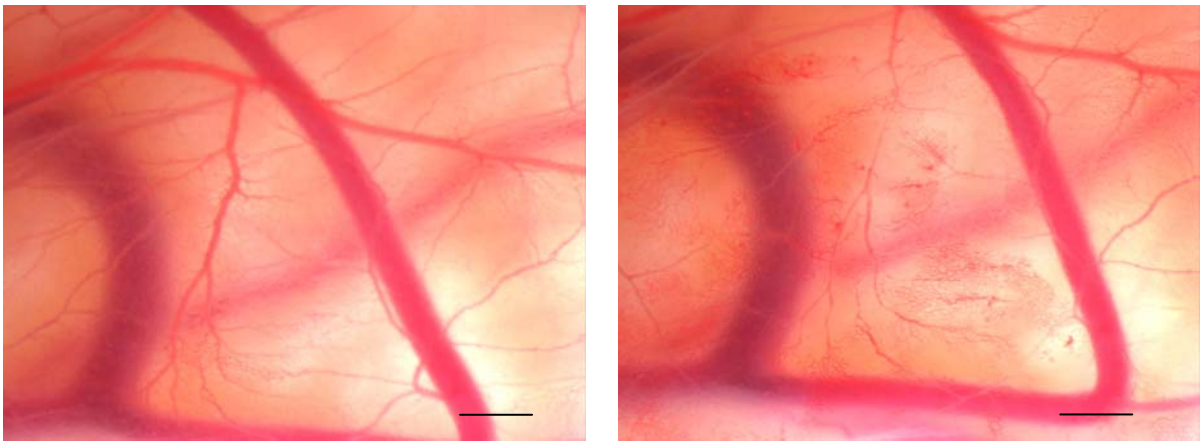

Figure 2.5.3.4-3: Picture of the CAM 63-times magnified before treatment (left) and after treatment with 2% Plantacare® 2000 for 3 min (right). The bars refer to 1 mm.

Table 2.5.3.4-2: Scores given for each of the 6 eggs tested after applying 2% Plantacare® 2000 solution for 3 min.

Egg	Haemorrhage	Lysis	Coagulation	Sum of scores
1.	0	0	0	0
2.	0	0	0	0
3.	1	0	0	1
4.	1	0	0	1
5.	0	0	0	0
6.	1	0	0	1

In Figure 2.5.3.4-4 an example of a CAM before treatment with PX-13 powder and after treatment with PX-13 powder for 3 min followed by rinsing with physiological saline can be seen. No changes on the CAM could be observed after treating the CAM with PX-13 powder. For PX-13 powder the sum of all scores (haemorrhage, lysis and coagulation) after 3 min is 0 (Table 2.5.3.4-3). Hence, it can be concluded that PX-13 applied as a powder has non/slight irritation potential.

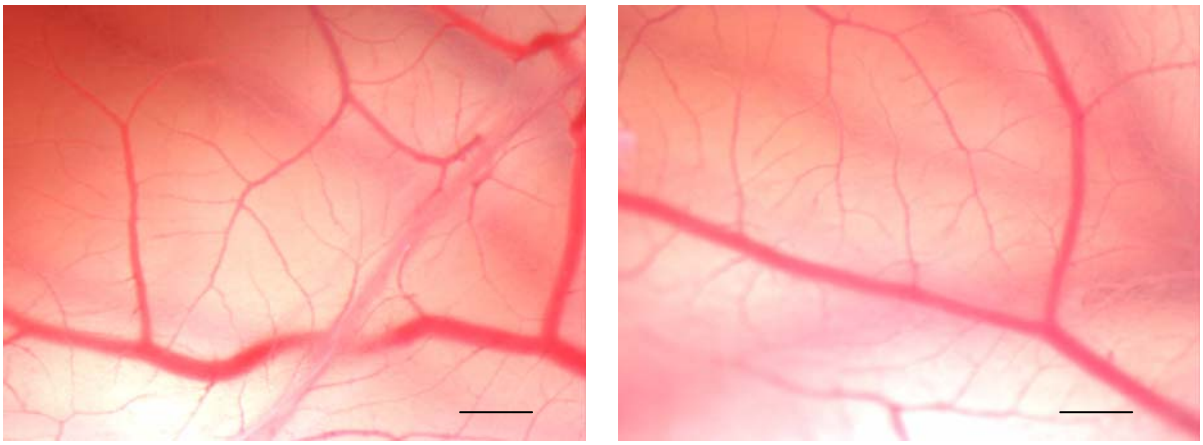

Figure 2.5.3.4-4: 63-times magnified pictures of the CAM before applying PX-13 powder to the CAM (left) and after treatment with PX-13 powder and rinsing with physiological saline (right). The bars refer to 1 mm.

Table 2.5.3.4-3: Scores given for each effect occurring on the CAMs of 6 eggs tested after applying PX-13 powder for 3 min and rinsing with physiological saline.

Egg	Haemorrhage	Lysis	Coagulation	Sum of scores
1.	0	0	0	0
2.	0	0	0	0
3.	0	0	0	0
4.	0	0	0	0
5.	0	0	0	0
6.	0	0	0	0

Figure 2.5.3.4-5 and Table 2.5.3.4-4 present the results obtained with PX-18 powder. In Figure 2.5.3.4-5 pictures of the CAM before and after the treatment with PX-18 powder are shown. It can be observed in the picture that no changes took place on the CAM after applying PX-18 powder for 3 min and rinsing it off afterwards. For PX-18 powder the sum of all scores (haemorrhage, lysis and coagulation) on all tested eggs is 1 (Table 2.5.3.4-4). PX-18 powder can therefore be classified as non/slightly irritant to the eye.

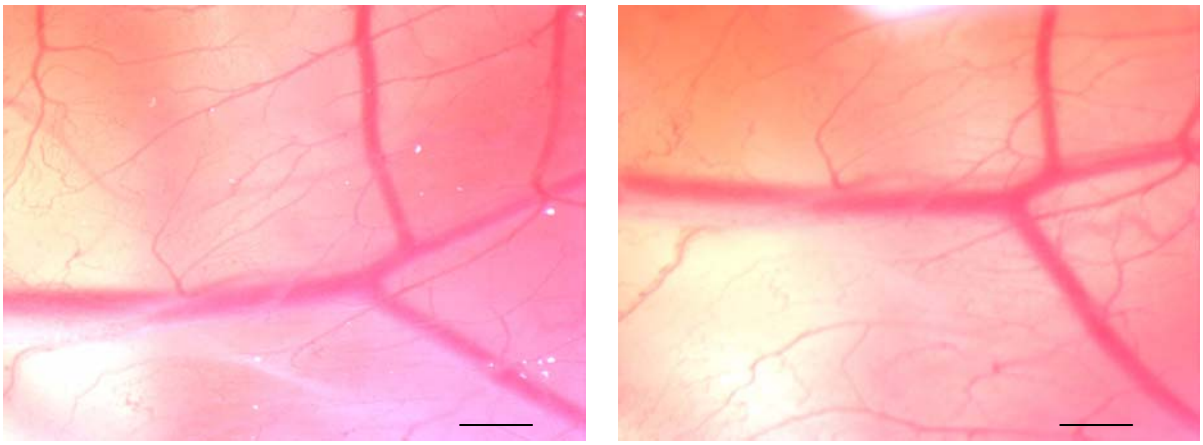

Figure 2.5.3.4-5: Pictures of the CAM before treatment with PX-18 powder (left) and after treatment with PX-18 powder for 3 min and rinsing with physiological saline (right). The pictures are magnified 63-times. The bars refer to 1 mm.

Table 2.5.3.4-4: Overview of the scores given for haemorrhage, lysis and coagulation on the 6 eggs tested with PX-18 powder.

Egg	Haemorrhage	Lysis	Coagulation	Sum of scores
1.	0	0	0	0
2.	0	0	0	0
3.	1	0	0	1
4.	0	0	0	0
5.	0	0	0	0
6.	0	0	0	0

Figure 2.5.3.4-6 shows an example of a CAM before and after treatment with 5% PX-13 nanosuspension. No changes on the CAM can be observed in this picture. Table 2.5.3.4-5 provides an overview of the results obtained with the 6 eggs tested. For 5% PX-13 nanosuspension the sum of all scores (haemorrhage, lysis and coagulation) on 6 treated eggs is 4. 5% PX-13 nanosuspension can be classified as non/slightly irritant to the eye.

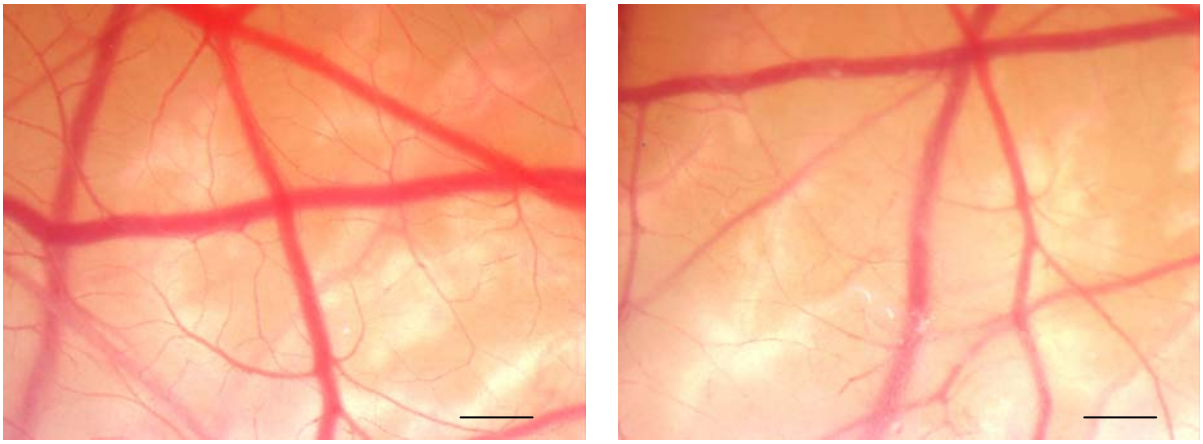

Figure 2.5.3.4-6: 63-times magnified pictures of the CAM before treatment with 5% PX-13 nanosuspension (left) and after treatment with 5% PX-13 nanosuspension for 3 min and rinsing with physiologic saline (right). The bars refer to 1 mm.

Table 2.5.3.4-5: Scores given for haemorrhage, lysis and coagulation after application of 5% PX-13 nanosuspension to the CAM of 6 eggs.

Egg	Haemorrhage	Lysis	Coagulation	Sum of scores
1.	0	0	0	0
2.	0	0	0	0
3.	0	1	0	1
4.	0	0	0	0
5.	1	1	0	2
6.	1	0	0	1

Figure 2.5.3.4-7 shows an example of a CAM before and after treatment with 5% PX-18 nanosuspension for 3 min followed by rinsing with physiological saline. It can be observed that no changes have taken place on the CAM. Table 2.5.3.4-6 gives an overview of the results obtained on each egg. For 5% PX-18 nanosuspension the sum of all scores (haemorrhage, lysis and coagulation) is 2. According to the applied test scheme 5% PX-18 nanosuspension can be classified as non/slightly irritant to the eye.

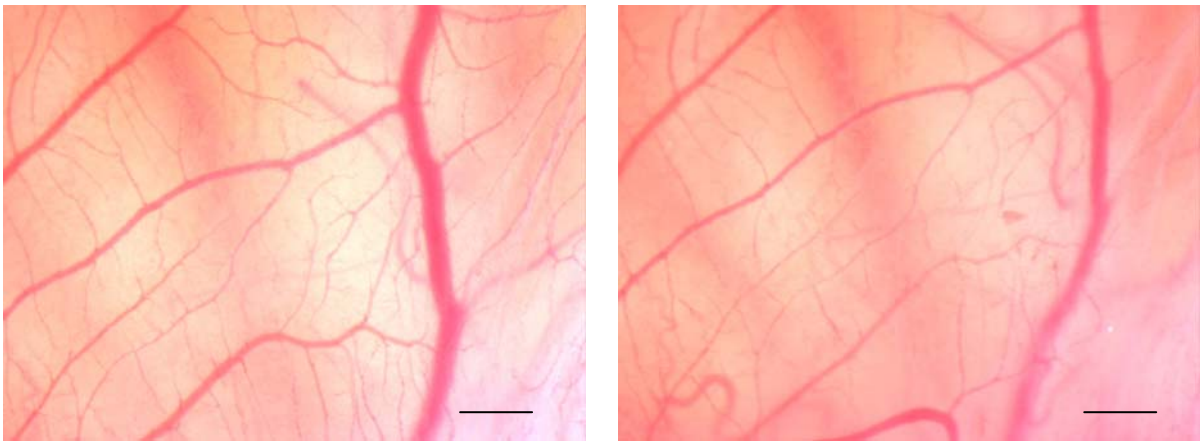

Figure 2.5.3.4-7: Picture of the CAM before treatment (left) and after treatment with 5% PX-18 nanosuspension for 3 min followed by rinsing with physiological saline (right). The pictures were taken with a 63-times magnification. The bars refer to 1 mm.

Table 2.5.3.4-6: Scores given for haemorrage, lysis and coagulation for each of the 6 eggs tested with 5% PX-18 nanosuspension.

Egg	Haemorrhage	Lysis	Coagulation	Sum of scores
1.	0	0	0	0
2.	0	1	0	1
3.	0	0	0	0
4.	0	0	0	0
5.	0	0	0	0
6.	0	1	0	1

All the tested materials did not show any moderate or strong reactions on the CAM. Intravascular or extravascular coagulation could not be observed after application of any of the test materials. Only weak haemorrhage and lysis could be seen on the CAM of some eggs after applying some of the test materials. Nevertheless, according to the test protocol applied, all tested formulations can be classified as non/slightly irritant to the eye because the scores given for haemorrhage, lysis and coagulation were smaller than 12 on the 6 eggs tested for all

test materials. Neither the powder of PX-13 or PX-18 nor the according nanosuspensions showed an irritation potential. Which means formulating the compounds as nanosuspensions does not increase the irritation potential.

Among all alternative tests developed to replace the Draize rabbit eye test the HET-CAM test is one of the most promising due to its sensitivity, reproducibility, simplicity and economy. The HET-CAM test has been intensively studied and validated. The results obtained with this test correlate well with the findings of the *in vivo* eye irritation test [254, 255]. The HET-CAM test was chosen to study the eye irritation potential of 1% Tween 80, 2% Plantacare® 2000, PX-13 powder, PX-18 powder, 5% PX-13 nanosuspension and 5% PX-18 nanosuspension because it has several advantages over other alternative tests because the technique can be applied to all types of chemicals and formulations, regardless of their properties (liquid or powder) or solubility [256-258]. Furthermore, with the HET-CAM test the effect of a compound or formulation is tested on a complex physiological system which gives a different test quality than cell culture studies. Considering all this, a good correlation of the results obtained with the HET-CAM test with *in vivo* results is expected and therefore no/only slight irritation of the eye is expected for all tested materials.

3 Coenzyme Q10-loaded NLC for dermal application

3.1 Introduction

3.1.1 Morphologic changes on the skin due to ageing

Ageing has been defined as the accumulation of molecular modifications which manifest as macroscopic clinical changes [259]. Like the entire organism the skin is ageing with time. With increasing age alterations in skin function occur because of structural and morphological changes. Factors of ageing have been classified as environmental (e.g. UV light, temperature extremes, humidity), lifestyle (e.g. food, psychological stressors, cigarette smoke) and genetic based factors [260]. Wrinkling is the most obvious sign of aged skin. The ageing wrinkles result of three main factors, the flattening of the dermo-epidermal junction, the influence of gravity and the loss of elastic properties of the skin. With ageing the face also develops facial lines, expression wrinkles (e.g. crow's foot, forehead wrinkles) caused by the repeated pull on the skin of underlaying facial mimetic muscles [261].

The epidermis of ageing skin becomes thinner because the cellular turn-over decreases [262, 263]. An increased heterogeneity in size of basal cells and an atrophy of the stratum spinosum can be observed. The keratinization in elderly skin takes longer. The corneocytes become less adherent, their shape changes and they become larger. The intercellular lipids of the stratum corneum change in quantity and composition reflecting a decrease in epidermal lipid biosynthesis [264, 265]. Melanocytes show an age-associated decrease in cumulative population doubling [266]. Furthermore, melanocytes may stop their activity which results in hypopigmentation or produce more melanosomes resulting in hyperpigmentation. With advanced age the number of Langerhans cells significantly decreases [267]. Often the cells become larger and less mobile resulting in a reduction of immune activity. The dermo-epidermal junction flatten which leads to a reduced cohesion between epidermis and dermis and a decreased exchange between the two tissues [268].

A decrement of the dermal thickness in ageing skin has been found. The number of fibroblasts decreases due to a diminishment of their replicative capacity and lifespan [266, 269]. The fibroblasts tend to become more globulous and their cytoplasma less dense. Furthermore, the synthesis of certain macromolecules e.g. collagens, elastin and proteoglycans is reduced. The

coutanious elasticity decreases in ageing skin. A dystrophy in elastic fibers can be observed [270]. Beside a decrease in elastin in ageing skin an increase in rigidity of elastic fibers due to the accumulation of calcium and cholesterol has been reported. The collagen fibers become thicker and more rigid [260]. Collagen fibers may be cross linked by Maillard reaction between collagen fibers and free glucose which results in a further increase of rigidity [271]. Additionally, a change in the quantitative composition of collagen can be observed in ageing skin [272]. Hyaluronan-bound water in the dermis and in the viable areas of the epidermis is important for skin hydration. In ageing skin epidermal hyaluronan decreases markedly whereas the total level of hyaluronan stays constant in the dermis. In the dermis an increased binding of hyaluronan with tissue was observed, which is accompanied with a diminished ability to take on water of hydration resulting in a loss in skin moisture. Furthermore, a progressive loss in size of the hyaluronan polymer in the skin as a function of age has been reported [273]. An age-associated reduction of cutaneous vessel size and a marked loss in dermal vessel density and surface area for exchange can be observed [274]. This results in a reduced cutanious vascular responsiveness, reduced UV-induced erythema, decreased skin temperature and disturbed nutrition supply [267]. Also a lymphatic vessel atrophy with age occurs in the skin [274]. Furthermore, the number of mast cells and lymphocytes decreases resulting in a diminishment in immune response. The sensitivity of the skin is reduced due to a reduction in the number of tactile corpuscles.

In ageing skin the thickness of the hypodermis diminishes. A reduction in subcutaneous fatty tissue can be observed. Sebaceous gland cells, which are responsible for sebum production and the lubrication of the skin, lose their morphological and functional characteristics with increasing age. Their size and secretory output decreases, resulting in a decrease in the surface lipid level and xerosis. Furthermore, a reduction in the density of sweat glands can be observed resulting in a reduced sweat output, higher core and skin temperature and a decrease in sensory thermal sensitivity [275].

3.1.2 Ageing theories

At the presence more than 300 ageing theories have been postulated [276]. Many ageing theories are interlinked with each other as the biological processes of the body and the factors affecting ageing are interlinked. In the following some of the major ageing theories with respect to skin ageing are outlined.

There are a number of DNA and genetic theories. The theory of ending telomeres first described by Hayflick is the most prominent one of them [277]. Telomeres are the ends of linear chromosomes, several thousand bases in length that consist of random repetitive DNA sequences. It was found *in vitro* in cultured human cells that the length of telomeres decreases by up to 150 base pairs with every cell division. Furthermore, it was reported, that the telomere length in cells obtained directly from tissue *in vivo* is inversely related to the age [278, 279]. Once the telomeres reach a critical length the cell cycle arrests or apoptosis occurs making ageing a genetically predetermined process [272].

The neuroendocrine theory by Dilman and Dean proposes that the ageing process is caused by an age-related loss of central (hypothalamic) and peripheral receptor sensitivity to inhibition by hormones and other signaling substances. This loss of hypothalamic sensitivity results in a progressive shifting of homeostasis and altered levels of hormones, neurotransmitters and cell signalers. These metabolic shifts are believed to cause ageing and ageing associated diseases [280-282]. According to this theory hormones also regulate the activity of all the enzymes involved in repair, recognition and elimination of cellular damages [1].

The cross link theory often also referred to as the glycosylation theory was developed by Bjorksten and modified by Bensusan [283, 284]. This theory describes the binding of glucose to various proteins which cause them to gradually stiffen and lose their function.

The most prominent ageing theory is the free radical theory postulated by Harman [285, 286]. Reactive oxygen species, such as superoxide radical, hydrogen peroxide, singulet oxygen and hydroxyl radical can cause oxidative damage to cellular macromolecules such as proteins, carbohydrates, lipids and nucleic acid and are thus cytotoxic. Exogenous agents like photochemical smog, ozone, pesticides, xenobiotics and ionizing radiation as well as a variety of endogenous processes such as mitochondrial respiration (mitochondrial theory of ageing [287, 288]), cytochrom P-450 detoxification reactions, phagocytic oxidative burst and peroxisomal leakage can generate significant amounts of reactive oxygen species [289]. Oxidative damage increases with age and contributes to the ageing phenotype as well as

various diseases due to the fact that the activity of antioxidant enzymes and the level of non-enzymatic antioxidants decline with age, allowing oxidative damage to occur [272, 290].

3.1.3 Coenzyme Q10

Ubidecarenone (Ubidecarenonum) is a synonym for coenzyme Q10. The chemical structure is shown in Figure 3.1.3-1. Coenzyme Q10 is composed of a tyrosine-derived quinone ring linked to a polyisoprenoid side chain consisting of 10 subunits [291]. It is a yellow till orange colored crystalline powder with a meting point at 48°C [213]. Under the influence of light coenzyme Q10 gets slowly darker and decomposes. The compound is practically insoluble in water and soluble in acetone. Coenzyme Q10 used in this work was obtained from BIK Internationaler Handel (Horgen, Switzerland).

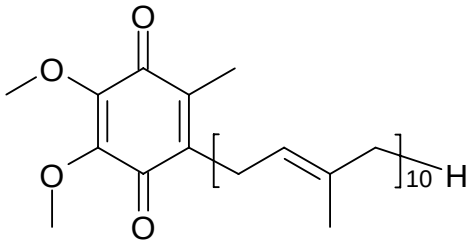

Figure 3.1.3-1: Chemical structure of coenzyme Q10 (2-[(all-E)-3,7,11,15,19,23,27,31,35,39-decamethyl-tetraconta-2,6,10,14,18,22,26,30,34,38-decaenyl]-5,6-dimethoxy-3-methylbenzol-1,4-dione).

The lipid soluble antioxidant coenzyme Q10 is synthesized endogenously by the mevalonate pathway [292, 293]. It exists in three redox states, fully oxidized ubiquninone (para-benzoquinone), semiquinone anion and fully reduced ubiquinol (hydroquinone) (Figure 3.1.3-2).

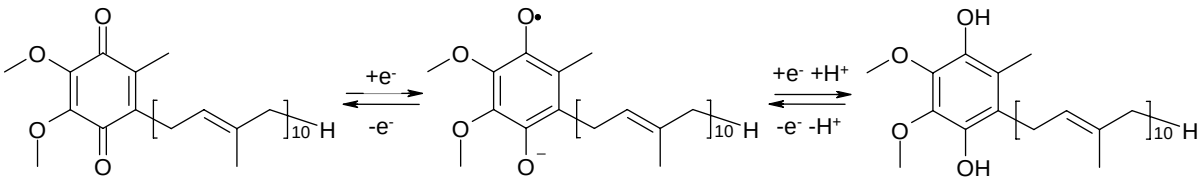

Figure 3.1.3-2: Redox equilibrium of para-benzoquinone (= ubiquinone) (left) with semiquinone anion (middle) and hydroquinone (=ubiquinol) (right) of coenzyme Q10.

Coenzyme Q10 is a cofactor in the mitochondrial respiratory chain, where it transfers free electrons from complex I and II to complex III during oxidative phosphorylation and ATP synthesis. Furthermore, the reduced form of coenzyme Q10 is a major chain-breaking

antioxidant, decreasing oxidative damage caused by lipid peroxidation. Therefore, ubiquinol donates a hydrogen atom to carbon- and oxygen-centered radicals generated during lipid peroxidation. Thereby the oxidative damage to lipids, proteins and DNA decreases [294, 295]. This autoxidation reaction generates a semiquinone anion that rapidly transforms into ubiquninone or ubiquinol. The ubiquinone is transferred back into ubiquinol by the mitochondrial respiratory chain [296]. Another function of coenzyme Q10 is the regeneration of α-tocopherol (vitamin E) from its oxidized form [292].

A decrease in coenzyme Q10 has been shown to contribute to cardiac failure, mitochondrial defects, immune deficiency, ischemic kidney, neurodegenerative conditions of the brain such as Alzheimer disease, degenerative muscle diseases, cancer and retinal damage [297-300] With increasing age the coenzyme Q10 synthesis is reduced, leading to lower plasma levels and tissue concentrations in elderly individuals. The decreasing coenzyme Q10 concentration upon ageing is consistent with the free radical theory of ageing [301].

Coenzyme Q10 has GRAS status and is widely used in food supplements and cosmetics [302]. In the skin coenzyme Q10 acts as an antioxidant with 10-fold higher levels in the epidermis than in the dermis [303]. A reduction in the efficiency of antioxidation systems has been proposed as a factor of skin ageing. It could be show in a pilot study that the topical application of coenzyme Q10 for six months led to a significant reduction in wrinkle depth in aged skin [272]. Therefore, investigations on dermal formulations containing coenzyme Q10 with regards to an optimized penetration into the skin and an optimized effect on aged skin are a promising approach.

3.2 Purpose of the study

In the first part of this work coenzyme Q10-loaded NLC as well as a coenzyme Q10-loaded o/w emulsion for topical application were prepared by high pressure homogenization. The systems were characterized and investigated with regard to physical (constant particle size distribution and constant melting behaviour) and chemical (constant active content) stability under different storage conditions.

Occlusion can increase the stratum corneum water content as well as the penetration of lipophilic active compounds into the skin. Therefore, in the second part of this work the occlusion properties of coenzyme Q10-loaded NLC and o/w emulsion were studied *in vitro*, *ex vivo* and *in vivo* and compared with coenzyme Q10 dissolved in highly occlusive liquid paraffin. Furthermore, the *in vitro* release of coenzyme Q10 from the three formulations was investigated using Franz diffusion cells and compared with the *in vivo* penetration of coenzyme Q10 into the stratum corneum evaluated by tape stripping test.

Different occlusion properties and different penetration profiles of active compounds can influence the effect on skin hydration of dermally applied products. Hence, in the third part of this work the effect on the skin hydration was evaluated *in vivo* after repetitive application of a cream containing coenzyme Q10-loaded NLC and a conventional o/w cream containing the same amount of coenzyme Q10 and having the same lipid content.

3.3 Preparation of coenzyme Q10-loaded NLC

3.3.1 Introduction

Many different techniques for the production of lipid nanoparticles have been described in the literature. These methods are high pressure homogenization [39, 167, 304], microemulsion technique [305-307], emulsification-solvent evaporation [308], emulsification-solvent diffusion method [309, 310], solvent injection (or solvent displacement) method [311], phase inversion [312], multiple emulsion technique [313], ultrasonication [314, 315] and membrane contractor technique [316, 317].

High pressure homogenization technique has many advantages compared to the other methods, e.g. easy scale up, avoidance of organic solvents, short production times, no regulatory problems for the production of topical pharmaceutical and cosmetic preparations due to the widely use of this technique in many industries including the pharmaceutical industry (e.g. production of emulsions for parenteral nutrition).

High pressure homogenization and the influence of the production parameters on the obtained particle size were described in details in chapter 2.4.2. For the production of lipid nanoparticles the hot or cold high pressure homogenization technique can be used. Figure 3.3.1-1 shows schematically the steps of these two techniques. For both techniques the active compound is dissolved or dispersed in melted solid lipid for SLN or in a mixture of liquid lipid (oil) and melted solid lipid for NLC. In the hot homogenization technique the lipid melt containing the active compound is dispersed in a hot surfactant solution of the same temperature (5-10°C above the melting point of the solid lipid or the lipid blend) by high speed stirring. The obtained emulsion (generally called pre-emulsion) is passed through a high pressure homogenizer adjusted to the same temperature, generally applying three cycles at 500 bar or two cycles at 800 bar. The obtained nanoemulsion recrystallizes upon cooling down. Applying the cold homogenization technique, the active containing lipid melt is cooled down. After solidification the mass is crushed and ground to obtain lipid microparticles. The lipid microparticles are dispersed in a cold surfactant solution yielding a cold pre-suspension of micronized lipid particles. This pre-suspension is passed through a high pressure homogenizer at or below room temperature applying typically 5-10 cycles at 500-1500 bar which leads to breaking of the micorparticles and hence the formation of lipid nanoparticles.

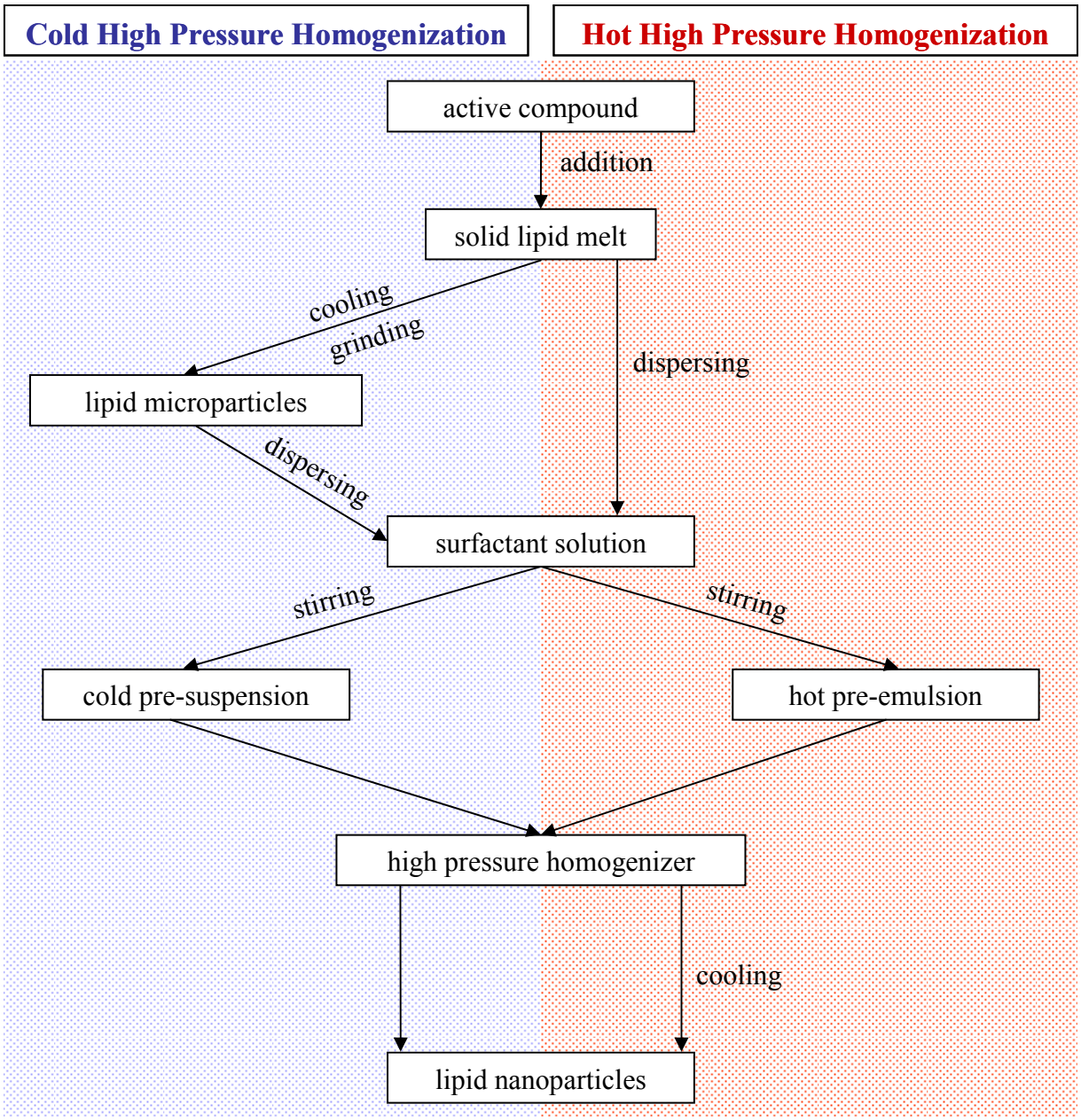

Figure 3.3.1-1: Schematic overview of the production process of lipid nanoparticles using cold (left, blue background) and hot (right, red background) high pressure homogenization technique.

Hot high pressure homogenization is the most frequently used technique. Cold high pressure homogenization is generally applied for extremely temperature sensitive compounds, to minimize the exposure to high temperatures, and hydrophilic compounds, to minimize the partitioning from the lipid phase to the water phase during the homogenization process [318].

3.3.2 Materials and methods

3.3.2.1 Materials

Cetyl palmitate

Cetyl palmitate (cetylii palmitas) is a mixture of esters from saturated natural fatty acids and saturated alcohols, mainly hexadecyl hexadecanoate ($C_{32}H_{64}O_2$), an ester of cetyl alcohol and palmitic acid. Beside palmic acid, cetyl palmitate may contain myristin acid and stearic acid. Cetyl alcohol may be partly replaced by myristyl alcohol or stearyl alcohol. Cetyl palmitate is a white wax which is supplied as pellets or flakes. Pure cetyl palmitate crystallizes in two modifications melting at 52.4-52.9°C and at 53.2-53.8°C. According to the composition of the ester mixture the melting point is increased or decreased [213]. Cetyl palmitate is insoluble in water and paraffin whereas it is soluble in chloroform and acetone. In this work Cutina® CP (Cognis, Düsseldorf, Germany) was used. In the following text cetyl palmitate is used as synonym for Cutina® CP.

Miglyol® 812

Medium chain triglyceride (Triglycerida saturate media) is a synonym for Miglyol® 812. It is produced from the oil which is extracted from the solid and dried part of the endosperms of Cocos mucifera L. and Elaeis guineensis JACQ. Miglyol® 812 consists of a mixture of triglycerides, mainly caprylic acid and capric acid. It consists of at least 95% saturated fatty acids with 8 or 10 carbon atoms. Miglyol® 812 is a colourless till light yellowish oily liquid which is insoluble in water but micsable with dichlormethane, ethanole, petroleum ether and fatty oils [213]. Miglyol® 812 used in this work was obtained from Caelo (Hilden, Germany).

Tego® Care 450

Polyglyceryl-3 methyl-glucose distearate is a synonym for Tego® Care 450. It is a non-ionic emulsifier with an HLB value of 11.5. Tego® Care 450 is supplied as amber coloured pellets. It exhibits a melting point at 55°C. At 20°C Tego® Care 450 is insoluble in water. At 60°C approximately 100 g/l are emulsifiable in water [319]. Tego® Care 450 used in this work was obtained from Goldschmidt (Essen, Germany).

3.3.2.2 Methods

High pressure homogenization

Coenzyme Q10-loaded NLC and o/w emulsion were produced by hot high pressure homogenization using a Micron LAB 40 (APV Deutschland GmbH, Unna, Germany) equipped with a water jacket for temperature control. The machine was operated discontinuously. Batches of 20-40 ml were prouced. Lipid phase and aqueous phase were heated separately to 85°C. Coenzyme Q10 and Tego® Care 450 were dissolved in the lipid phase. The water phase was admixed to the coenzyme Q10 containing lipid phase and a pre-emulsion was formed by 30 sec high speed stirring applying 8000 rpm using an Ultra Turrax T25 (Janke and Kunkel, Staufen, Germany). The obtained pre-emulsion was homogenized applying three cycles at 500 bar at 85°C. Dingler reported a sufficient stability of coenzyme Q10 under the applied production conditions [320].

Particle size analysis

The particle size of the coenzyme Q10-loaded NLC and o/w emulsion was determined by PCS and LD as described in chapter 2.4.2. For LD data evaluation the Mie theory was used. Water with a RI of 1.33 was used as measurement medium. The real refractive index and the imaginary refractive index were set at 1.456 and 0.01, respectively [320-322].

3.3.3 Results and discussion

Coenzyme Q10-loaded NLC and o/w emulsion were produced by hot high pressure homogenization (3 cycles, 500 bar, 85°C). The composition of these two formulations is shown in Table 3.3.3-1. In the o/w emulsion the cetyl palmitate was replaced by Miglyol® 812. The coenzyme Q10-loaded o/w emulsion served as a reference for coenzyme Q10-loaded NLC in this work for the determination of occlusive properties, the *in vitro* release profile using Franz diffusion cells and the *in vivo* skin penetration by tape-stripping test and is therefore described in details.

Table 3.3.3-1: Composition of coenzyme Q10-loaded NLC and o/w emulsion [% (w/w)].

Ingredients	NLC	Emulsion
Coenzyme Q10	4.80%	4.80%
Cetyle palmitate	14.45%	-
Miglyol® 812	0.75%	15.2%
Tego® Care 450	1.80%	1.80%
Bidistilled water	78.20%	78.20%

Figure 3.3.3-1 shows the average particle size and PI measured by PCS for coenzyme Q10-loaded NLC and o/w emulsion related to the production cycle number applying 500 bar at 85°C. The average particle diameter measured by PCS after cycle 1 was decreased about 25% for NLC and about 20% for the o/w emulsion applying a further production cycle. Between cycle 2 and 3 a reduction of the particles size by 10 nm was found for both formulations. With increasing cycle number the PI decreased. After 3 cycles a PI of 0.075 and 0.095 was obtained for NLC and o/w emulsion, respectively. This indicates a narrow particle size distribution. Figure 3.3.3-2 provides a summary of the LD 50, LD 90 and LD 95 values obtained after each production cycle for both formulations. With increasing cycle number a decrease in the LD values can be observed whereby the particle size decreased more between cycle 1 and 2 than between cycle 2 and 3. After 3 homogenization cycles the particle size of both formulations was well within the nanometer range. The presence of microparticles can be excluded (LD 99 = 0.531 µm for NLC; LD 99 = 0.532 µm for o/w emulsion). A similar particle size was obtained for coenzyme Q10-loaded NLC and o/w emulsion. Therefore, an influence of the particles size on the results of the following experiments can be excluded.

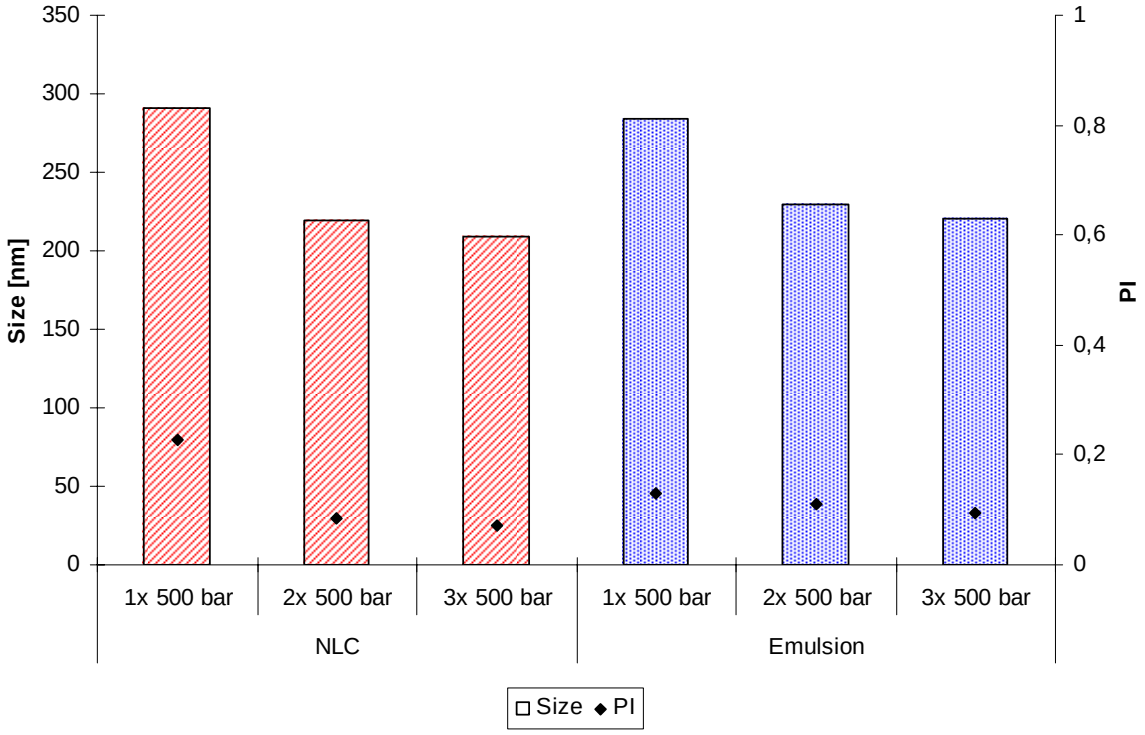

Figure 3.3.3-1: Average particle size and PI measured by PCS of coenzyme Q10-loaded NLC and o/w emulsion after 1, 2 and 3 cycles at 500 bar at 85°C.

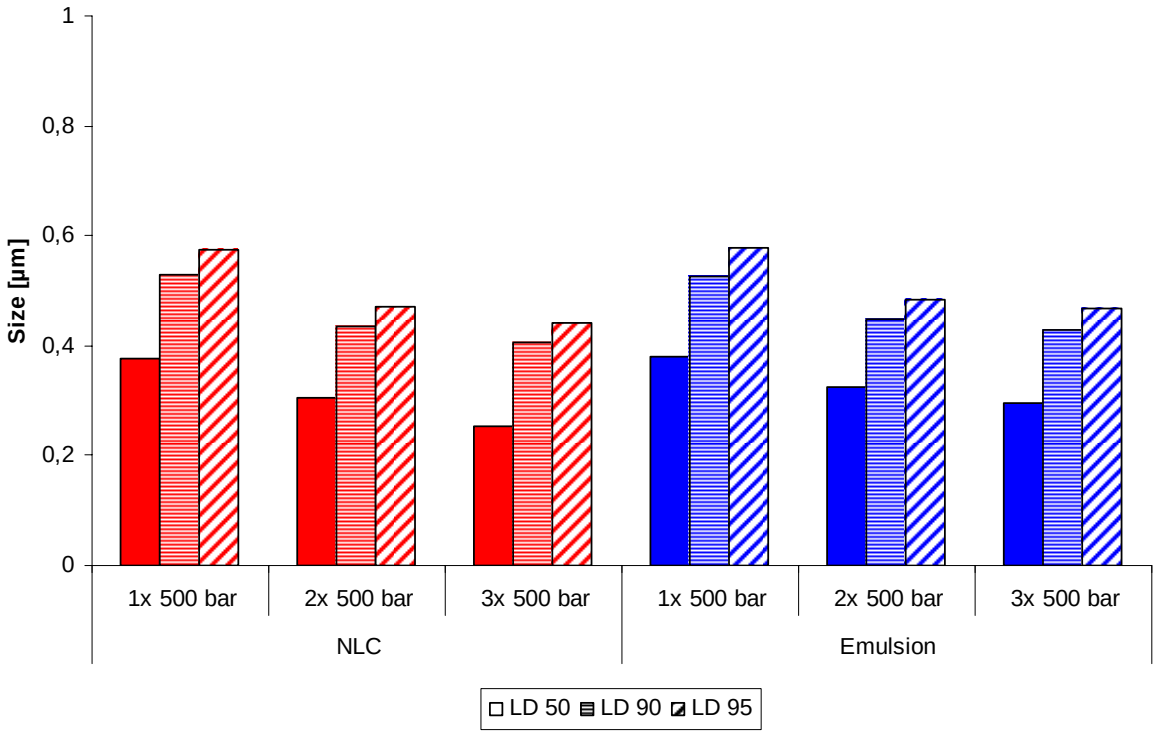

Figure 3.3.3-2: LD 50, LD 90 and LD 95 of coenzyme Q10-loaded NLC and o/w emulsion after 1, 2 and 3 homogenization cycles at 500 bar at 85°C.

To evaluate the reproducibility of the particle size of coenzyme Q10-loaded NLC and o/w emulsion three batches of each formulation were prepared. The particle size of each batch was evaluated by PCS and LD. The mean particle size and PI obtained by PCS as well as the mean LD 50, LD 90 and LD 95 values were calculated from the three different batches. For the evaluation of the reproducibility the relative standard deviation was used. The results of this study are shown in Table 3.3.3-2.

Table 3.3.3-2: Average particle size measured by PCS, PI, LD 50, LD 90 and LD 95 of three batches of coenzyme Q10-loaded NLC and o/w emulsion. The mean values of the particle size and PI as well as the according relative standard deviation (RSD) of the three batches were calculated.

Formulation	Value	Average particle size			Mean	RSD
		Batch 1	Batch 2	Batch 3		[%]
NLC	PCS [nm]	209	206	213	209	1.7
	PI	0.075	0.085	0.091	0.084	9.7
	LD 50 [µm]	0.254	0.252	0.240	0.249	3.0
	LD 90 [µm]	0.390	0.406	0.396	0.397	2.0
	LD 95 [µm]	0.446	0.443	0.433	0.441	1.5
Emulsion	PCS [nm]	220	227	207	218	4.7
	PI	0.095	0.081	0.098	0.091	9.9
	LD 50 [µm]	0.294	0.274	0.294	0.287	4.0
	LD 90 [µm]	0.430	0.419	0.427	0.425	1.3
	LD 95 [µm]	0.466	0.453	0.462	0.462	1.5

A good reproducibility of the mean particle size in between the batches was obtained for both coenzyme Q10-loaded NLC and o/w emulsion. The relative standard deviation was ≤ 4% for all analysed LD values. The relative standard deviation of the average particle diameter measured by PCS was 1.7% for the NLC formulation and 4.7% for the o/w emulsion indicating a good reproducibility. For the PI values a relative standard deviation < 10% was found indicating only little deviation in particle size distribution between the batches. This is well in agreement with earlier findings, where a good reproducibility of the particles size was reported for lipid nanoparticles and o/w emulsions produced by high pressure homogenization [320].

3.4 Stability of coenzyme Q10-loaded NLC

3.4.1 Introduction

Many compounds have been successfully incorporated in lipid nanoparticles [323-327]. Furthermore, it could be shown that lipid nanoparticles are able to enhance the chemical stability of compounds sensitive to light, oxidation and hydrolysis e.g. coenzyme Q10 [320], ascorbyl palmitate [60], tocopherol (vitamin E) [320] and retinol (vitamin A) [61, 62]. However, possible problems associated with lipid nanoparticles stability as drug expulsion from the lipid matrix, the formation of supercooled melts and gelation phenomena have been reported [167]. Drug expulsion from lipid nanoparticles is caused by polymorphic transformation of the lipid during the storage time. This problem is pronounced in SLN compared to NLC due to the fact that SLN are produced from solid lipids only and after preparation at least a part of the particles crystallizes in a higher energy modification (α or β`). During storage, these modifications can transform to the low energy, more ordered β modification. Due to its high degree of order, the number of imperfections in the crystal lattice is reduced leading to drug expulsion. In NLC due to blending a solid lipid with a liquid lipid a less ordered solid lipid matrix is created. This increases the loading capacity of active compounds and also avoids or minimizes the expulsion of the active compound during storage [328]. The formation of supercooled melts might occur in lipid nanoparticles due to size dependency of crystallization processes, emulsifiers and incorporated active compounds. In case a supercooled melt is formed the advantages of lipid nanoparticles over o/w emulsions will be neglected due to the liquid state of the lipid in both systems. This problem can be overcome by cooling down the lipid nanoparticles in liquid nitrogen straight after production [329]. Gelation phenomena describe the transformation of lipid nanoparticle dispersions with low viscosity into viscous gels. This irreversible process involves the loss of the colloidal particle size. It was found that a decrease in zeta potential values below |-15 mV| and a change in crystallinity are associated with this phenomena [330, 331].

The particle charge, the particle size, the melting behaviour and the chemical stability were investigated of coenzyme Q10-loaded NLC and o/w emulsion to obtain information about their physical and chemical stability.

3.4.2 Methods

Stability investigations

For stability investigations coenzyme Q10-loaded NLC and o/w emulsion were stored for 180 days at 5°C ± 3°C, 25°C ± 2°C and 40°C ± 2°C in darkness. As a reference for chemical stability investigations 4.8% (w/w) coenzyme Q10 were dissolved in liquid paraffin (Caelo, Hilden, Germany) and stored at the same conditions. Due to the fact that photolytic degradation of coenzyme Q10 was reported, a short time chemical stability study exposing coenzyme Q10-loaded NLC, o/w emulsion and coenzyme Q10 dissolved in liquid paraffin to artificial sun light for 60 day was performed. For artificial illumination the samples were placed between two fluorescent lamps in a defined distance to avoid warming up. As florescent lamps two 58 W tubes with the light spectrum of day light were used.

The zeta potential was measured as described in chapter 2.4.3. To asses the particle size PCS and LD measurements were performed following the methods described in chapter 2.4.2 and chapter 3.3.2.

Differential scanning calorimetry (DSC)

The method is described in details in chapter 2.3.1. Therefore, only the relevant facts for the performance of the method to study lipid nanoparticles are outlined here. For the experiments a heat flux DSC instruments (Mettler DSC 821e, Mettler Toledo, Gießen, Germany) was used. 1-3 mg sample, calculated on the base of lipid phase, were analyzed in sealed and pin-holed standard 40 µl aluminum pans. With a heating rate of 5 K/min the samples were heated from 25°C to 85°C and cooled down from 85°C to 25°C. During the measurement the sample cell was continuously purged with nitrogen at a flow rate of 80 ml/min.

The onset and melting point (peak maximum) were evaluated to describe the melting behavior. The melting enthalphy (ΔH) was evaluated to gain information about the recrystallization of the lipid. The crystallinity index (CI) was calculated from the melting enthalpy using the following equation:

$$CI\,[\%] = \left(\frac{\Delta H_{NLC\ dispersion}}{\Delta H_{bulk\ material} \times concentration_{solid\ lipid\ phase\,[\%]}} \right) \times 100$$

HPLC method for the quantification of coenzyme Q10

Coenzyme Q10 was quantified in this work using an HPLC method modified after Dingler [320]. The HPLC system used consisted of an auto sampler model 560, a pump system model 525 and a diode array detector model 540 (Kontron Instruments, Groß-Zimmern, Germany). This system was linked to a KromaSystem 2000 v. 1.70 data acquisition and process system, which also controlled the HPLC modules. 20 µl of the sample were injected onto a Betasil C8 (5 µm) 125x 4 mm column with a matching pre-column (Thermo Fisher Scientific, Waltham, USA). The column was kept at room temperature during the measurement. The mobile phase consisted of acetonitrile HPLC grade (Mallinckrodt Baker, Deventer, Netherlands) and tetrahydrofurane HPLC grade (Mallinckrodt Baker, Deventer, Netherlands) in a ratio 9:1 (v/v). The mobile phase was run with a flow rate of 1.5 ml/min. The UV-spectrum was recorded at a wavelength of 280 nm. The coenzyme Q10 containing samples as well as coenzyme Q10 powder for the standard curves were dissolved in acetone HPLC grade (Mallinckrodt Baker, Deventer, Netherlands). Table 3.4.2-1 provides a summary of the specificity, linearity, LOD, LOQ, accuracy, precision and range of the HPLC method used in this work.

Table 3.4.2-1: Summary of the specificity, linearity, LOD, LOQ, accuracy, precision and range of the HPLC method used to quantify coenzyme Q10.

Parameter	Specification
Specificity	Retention time: 8 min
Linearity	$R^2 \geq 0.99$
LOD	0.33 µg/ml
LOQ	1 µg/ml
Accuracy (inter and intra assay)	98-100%
Precision (inter and intra assay)	1-3%
Range	10-100 µg/ml

3.4.3 Results and discussion

Zeta potential

The zeta potential is a useful tool to predict the physical long term stability of colloidal systems. At the day of production a zeta potential of |-54.1 ± 6.2 mV| and |-57.4 ± 7.0 mV| was measured for coenzyme Q10-loaded NLC and o/w emulsion, respectively. Zeta potential values of this order of magnitude indicate a good physical stability [193]. Particle aggregation or coalescence, respectively, is not likely to occur due to electrostatic repulsion between the lipid particles in case of NLC and between the oil droplets in case of o/w emulsion. Furthermore, Tego® Care 450 performs an additional sterical stabilization of the formulations. Table 3.4.3-1 provides a summary of the zeta potential values of coenzyme Q10-loaded NLC and o/w emulsion obtained at the day of production and after 180 day of storage at 5°C ± 3°C, 25°C ± 2°C and 40°C ± 2°C.

Table 3.4.3-1: Zeta potential values of coenzyme Q10-loaded NLC and o/w emulsion at the day of production and after 180 days of storage at 5°C ± 3°C, 25°C ± 2°C and 40°C ± 2°C (measured in water with 50 µS/cm conductivity).

Formulation	Day 0 [mV]	Day 180 [mV]		
		5°C ± 3°C	25°C ± 2°C	40°C ± 2°C
NLC	-54.1 ± 6.2	-56.8 ± 6.5	-55.4 ± 6.5	-59.2 ± 6.3
Emulsion	-57.4 ± 7.0	-63.6 ± 6.9	-62.5 ± 6.9	-63.9 ± 8.6

The zeta potential values of both formulations were of the same order of magnitude after 180 days of storage at all three temperatures as on the day of production. This indicates a further physical stability of the samples at all storage temperatures.

Particle size

Freitas and Müller found that particle growth could be induced by an input of kinetic energy (e.g. temperature) to the system [330]. The authors found that the particle size measured by LD increased rapidly at elevated temperature and remained stable for more than 180 days when stored refrigerated. However, Saupe reported a constant particle size of cetyl palmitate SLN stabilized with Tego® Care 450 and NLC composed of cetyl palmitate and Miglyol® 812 stabilized with Tego® Care 450 over an observation period of one year at low and high temperatures [332]. Radtke could show a good physical stability with regards to particle size for drug-free and cyclosporine A-loaded SLN, NLC and nanoemulsion over three years

storing the samples at room temperature [333]. These findings indicate that no general statement over the physical stability with regards to particle size of lipid nanoparticles can be done. Each system needs to be investigated separately.

The average particle diameter measured by PCS and the PI of coenzyme Q10-loaded NLC and o/w emulsion are shown in Figure 3.4.3-1 and Figure 3.4.3-2. The average particle diameter and PI stayed constant over the observation period for both formulations at all three test temperatures.

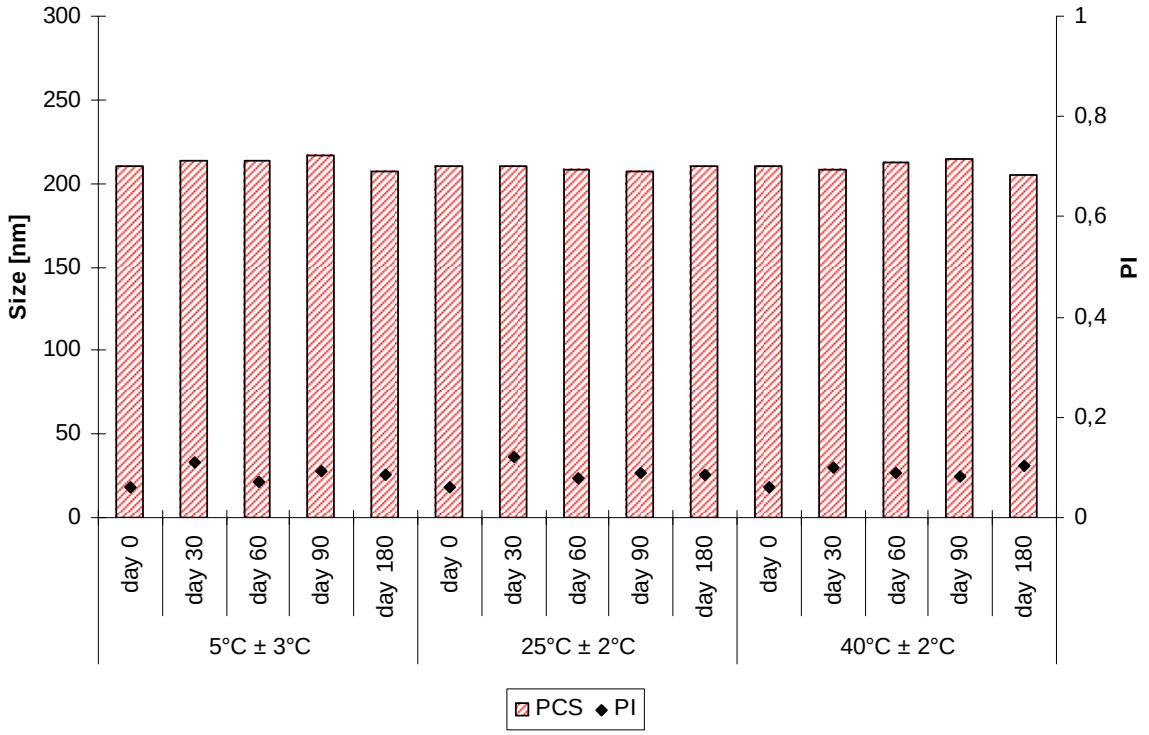

Figure 3.4.3-1: Particles size and PI of coenzyme Q10-loaded NLC measured by PCS over a period of 180 days stored at 5°C ± 3°C, 25°C ± 2°C and 40°C ± 2°C.

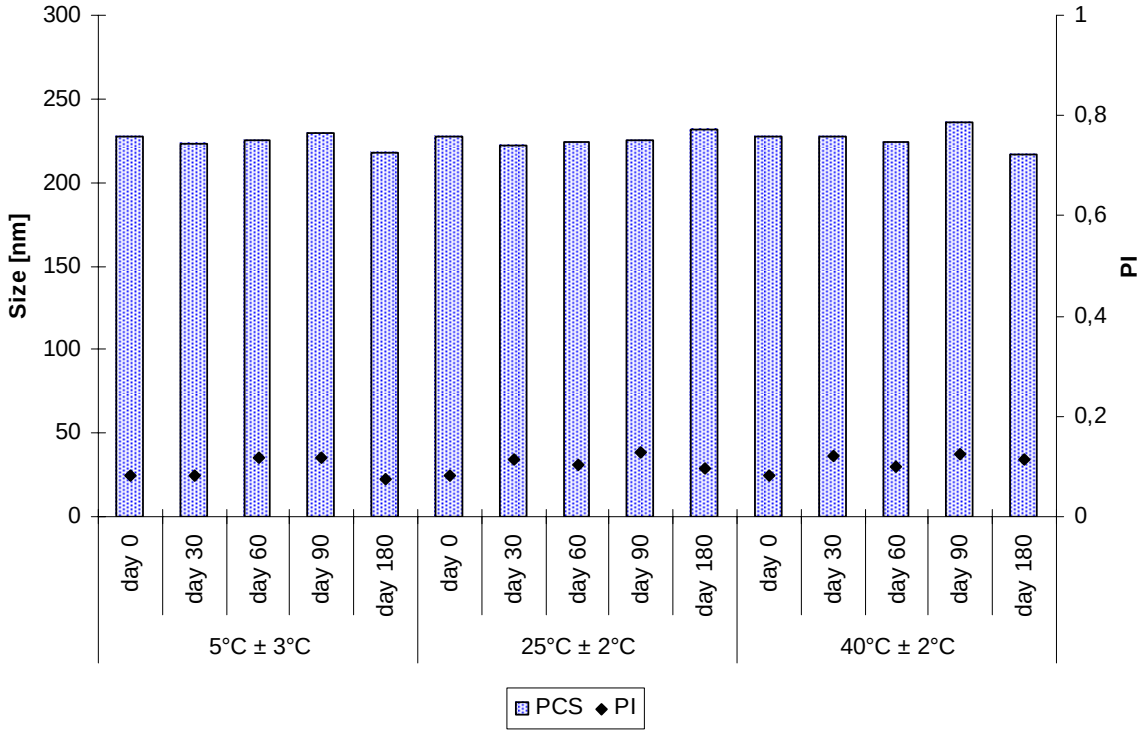

Figure 3.4.3-2: Particles size and PI of coenzyme Q10-loaded o/w emulsion measured by PCS over a period of 180 days stored at 5°C ± 3°C, 25°C ± 2°C and 40°C ± 2°C.

PCS is a good tool for the characterization of particles in the nanometer range but it is not able to detect larger particles. Therefore, for the detection of aggregates and agglomerates or coalescence and flocculation, respectively, LD measurements were performed. Figure 3.4.3-3 and Figure 3.4.3-4 summarize the results obtained by LD measurement for coenzyme Q10-loaded NLC and o/w emulsion. Neither for the NLC formulation nor for the o/w emulsion an increase in LD values was found. The LD measurements confirm a good physical stability with regards to the particles size for both formulations at all tested storage temperatures. The presence of larger particles can be excluded. Hence, the results of the particle size investigations support the findings of the zeta potential measurements which suggested a good physical stability of both carrier systems.

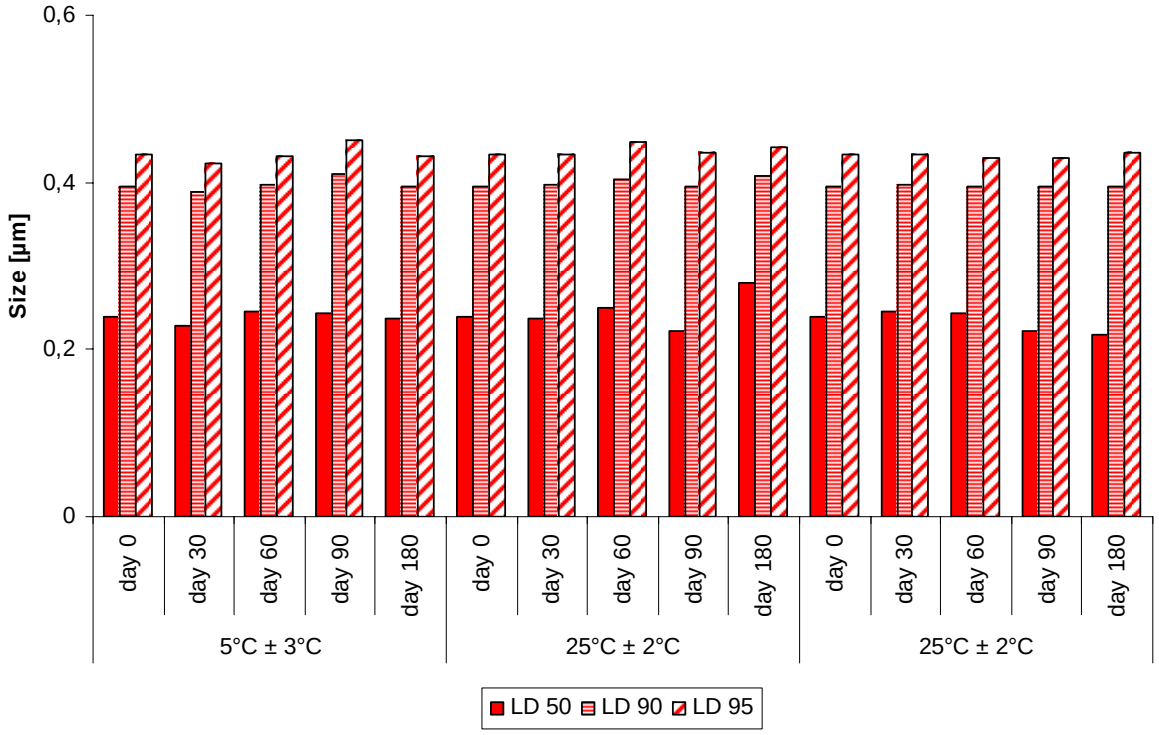

Figure 3.4.3-3: LD 50, LD 90 and LD 95 of coenzyme Q10-loaded NLC measured over a period of 180 days stored at 5°C ± 3°C, 25°C ± 2°C and 40°C ± 2°C.

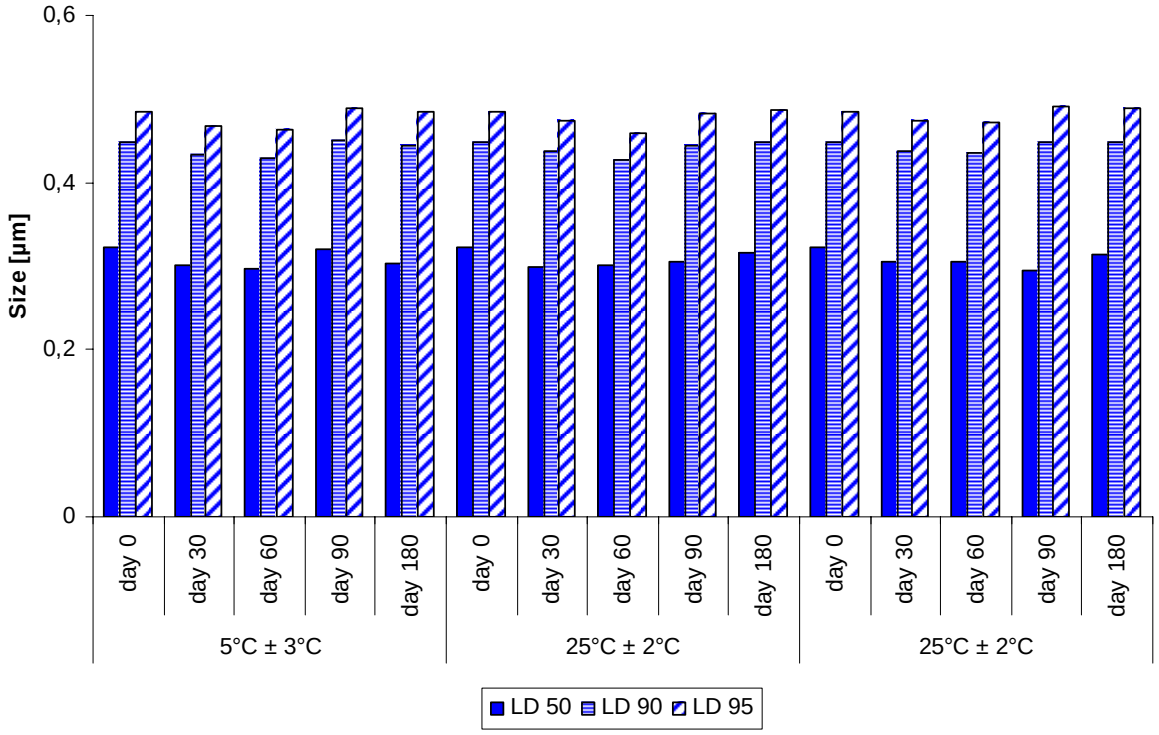

Figure 3.4.3-4: LD 50, LD 90 and LD 95 of coenzyme Q10-loaded o/w emulsion measured over a period of 180 days stored at 5°C ± 3°C, 25°C ± 2°C and 40°C ± 2°C.

The findings of this study are well in agreement with the literature about coenzyme Q10-loaded cetyl palmitate based lipid nanoparticles stabilized with Tego® Care 450. Dingler reported a good physical stability with regards to particle size for coenzyme Q10-loaded cetyl palmitate SLN (20% lipid phase; 24% coenzyme Q10 related to the lipid phase) storing the samples at room temperature and 40°C for 180 days [320]. Teeranachaideekul observed a good physical stability of coenzyme Q10-loaded NLC (10% and 20% lipid phase (mixture of cetyl palmitate and Miglyol® 812); 24% coenzyme Q10 related to the lipid phase) at 4°C, 25°C and 40°C over 12 month [322].

DSC investigations

To gain information on the melting behaviour, the polymorphism and the degree of crystallinity of the NLC under investigations as well as the according bulk materials used, DSC measurements were performed. Figure 3.4.3-5 shows the obtained melting curves of cetyl palmitate bulk material, a bulk mixture of cetyl palmitate and Miglyol® 812 in the ratio 19:1, a bulk mixture of cetyl palmiate, Miglyol® 812 and coenzyme Q10 in the ratio used in the NLC (96:289:15), coenzyme Q10-loaded NLC and coenzyme Q10-loaded o/w emulsion. The bulk material as well as the bulk mixtures were heated up to 85°C and kept at that temperature for one hr to mimic the production conditions of the NLC. The DSC curves were recorded one day after tempering of the materials or production in case of NLC and o/w emulsion, respectively.

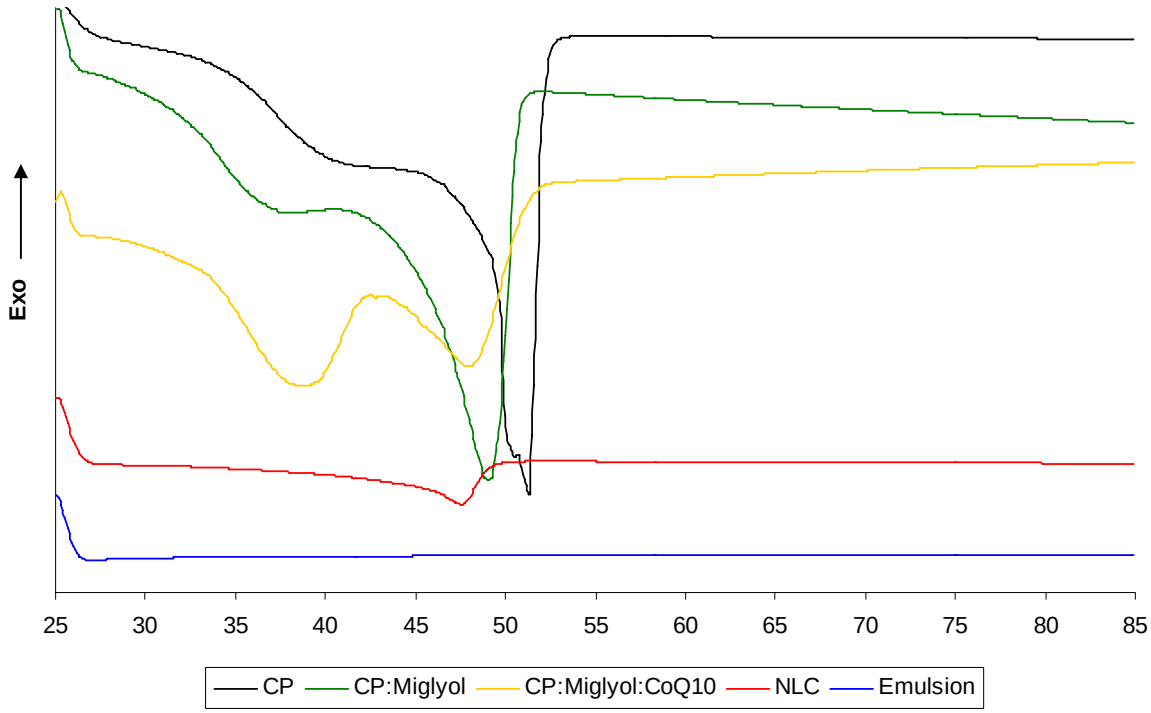

Figure 3.4.3-5: DSC melting curves of cetyl palmitate bulk material (CP), a bulk mixture of cetyl palmitate and Miglyol® 812 in the ratio 19:1 (CP:Miglyol), a bulk mixture of cetyl palmiate, Miglyol® 812 and coenzyme Q10 in a ration 96:289:15 (CP:Miglyol:CoQ10), coenzyme Q10-loaded NLC (NLC) and coenzyme Q10-loaded o/w emulsion (emulsion).

The literature is describing two modifications of pure cetyl palmitate (hexadecyl hexadecanoate) melting at 52.2-52.9°C and 53.2-53.8°C [213]. In the present work Cutina® CP was used. For Cutina® CP two modifications with melting points at 39.8°C and 51.1°C were found. This indicates the presence of alcohol and fatty acid compounds with shorter chain length than in pure cetyl palmitate in the marketed product Cutina® CP which led to a melting point depression of both modifications. However, in this work cetyl palmitate is used as a synonym for Cutina® CP.

The tempered bulk mixture of cetyl palmitate and Miglyol® 812 in a ratio 19:1, which is the same ratio used in coenzyme Q10-loaded NLC, was investigated by DSC in order to obtain information on the inclusion of the liquid lipid in the solid lipid and the influence on the melting behavior. Due to mixing cetyl plamitate with Miglyol® 812 a decrease of the melting points of both modifications of cetyl palmitate could be observed. The melting points of the modifications in this mixture were 36.4°C and 48.9°C. This indicates that Miglyol® 812 is dissolved in cetyl pamitate and therefore the crystal structure of cetyl plamitate is less pronounced [332, 334].

In the next step the tempered mixture of cetyl palmitate, Miglyol® 812 and coenzyme Q10 in the ratio used in coenzyme Q10-loaded NLC was analysed by DSC. For this mixture two

modifications with melting points at 38.4°C and 48.2°C were found. In this mixture the creation of the lower melting modification was pronounced compared to cetyl palmitate and the mixture of cetyl palmitate and Miglyol® 812. That means coenzyme Q10 present in the mixture suppresses the crystallisation in the more ordered and more stable modification. Furthermore, the melting peaks were broader than in the previously analysed systems. The melting point of coenzyme Q10 used in this work was found to be 50.9°C. In the melting curve of the tempered bulk mixture of cetyl palmitate, Miglyol® 812 and coenzyme Q10 the melting peak of coenzyme Q10 is absent which also provides evidence that coenzyme Q10 is dissolved in the mixture.

Coenzyme Q10-loaded NLC show one melting peak with an onset temperature at 43.4°C and a peak maximum at 47.3°C. Due to the presence of a melting endotherm the formation of a supercooled melt can be excluded. Furthermore, the onset temperature and the melting point of the NLC are above 32°C which is necessary to remain the solid state of the NLC after dermal application. The instable lower melting modification observed in the melting curves of cetyl palmitate and the bulk mixtures was not observed in coenzyme Q10-loaded NLC. This is caused by the fact that polymorphic transitions can occur more rapidly in lipid nanoparticles than in bulk state [335]. The melting point obtained for the more stable modification was lower than the melting point of this modification in the bulk mixture of cetyl palmitate, Miglyol® 812 and coenzyme Q10. In addition to a possible effect of the surfactant used to stabilize the NLC dispersion, this can be explained by the small particle size and the high specific surface area of the NLC according to the Gibbs-Thomson equation [334, 335]. Furthermore, broadening of the melting peak could be observed. This is caused by the fact that the particle size distribution of coenzyme Q10-loaded NLC differs from an ideal monodispers particle size distribution and the fractions of different sizes melt at different temperatures [335].

In case of the coenzyme Q10-loaded o/w emulsion no melting event was detected. This provides evidence that coenzyme Q10 was completely dissolved in the oil phase.

Table 3.4.3-2 provides a summary of the melting points, onsets and crystallinity indices found for coenzyme Q10-loaded NLC at the three different storage temperatures over an observation period of 180 days.

Table 3.4.3-2: Melting point (peak maximum), onset and crystallinity index (CI) of coenzyme Q10-loaded NLC stored at 5°C ± 3°C, 25°C ± 2°C and 40°C ± 2°C for 180 days.

Storage condition	Parameter	Day					
		1	14	30	60	90	180
5°C	Melting point [°C]	47.3	47.0	47.1	47.1	47.1	46.8
	Onset [°C]	43.4	43.1	43.4	43.4	43.1	43.1
	CI [%]	57.1	73.7	83.3	83.4	84.6	77.5
25°C	Melting point [°C]	47.3	47.0	47.3	47.1	47.2	47.2
	Onset [°C]	43.4	43.2	43.6	43.5	43.0	43.4
	CI [%]	57.1	77.7	78.9	78.9	82.9	74.6
40°C	Melting point [°C]	47.3	46.8	46.9	46.9	47.0	47.2
	Onset [°C]	43.4	42.6	41.7	44.4	43.8	42.4
	CI [%]	57.1	8.0	12.5	32.0	54.5	9.8

The onsets and melting points stayed constant over the observation period at all temperatures indicating no change in lipid modification. At 5°C ± 3°C and 25°C ± 2°C an increase of the CI within the first 14 days was found. This might be caused by incomplete solidification on day 1. It has been previously reported, that freshly crystallized material, even when the material crystallizes into stable polymeric forms, often have a lower melting enthalpy than after a certain storage time [335]. However, the CI reached at day 14 stayed constant over 180 days at these two storage conditions and was well below 100%. A constant crystallinity is quite impotent as an increase in crystallinity leads to an increase in the packing order in the lipid matrix and therefore it can result in the exclusion of incorporated active compounds. The investigations on CI are well in agreement with the observations on zeta potential and particle size, as decreasing zeta potential values and increasing CI lead to particle growth and gelation of lipid nanoparticles dispersions, which was not observed in the present study. Storing coenzyme Q10-loaded NLC at 40°C ± 2°C led to a decrease of the CI within the first 14 days. This might be caused by softening of the lipid particle matrix due to the fact that the storage temperature was very close to the onset and melting point of the formulation.

Chemical stability

The reaction rate of the chemical degradation of active compounds can be increased with an increasing temperature. The effect of the temperature on the rate of reaction can be explained by the Arrhenius equation [189]. Therefore, the chemical stability of coenzyme Q10-loaded NLC and o/w emulsion was assessed by HPLC and compared to coenzyme Q10 dissolved in liquid paraffin stored at three different temperatures. Figure 3.4.3-6 shows the percentage coenzyme Q10 remaining in the formulations related to the coenzyme Q10 content found at day 0 after 180 days of storage at 5°C ± 3°C, 25°C ± 2°C and 40°C ± 2°C in darkness.

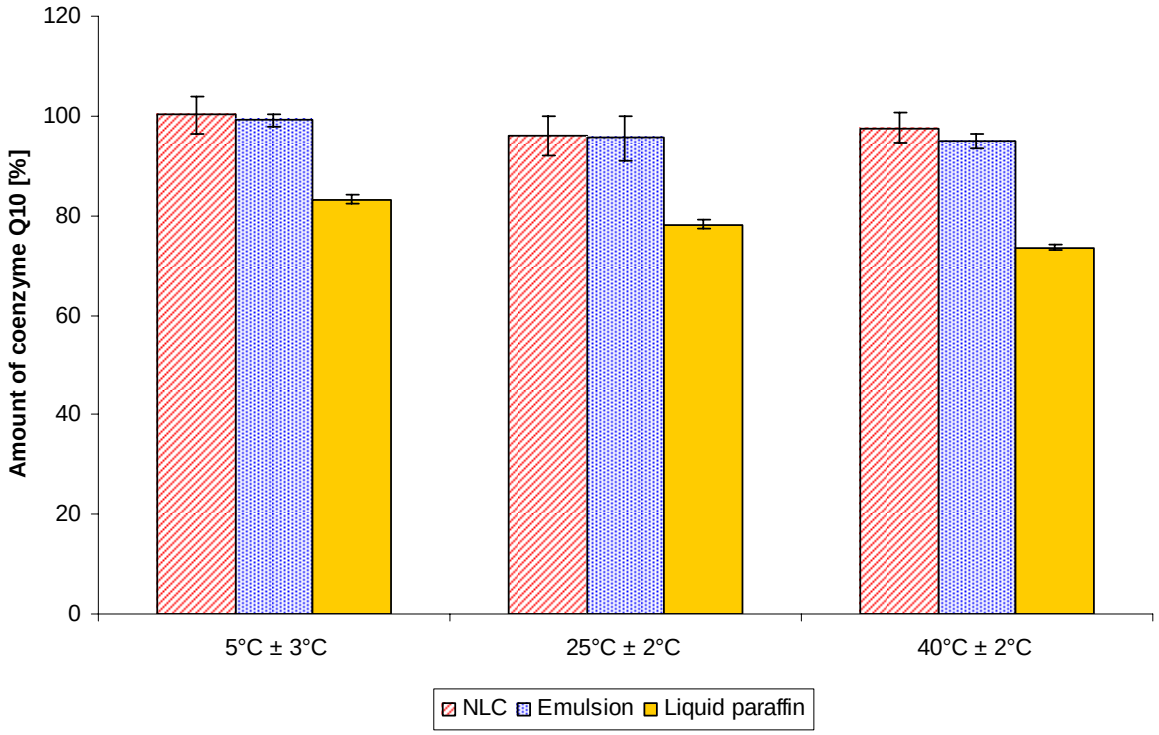

Figure 3.4.3-6: Percentage coenzyme Q10 remaining in NLC, o/w emulsion and liquid paraffin after 180 days of storage at 5°C ± 3°C, 25°C ± 2°C and 40°C ± 2°C.

A good chemical stability of coenzyme Q10-loaded NLC and o/w emulsion was found at all three storage temperatures in darkness. Neither for coenzyme Q10-loaded NLC nor for coenzyme Q10-loaded o/w emulsion a decrease in coenzyme Q10 content could be observed with increasing storage temperature. Pronounced chemical degradation was observed with increasing storage temperature when coenzyme Q10 was dissolved in liquid paraffin. Therefore, the findings of this study indicate that both NLC and o/w emulsion are able to protect coenzyme Q10 from chemical degradation when stored in darkness.

The degradation of coenzyme Q10 is accelerated under light exposure [336]. To evaluate the influence of the carrier system on the chemical stability of coenzyme Q10 under light exposure a short time study was performed where coenzyme Q10-loaded NLC, o/w emulsion and coenzyme Q10 dissolved in liquid paraffin were exposed continuously to artificial sun light for 60 day. The results of this study are shown in Figure 3.4.3-7.

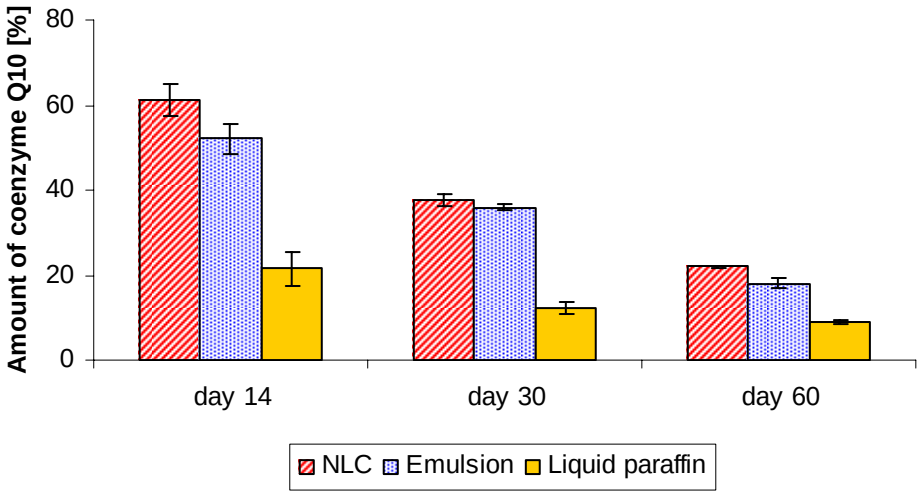

Figure 3.4.3-7: Percentage coenzyme Q10 remaining in NLC, o/w emulsion and liquid paraffin after 14, 30 and 60 days of storage under artificial light exposure.

Within 14 days already 78.5% of the coenzyme Q10 dissolved in liquid paraffin were degraded where as only 38.7% of coenzyme Q10 incorporated in NLC and 47.9% coenzyme Q10 incorporated in o/w emulsion were degraded within the same time. Both NLC and o/w emulsion are able to protect coenzyme Q10 better from degradation compared to a solution in liquid paraffin. The protective effect against chemical degradation preponderate if coenzyme Q10 was incorporated in NLC compared to o/w emulsion. Coenzyme Q10 dissolved in the oil droplets of an o/w emulsion can diffuse within the oil droplets freely whereas the coenzyme Q10 embedded in the solid lipid matrix of NLC has a decreased diffusion velocity. This can be explained by the Stokes-Einstein equation which shows that the diffusion velocity is reverse proportional to the viscosity of the medium. Faster diffusion of coenzyme Q10 in o/w emulsion leads to a faster exchange of coenzyme Q10 molecules exposed to light on the surface of the oil droplets compared to NLC. By that effect a pronounced degradation of coenzyme Q10 in o/w emulsion compared to NLC can be explained.

In summary it can be noted that both coenzyme Q10-loaded NLC and o/w emulsion showed a good physical and chemical stability. Zeta potential values of a sufficient height for a good electrostatic stabilization were found for both carrier systems. The zeta potential values stayed unchanged over the investigation time at low and high temperature indicating a good physical stability of both carriers. This was confirmed by PCS and LD measurements as a constant particle size could be observed at all storage temperatures over 180 day. Furthermore, DSC investigations showed no changes in the crystallinity of the NLC and no changes of the onset and melting temperature during storage. This indicates that no changes in the lipid modification occurred. Therefore, no expulsion of coenzyme Q10 from NLC is expected during the storage time. In addition absence of supercooled melts and gelation phenomena could be shown in this study. Beside a good physical stability a good chemical stability of coenzyme Q10-loaded NLC and o/w emulsion was observed. However, under light exposure NLC provide a more efficient protection of the chemical labile coenzyme Q10 than the o/w emulsion.

3.5 Occlusive properties of coenzyme Q10-loaded NLC

3.5.1 Introduction

Water plays an important role in the physical properties of the stratum corneum. Occlusive properties of dermally applied products can increase the stratum corneum water content from a normal range of 10-20% up to 50% [58]. Associated with occlusion are also increases in skin temperature, skin pH, epidermal thickness, transepidermal water loss and mitotic rate as well as a pronounced local blood flow. The absorption of some topically applied drugs and cosmetic actives can be promoted due to occlusion [154]. Therefore, occlusion can be a desired effect for the topical application of cosmetics and pharmaceutics. Skin occlusion can be reached by the application of occlusive foils (e.g. polyacrylate foils), lipophilic compounds (e.g. oils, liquid paraffin, petrolatum, Lanolin, fats) and w/o ointments. Lipid nanoparticles also exhibit occlusive properties whereby the occlusive effect depends on various factors such as particle size, applied sample volume, lipid concentration and crystallinity of the lipid matrix [337, 338]. It was reported by Wissing et al. that the highest occlusion will be reached using low melting lipids, highly crystalline particles and very small particles [337]. Nanoparticles have been found to be 15-folds more occlusive than microparticles [339, 340]. Comparing the occlusive effect of SLN and NLC, Souto et al. found a higher occlusive factor for SLN in comparison to NLC of the same lipid content due to a higher crystallinity of SLN [48]. Comparing NLC with different oil content led to the conclusion that an increase in oil content leads to a decrease of the occlusive factor [341]. These findings indicate that the degree of occlusion of lipid nanoparticles can be influenced by various parameters and thereby the degree of occlusion can be adjusted in a controlled way [342]. Another advantage of lipid nanoparticles is that they are easily admixable to hydrogels or o/w creams, which introduces occlusive properties to these formulations without changing their light character and therefore avoids a glossy skin appearance after dermal application.

3.5.2 Methods

***In vitro* occlusion test**

The *in vitro* occlusion test was performed as described by de Vringer [343]. Beakers (100 ml) with a diameter of 5 cm were filled with 50 ml bidistilled water, covered with a cellulose acetate filter (Macherey-Nagel, Düren, Germany) and sealed. Coenzyme Q10 containing NLC, o/w emulsion and liquid paraffin (4.8% (w/w) coenzyme Q10, 95.2% (w/w) liquid paraffin) were applied evenly to the cellulose acetate filter with a final amount of 10.2 mg/cm^2 (n = 5). The samples were stored at 32°C ± 1°C and 60% ± 5% relative humidity. Water evaporation was investigated by weighing the beakers after 6, 24 and 48 hrs. The occlusion factor (F) was calculated using the following equation:

$$F\,[\%] = \left(\frac{A-B}{A}\right) \times 100$$

A = amount of water evaporated through the cellulose acetate filter without application of a test sample

B = amount of water evaporated through the cellulose acetate filter after application of a test sample

In case the applied formulation has no occlusive properties an occlusion factor of 0%, in case of maximum occlusion an occlusion factor of 100% would be obtained.

Microscopic investigation of film formation

To investigate the film formation 10 µl of NLC and o/w emulsion were applied to a microscope slide, spread with a glass rod, dried at 32°C and observed using a light microscope (Leitz, Wetzlar, Germany) equipped with a CMEX-1 digital camera (Euromex microscopes, Arnheim, Netherlands) connected to Image Focus software version 1.3.1.4. (Euromex microscopes, Arnheim, Netherlands).

***Ex vivo* occlusion test using porcine skin**

The *in vitro* occlusion test of de Vringer was modified for this experiments [343]. Porcine skin was obtained from the outer pig ear. Beakers (20 ml) with a diameter of 3 cm were filled to the top with freshly prepared PBS, covered with porcine skin and sealed. Coenzyme Q10

containing NLC, o/w emulsion and liquid paraffin were applied evenly to the porcine skin with a final amount of 10.2 mg/cm^2 (n = 6). The samples were stored at 32°C ± 1°C and 60% ± 5% relative humidity. Water evaporation was investigated by weighing the beakers after 6, 24 and 48 hrs. The according occlusion factor F was calculated. Untreated porcine skin served as control.

***In vivo* occlusion test – Single application Corneometer study**

In a short time *in vivo* study, the skin hydration was measured using a Corneometer CM 825 (Courage and Khazaka, Cologne, Germany) connected to a Multi Probe Adapter MPA 5 (Courage and Khazaka, Cologne, Germany) (see chapter 3.8.16). The volunteers obtained detailed information about the purpose and the aim of the study as well as possible risks associated with the study. Each volunteer had to document his willingness to take part in the study by his signature. Furthermore, the volunteers agreed with their signature in the evaluation, processing, use and publishing of the data in pseudonymized form. At the beginning all volunteers were asked to wash their arms and dry them afterwards. Three test areas and one control area were defined on the volar forearms of 10 female volunteers with healthy skin in the testing areas. After an incubation time of 30 min at 20°C ± 1°C and 45% ± 5% relative humidity, the base values were determined by Corneometer measurement. 100 mg of coenzyme Q10 containing NLC and o/w emulsion were applied to 10.4 cm^2 test areas. A further test area was occluded using Parafilm®. The skin hydration was measured 30, 60 and 120 min after application of the test formulations. The average percentage change of skin hydration at each measurement point was calculated using the following equation:

$$\textit{Change in skin hydration}\,[\%] = \left(\frac{\sum Q_{ti}}{\sum Q_{0i}} - 1 \right) \times 100$$

t = time point

i = number of volunteer

Q_{ti} = quotient of measured value in the test area and the control area at the time point t for volunteer i

Q_{0i} = quotient of measured value in the test area and the control area at the begin of the study for volunteer i

3.5.3 Results and discussion

In vitro occlusion test

Figure 3.5.3-1 shows the occlusion factor of NLC, o/w emulsion and liquid paraffin. The occlusion factor of the NLC was much higher than the occlusion factor of the o/w emulsion. NLC show the same occlusion properties like highly occlusive liquid paraffin. NLC and o/w emulsion were produced under the same conditions, had the same lipid content, a similar particle size and were applied with the same amount. Therefore, these factors can be excluded for causing different occlusive behavior of NLC and o/w emulsion. NLC used for these investigations had a melting point of 47.3°C. That means they are still solid at both room and skin temperature whereas the oil of the o/w emulsion is liquid at these temperatures. The difference in the occlusive behavior is therefore caused by the difference in crystallinity [338].

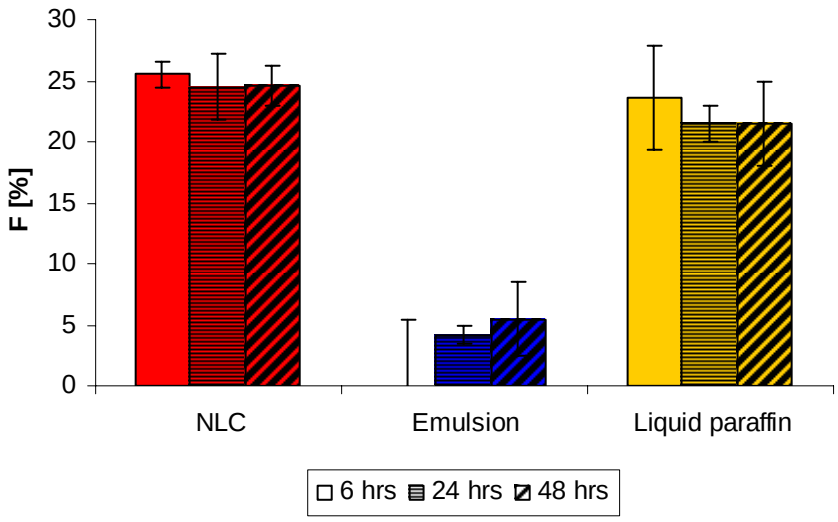

Figure 3.5.3-1: Occlusion factor (F) of NLC, o/w emulsion and liquid paraffin.

The high occlusive effect of NLC can be explained by the film formation of NLC. Nanoparticles exhibit distinct adhesive properties to surfaces. Hence, after the water is evaporated from the NLC dispersion only the solid NLC particles stay on the filter surface or on the skin, respectively. The capillary force of the nanometer pores between the NLC particles are contractive promoting fusion and dense film formation which is also promoted by application pressure [344, 345]. The microscopic picture of NLC shows clearly a film formation on the slide whereas after application of the o/w emulsion no film formation could be observed (Figure 3.5.3-2).

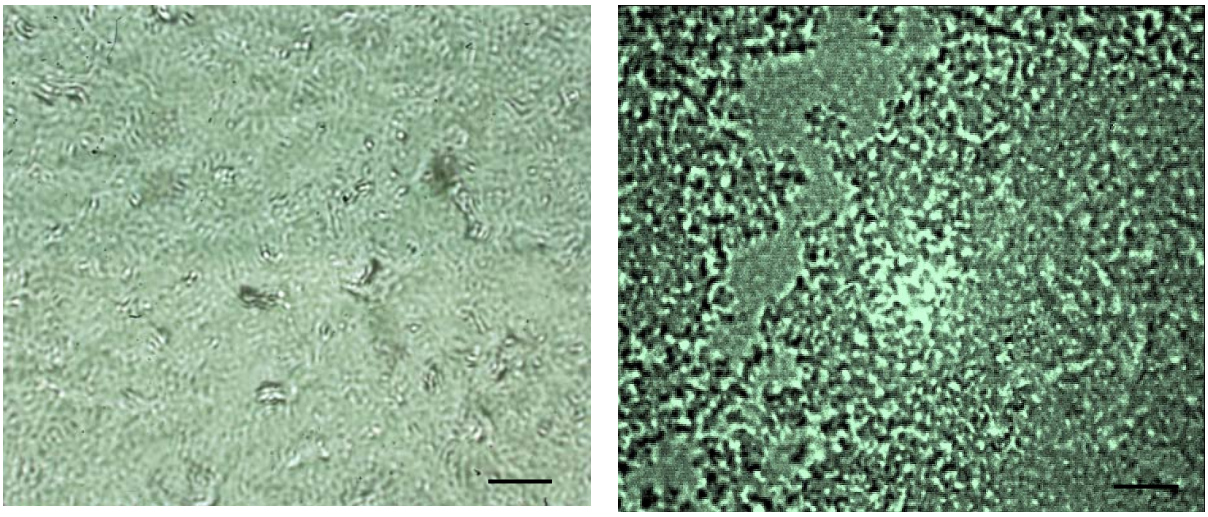

Figure 3.5.3-2: Appearance of NLC (left) and o/w emulsion (right) after drying on a microscope slide magnified 100x10-times. The bar refers to 4 µm.

It should be pointed out that the lipid concentration of the NLC dispersion was 20%. That means only about 2 mg/cm^2 pure lipid phase were applied to the cellulose acetate filter in the occlusion test. Even with that low lipid concentration NLC performed the same occlusivity like the highly occlusive liquid paraffin whereas the o/w emulsion, having the same lipid concentration as NLC, had relatively low occlusive properties.

Ex vivo occlusion test using porcine skin

Figure 3.5.3-3 shows the occlusion factors obtained for NLC, o/w emulsion and liquid paraffin in the *ex vivo* occlusion test using porcine skin. The occlusion factor of NLC was higher than the occlusion factor of the o/w emulsion. NLC show similar occlusion properties as highly occlusive liquid paraffin.

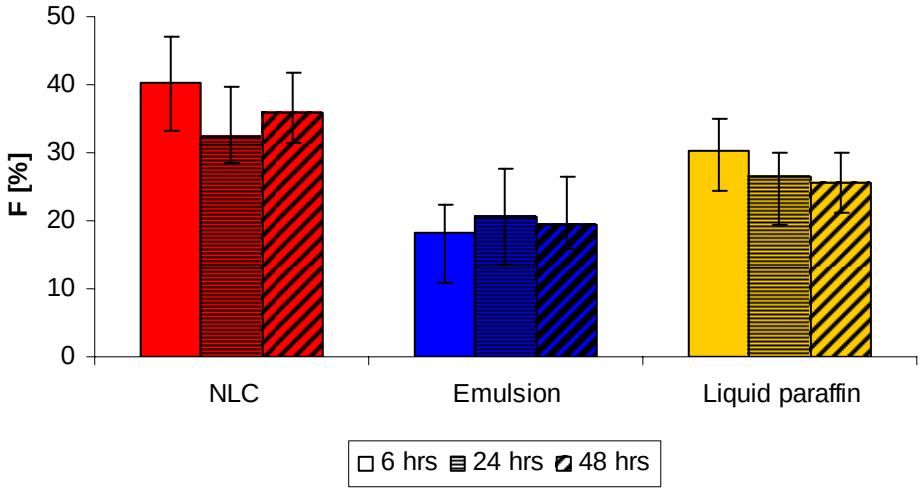

Figure 3.5.3-3: Occlusion factor (F) of NLC, o/w emulsion and liquid paraffin obtained on *ex vivo* porcine skin.

The results obtained in the *ex vivo* occlusion test confirm the findings of the *in vitro* test. This confirms the theory that lipid nanoparticles adhere to the skin and form a dense film which inhibits water evaporation from the skin. Jenning et al. could show previously by microscopic investigations on porcine skin that the application of SLN containing o/w cream induced swelling and increased the thickness of the stratum corneum which indicates occlusion whereas an o/w cream without SLN did not show this effect [59].

In vivo occlusion test – Single application Corneometer study

The Corneometer is a capacity measuring device which is sensitive to the relative dielectric constant of materials placed in contact with the electrode. Water has a relatively high dielectric constant whereas the dielectric constants of lipids are relatively low. Hence, an increase in water content in the skin increases the Corneometer values whereas placing materials with a low dielectric constant in contact with the sensing head of the Corneometer decreases the readings [346]. The results of the *in vivo* occlusion study are shown in Figure 3.5.3-4. Placing Parafilm® on the skin and measuring on this occlusive material reduces the measured skin hydration by about 80% over the observation period. After applying coenzyme Q10 containing NLC to the skin, the measured skin hydration was reduced by 38.5% within the first 30 min, by 38.9% after 60 min and by 34.2% after 120 min. The reduction of the Cornemoeter values after application of NLC to the skin indicates the formation of an occlusive film. Due to the presence of an occlusive film on the skin surface the measuring condensator of the Corneometer is insulated from the water in the stratum corneum. This results, what was also shown for Parafilm®, in a reduction of the measured skin

hydration although an accumulation of water takes place under occlusive material. The o/w emulsion with less occlusive properties increased the skin hydration by 42% within 30 min, by 24.7% within 60 min and by 23.3% within 120 min because in this case no film formation interferes with the measuring condensator an increase in skin hydration can be directly measured. A decrease in skin hydration over the observation period was found for the o/w emulsion due to evaporation of water from the formulation.

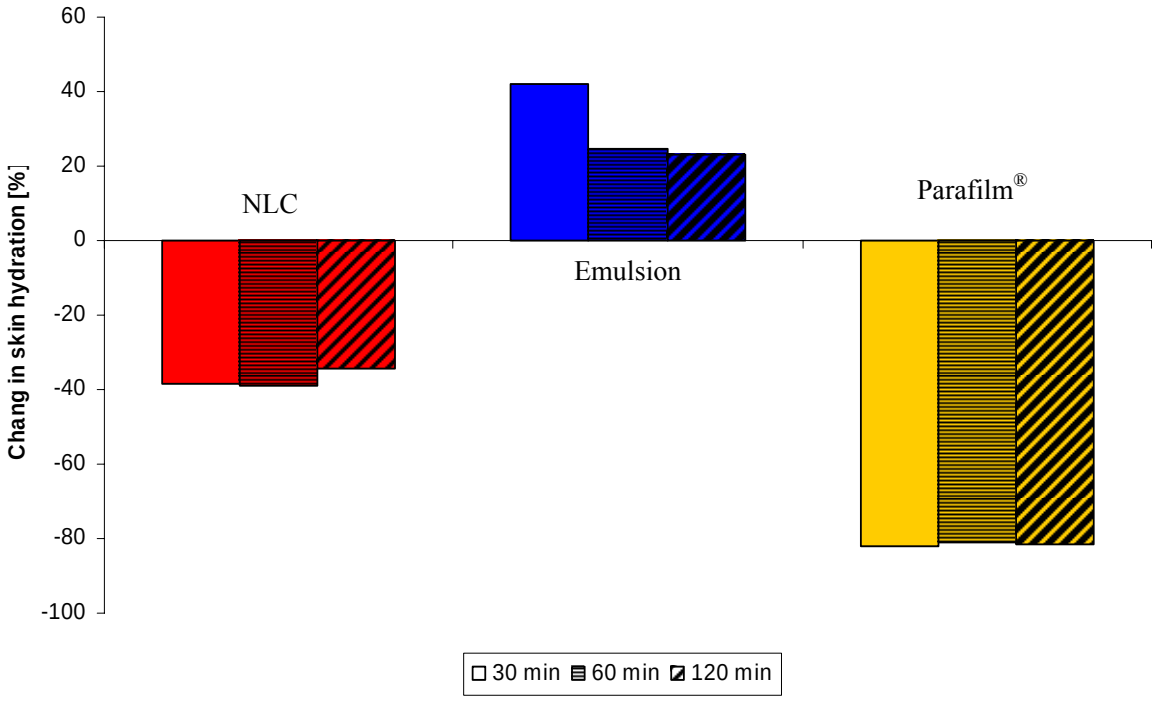

Figure 3.5.3-4: Change in measured skin hydration [%] after applying NLC, o/w emulsion and Parafilm® to the volar forearm of 10 female volunteers for 30, 60 and 120 min.

The theory by Jenning and Wissing of the formation of a dense film on the skin after application of NLC which leads to occlusion can be supported with the findings of the *in vitro*, *ex vivo* and *in vivo* tests performed to investigate the occlusive properties of coenzyme Q10-loaded NLC. In the *in vitro* and *ex vivo* test coenzyme Q10-loaded NLC performed a similar occlusivety like highly occlusive liquid paraffin. *In vivo* the formation of a dense film on the skin could be shown by the reduction of the Corneometer values.

3.6 *In vitro* release of coenzyme Q10

3.6.1 Introduction

Burst release as well as sustained release have been reported for SLN and NLC dispersions [53, 347-349]. For dermal application both features are of interest. Burst release might improve the penetration of active compounds. Sustained release becomes important for active ingredients that are irritating at high concentrations or to supply the skin over a prolonged period of time with an active compound (e.g. anti-mycotics). The main factors influencing the release of actives from lipid nanoparticles are the physicochemical properties of the incorporated active itself [350, 351], the active content [48, 352], the lipid matrix composition [48, 353], the surfactants used [49], the surface charge [353], the active distribution throughout the particle matrix [43, 351, 352], the production method and production parameters [50, 351], the release media [354, 355] and the release model used [352].

With regards to the active distribution throughout the matrix three different models have been proposed, which are the homogeneous matrix model, the active-enriched shell model and the active-enriched core model. The homogeneous matrix model is characterized by molecularly dispersed actives throughout the matrix. This model can be mainly obtained by cold homogenization technique or hot homogenization technique incorporating very lipophilic actives. Slow release of active compounds over a long time interval has been reported for this model [356]. In the active-enriched shell model the active is located on the particles surface surrounding an active-free lipid core. The formation of this model by hot high pressure homogenization can be explained by partitioning of the active into the water phase during the production. Cooling the system leads to lipid precipitation while the active re-partitions into the liquid lipid phase and is therefore concentrated in the outer shell. A burst release is likely for this model [351]. In the active-enriched core model the active-enriched core is surrounded by an active-free lipid shell or a lipid shell with a low active concentration. This model forms if after hot high pressure homogenization cooling leads to supersaturation of the active in the lipid and the active precipitates before the lipid crystallizes. Due to an increased diffusional distance and a hindering effect of the lipid shell this particles show sustained release profiles [43]. However, in practice also mixtures of the three models are obtained.

In the present study the *in vitro* release of coenzyme Q10 from NLC, o/w emulsion and liquid paraffin was studied using Franz diffusion cells.

3.6.2 Methods

***In vitro* release study**

The *in vitro* release of coenzyme Q10 from NLC, o/w emulsion and liquid paraffin was studied using static Franz diffusion cells (Crown Scientific, Somerville, USA) with a diameter of 0.9 cm (0.64 cm^2 surface area) and 6.0-6.5 ml acceptor volume. As acceptor medium 20% (w/w) Labrasol® (Gattefossé, Saint-Priest, France) in PBS was used, which was stirred by a magnetic bar at 600 rpm. The experiment was carried out under sink conditions with infinite dose. Coenzyme Q10 containing NLC and emulsion were prepared as described in chapter 3.3 and diluted in a ratio 1:10 with bidistilled water. 0.48% (w/w) coenzyme Q10 were dissolved in liquid paraffin and served as a reference. 300 µl of each formulation were applied to cellulose acetate membrane filters (Sartorius, Göttingen, Germany) with a pore size of 0.1 µm, which were socked in acceptor medium over night. The release study was carried out at 32°C to mimic skin temperature. To ensure a temperature of 32°C throughout the system Franz diffusion cells filled with acceptor medium and cellulose acetate membranes mounted to them were acclimatized for one hr before the start of the experiment. Samples of 300 µl were withdrawn after 1, 2, 3, 4, 5, 6 and 24 hrs. The same volume was replaced by fresh acceptor medium maintained at 32°C. The samples were analyzed by HPLC as described in chapter 3.4. The obtained data were statistically evaluated using the Wilcoxon test ($\alpha = 0.05$). Furthermore, to describe the kinetics of the coenzyme Q10 release mathematic models such as zero-order, first-order and Higuchi model were used. The criterion for selecting the most appropriate model was based on the goodness of fit test.

3.6.3 Results and discussion

To evaluate the mechanism of coenzyme Q10 release from NLC, o/w emulsion and liquid paraffin an *in vitro* release study using Franz diffusion cells has been performed. Figure 3.6.3-1 shows the cumulative amount of coenzyme Q10 released from NLC, o/w emulsion and liquid paraffin related to the applied amount of coenzyme Q10. The released amount of coenzyme Q10 from NLC and o/w emulsion was of the same order of magnitude at each time point. No significant difference in the released amount of coenzyme Q10 from these formulations was found ($\alpha = 0.05$). The released amount of coenzyme Q10 from liquid paraffin was significant lower than from NLC and o/w emulsion ($\alpha = 0.05$). The release profiles of all three formulations can be described by zero-order release kinetic ($r > 0.99$, $p < 0.01$), which means that per time interval the same amount of coenzyme Q10 was released from the formulations. The premises for zero-order release kinetic were fulfilled in the test system due to performing infinite dose experiments under sink conditions.

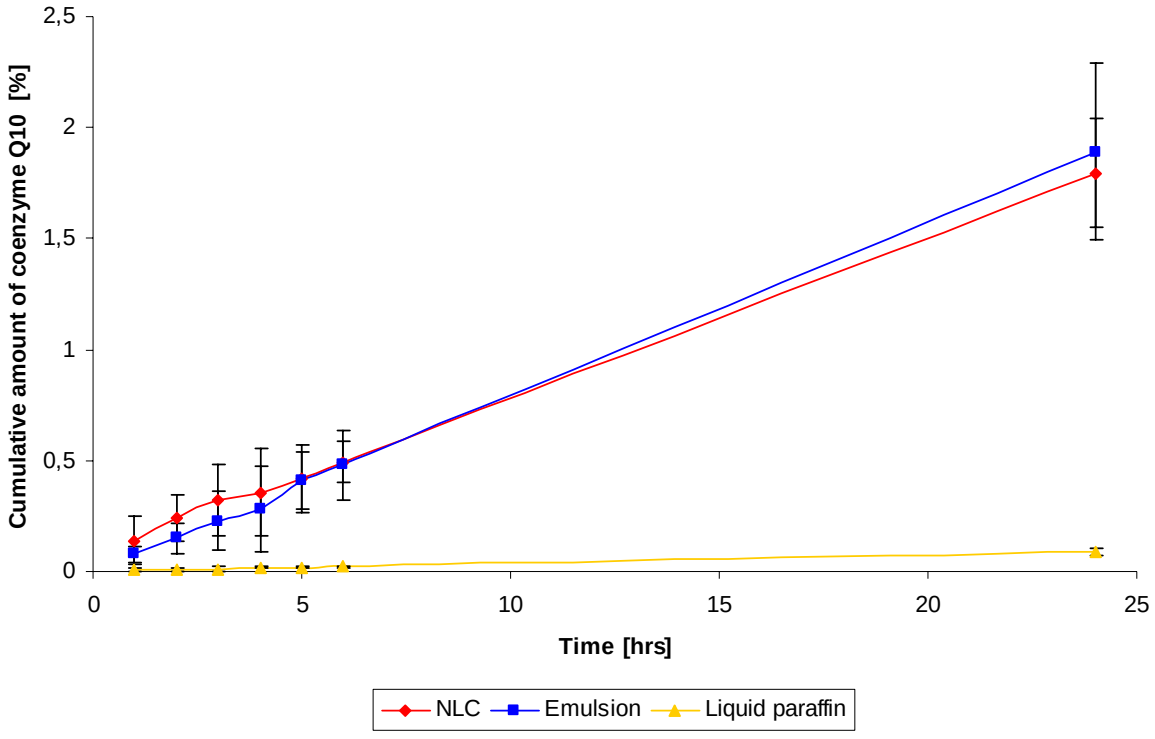

Figure 3.6.3-1: Cumulative amount of coenzyme Q10 released from NLC, o/w emulsion and liquid paraffin related to the applied amount of coenzyme Q10 (n = 6).

The steady-state flux values obtained as the slop of the linear regression equation ($r > 0.99$, $p < 0.01$) when plotting the cumulative amount coenzyme Q10 permeated per cm^2 versus time are shown in Table 3.6.3-1 for NLC, o/w emulsion and liquid paraffin. The flux values of coenzyme Q10 from NLC and o/w emulsion were higher than the flux value of coenzyme Q10 from liquid paraffin. The low flux value of coenzyme Q10 from liquid paraffin can be explained by the highly lipophilic character of both coenzyme Q10 and liquid paraffin. The tendency that coenzyme Q10 diffuses into the less lipophilic acceptor medium is therefore low. In case of o/w emulsion and NLC dispersion only 2% lipid content were present in the donor chamber surrounded by 98% aqueous phase. The aqueous solubility of coenzyme Q10 is very low. Therefore, if coenzyme Q10 is released from the oil droplets of the emulsion or from the lipid particles of the NLC dispersion, respectively, a fast diffusion of coenzyme Q10 into the acceptor medium, where the solubility of coenzyme Q10 is higher than in water, takes place. Hence, higher flux values for coenzyme Q10 from NLC and o/w emulsion are obtained than from liquid paraffin.

Table 3.6.3-1: Steady-state flux values of coenzyme Q10 from NLC, o/w emulsion and liquid paraffin.

Formulation	Flux [µg/cm²/h]
NLC	1.47
Emulsion	1.51
Liquid paraffin	0.08

In summary, no significant difference in the release profile of coenzyme Q10 from NLC and o/w emulsion was found under the applied test conditions. The release of coenzyme Q10 from liquid paraffin was significant lower than from NLC and o/w emuslion. These findings were confirmed by the steady-state flux values. Moreover, it could be shown that the release of coenzyme Q10 from all tested formulations followed zero-order kinetic. Hence, neither burst release nor sustained release was obtained for coenzyme Q10-loaded NLC under the applied test conditions.

3.7 *In vivo* evaluation of the skin penetration of coenzyme Q10 by tape stripping test

3.7.1 Introduction

The skin acts as a barrier in two directions, controlling the loss of water, electrolytes and other body constitutes, while preventing the entry of harmful or unwanted molecules from the external environment [2, 357]. Factors influencing the penetration of actives into the skin are the structure of the skin, the physico-chemical properties of the active, physico-chemical properties of the vehicle in which the active is applied as well as the dosing conditions.

The stratum corneum represents the major barrier for the penetration of actives into the skin or the permeation of actives across the skin. There are two general options for active molecules to permeate the stratum corneum, the transepidermal route and the route via pores (Figure 3.7.1-1) [3]. The transepidermal route can be divided into the transcellular route and the intercellular route. In case of intercellular penetration, which is the more common case, the active penetrates through the lipid bilayers between the corneocytes. In case of transcellular penetration the active passes through lipid bilayer structures of the stratum corneum and the corneocytes. The transport of actives via pores i.e. along the hair follicles, sebaceous glands and sweet glands, is considered to be of minor importance because of their relatively small area (less than 0.1% of the total skin surface).

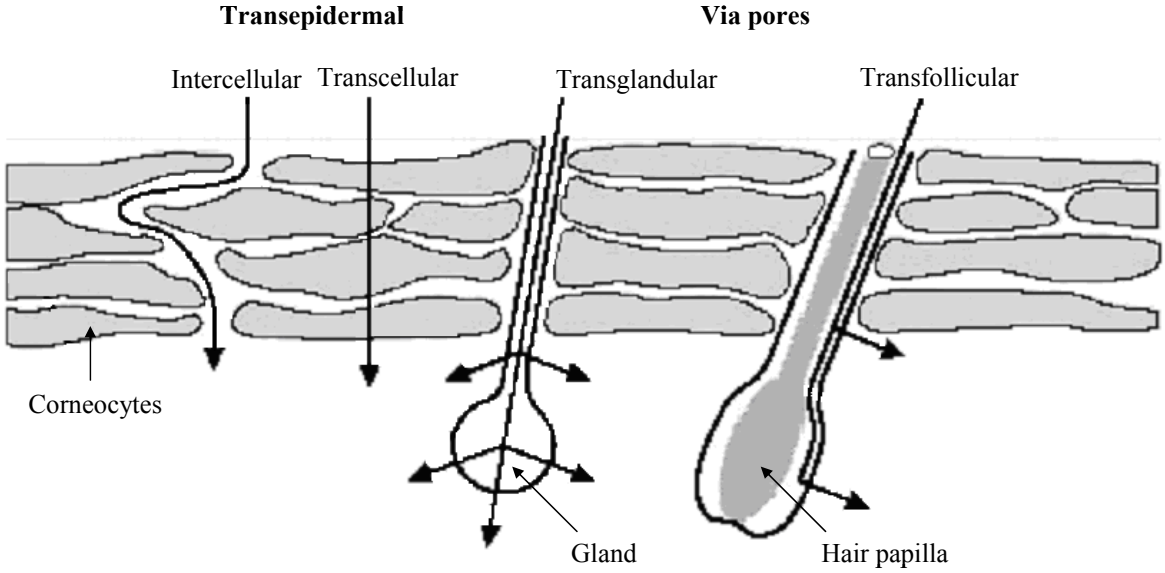

Figure 3.7.1-1: Schematic overview of penetration ways of actives across the stratum corneum (modified after [3]).

To study the penetration, the distribution within the stratum corneum and dermato-pharmacokinetics of dermally applied cosmetic actives or drugs as well as to study stratum corneum physiology the serial removal of the stratum corneum by adhesive tape strips (tape stripping) is a useful and noninvasive technique [358-361]. Although the forearm, back, thigh or other parts of the body can be used for tape stripping studies, most studies are carried out on the forearm for reasons of convenience [362]. On the volar forearm the thickness of the stratum corneum ranges between 5 µm and 20 µm [363]. To completely remove the stratum corneum from this area 50 up to 100 tape strips need to be applied [364]. However, to asses the majority of the active compound penetrated into the stratum corneum an FDA draft guidance recommends to remove ten tape strips whereby the first tape strip is discarded because it may contains unabsorbed actives from the skin surface and the active content in the following nine tape strips is analyzed [365].

3.7.2 Methods

Tape stripping test

The penetration of coenzyme Q10 from NLC, o/w emulsion and liquid paraffin into the stratum corneum was studied by tape stripping test. Coenzyme Q10-loaded NLC and o/w emulsion were prepared as described in chapter 3.3. The obtained formulations were diluted in a ratio 1:10 with bidistilled water. 0.48% (w/w) coenzyme Q10 were dissolved in liquid paraffin. The volunteers obtained detailed information about the purpose and the aim of the study as well as possible risks associated with the study. Each volunteer had to document his willingness to take part in the study by his signature. Furthermore, the volunteers agreed with their signature in the evaluation, processing, use and publishing of the data in pseudonymized form. Five 23-25 years old female volunteers with healthy skin on the volar forearm participated in this study. At the beginning the volunteers were ask to wash their arms and dry them afterwards. After an incubation period of 30 minutes at 20°C ± 1°C and 45±5% relative humidity four 10.4 cm^2 test areas were marked on the volar forearm of the volunteers. 150 mg of coenzyme Q10 containing NLC, o/w emulsion and liquid paraffin were applied to the test areas and spread evenly. 30 minutes after application the samples were washed off. The stratum corneum was removed with 10 strips of Scotch Tape No. 90. Each tape was taken in a controlled way, i.e. a 1 kg rubber weight was rolled over it 10 times. The first tape was discarded because of possible remains of the formulations on the tape. The coenzyme Q10 was extracted from the following 9 tape strips (number 1-9) with 2.00 ml of acetone. The

concentration of coenzyme Q10 was determined using the HPLC method described in chapter 3.4. Strip 4 and 5, 6 and 7 and 8 and 9 were analyzed together. The obtained data were statistically evaluated using the Wilcoxon test ($\alpha = 0.05$).

One test area stayed untreated and surfed for the determination of the amount of stratum corneum removed with each tape strip applying the above described method. Therefore, the tape strips were weight before and after stripping. Furthermore, the stratum corneum removed with each tape strip was visualized using a light microscope (Leitz, Wetzlar, Germany) equipped with a CMEX-1 digital camera (Euromex microscopes, Arnheim, Netherlands) connected to Image Focus software version 1.3.1.4. (Euromex microscopes, Arnheim, Netherlands).

3.7.3 Results and discussion

Jacobi et al. reported a linear relationship between the number of tape strips and the stratum corneum amount removed up to 20 tape strips. Whereas with a further increasing number of tape strips a non-linear correlation exists between the number of the tape strip and the stratum corneum amount removed [364]. Generally the amount of stratum corneum removed by tape stripping depends on a variety of parameters e.g. the type of adhesive tape used, the pressure applied, the person performing the tape stripping test, the side of application, the age and the gender of the volunteers, the ambient temperature and humidity and inter-seasonal differences in the stratum corneum structure [360]. Therefore, the relationship between the amount of stratum corneum removed and the tape strip number under the applied test conditions was investigated. Figure 3.7.3-1 shows the cumulative amount of stratum corneum removed related to the tape strip number.

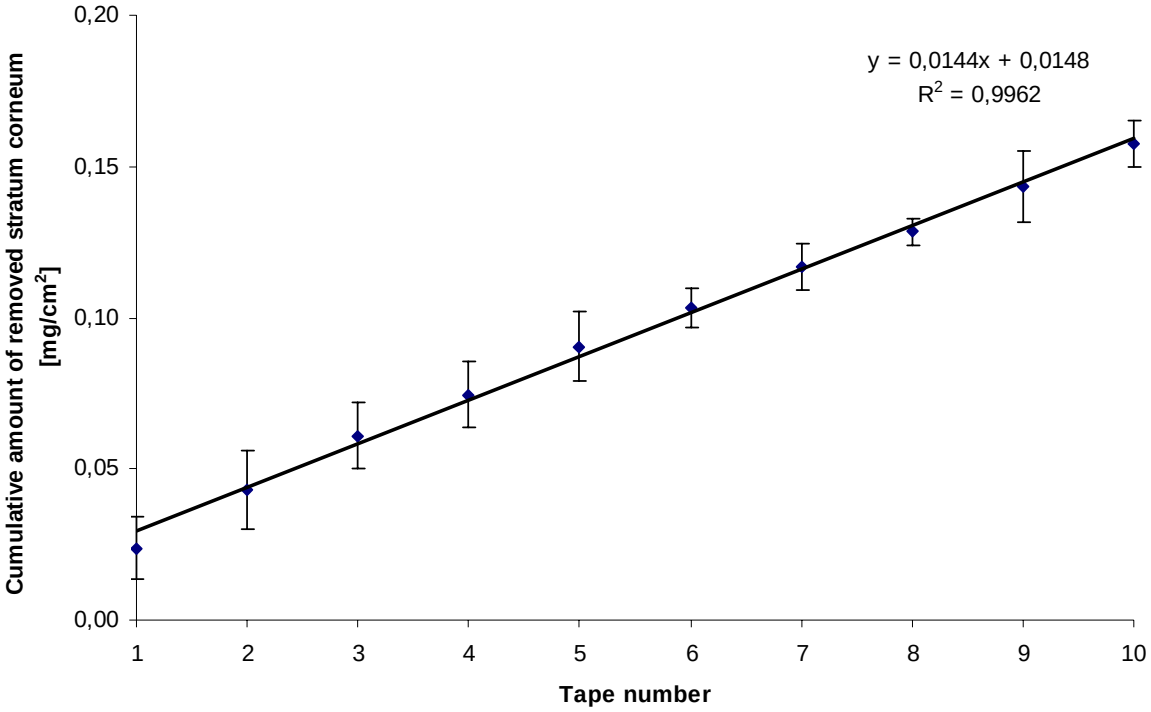

Figure 3.7.3-1: Cumulative amount of stratum corneum removed [mg/cm^2] related to the tape strip number (n = 5).

A linear correlation between the cumulative amount of removed stratum corneum and the tape strip number was found, which was confirmed by linear regression analyses ($r > 0.99$, $p < 0.01$)). That means with each of the 10 tapes approximately the same amount of the stratum corneum is removed. To obtain detailed information on the covering density of the corneocytes on each removed tape strip, light microscopy pictures were taken. Figure 3.7.3-2 shows exemplary the microscopy pictures of the stratum corneum removed with each of 10 tape strips from the volar forearm of one of the five female volunteer, who participated in this study. These pictures confirm the findings as on each tape approximately the same amount of stratum corneum can be seen. Hence, the penetrated amount of coenzyme Q10 into the stratum corneum from the test formulations was directly related to the tape strip number.

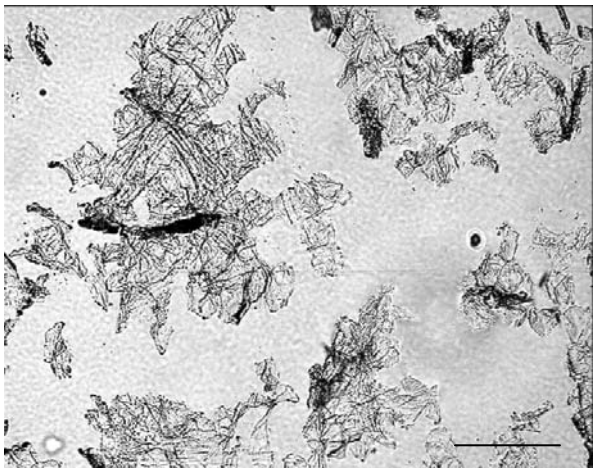

Tape 1

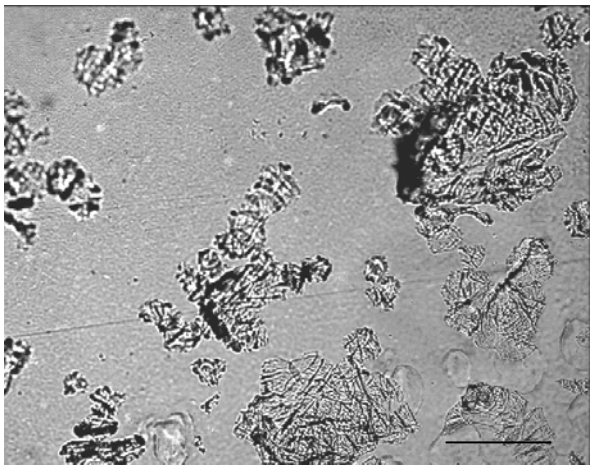

Tape 2

Tape 3

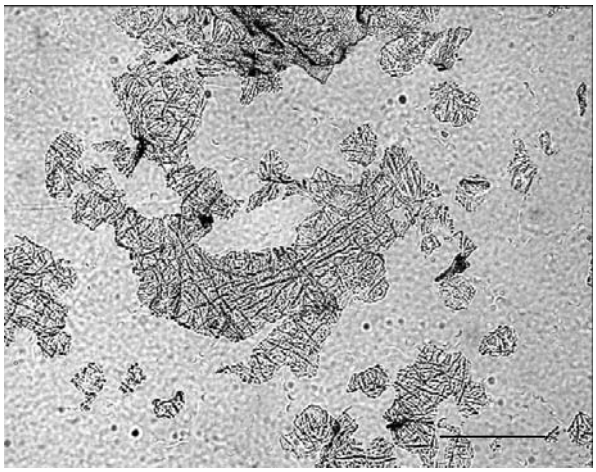

Tape 4

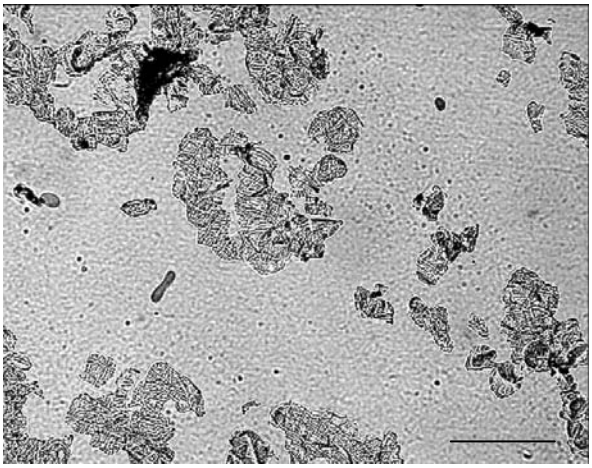

Tape 5

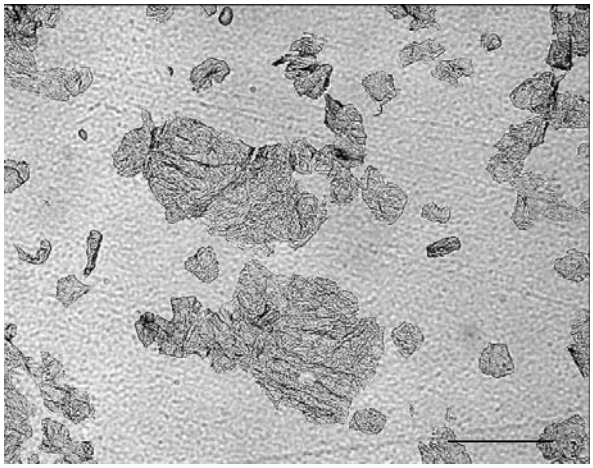

Tape 6

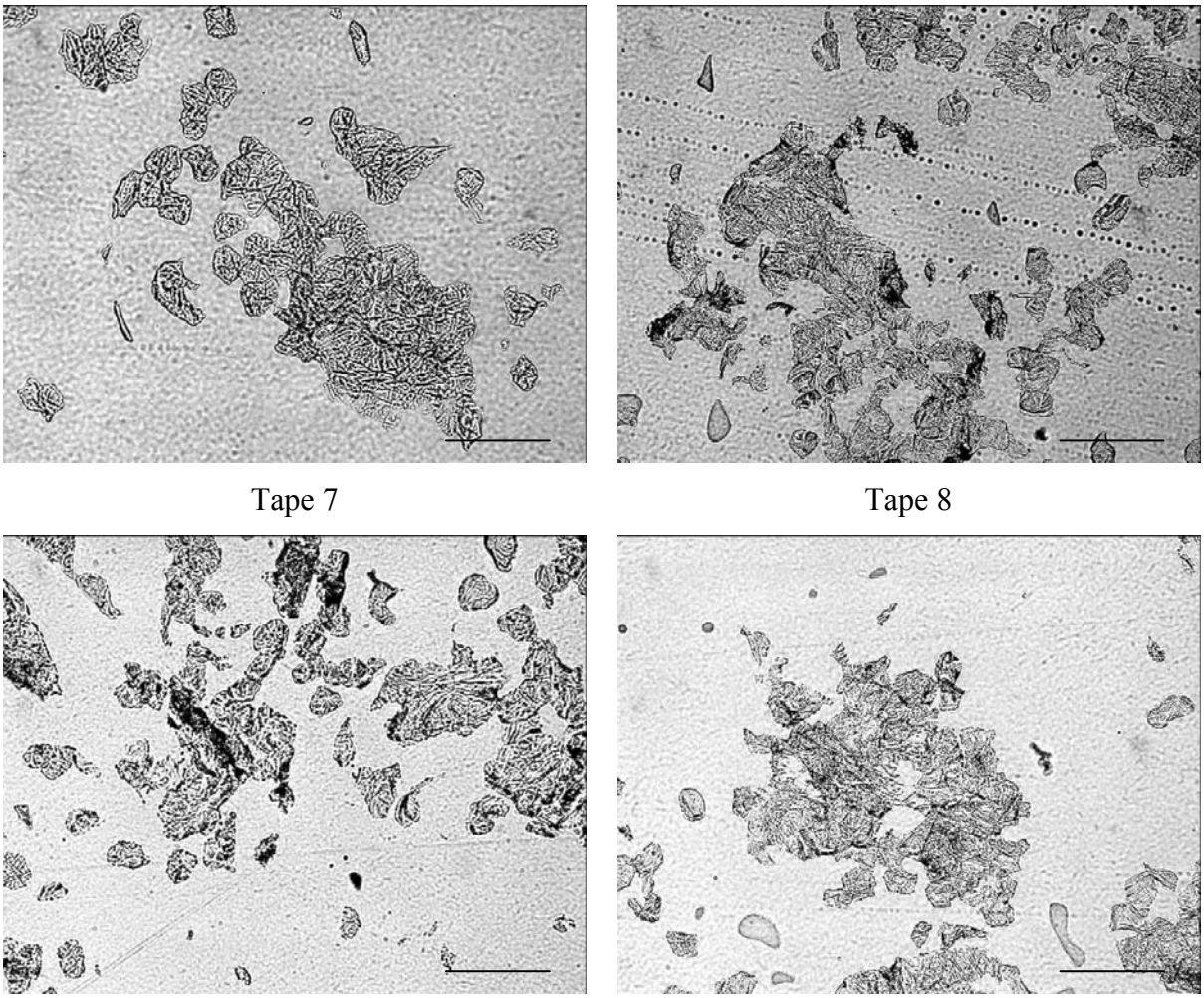

Figure 3.7.3-2: Visualization of the stratum corneum removed with each of 10 tape strips from the volar forearm of a female volunteer (bar refers to 200 µm).

Figure 3.7.3-3 shows the results of the tape stripping test obtained after applying coenzyme Q10 containing NLC, o/w emulsion and liquid paraffin to the skin. It was found that the penetration of coenzyme Q10 into the stratum corneum from NLC and o/w emulsion was significant higher than from liquid paraffin ($\alpha = 0.05$). The highest amount of coenzyme Q10 penetrated into the stratum corneum was found after the application of coenzyme Q10-loaded NLC. The amount of coenzyme Q10 penetrated into the stratum corneum from the NLC formulation was significant higher than the amount penetrated into the stratum corneum from the o/w emulsion ($\alpha = 0.05$).

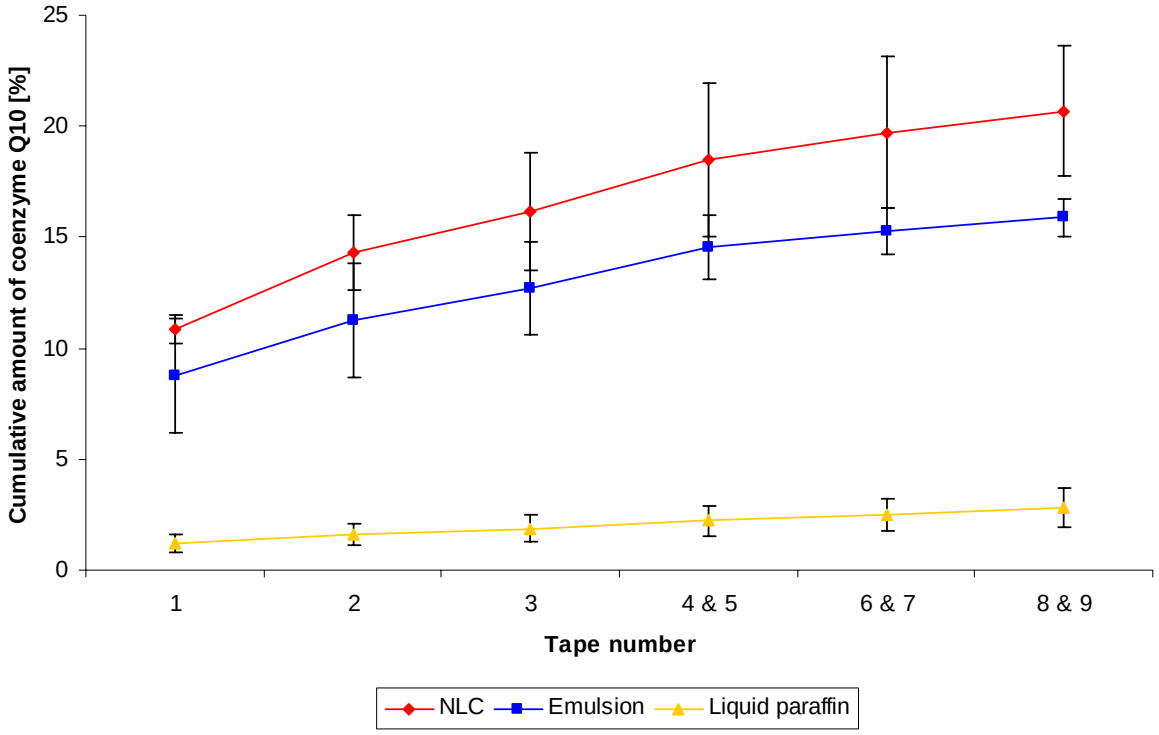

Figure 3.7.3-3: Cumulative amount of coenzyme Q10 found in the tapes after application of coenzyme Q10 containing NLC, o/w emulsion and liquid paraffin related to the applied amount (n = 5).

The shape of the penetration curves indicates a logarithmic relationship between the cumulative values of coenzyme Q10 penetrated into the stratum corneum and the tape strip numbers as with low tape strip numbers a high increase in the cumulative amount of coenzyme Q10 was found whereas with higher tape strip numbers the cumulative amount of coenzyme Q10 increased only slightly. Logarithmic relationships between a penetrated compound and the tape strip number have been reported previously [361]. When performing regression analysis, functions of the type:

$$y = n \log x + m$$

can fit the data, where y is the cumulative percentage of coenzyme Q10 found inside the stratum corneum, x is the corresponding tape strip number and n and m the estimate equilibration coefficients. Table 3.7.3-1 provides a summary of the parameters describing the logarithmic relation between the cumulative amount of coenzyme Q10 and the tape strip number for NLC, o/w emulsion and liquid paraffin. Slope n accounts for the gradient of coenzyme Q10 content inside the stratum corneum layers. For the NLC the highest gradient of coenzyme Q10 content into the stratum was obtained. That shows that the penetration of

coenzyme Q10 into the stratum corneum from NLC was superior to the penetration obtained from the o/w emulsion and liquid paraffin. The liquid paraffin showed the smallest slope n, indicating a poor penetration of coenzyme Q10 into the stratum corneum. The value of the constant m stands for the amount of coenzyme Q10 found at the first tape strip. Here the values of NLC and o/w emulsion were also much higher than the one from liquid paraffin. That means even close to the skin surface a higher coenzyme Q10 content could be detected for NLC and o/w emulsion than for liquid paraffin.

Table 3.7.3-1: Parameters describing the logarithmic relation between the cumulative amount of coenzyme Q10 and the tape number for NLC, o/w emulsion and liquid paraffin ($p<0.01$).

Parameter	NLC	Emusion	Liquid paraffin
n	4.466	3.290	0.711
m	11.086	8.928	1.141
R^2	0.997	0.994	0.981

In the *in vitro* release study it was found that the release of coenzyme Q10 from liquid paraffin was significantly lower than from coenzyme Q10-loaded NLC and o/w emulsion. A good correlation between the *in vitro* release study and the *in vivo* tape stripping test was found for the coenzyme Q10 containing liquid paraffin. The poor penetration of coenzyme Q10 into the stratum corneum from liquid paraffin is likely to be caused by the poor release of coenzyme Q10 from the formulation. The solubility of coenzyme Q10 in liquid paraffin is much higher than in the stratum corneum and no push or pull effect can be obtained [2].

There was no significant difference found in the *in vitro* release profiles of coenzyme Q10-loaded NLC and o/w emulsion whereas in the *in vivo* tape stripping test a significant higher amount of coenzyme Q10 penetrated into the stratum corneum from the NLC formulation. Having the same lipid content, the same coenzyme Q10 content, a similar particle size and the same release profiles, the higher occlusive properties of coenzyme Q10-loaded NLC might cause the pronounced penetration of coenzyme Q10 into the stratum corneum compared to o/w emulsion. By occluding the skin the transepidermal water loss is prevented and endogenous water is trapped in the stratum corneum, which therefore becomes more hydrated. The presence of water in the stratum corneum results in hydration shells around the polar head groups of the lipid bilayer via hydrogen bonds, which loosens its packing. A more fluid and more permeable lipophilic route will be obtained leading to a better permeation of lipophilic compounds like coenzyme Q10 [9, 58]. The penetration of coenzyme Q10 from liquid

paraffin, which has the same occlusive properties as coenzyme Q10-loaded NLC, could not be enhanced due to the poor release from this formulation.

The findings of this *in vivo* study are well in agreement with earlier findings, where an enhanced penetration of lipophilic compounds into the stratum corneum was reported from lipid nanoparticles. For example, loading the non-steroidal anti-inflammatory drugs ketoprofen, naproxen and indomethacin to NLC could increase their penetration into the stratum corneum compared to reference formulations [315, 366]. The glucocorticoids prednicabate and betamethasone 17-valerate penetrated better into the skin when applied as an SLN containing formulations compared to conventional creams [325, 367]. An increased penetration of cyproterone acetate from SLN was reported [52]. Jenning et al. could show an increased concentration of vitamin A in the stratum corneum after application of vitamin A-loaded SLN compared to o/w emulsion [59]. Studying the *in vivo* penetration of coenzyme Q10 from SLN into the stratum corneum, Dingler could show an enhanced penetration compared to isopropanol and liquid paraffin [320]. The present study could show that also NLC are able to enhance the penetration of coenzyme Q10 into the stratum corneum.

In the present study it could be shown by weighing the tape strips before and after removal as well as by light microscopy investigations that approximately the same amount of stratum corneum was removed with each tape strip under the applied test conditions. Comparing the penetration of coenzyme Q10 from NLC, o/w emulsion and liquid paraffin, it was found that the penetration of coenzyme Q10 from NLC into the stratum corneum was significant higher than from the other two formulations. The penetration of coenzyme Q10 from liquid paraffin into the stratum corneum was the lowest, which correlated well with the findings of the *in vitro* release study. No significant difference in the *in vitro* release profiles of coenzyme Q10-loaded NLC and o/w emulsion was found, whereas the *in vivo* penetration of coenzyme Q10 was significant higher from NLC, which was related to the highly occlusive properties of NLC, which can enhance the penetration of the lipophilic coenzyme Q10.

3.8 Effect of NLC on skin hydration: *in vivo* study

3.8.1 Background

If the effect of a cosmetic product should be claimed on its package, the proof of this effect is required by law [368, 369]. One important criterion for the evaluation of cosmetic products is their effect on skin hydration, which was evaluated in the following *in vivo* study for two test formulations using a Corneometer CM 825 (Courage and Khazaka, Colongne, Germany) [346]. The test formulations were a conventional o/w cream and an o/w cream containing NLC. Both test formulations had the same lipid content and the same content of the cosmetic active coenzyme Q10. The study was carried out from December 2005 until January 2006 at the Department of Pharmaceutical Technology, Biopharmaceutics and NutriCosmetics at the Freie Universität Berlin.

3.8.2 Aim of the study

The aim of the study was to evaluate if Cutanova Nanorepair Q10 cream (Dr. Rimpler GmbH, Wedemark, Germany) and a placebo cream, with the same lipid and coenzyme Q10 content but without NLC, increase the skin hydration significantly after repetitive application. Furthermore, it should be evaluated if the NLC containing Cutanova Nanorepair Q10 cream increases the skin hydration more than the placebo cream.

3.8.3 Benefit-risk-evaluation

The ingredients of the two cosmetic products under evaluation are consistent with the requirements outlined in the cosmetic ordinance [369]. The test formulations are market products. For the topical application of the test formulations under investigations were no specific disadvantages or risks known, which are pronounced over the basically always existing risk of intolerance in case of sensitization. The benefit for a future customer to obtain a product with evaluated effectiveness preponderances the potential risk of the evaluation according to today's knowledge. The performance of the *in vivo* study is therefore considered to be ethically justifiable. The method for the evaluation of the skin hydration is not invasive and exhibits no danger to the volunteers.

3.8.4 Design of the study

The study was designed as a one-side-blind, placebo controlled study with intra individual comparison of two test formulations and two untreated control areas. The test formulations were applied to the test areas on the volar forearm twice daily (in the morning and in the evening) for six weeks. An untreated control area was defined on each volar forearm. Hence, the intra and inter individual comparison of the test formulations as well as of the untreated control areas was possible. All volunteers got the same treatment. The volunteers were not subdivided in groups. The volunteers obtained the two test formulations marked with a formulation code and the test area for home application. The skin hydration was evaluated at day 1, 7, 28, 42 and 49. In the morning of day 7, 28 and 42 no cream was applied. Therefore, the skin hydration was measured 12 to 16 hrs after the last application.

3.8.5 Composition of the creams

Cutanova Nanorepair Q10 cream (Dr. Rimpler GmbH, Wedemark, Germany) with an NLC content of 10% and a placebo cream, where the NLC were replaced by a conventional o/w emulsion, were tested. Both test formulations had the same lipid content (approximately 40%) and the same content of coenzyme Q10 (0.48%). Therefore, the effect of the NLC containing cream could be compared with the effect of a conventional o/w cream. Table 3.8.5-1 summarizes the ingredients of the two test formulations.

Table 3.8.5-1: Summary of the ingredients of the two test formulations.

Cutanova Nanorepair Q10 Cream	Placebo cream
Aqua, Cetearyl Alcohol, Octyldodecanol, Glycerin, Squalane, Cannabis Sativa, Dimethicone, Cyclopentasiloxane, Arachidyl Alcohol, Cetyl Palmitate, Behenyl Alcohol, Cetearyl Glucoside, Ubiquinone, Hibiscus Sabdariffa Flower Extract, Hydrolyzed Wheat Protein, Hydrolyzed Soy Protein, Zingiber Officiale Root Extract, Beta-Carotene, Zea Mays, Erythrulose, Tocopherol, Tripeptide-1, Xanthan Gum, Tetrasodium Edta, Arachidyl Glucoside, Hydrogenated Palm Glycerides Citrate, Dimethicone Crosspolymer, Polyglyceryl-3 Methylglucose Distearate, Caprylic/Capric Glycerides, Phenoxyethanol, Methylparaben, Ethylparaben, Propylparaben, Butylparaben, Isobutylparaben, Parfum	Aqua, Cetearyl Alcohol, Octyldodecanol, Glycerin, Squalane, Cannabis Sativa, Dimethicone, Cyclopentasiloxane, Arachidyl Alcohol, Caprylic/Capric Triglyceride, Cetearyl Glucoside, Behenyl Alcohol, Ubiquinone, Hibiscus Sabdariffa Flower Extract, Zingiber Officiale Root Extract, Erythrulose, Tocopherol, Tetrasodium Edta, Hydrolyzed Soy Protein, Xanthan Gum, Dimethicone Crosspolymer, Arachidyl Glucoside, Hydrolyzed Wheat Protein, Tripeptide-1, Hydrogenated Palm Glycerides Citrate, Zea Mays, Beta-Carotene, Phenoxyethanol, Methylparaben, Ethylparaben, Propylparaben, Butylparaben, Isobutylparaben, Parfum

3.8.6 Particle size

With LD NLC and microparticulate oil droplets of the cream can be detected simultaneously. Before the LD measurement the creams were diluted with bidistilled water to obtain a homogeneous distribution of the formulation in the measurement cell. Furthermore, the formulations were filtered through a 5.0 µm cellulose acetate filters (Sartorius, Göttingen, Germany) because in the volume distribution the larger particle fraction is pronounced over the smaller one and the presence of NLC should be shown. Figure 3.8.6-1 shows the volume distribution measured by LD for Cutanova Nanorepair Q10 cream and the placebo cream. For the placebo cream a monomodal particle size distribution was found in the range of 1 µm to 10 µm. The Cutanova Nanorepair Q10 cream showed a bimodal particle size distribution with one discrete peak in the nanometer range indicating the presence of NLC and one discrete

peak in the micrometer range due to the oil droplets of the cream. These findings indicate that NLC are still present in the formulation and did not dissolve in the cream. Furthermore, agglomeration of NLC can be excluded with these results [64].

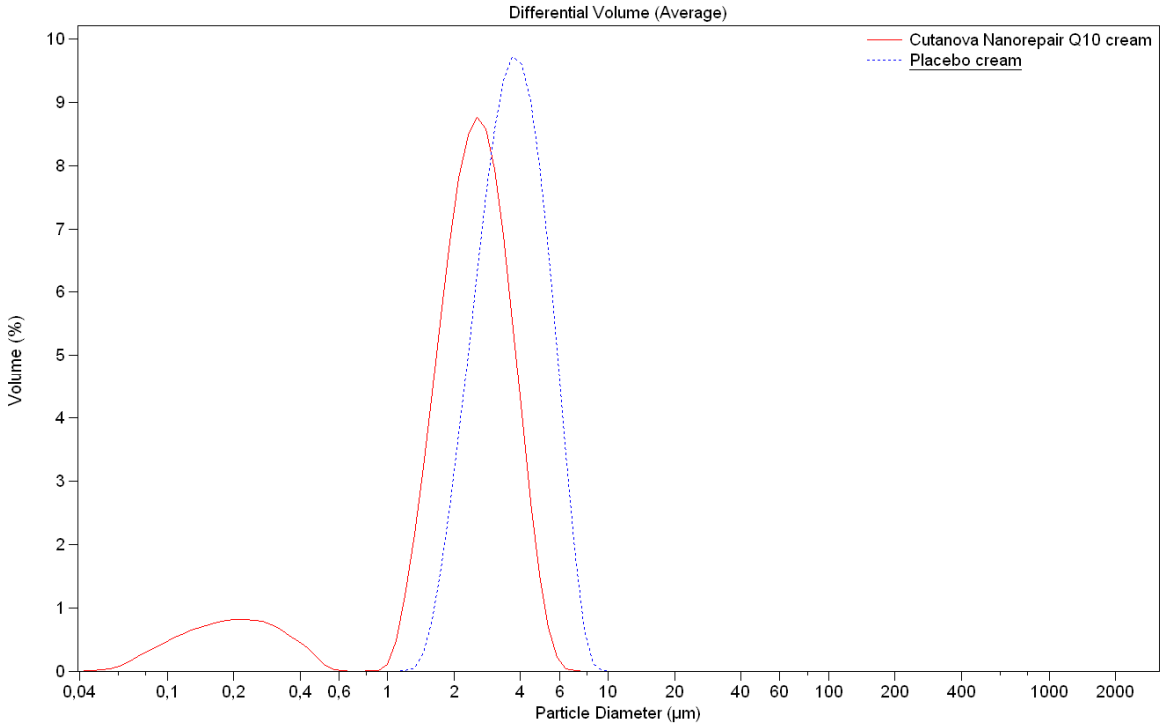

Figure 3.8.6-1: LD data of Cutanova Nanorepair Q10 cream and placebo cream.

3.8.7 Rheological properties

Rheology is a branch of physics which deals with deformation and flow of matters under the influence of outer forces [370]. The two extremes are the ideal elastic solid and the ideal viscous liquid. However, most pharmaceutical and cosmetic formulations are neither ideal elastic solids nor ideal viscous liquids [66, 371]. They mostly show elastic and viscous properties and are therefore visco-elastic materials. An ideal elastic solid is deformed when stress is applied and regains its original shape completely when the stress is released. Ideal viscous liquids are irreversible deformed due to the influence of outer forces. These liquids follow Newton's law of direct proportionality between shear stress and shear rate. The factor of proportionality is called dynamic viscosity. This flow behaviour is also called Newtonian flow [372]. However, for the majority of dermal applied vehicles (e.g. creams, gels, pasts) exists no linearity between shear stress and shear rate at a constant temperature due to their inner structure. Their flow behaviour is called non-Newtonian flow. The apparent viscosity

depends on the applied shear stress or shear rate [372]. Time-independent non-Newtonian flow can be classified as pseudoplastic, dilatant or plastic flow. Pseudoplasic flow is characterised by a decreasing apparent viscosity related to an increasing shear stress or shear rate (shear thinning). The cause of pseudoplastic flow is the progressive breakdown of the structure in the liquid medium by increasing shear and the rebuilding of the structure by Brownian motion. The opposite behaviour, shear thickening or an increase in apparent viscosity with increasing shear is called dilatant flow. Plastic materials do not flow at low shear stress but undergo reversible deformation like elastic solids. When a characteristic shear stress, called yield value, is exceeded the material starts to flow. Yield values are usually caused by structural networks (e.g. van der Waals forces, hydrogen bonds) extending through the entire system. Flow behaviour where the apparent viscosity depends not only on temperature, composition, and shear rate or shear stress but also on the previous shear history and time under shear is called time-dependent non-Newtonian behaviour [370]. In contrast to time-independent non-Newtonian flow the up-curve and down-curve of the flow curves of time-dependent non-Newtonian flow are not identical. The area enclosed by the two curves is called hysteresis loop and is a measure for the extend of the breakdown of the inner structure. If the apparent viscosity decreases with increasing shear time and the basal viscosity is reached again after a certain rest period the behaviour is called thixotropic flow. If the apparent viscosity is decreased with increasing shear time and the apparent viscosity is changed irreversible, the flow behaviour is called rheodestruction. Rheopex flow behaviour is characterised by an increase in the apparent viscosity with increasing shear time due to the induction of the formation of a three-dimensional network due to shearing.

The rheological measurements were performed with a rheometer Rheo Stress RS 100 (Haake, Karlsruhe, Germany) equipped with a cone-and-plate test geometry (plate diameter 20 mm, cone angle 4°). All measurements were carried out at 20°C ± 0.1°C. Continuous flow measurements were performed by increasing the shear rate from 0.00 to 100.00 s^{-1} over 250 seconds followed by decreasing the shear rate from 100 to 0.15 s^{-1} over 250 seconds. The yield points were determined by stress ramp with data sampling in log rate and performing two power law regression analyses. All measurements were performed in triplicate.

Figure 3.8.7-1 shows the flow patterns of Cutanova Nanorepair Q10 cream and placebo cream. Plastic flow characteristics were found for both test formulations by continuous shear rheometry. Furthermore, ascending and descending flow curve do not overlap. The

descending flow curve is located below the ascending flow curve. That means the apparent viscosity is at each shear rate on the descending curve lower than on the ascending curve. The plastic flow of the two test formulations is therefore superposed with thixotropic flow behaviour. The hysteresis loop of the Cutanova Nanorepair Q10 cream encloses a larger area than the one of the placebo cream indicating a more distinct thixotropy of the Cutanova Nanorepair Q10 cream. At the same shear rate the Cutanova Nanorepair Q10 cream exhibits a higher shear stress than the placebo cream indicating a higher apparent viscosity of the Cutanova Nanorepair Q10 cream. Yield point measurements showed a yield point of 59.4 Pa for Cutanova Nanorepair Q10 cream and a yield point of 30.2 Pa for placebo cream. These results indicate a more pronounced structural network in Cutanova Nanorepair Q10 cream. Cutanova Nanorepair Q10 cream contains 10% NLC dispersion with a particle content of 20%, i.e. 14.45%, cetyl palmitate, 0.75% Miglyol® 812 and 4.8% coenzyme Q10. The lipid nanoparticles (cetyl palmitate) in Cutanova Nanorepair Q10 cream increases the yield point, apparent viscosity and thixotropy compared to placebo cream [373].

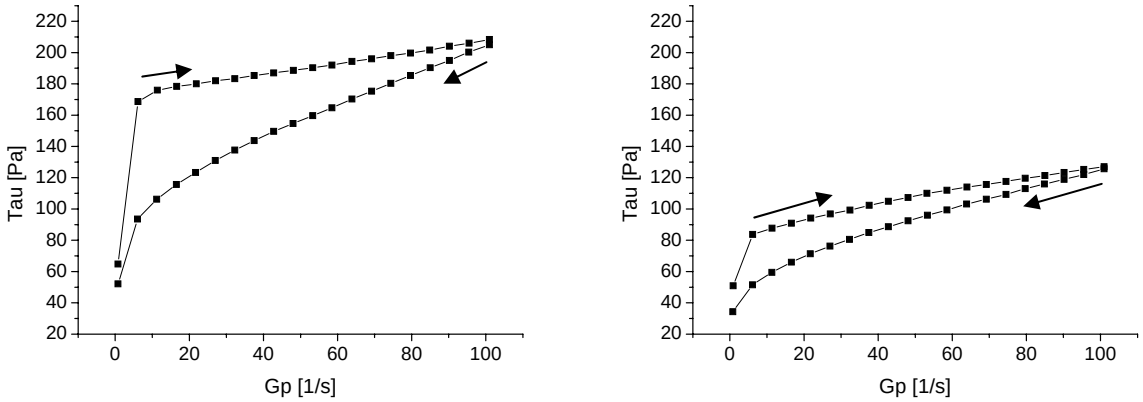

Figure 3.8.7-1: Shear stress of Cutanova Nanorepair Q10 cream (left) and placebo cream (right) as a function of shear rate at 20°C (n=3).

3.8.8 Volunteers

31 female volunteers with healthy skin in the test and control areas participated in this study. The volunteers were selected according to the including and excluding criteria. Each volunteer used two test formulations. For every volunteer two test areas and two control areas were evaluated. Age, gender, BMI, profession, smoking habit, shower habit, daily drink volume, sporting habits, amount of visits of a solarium per month, medication as well as local treatment in the test areas were recorded for each volunteer.

3.8.9 Including and excluding criteria

3.8.9.1 Including criteria

Volunteers who were included into the study had to fulfil the following criteria:

- female volunteers
- healthy skin in the test areas
- Corneometer values ≤ 75 arb. units

3.8.9.2 Excluding criteria

Volunteers were excluded from the study if they fulfilled one of the following criteria:

- sunburn, wounds, scars, hyper pigmentation, skin diseases or tattoo in the test or control areas
- known allergic reaction to one of the ingredients of the test formulations
- topical use of medication in the test or control areas within two weeks before the study
- major diseases within four weeks before the study
- pregnancy and lactation
- Corneometer values > 75 arb. units
- non-compliance

3.8.10 Limitations during the test period

No further cosmetic products or other externa should have been used in the test and control areas during the study. The volar forearm should not have been exposed directly to the sun or to UV-light in solaria.

3.8.11 Laws and regulations

The design and performance of this study was not regulated by §§ 40 and 41 of the German Medicines law due to the fact that the formulations under evaluation are no medicine after the German Medicines law [374]. The test of the cosmetic products was performed under consideration of the declaration of Helsinki (adopted in Hong Kong, 1989) and GCP ordinance (4th of August 2004).

Each volunteer obtained detailed written information about the purpose and the aim, the importance and the extent of the study as well as about possible risks associated with the study. Additionally, the study procedure and the associated risk were explained in details during an informational conversation, where every volunteer had the chance and enough time to ask still uncovered questions. Each volunteer documented his willingness to take part in the study by his signature. The willingness to take part in the study could be countermanded at any time without any personal disadvantages.
According to the Data Protection Act the agreement of the volunteer in the evaluation, processing, use and publishing of data in a pseudonymized way is needed [375]. The volunteers agreed with that by their signature.

3.8.12 Protocol of the study

Three days before the start of the study and during the study no externa were used at the volar forearm. At day 1 the skin hydration in the test and control areas was evaluated. Furthermore, the test formulations were applied for the first time to the test areas whereby the control areas stayed untreated. 0.08 g to 0.12 g of the test formulation were applied to the test areas each application. To obtain a constant application during the test period for each volunteer, the first application was performed under instruction and a leaflet about the application of the test formulations and the location of the test and control areas was handed out. Each volunteer obtained a standardized user protocol in which he had to note the time of application or if an application was forgotten. Furthermore, each volunteer could document incompatibilities and other particularities during the use in the user protocol. The volunteers were asked to apply the test formulations self dependent at home in the morning and in the evening, integrated in the daily personal hygiene, at the according test areas and document the application in the user protocol. In the morning of day 7, 28 and 42 the test formulations were not applied. At these days the skin hydration was measured. Due to skipping the application in the morning the test parameters were evaluated about 12 to 16 hrs after the last application. The last application was performed at day 41. At day 42 the containers with the test formulations and the user protocols were collected to evaluate the compliance of the volunteers. At day 49 the skin hydration was evaluated. Furthermore, at day 49 the volunteers could perform a product evaluation using a standardized questionnaire. Each measurement was performed after 30 min acclimatisation at 20°C ± 1°C and 40-50% relative humidity. Table 3.8.12-1 provides a summary of the protocol of the study.

Table 3.8.12-1: Summary of the protocol of the study.

Day	Implemented action
-3	● information and collection of demographic data
1	● measurement of the skin hydration after 30 min acclimatization ● first application under supervision ● handing out of test formulations and user protocol
2-6	● application of the test formulations in the morning and in the evening
7	● no application in the morning ● measurement of the skin hydration after 30 min acclimatization
8-27	● application of the test formulations in the morning and in the evening
28	● no application in the morning ● measurement of the skin hydration after 30 min acclimatization
29-41	● application of the test formulations in the morning and in the evening
42	● no application in the morning ● measurement of the skin hydration after 30 min acclimatization ● collection of the test formulations to control the compliance ● collection of the user protocol to control the compliance
43-48	● application free time
49	● measurement of the skin hydration after 30 min acclimatization ● product evaluation using a standardized questionnaire

3.8.13 Methods for the safety of the volunteers

Discomfort should be documented related to the time of application, duration, intensity and possibility of a correlation with the test formulations. In case of unwanted side reactions in the test areas no further application of the test formulations should be performed and the director of studies should be informed.

3.8.14 Control of compliance

The first application was performed under detailed instruction and a leaflet about the application of the test formulations with pictures of the location of the test and control areas was handed out. The test formulations were labelled with the test area where they should be applied. Each volunteer obtained a standardized user protocol in which he had to note the time

of application or if an application was forgotten. The containers of the test formulations were weighed before and after the study for the evaluation of the usage of the creams and therefore the compliance.

3.8.15 Acclimatization

The study was performed in an air-conditioned room at the Freie Universität Berlin in the Department of Pharmaceutical Technology, Biopharmaceutics and NutriCosmetics. The volunteers were seated for acclimatisation for at least 30 min at 20°C ± 1°C and 40-50% relative humidity before the measurements were performed.

3.8.16 Evaluation of skin hydration

The skin surface hydration was measured using a Corneometer CM 825 (Courage and Khazaka, Cologne, Germany) connected to a Multi Probe Adapter MPA 5 (Courage and Khazaka, Cologne, Germany). For the measurement the relatively high dielectric constant of water ($\varepsilon = 80.1$ at 20°C; $\varepsilon = 78$ at 32°C) is used which differs a lot from the dielectric constant of other materials (mostly $\varepsilon < 7$). The sensing head of the Corneometer is a condenser. If the sensing head is placed on the skin, the strateum corneum is in the scatter zone of the condenser. Depending on the water content, different changes in capacity are obtained. The capacity changes of the measuring condenser are automatically converted by the device into a digital value which is proportional to the hydration level of the skin surface. Between the skin and the measuring device is no ohmic contact because the metal conductor is placed behind a glass slide. Due to that the current conduction through the skin is minimized. One single measurement takes one second. Due to the short measurement time the measurement result is not influenced by occlusion or movements of the volunteer. The mean value of five single measurements at five different places within the test and control areas were saved and analyzed. The measurement values are expressed in arbitrary units (arb. units).

3.8.17 Biometric planning and evaluation

3.8.17.1 Targeted parameters

The targeted parameter for the statistical evaluation was the average percentage change of the measured skin hydration due to the application of the test formulations at each measurement

point related to the base value as well as to the measured value at the same time point in the control area.

3.8.17.2 Statistical methods

The raw data of all volunteers as well as all variables were documented. The mean, standard deviation, median, minimum and maximum were calculated and summarized in a table. The targeted parameter for the statistical evaluation was the average percentage change of the measured skin hydration in the treated test areas. The average percentage change of skin hydration due to the application of Cutanova Nanorepair Q10 cream and placebo cream at each measurement point was calculated using the following equation:

$$Change\ in\ skin\ hydration\,[\%] = \left(\frac{\sum Q_{ti}}{\sum Q_{0i}} - 1 \right) \times 100$$

t = time point

i = number of volunteer

Q_{ti} = quotient of measured value in the test area and the control area at the time point t for volunteer i

Q_{0i} = quotient of measured value in the test area and the control area at the begin of the study for volunteer i

3.8.17.3 Hyopthesis

Situation at the beginning of the study

At the beginning of the study a homogeneous starting situation was expected in the test and control areas of the right and the left forearm. That means, before the application of Cutanova Nanorepair Q10 cream and placebo cream the conditions in the test and control areas are equal on both forearms.

Null hypothesis: The quotients of the measuring values in the test area and control area belong to the same population.

Alternative hypothesis: The quotients of the measuring values in the test area and control area do not belong to the same population.

It was expected that the null hypothesis for day 1 can be retrained with a probability of error of $\alpha = 0.05$.

Evaluation of the increase in skin hydration

Due to the application of the test formulations a change in skin hydration is expected. A change of skin hydration is expected at day 7, 28, 42 and 49 compared to day 1 as well as a different change in skin hydration for Cutanova Nanorepair Q10 cream and the placebo cream at the according measurement days.

Null hypothesis: The quotients of the measuring values in the test area and control area belong to the same population.

Alternative hypothesis: The quotients of the measuring values in the test area and control area do not belong to the same population.

It was expected that the null hypothesis for the comparison of quotients at day 7, 28, 42 and 49 with day 1 can be rejected with a probability of error of $\alpha = 0.05$. Furthermore, it was expected, that the null hypothesis can be rejected with a probability of error of $\alpha = 0.05$ for the comparison of the effect on skin hydration of Cutanova Nanorepair Q10 cream and placebo cream.

Verification of the hypothesises

To verify the hypothesises the individual quotients of the test area and control area of each volunteer at each time point for each test formulation was calculated from the raw data of the Corneometer measurement. The obtained data were statistically evaluated using the Wilcoxon test.

3.8.18 Results

3.8.18.1 Drop outs

During the study one volunteer droped out. The volunteer broke her nasal bone and did spend one week in hospital. There is no obvious causal correlation between the drop out and the application of the test formulations. All other volunteers terminated the study at the predetermined end point. None of these volunteers showed unwanted side reactions.

3.8.18.2 Demographic data

A summary of the demographic data of the volunteers is given in Table 3.8.18.2-1. The average age of the volunteers was 25.5 years (median = 23 years; SD = 6.3). However, 91% of the volunteers were under 30 years old. 74% of the volunteers had a BMI in the range of 19 to 24 and had therefore a normal body weight. 13% had a BMI < 19 or > 24 respectively. With regards to the profession the collective of the volunteers was quite homogeneous, 91% were students, one volunteer was a laboratory assistant, one volunteer was a secretary and one volunteer was a pharmacist. The majority of the volunteers were non-smokers (81%). The drink volume per day was 1 to 2 litres for 81% of the volunteers. Only 8% drunk less than 1 litre whereas 13% drunk more than 2 litres a day. Approximately half of the volunteers did some sports at least once a week. 65% of the volunteers showered once a day, 32% less than once daily and only 3% twice daily. 91% of the volunteers did not go to a solarium whereas 9% went once or twice a month. With regards to the medication 68% of the volunteers took oral contraception during the study. Furthermore, one volunteer took Thyronajod 75 another one took Maprotilin. None of the volunteers used topical treatments on the volare forearm.

Table 3.8.18.2-1: Summary of demographic data of the volunteers.

Nr.	Age	BMI	Smoker	Profession	Drink volume [l/day]	Shower habit [times/day]	Sport [times/week]
1	22	18.8	no	student	1-2	<1	1
2	23	17.8	no	student	1-2	1	2
3	22	30	no	student	1-2	<1	0
4	23	23.6	no	student	<1	<1	1-2
5	22	19.5	no	student	1-2	1	2-3
6	24	19.5	no	student	1-2	1	0
7	23	23.7	no	student	1-2	1	1
8	22	19.5	yes	student	1-2	1	0
9	22	23	no	student	1-2	1	0
10	23	20.3	no	student	1-2	1	0
11	22	23.0	no	student	>2	1	2
12	22	20.9	no	student	1-2	1	0
13	24	21.7	yes	student	1-2	<1	0
14	25	20.3	no	student	1-2	1	2-3
15	27	25.0	no	student	1-2	1	0
16	28	20.1	no	student	<1	<1	1-2
17	23	19.4	yes	student	1-2	1	1-2
18	22	21.0	no	student	>2	1	0
19	23	19.0	no	student	>2	2	2
20	25	20.0	no	pharmacist	1-2	1	1
21	27	21.4	no	student	1-2	1	0
22	47	21.4	no	secretary	1-2	1	1
23	26	21.1	no	student	1-2	1	2
24	24	23.0	yes	student	1-2	<1	0
25	32	17.8	no	student	1-2	1	2-3
26	24	22.1	no	student	1-2	<1	0
27	48	28.6	yes	student	1-2	<1	0
28	24	19.9	no	student	>2	<1	1
29	22	20.6	no	student	1-2	<1	0
30	23	21.6	no	student	1-2	1	2
31	27	18.4	no	laboratory assistant	1-2	1	0

3.8.18.3 Evaluation of the volunteers safety

During the test period none of the volunteers showed adverse effects. None of the volunteers reported adverse effects in the user protocol.

3.8.18.4 Compliance

Table 3.8.18.4-1 provides a summary of the consumption of the test formulations by each volunteer. During the study approximately the same amount of Cutanova Nanorepair Q10 cream and placebo cream were consummated. From Cutanova Nanorepair Q10 cream the volunteers used on average 10.14 g (median = 8.79 g; SD = 5.07). An average use of 10.74 g (median = 9.17 g; SD = 5.04) of the placebo cream was found. The individual volunteers used approximately the same amounts of both test formulations. After detailed evaluation of the user protocols and comparison of the entries in the user protocol with the consumption of the test formulations as well as with the application mass of each volunteer evaluated at the beginning of the study, all volunteers seamed to be compliant during the study.

Table 3.8.18.4-1: Consumption of the test formulations during the study by each volunteer.

Nr.	Consumption of Cutanova Nanorepair Q10 cream [g]	Consumption of placebo cream [g]
1	7.71	8.74
2	13.52	13.37
3	14.15	16.09
4	4.41	4.81
6	6.13	6.78
7	11.65	11.11
8	5.03	6.91
9	7.32	8.86
10	7.02	8.87
11	6.08	4.80
12	8.69	9.33
13	6.53	7.68
14	8.03	9.00
15	12.91	16.5
16	11.06	11.53
17	9.62	8.17
18	26.58	25.07
19	22.34	21.85
20	8.89	8.00
21	10.60	12.16
22	11.86	11.06
23	7.06	6.93
24	7.99	10.03
25	1.39	1.71
26	16.4	18.23
27	12.34	13.98
28	11.09	12.93
29	11.92	12.93
30	8.29	7.72
31	7.71	7.17

3.8.18.5 Results of the statistic evaluation

3.8.18.5.1 Evaluation of the raw data

Table 3.8.18.5-1 shows the calculated mean values, standard deviations, medians, minima and maxima of the raw data.

Table 3.8.18.5-1: Mean, standard deviation (SD), median, minimum (min.) and maximum (max.) of the raw data obtained in the test and control areas for Cutanova Nanorepair Q10 cream and the placebo cream.

Area	Day	Mean	SD	Median	Min.	Max.
Control for Cutanova	1	31.02	6.26	30.60	20.06	47.00
Test for Cutanova		24.80	5.37	25.00	16.40	34.00
Control for placebo		30.34	6.80	29.00	20.72	53.80
Test for placebo		24.08	5.11	23.42	15.72	34.20
Control for Cutanova	7	34.66	4.27	34.20	24.00	42.00
Test for Cutanova		34.19	5.36	34.60	25.60	45.60
Control for placebo		34.70	5.28	34.20	25.00	46.20
Test for placebo		32.42	4.44	32.40	22.20	41.20
Control for Cutanova	28	33.97	4.73	34.20	25.00	42.40
Test for Cutanova		33.61	3.90	33.20	27.6	42.8
Control for placebo		32.25	4.83	34.00	25.40	44.40
Test for placebo		31.37	4.46	30.20	23.60	41.40
Control for Cutanova	42	32.68	5.28	31.80	23.60	47.00
Test for Cutanova		32.56	5.06	31.30	24.40	43.60
Control for placebo		32.16	5.85	30.70	21.60	47.40
Test for placebo		30.27	5.02	30.00	25.20	46.20
Control for Cutanova	49	31.94	4.48	31.60	23.80	41.20
Test for Cutanova		26.94	4.16	26.00	21.00	35.00
Control for placebo		31.39	4.99	30.00	23.80	41.40
Test for placebo		25.25	4.68	24.60	18.60	38.40

At day 1 in the control areas similar data were obtained (31.02 arb. units and 30.34 arb. units). Also both test areas showed similar Corneometer values, 24.80 arb. untits and 24.08 arb. untits respectively. The difference between the Corneometer value in the control area and in the test area was therefore before application of Cutanova Nanorepair Q10 cream 6.22 arb.

untits and 6.26 arb. units before application of placebo cream. An increase in skin hydration due to the application of the test formulations will lead to a decrease of the difference between the control and test area.

After an application time of 7 days an increase in skin hydration was found in the control and test areas. The values measured in the control areas were 34.66 arb. units and 34.70 arb. units respectively. In the test area of Cutanova Nanorepair Q10 cream a value of 34.19 arb. units was measured. The measured value in the test area of the placebo cream was 32.42 arb. units. The difference between the control and the test area therefore decreased to 0.47 arb. units for Cutanova Nanorepair Q10 cream and to 2.28 arb. units for placebo cream.

At day 28, 33.97 arb. units and 33.25 arb. units were measured in the control areas and 33.61 arb. units and 31.37 arb. units in the test areas for Cutanova Nanorepair Q10 cream and placebo cream respectively. The difference between control and test area was for Cutanova Nanorepair Q10 cream 0.36 arb. units and 1.88 arb. units for placebo cream.

At day 42 32.68 arb. units and 32.16 arb. units were measured in the control areas and 32.56 arb. units and 30.27 arb. units in the test areas for Cutanova Nanorepair Q10 cream and placebo cream respectively. For Cutanova Nanorepair Q10 cream a difference between the values in the control and test area of 0.12 arb. units was obtained after 42 days of application which corresponds to an increase of the skin hydration by 6.10 arb. units during the application period. The difference between control and test area at day 42 was 1.89 arb units for the placebo cream. Hence, for the placebo cream the Corneometer value increased by 4.37 arb. units during the 42 application days.

After one week without application of the test formulations, at day 49 of the study, 31.94 arb. units and 31.39 arb. units were measured in the control areas and 26.94 arb. units and 25.25 arb. units in the test areas for Cutanova Nanorepair Q10 cream and placebo cream respectively. A difference between the values in the control and test areas after one week application free time of 5.00 arb. units and 6.14 arb. units was found for Cutanova Nanorepair Q10 cream and placebo cream respectively. The Corneometer values at day 1 and day 49 differed by 1.22 arb units for the Cutanova Nanorepair Q10 cream and by 0.12 arb. units for the placebo cream. The standard deviation of the averaged Corneometer values was ranging between 4.16 and 6.80.

3.8.18.5.2 Evaluation of the quotients of the measured values in the test and control areas

Table 3.8.18.5-2 provides a summary of the calculated mean values, standard deviations, medians, minima and maxima of the quotients of test and control area.

Table 3.8.18.5-2: Mean, standard deviation (SD), median, minimum (min.) and maximum (max.) of the quotients of the test and control areas.

Test formulation	Day	Mean	SD	Median	Min.	Max.
Cutanova	1	0.80	0.12	0.78	0.64	1.26
Placebo		0.80	0.10	0.80	0.61	0.09
Cutanova	7	0.99	0.11	0.97	0.77	1.15
Placebo		0.94	0.12	0.97	0.76	1.14
Cutanova	28	1.00	0.11	1.02	0.77	1.16
Placebo		0.95	0.11	0.94	0.70	1.13
Cutanova	42	1.01	0.12	1.04	0.74	1.25
Placebo		0.95	0.12	0.96	0.71	1.19
Cutanova	49	0.85	0.11	0.84	0.68	1.04
Placebo		0.81	0.11	0.82	0.65	1.01

With regards to the average quotients of the test area and control area it can be seen that the quotient for Cutanova Nanorepair Q10 cream and the placebo cream with 0.80 were similar at day 1. At day 7 the quotient for Cutanova Nanorepair Q10 cream was increased to 0.99 and the one for the placebo cream to 0.94. The quotient for the placebo cream was 0.95 on day 28 and 42. For Cutanova Nanorepair Q10 cream a quotient of 1.00 at day 28 and 1.01 at day 42 was obtained. The quotients for Cutanova Nanorepair Q10 cream were therefore higher than the ones of the placebo cream. At day 49, after one week application free time, a quotient of 0.85 was found for Cutanova Nanorepair Q10 cream and of 0.81 for the placebo cream.

3.8.18.5.3 Verification of the hypothesises

Situation at the beginning of the study

With the Wilcoxon test with a probability of error of $\alpha = 0.05$ it was found that the differences between the quotients of the test area and the control area of the left and the right forearm can be considered to be random. The null hypothesis is retrained. It is therefore assumed that a homogeneous starting situation exists before the application of the test formulations.

Increase in skin hydration compared to day 1

At day 7, 28 and 42 a significant increase in skin hydration was found for Cutanova Nanorepair Q10 cream and placebo cream compared to day 1. The null hypothesis can therefore be rejected for day 7, 28 and 42. The difference between the quotients of the test and the control areas at day 1 and 49 can be considered to be random with a probability of error of $\alpha = 0.05$ for both test formulations. The null hypothesis will be retrained for day 49.

Comparison of the increase in skin hydration by Cutanova Nanorepair Q10 cream and placebo cream at the same day

The differences in skin hydration after application of Cutanova Nanorepair Q10 cream and placebo cream at day 7 can be considered to be random with a probability of error of $\alpha = 0.05$. The null hypothesis is not rejected for day 7. The obtained differences in skin hydration at day 28, 42 and 49 between the two tested formulations are significant. The null hypothesis is therefore rejected with a probability of error of $\alpha = 0.05$.

3.8.18.5.4 Percentage increase in skin hydration related to the base value

The average percentage changes of the measured skin hydration after treatment with the two test formulations were calculated for each measurement point and are summarized in Figure 3.8.18.5-1.

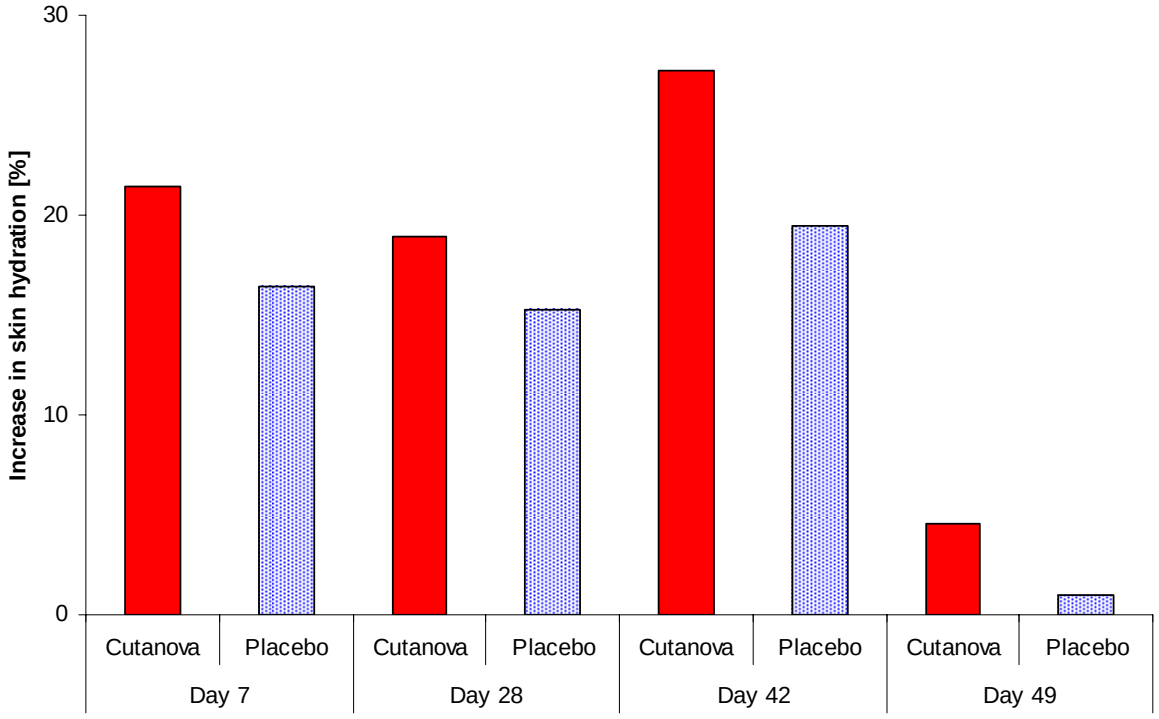

Figure 3.8.18.5-1: Increase in skin hydration in percent after application of Cutanova Nanorepair Q10 cream and placebo cream for 7, 28 and 42 days and at day 49 after 7 days application free time.

Both test formulation increased the skin hydration already significantly after 7 days of application. Due to the application of Cutanova Nanorepair Q10 cream the skin hydration increased within 7 days by 21.4%. The placebo cream increased the skin hydration in the same time period by 16.4%. The difference in the increase in skin hydration of the two test formulation after 7 days of application was not significant. After 28 days an increase in skin hydration by 18.9% compared to the base value was found for Cutanova Nanorepair Q10 cream. At day 42 the increase in skin hydration was 27.2% compared to the base value for this formulation. The increase in skin hydration was significant at these measurement points compared to day 1. For the placebo cream an increase in skin hydration of 15.3% at day 28 and 19.4% at day 42 was found. These increases were significant compared to the base value. The increase in skin hydration obtained by Cutanova Nanorepair Q10 cream was significantly higher than the one obtained with placebo cream at day 28 and day 42. After one week without any treatment, the skin hydration was still increased by 4.5% in the teat area of the Cutanova Nanorepair Q10 cream. At the same time point an increase in skin hydration by 1% was measured for the placebo cream. The difference in skin hydration is significant in the test areas of both formulations. However, the increase in skin hydration was found not to be significant compared to the value obtained at day 1.

3.8.18.6 Results of the product evaluation

In a standardized questionnaire the volunteers were ask to rate the visual impression (colour), the consistency, the dissemination on the skin, the skin feeling after application and the subjective feeling of increase in skin hydration for both test formulations as very good, good, moderate or poor. Figure 3.8.18.6-1 summarizes the results of the product evaluation.

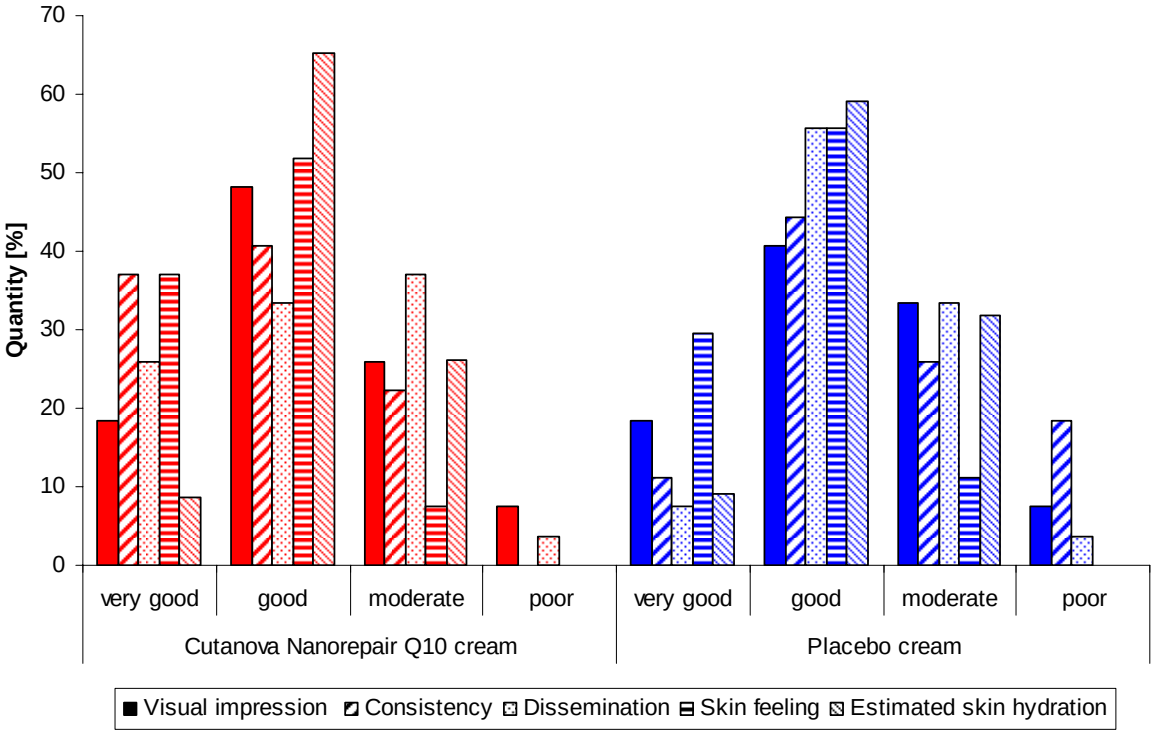

Figure 3.8.18.6-1: Results of the product evaluation.

Due to the high amount of coenzyme Q10 in the test formulations the creams appear to be yellow. The visual impression of Cutanova Nanorepare Q10 cream was rated as very good or good by 66.7% of the volunteers. 33.3% of the volunteers found the colour moderate or poor. The visual impression of the placebo cream was rated as very good or good by 59.3% of the volunteers and as moderate or poor by 40.7%. Therefore, the overall visual impression of the Cutanova Nanorepair Q10 cream was estimated better than the one of the placebo cream although the two formulations were identical in colour. As outlined in chapter 3.8.7 Cutanova Nanorepair Q10 cream had a higher apparent viscosity, a higher yield point and a more pronounced thixotropy than the placebo cream. The consistency of the Cutanova Nanorepair Q10 cream was rated as very good by 37% and as good by 40.7% of the volunteers. 22.3% found the consistency of this cream moderate. None of the volunteers rated the consistency as poor. Only 11.1% of the volunteers found the consistency of the placebo cream very good.

44.4% rated the consistency as good and 25.9% as moderate. The consistency of the placebo cream was judge as poor by 18.6% of the volunteers. Therefore, the overall impression of the consistency of the Cutanova Nanorepair Q10 cream was better than the one of the placebo cream. The dissemination on the skin of the Cutanova Nanorepair Q10 cream was estimated as very good by 25.9%, good by 33.3%, moderate by 37% and as poor by 3.7%. The dissemination on the skin of the placebo cream was rated as very good by only 7.4% of the volunteers. 55.6% found the dissemination of placebo cream good, 33.3% moderate and 3.7% poor. The skin feeling after application of Cutanova Nanorepair Q10 cream was rated as very good by 38.5%, as good by 53.5% and moderate by 8% of the volunteers. 30.8% found the skin feeling very good after the application of placebo cream, 57.7% good and 11.1% moderate. Therefore, the skin feeling after application of the Cutanova Nanorepair Q10 cream was rated better than the one of the placebo cream. 73.9% of the volunteers rated the increase in skin hydration after application of Cutanova Nanorepair Q10 cream as very good or good. In case of placebo cream 69.6% rated the increase in skin hydration as very good or good. The increase in skin hydration was rated to be moderate by 26.1% for Cutanova Nanorepair Q10 cream and by 30.4% for placebo cream. No volunteer found the increase skin hydration of the test formulations poor. However, the subjective impression of the increase in skin hydration was found to be better for the Cutanova Nanorepair Q10 cream than for placebo cream. Furthermore, the volunteers were asked which formulation in direct comparison they found better. Here 66.7% answered Cutanova Nanorepair Q10 cream and 33.3% placebo cream.

3.8.19 Summary and discussion

In the *in vivo* study it could be shown that both coenzyme Q10 containing creams were able to increase the skin hydration significantly compared to the base value within 7 days of application. After 28 days of application a significant difference in the skin hydrating effect of Cutanova Nanorepair Q10 cream and placebo cream could be shown. The NLC containing Cutanova Nanorepair Q10 cream increased the skin hydration significantly more than the NLC-free placebo cream. After an application period of 6 weeks the Cutanova Nanorepair Q10 cream was still significantly superior with regards to skin hydration compared to the placebo cream. The increase in skin hydration obtained at day 42 with the placebo cream was of the same order of magnitude as the increase in skin hydration obtained after 28 days of application of Cutanova Nanorepair Q10 cream. After an application free time of one week, the increase in skin hydration in the test area of the Cutanova Nanorepair Q10 cream was still

significant higher than the one in the test area of the placebo cream. However, the differences to the base values for both formulations were not significant. In a subjective product evaluation using a questionnaire the volunteers estimated that the skin hydration effect of the Cutanova Nanorepair Q10 cream was better than the one of the placebo cream. Reasons for the increased effect on skin hydration of the NLC containing Cutanova Nanorepair Q10 cream compared with the NLC-free placebo cream are the distinctively occlusion effect of NLC as well as the enhanced penetration of coenzyme Q10 from NLC into the stratum corneum compared to a conventional formulation [48, 58, 320, 341, 376]. Wissing and Müller reported previously the ability of an SLN containing o/w cream to increase the skin hydration significantly more than a conventional o/w cream without SLN within 28 days [377]. The results obtained by these authors for the first generation of lipid nanoparticles could be confirmed for the second generation of lipid nanoparticles in the present study.

4 Summary

4.1 PLA_2 inhibitors: PX-13 and PX-18

PLA_2 has attracted considerable interest as a pharmacological target due to its role in lipid signalling and its involvement in a number of inflammatory conditions. An increased expression of $sPLA_2$, especially $sPLA_2$-IIA, in psoriatic epidermis and dermis has been reported. For the treatment of psoriasis the topical application of the $sPLA_2$ inhibitors PX-18 and PX-13, with a preference to $sPLA_2$-IIA, was suggested.

Synthesis optimization, characterisation and validation of an analytical method

The first part of the work was focused on the optimization of the synthesis and the characterization of PX-18 and PX-13 as well as the development and validation of a quantitative analytical method. The synthesis of both PX-18 and PX-13 was optimized by changing the solvent mixture for the reaction and changing the purification methods. With the new methods PX-18 and PX-13 of a high purity could be obtained. A yield of 65.8% in case of PX-18 and a yield of 61.3% in case of PX-13 were obtained. An overview of the most important spectral data (^{1}H-NMR, ^{13}C-NMR, IR and MS) is given, which helps to identify the two compounds. Furthermore, PX-18 and PX-13 were investigated for the first time with respect to decomposition, pseudo-polymorphism and polymorphism. It was found that PX-18 starts to decompose at a temperature of 235°C and PX-13 at a temperature of 245°C. The results obtained by thermal investigations suggest, that one molecule of PX-18 is associated with two molecules of water whereas one molecule of PX-13 is associated with twelve molecules of water. Two polymorph forms of PX-18 were found in the present study. However, PX-13 showed a more complex polymorphism. For quantitative analysis of PX-18 and PX-13, a reversed-phase HPLC-UV method was developed and validated. A chromphore system was introduced to the compounds by a pre-chromatogarphic off-line derivatization reaction using PNBDI as derivatization agent. The range of the HPLC-UV method is 7-500 µg/ml for both compounds.

Preparation, characterization and stability investigation of PX-18 and PX-13 nanosuspensions

A poor aqueous solubility was reported for PX-18 and PX-13. To overcome this problem, in the second part of this work, the new compounds were formulated as nanosuspensions using

high pressure homogenization. It was found by contact angle measurements on compressed discs of PX-18 and PX-13 that Tween 80 performed the best wetting of PX-18 and Plantacare® 2000 the best wetting of PX-13 among all tested surfactants. Applying 20 homogenization cycles at 1500 bar at 5°C, PX-18 nanosuspensions with an active content of 1%, 5% and 10%, stabilized with 1% Tween 80, with a particles size below 1 µm could be achieved. For the 1% PX-18 nanosuspension an average particle size measured by PCS < 50 nm was obtained. Particle sizes as small as this have previously only been reported for nanosuspensions produced by a combination technology, where the material is lyophilized and subsequently subjected to high pressure homogenization. Applying 20 cycles at 1500 bar at 5°C to 1% and 5% PX-13 dispersions has not proved satisfactory, neither with 1% nor with 2% Plantacare® 2000 used as stabilizer. Melting 1% or 5% PX-13 in a 2% Plantacare® 2000 solution and homogenizing the obtained emulsion applying three homogenization cycles at 500 bar at 95°C, led to nanosuspensions with particles sizes well in the nanometer range. A good reproducibility of the mean particle size in between the batches was obtained for PX-18 and PX-13 nanosuspensions. For PX-18 and PX-13 an increase in saturation solubility as well as in the dissolution velocity could be shown by decreasing the particle size from the micrometer range to the nanometer range. The best physical stability was found for PX-18 nanosuspensions when stored at 5°C ± 3°C and for PX-13 nanosuspensions when stored at 25°C ± 2°C. The nanosuspensions were also chemical stable at these storage temperatures.

Dermal and ocular safety of PX-18 and PX-13

In the third part of this work the dermal and ocular safety of PX-18 and PX-13 was evaluated using *in vitro* test systems. The cytotoxic potential of PX-18 and PX-13 on primary human keratinocytes and fibroblasts monolayer cell cultures was investigated by two quantitative colorimetric cytotoxicity assays, the MTT assay and the Neutral red assay using betamethasone for comparison. It was found that the cytotoxic potential of PX-18 and PX-13 on primary human keratinocytes and fibroblast monolayer cell cultures is similar to, or even less than, the cytotoxic potential of betamethasone, one of the compounds used as standard therapy for inflammatory skin diseases. Evaluating the skin irritation potential using the EPISKIN test, a reconstructed human epidermis model, it could be shown that the $sPLA_2$ inhibitors PX-18 and PX-13 as well as the according nanosuspensions with an active concentration of 5% can be classified as non irritant to the skin according to the EU classification system. Hence, no skin irritation is expected after applying these compounds and nanosuspensions to the skin. To evaluate the eye irritation potential the HET-CAM test

was performed. It was found that neither the powder of PX-18 and PX-13 nor the according nanosuspensions showed an irritation potential on the CAM. That means, according to the test protocol applied, all tested formulations can be classified as non/slightly irritant to the eye. Furthermore, the results indicate that formulating the compounds as nanosuspensions is not increasing their irritation potential on the eye.

4.2 Coenzyme Q10-loaded NLC for dermal application

Reactive oxygen species are believed to play a key role in the ageing process. Human skin is continuously exposed to various types of stressful events causing oxidative stress. In aged skin the internal defense mechanisms, that help to control reactive oxygen species levels, lose efficiency, which will lead to an additional increase in oxidative stress. Coenzyme Q10 has antioxidant properties and is therefore widely used in dermal applied anti-ageing products. Problems associated with coenzyme Q10 containing formulations are a light and temperature induced decomposition of coenzyme Q10 and a poor delivery of coenzyme Q10 into the skin from conventional formulations.

Preparation, characterization and stability investigation of coenzyme Q10-loaded NLC and o/w emulsion

A similar particle size, well within the nanometer range, was obtained for coenzyme Q10-loaded NLC and o/w emulsion. A good reproducibility of the particle size was found for both carrier systems. Coenzyme Q10-loaded NLC and o/w emulsion showed a good physical and chemical stability. Zeta potential values of a sufficient height for a good electrostatic stabilization were found for both carrier systems. The zeta potential values stayed unchanged over the investigation time at low and high temperature indicating a good physical stability. A constant particle size could be observed at all storage temperatures (4°C ± 3°C, 25°C ± 2°C and 40°C ± 2°C) over 180 day by PCS and LD measurements. Furthermore, DSC investigations showed no changes of the onset and melting temperature and no changes in the crystallinity of the NLC during storage. This indicates that no changes in the lipid modification occurred. Beside a good physical stability a good chemical stability of coenzyme Q10-loaded NLC and o/w emulsion was observed when stored in darkness whereas coenzyme Q10 dissolved in lipid paraffin decomposed fast. However, under light exposure NLC provided a more sufficient protection of the chemical label coenzyme Q10 than the o/w emulsion.

Occlusion properties, release profiles and skin penetration

Due to the fact that occlusion can increase the stratum corneum water content as well as the penetration of lipophilic active compounds into the skin, the occlusive properties, the release profiles and skin penetration of coenzyme Q10 from coenzyme Q10 containing formulations were investigated in the second part of this study. Film formation after application of NLC could be shown with the *in vitro*, *ex vivo* and *in vivo* occlusion test. In the *in vitro* and *ex vivo* test coenzyme Q10-loaded NLC performed a similar occlusivety like highly occlusive liquid paraffin whereas the coenzyme Q10-loaded o/w emulsion showed much less occlusive properties. Microscopic pictures of coenzyme Q10-loaded NLC clearly showed a film formation on the slide whereas after application of o/w emulsion no film formation could be observed. *In vivo* the formation of a dense film on the skin could be shown by the reduction of the Corneometer values. In an *in vitro* release study using Franz diffusion cells no significant difference in the release of coenzyme Q10 from NLC and o/w emulsion was found under the applied test conditions whereas the release of coenzyme Q10 from liquid paraffin was significant lower. The coenzyme Q10 release followed zero-order release kinetic from all three formulations. Comparing the penetration of coenzyme Q10 from NLC, o/w emulsion and liquid paraffin into the stratum corneum, it was found that the penetration of coenzyme Q10 from NLC was significant higher than from the other two formulations. The penetration of coenzyme Q10 from liquid paraffin into the stratum corneum was the lowest, which correlated well with the findings of the *in vitro* release study. The *in vivo* penetration of coenzyme Q10 was significant higher from NLC than from o/w emulsion although no difference was found in the *in vitro* release. This was related to the highly occlusive properties of NLC, which can enhance the penetration of the lipophilic compounds like coenzyme Q10.

Effect of NLC on skin hydration: *in vivo* study

Different occlusion properties and different penetration profiles of active compounds can influence the effect on skin hydration of dermally applied products. Hence, in the third part of this work the effect on the skin hydration was evaluated *in vivo* after repetitive application of a cream containing coenzyme Q10-loaded NLC (Cutanova Nanorepair Q10 cream) and a conventional o/w cream (placebo cream) containing the same amount of coenzyme Q10 and having the same lipid content. Both creams increased the skin hydration significantly within seven days. A significant higher skin hydration was found in the test areas of Cutanova Nanorepair Q10 cream than in those of the placebo cream after 28 days. Applying the creams for six weeks, Cutanova Nanorepiar Q10 cream was still significantly superior with regards to

skin hydration compared to the placebo cream. After an application free time of one week, the increase in skin hydration in the test area of the Cutanova Nanorepair Q10 cream was still significantly higher than the one in the test area of the placebo cream. However, the differences to the base values for both formulations were not significant. Also in a subjective product evaluation using a questionnaire the volunteers estimated that the skin hydration effect of the Cutanova Nanorepair Q10 cream was better than the one of the placebo cream.

5 Zusammenfassung

5.1 PLA_2 Inhibitoren: PX-13 und PX-18

PLA_2 ist ein interessanter pharmakologischer Angriffspunkt, da PLA_2 eine bedeutende Rolle in der Eicosanoidbiosynthese spielt und an einer Reihe von entzündlichen Prozessen beteiligt ist. In psoriatischer Epidermis und Dermis wurde eine vermehrten Expression von $sPLA_2$, ins besonderem von $sPLA_2$-IIA, gefunden. Eine topische Behandlung von Psoriasis mit den $sPLA_2$ Inhibitoren PX-18 und PX-13, die eine Präferenz zu $sPLA_2$-IIA haben, erscheint daher sinnvoll.

Syntheseoptimierung, Charakterisierung und Validierung einer analytischen Methode

Der erste Teil dieser Arbeit befasst sich mit der Optimierung der Synthese und der Charakterisierung von PX-18 und PX-13 sowie mit der Entwicklung und Validierung einer quantitativen analytischen Methode. Die Synthese von PX-18 und PX-13 konnte durch den Wechsel des Lösungsmittelgemischs für die Reaktion und die Änderung der Aufreinigungsmethode optimiert werden. Mit den neuen Methoden können PX-18 und PX-13 mit einem hohen Reinheitsgrad hergestellt werden. Die Ausbeute der Synthesen beträgt 65,8% für PX-18 und 61,3% für PX-13. In der Arbeit wird ein Überblick über die wichtigsten Spektraldaten (^{1}H-NMR, ^{13}C-NMR, IR und MS) gegeben, mit deren Hilfe PX-18 und PX-13 identifiziert werden können. Des Weiteren wurden zum ersten Mal Untersuchungen zur Zersetzungstemperatur, zum Pseudopolymorphismus und zum Polymorphismus durchgeführt. Die Untersuchungen ergaben, dass PX-18 sich bei einer Temperatur von 235°C und PX-13 sich bei einer Temperatur von 245°C zu zersetzen beginnt. Weiterhin legen die Ergebnisse der thermischen Analyse nahe, dass ein Molekül PX-18 mit zwei Molekülen Wasser und ein Molekül PX-13 mit zwölf Molekülen Wasser assoziiert ist. Zwei polymorphe Formen von PX-18 konnten mit den gewählten Methoden nachgewiesen werden. Der Polymorphismus von PX-13 erscheint dahingegen etwas komplexer. Um PX-18 und PX-13 qualitativ analysieren zu können, wurde eine Reversed-Phase-HPLC-UV Methode entwickelt und validiert. Mit Hilfe einer der chromatographischen Trennung in einem separaten Arbeitsschritt vorangestellten Derivatisierungsreaktion wurde ein chromophores System in PX-18 und PX-13 eingeführt. Als Derivatisierungsreagenz diente PNBDI. Der Bestimmungsbereich der HPLC-UV Methode liegt zwischen 7 µg/ml und 500 µg/ml.

Herstellung, Charakterisierung und Stabilität von PX-18 und PX-13 Nanosuspensionen

PX-18 und PX-13 sind praktisch unlöslich in Wasser. Um das Löslichkeitsproblem zu umgehen, wurden im zweiten Teil der Arbeit Nanosuspensionen mit Hilfe der Hochdruckhomogenisation hergestellt. Hierfür wurden vorab über Kontaktwinkelmessungen auf komprimierten Scheiben aus PX-18 und PX-13, Tween 80 als bestes Netzmittel für PX-18 und Plantacare® 2000 als bestes Netzmittel für PX-13 ermittelt. Nanosuspensionen mit einem Gehalt von 1%, 5% und 10% PX-18, stabilisiert mit 1% Tween 80, mit einer Partikelgröße < 1 µm konnten mit 20 Homogenisationszyklen mit einem Druck von 1500 bar bei einer Temperatur von 5°C hergestellt werden. PCS Messungen ergaben eine Partikelgröße < 50 nm für die 1%ige Nanosuspension. Solch kleine Partikelgrößen konnten bisher nur erreicht werden, wenn Nanosuspensionen mit einer kombinierten Technologie hergestellt wurden, bei der das Material erst lyophilisiert und anschließend homogenisiert wurde. Hochdruckhomogenisation unter den gleichen Produktionsbedingungen (20 Zyklen, 1500 bar und 5°C) von 1% bzw. 5% PX-13 Dispersionen, stabilisiert mit 1% Plantacare® 2000 bzw. 2% Plantacare® 2000, führte nicht zu Nanosuspensionen von zufriedenstellender Qualität. Das Schmelzen von 1% bzw. 5% PX-13 in einer wässrigen 2%igen Plantacare® 2000 Lösung und die nachfolgende Homogenisation der erhaltenen Emulsion bei 500 bar und 95°C mit drei Zyklen, führte zu Nanosuspensionen mit einer Partikelgröße im Nanometerbereich. Eine gute Reproduzierbarkeit der mittleren Partikelgröße zwischen den einzelnen Chargen konnte für die PX-18 und PX-13 Nanosuspensionen nachgewiesen werden. Für PX-18 und PX-13 konnte ein Anstieg der Sättigungslöslichkeit und der Lösungsgeschwindigkeit gezeigt werden, wenn die Partikelgröße vom Mikrometerbereich in den Nanometerbereich überführt wurde. Die beste physikalische Stabilität der PX-18 Nanosuspension wurde bei Lagerung bei 5°C ± 3°C erhalten, während die beste physikalische Stabilität von PX-13 Nanosuspensionen bei 25°C ± 2°C gefunden wurde. Bei den genannten Lagertemperaturen waren die Nanosuspensionen auch chemisch stabil.

Dermale Sicherheit und Gefahrlosigkeit am Auge von PX-18 und PX-13

Im dritten Teil dieser Arbeit wurde das Gefahrenpotential von PX-18 und PX-13 an der Haut und am Auge mit Hilfe von *in vitro* Testsystemen untersucht. Die Zytotoxizität von PX-18 und PX-13 wurde an Monolayer-Zellkulturen primärer, humaner Keratinozyten und Fibroblasten mit zwei quantitativen colorimetrischen Zytotoxizitätstests, dem MTT Test und dem Neutralrot Test durchgeführt, wobei Betamethason als Vergleich diente. Das zytotoxische Potential von PX-18 und PX-13 an Momolayer-Zellkulturen primärer, humaner

Keratinozyten und Fibroblasten war vergleichbar mit dem vom Betamethason oder sogar geringer. Betamethason ist ein Arzneistoff, der standardmäßig zur Behandlung entzündlicher Hauterkrankungen eingesetzt wird. Bei der Ermittlung des Hautirritationspotentials mittels EPISKIN Test, einem rekonstruierten humanen Epidermismodell, konnte gezeigt werden, dass die $sPLA_2$ Inhibitoren PX-18 und PX-13 sowie die entsprechenden Nanosuspensionen mir einem Gehalt von 5% als nicht irritierend an der Haut nach dem EU Klassifizierungssystem eingestuft werden können. Dementsprechend werden keine Hautirritationen erwartet, wenn PX-18 und PX-13 oder die entsprechenden Nanosuspensionen auf die Haut aufgetragen werden. Um das Irritationspotential am Auge festzustellen, wurde der HET-CAM Test durchgeführt. Weder PX-18 und PX-13 Pulver noch die entsprechenden 5%igen Nanosuspensionen zeigten ein Irritationspotential an der CAM. Das heißt nach dem angewendeten Testprotokoll können alle getesteten Formulierungen als nicht bzw. leicht irritierend am Auge eingestuft werden. Weiterhin weisen die Ergebnisse darauf hin, dass durch die Formulierung von PX-18 und PX-13 als Nanosuspension ihr Irritationspotential am Auge nicht erhöht wird.

5.2 Coenzym Q10-beladene NLC zur dermalen Applikation

Es wird angenommen, dass reaktive Sauerstoffspezies eine bedeutende Rolle im Alterungsprozess spielen. Die menschliche Haut ist kontinuierlich oxidativem Stress ausgesetzt. Im Verlauf der Hautalterung verlieren die internen Verteidigungsmechanismen, die die Konzentration an reaktiven Sauerstoffspezies kontrollieren, an Effektivität, was zu einer weiteren Erhöhung des oxidativen Stresses führt. Coenzym Q10 besitzt antioxidative Eigenschaften und wird daher in dermal zu applizierenden Anti-Ageing Produkten eingesetzt. Probleme die bei diesen Produkten auftreten sind die licht- und temperaturabhängige Zersetzung von Coenzym Q10 sowie eine schlechte Penetration von Coenzym Q10 in die Haut aus herkömmlichen Formulierungen.

Herstellung, Charakterisierung und Untersuchungen zur Stabilität von Coenzym Q10-beladenen NLC und O/W-Emulsion

Für die Coenzym Q10-beladenen NLC und die entsprechende O/W-Emulsion wurde eine ähnliche Partikelgröße im Nanoeterbereich erhalten. Für beide Formulierungen ergab sich eine gute Reproduzierbarkeit der Partikelgröße. Die Coenzym Q10-beladenen NLC und die entsprechende O/W-Emulsion hatten eine gute physikalische und chemische Stabilität. Für

beide Systeme wurden Zetapotentiale von ausreichender Höhe für eine gute elektrostatische Stabilisierung gemessen. Die Zetapotentiale blieben über den Beobachtungszeitraum bei niedrigen und hohen Lagerungstemperaturen konstant, was auf eine gute physikalische Stabilität hinweist. Mit PCS- and LD-Messungen konnte über einen Zeitraum von 180 Tagen eine konstante Partikelgröße bei allen Lagerungstemperaturen (4°C ± 3°C, 25°C ± 2°C, 40°C ± 2°C) gemessen werden. DSC-Untersuchungen ergaben über den Beobachtungszeitraum gleich bleibende Onset- und Schmelztemperaturen sowie konstante Kristallinitätsindices für die NLC. Das bedeutet, dass keine Änderungen in der Lipidmodifikation während der Lagerung auftraten. Neben einer guten physikalischen Stabilität wurde eine gute chemische Stabilität von Coenzym Q10-beladenen NLC und der entsprechenden O/W-Emulsion gefunden, wenn diese unter Lichtausschluss gelagert wurden, während in flüssigem Paraffin gelöstes Coenzym Q10 sich schnell zersetzte. Unter Lichteinfluss zeigten die NLC eine bessere chemische Stabilisierung von Coenzym Q10 als die O/W-Emulsion.

Okklusive Eigenschaften, Freisetzungsprofile und Penetration in die Haut

Da Okklusion zu einer Erhöhung des Wassergehalts im Stratum corneum führt sowie die Penetration von lipophilen Stoffen in die Haut fördern kann, wurden im zweiten Teil der Arbeit die okklusiven Eigenschaften, die Freisetzungsprofile und die Coenzym Q10-Penetration in die Haut von Coenzym Q10 enthaltenden Formulierungen untersucht. Nach dem Auftragen von NLC konnte eine Filmbildung im *in vitro*, *ex vivo* und *in vivo* Okklusionstest nachgewiesen werden. Im *in vitro* und *ex vivo* Okklusionstest ergab sich für die Coenzym Q10-beladenen NLC eine vergleichbare Okklusivität wie die des hoch okklusiven flüssigen Paraffins, während die Coenzym Q10-beladene O/W-Emulsion weitaus geringere okklusive Eigenschaften zeigte. Mikroskopbilder von Coenzym Q10-beladenen NLC zeigten deutlich eine Filmbildung auf dem Objektträger. Nach dem Auftragen der O/W-Emulsion konnte keine Filmbildung beobachtet werden. *In vivo* konnte die Bildung eines dichten Films auf der Haut über die Abnahme der Corneometerwerte gezeigt werden. In *in vitro* Freisetzungsversuchen an Franz-Diffusionszellen konnte unter den angewendeten Testbedingungen kein signifikanter Unterschied im Freisetzungsverhalten von Coenzym Q10 aus den NLC und der O/W-Emulsion gefunden werden. Die Freisetzung von Coenzym Q10 war aber signifikant geringer aus flüssigem Paraffin als aus den anderen beiden Formulierungen. Die Freisetzung von Coenzym Q10 aus allen drei Formulierungen verlief nach einer Freisetzungskinetik 0. Ordnung. Beim Vergleich der Penetration von

Coenzym Q10 aus NLC, O/W-Emulsion und flüssigem Paraffin ins Stratum corneum ergab sich, dass die Penetration von Coenzym Q10 aus NLC signifikant höher war als aus den anderen beiden Formulierungen. Die Penetration von Coenzym Q10 aus flüssigem Paraffin ins Stratum corneum war am geringsten, was gut mit den Ergebnissen des *in vitro* Freisetzungsversuchs korrelierte. Die *in vivo* Penetration von Coenzym Q10 war signifikant höher aus NLC als aus der O/W-Emulsion obwohl kein Unterschied im *in vitro* Freisetzungsverhalten gefunden wurde. Dies wurde über die okklusiven Eigenschaften der NLC erklärt, die zu einer erhöhten Penetration von lipophilen Verbindungen wie Coenzym Q10 führen können.

Effekt von NLC auf die Hautfeuchtigkeit: *in vivo* Studie

Unterschiedliche okklusive Eigenschaften und unterschiedliche Penetrationsprofile von Wirkstoffen können einen Einfluss auf die hautfeuchtigkeitserhöhende Wirkung von dermal zu applizierenden Produkten haben. Deshalb wurde im dritten Teil dieser Arbeit der *in vivo* Effekt auf die Hautfeuchtigkeit nach wiederholter Anwendung einer Creme, die Coenzym Q10-beladene NLC enthielt (Cutanova Nanorepair Q10 Creme), und einer konventionellen O/W Creme (Placebocreme) mit dem gleichen Coenzym Q10- und Fettgehalt ermittelt. Beide Cremes erhöhten bereits nach 7 Tagen die Hautfeuchtigkeit signifikant. Eine signifikante Erhöhung der Hautfeuchtigkeit über die der Placebocreme hinaus wurde in den Testarealen der Cutanova Nanorepair Q10 Creme nach 28 Tagen gefunden. Nach einem Applikationszeitraum von sechs Wochen war die Cutanova Nanorepair Q10 Creme der Placebocreme in Hinblick auf die hautfeuchtigkeitserhöhende Wirkung immer noch signifikant überlegen. Nach einer Applikationspause von einer Woche wurde in den Testgebieten der Cutanova Nanorepair Q10 Creme eine signifikant höhere Hautfeuchtigkeit als in den Testgebieten der Placebocreme gemessen. Der Unterschied zum Ausgangswert erwies sich allerdings für beide Formulierungen als nicht signifikant. In einer subjektiven Produktbewertung anhand eines Fragebogens bewerteten die Studienteilnehmer die hautfeuchtigkeitserhöhende Wirkung der Cutanova Nanorepair Q10 Creme besser als die der Placebocreme.

6 References

1. W. Umbach, Kosmetik und Hygiene von Kopf bis Fuß. 3 ed. 2004, Weinheim: WILEY-VCH. 569.
2. J.W. Wiechers, The barrier function of the skin in relation to percutaneous absorption of drugs, Pharm Weekbl Sci, 1989. 11(6): p. 185-98.
3. H. Trommer, R.H. Neubert, Overcoming the stratum corneum: the modulation of skin penetration. A review, Skin Pharmacol Physiol, 2006. 19(2): p. 106-21.
4. A.P. Lavrijsen, I.M. Higounenc, A. Weerheim, E. Oestmann, E.E. Tuinenburg, H.E. Bodde, M. Ponec, Validation of an in vivo extraction method for human stratum corneum ceramides, Arch Dermatol Res, 1994. 286(8): p. 495-503.
5. S. Mac-Mary, S.M. Sainthillier, P. Humbert, Dry skin and the environment, Exog Dermatol, 2005. 3: p. 72-80.
6. E. Houben, K. De Paepe, V. Rogiers, A keratinocyte's course of life, Skin Pharmacol Physiol, 2006. 20: p. 122-32.
7. L. Norlén, Molecular skin barrier models and some central problems for the understanding of skin barrier structure and function, Skin Pharmacol Physiol, 2002. 16: p. 203-11.
8. M.H. Schmid-Wendtner, H.C. Korting, The pH of the skin surface and its impact on the barrier function, Skin Pharmacol Physiol, 2006. 19(6): p. 296-302.
9. R.H. Guy, J. Hadgraft, Physicochemical aspects of percutaneous penetration and its enhancement, Pharm Res, 1988. 5(12): p. 753-8.
10. R.H. Guy, J. Hadgraft, Physicochemical interpretation of the pharmacokinetics of percutaneous absorption, J Pharmacokinet Biopharm, 1983. 11(2): p. 189-203.
11. R.O. Potts, R.H. Guy, Predicting skin permeability, Pharm Res, 1992. 9(5): p. 663-9.
12. R.O. Potts, R.H. Guy, A predictive algorithm for skin permeability: the effects of molecular size and hydrogen bond activity, Pharm Res, 1995. 12(11): p. 1628-33.
13. J. Pardeike, A. Hommoss, R.H. Müller, Lipid nanoparticles (SLN, NLC) in cosmetic and pharmaceutical dermal products, Int J Pharm, 2008. doi:10.1016/j.ijpharm.2008.10.003.
14. G.C. Rao, M.S. Kumar, N. Mathivanan, M.E. Rao, Nanosuspensions as the most promising approach in nanoparticulate drug delivery systems, Pharmazie, 2004. 59(1): p. 5-9.
15. D. Cosco, C. Celia, F. Cilurzo, E. Trapasso, D. Paolino, Colloidal carriers for the enhanced delivery through the skin, Expert Opin Drug Deliv, 2008. 5(7): p. 737-55.
16. P. Santos, A.C. Watkinson, J. Hadgraft, M.E. Lane, Application of microemulsions in dermal and transdermal drug delivery, Skin Pharmacol Physiol, 2008. 21(5): p. 246-59.
17. S. Gohla, Emulsionen vom Typ Wasser-in-Öl-in-Wasser (WOW) in Kosmetika, in *Pharmazeutische Technologie: Moderne Arzneiformen*, R.H. Müller, G.E. Hildebrand;, Editors. 1997, Wissenschaftliche Verlagsgesellschaft: Stuttgart. p. 143-154.
18. R.H. Müller, A. Akkar, Drug nanocrystals of poorly solible drugs, Encyclopedia of Nanoscience and Nanotechnology, 2004. 2(2004): p. 627-638.
19. C.M. Keck, R.H. Müller, Drug nanocrystals of poorly soluble drugs produced by high pressure homogenisation, Eur J Pharm Biopharm, 2006. 62(1): p. 3-16.
20. M. List, H. Sucker, Pharmaceutical colloidal hydrosols for injection. 1988, 2200048.

21. P. Grassmann, M. List, A. Scheitzer, H. Sucker, Hydrosols - Alternatives for the Parenteral Applikation of Poorly Water Soluble Drugs, Eur J Pharm Biopharm, 1994. 40: p. 64-72.
22. G.G. Liversidge, K.C. Cundy, J.F. Bishop, D.A. Czekai, Surface modified drug nanoparticles. 1992, 5,145,684.
23. R.H. Müller, R. Becker, B. Kruss, K. Peters, Pharmaceutical nanosuspensions for medicament administration as system with increased saturation solubility and rate of solution. 1999, 5,858,410: U.S.
24. R.H. Müller, K. Mäder, K.P. Krause, Verfahren zur schonenden Herstellung von hochfeinen Micro-/Nanopartikeln. 2000, PCT/EP00/06535.
25. J.E. Kipp, J.C.T. Wong, M.J. Doty, C.L. Rebbeck, Microprecipitation method for preparing submicron suspensions. 2003, 6,607,784.
26. J. Möschwitzer, A. Lemke, Method for the gentle production of ultrafine particle suspensions. 2005, 017 777.8 DE 10.
27. C. Jacobs, O. Kayser, R.H. Müller, Nanosuspensions as a new approach for the formulation for the poorly soluble drug tarazepide, Int J Pharm, 2000. 196(2): p. 161-4.
28. F.N. Bushrab, R.H. Müller, Nanocrystals of poorly soluble drugs for oral administration, DrugNews, 2003. 5: p. 20-22.
29. J. Hecq, M. Deleers, D. Fanara, H. Vranckx, K. Amighi, Preparation and characterization of nanocrystals for solubility and dissolution rate enhancement of nifedipine, Int J Pharm, 2005. 299(1-2): p. 167-77.
30. R.H. Müller, C. Jacobs, Buparvaquone mucoadhesive nanosuspension: preparation, otimisation and long-term stability, Int J Pharm, 2002. 237(2002): p. 151-61.
31. R.H. Müller, B.H.L. Böhm, M.J. Grau, Nanosuspensionen - Formulierungen für schwerlösliche Arzneistoffe mit geringer Bioverfügbarkeit 2. Mitteilung: Stabilität, biopharmazeutische Aspekte, mögliche Arzneiformen und ZUlassungsfragen, Die Pharmazeutische Industrie, 1999. 61(2): p. 175-178.
32. N. Hernandez-Kirstein, Development and characterisation of buparvaquone nanosuspensions for pulmonary delivery in the treatment of Pneumocystis pneumonia, in Institut für Pharmazie. 2006, Freie Universität Berlin: Berlin.
33. C. Jacobs, R.H. Müller, Production and characterization of a budesonide nanosuspension for pulmonary administration, Pharm Res, 2002. 19(2): p. 189-94.
34. J. Lademann, H. Richter, A. Teichmann, N. Otberg, U. Blume-Peytavi, J. Luengo, B. Weiss, U.F. Schäfer, C.M. Lehr, R. Wepf, W. Sterry, Nanoparticles--an efficient carrier for drug delivery into the hair follicles, Eur J Pharm Biopharm, 2007. 66(2): p. 159-64.
35. J.S. Lucks, R.H. Müller, Medication vehicles made of solid lipid particles (solid lipid Nanospheres SLN). 1991, EP0000605497.
36. R.H. Müller, K. Mäder, A. Lippacher, V. Jenning, Solid-lipid (semi-solid) liquid particles and method of producing highly concentrated particles dispersions. 2000, PCT/EP00/04565.
37. R.H. Müller, K. Mäder, A. Lippacher, V. Jenning, Fest-flüssig (halbfeste) Lipidpartikel (Nano-Compartiment-Carrier-NCC) und Verfahren zur Herstellung hochkonzentrierter Lipidpartikel. 1999, DE19945203A1.
38. M.D. Joshi, R.H. MÜller, Lipid nanoparticles for parenteral delivery of actives, Eur J Pharm Biopharm, 2008.
39. S.A. Wissing, O. Kayser, R.H. Müller, Solid lipid nanoparticles for parenteral drug delivery, Adv Drug Delivery Rev, 2004. 56: p. 1257-72.

40. R.H. Müller, S. Runge, V. Ravelli, W. Mehnert, A.F. Thunemann, E.B. Souto, Oral bioavailability of cyclosporine: Solid lipid nanoparticles (SLN) versus drug nanocrystals, Int J Pharm, 2006. 317(1): p. 82-9.
41. B. Sarmento, S. Martins, D. Ferreira, E.B. Souto, Oral insulin delivery by means of solid lipid nanoparticles, Int J Nanomedicine, 2007. 2(4): p. 743-9.
42. H. Yuan, J. Chen, Y.Z. Du, F.Q. Hu, S. Zeng, H.L. Zhao, Studies on oral absorption of stearic acid SLN by a novel fluorometric method, Colloids Surf B Biointerfaces, 2007. 58(2): p. 157-64.
43. R.H. Müller, M. Radtke, S.A. Wissing, Solid lipid nanoparticles (SLN) and nanostructured lipid carriers (NLC) in cosmetic and dermatological preparations, Adv Drug Delivery Rev, 2002. 54: p. 131-55.
44. M. Schäfer-Korting, W. Mehnert, H.C. Korting, Lipid nanoparticles for improved topical application of drugs for skin diseases, Adv Drug Deliv Rev, 2007. 59(6): p. 427-43.
45. A.A. Attama, S. Reichl, C.C. Müller-Goymann, Diclofenac sodium delivery to the eye: in vitro evaluation of novel solid lipid nanoparticle formulation using human cornea construct, Int J Pharm, 2008. 355(1-2): p. 307-13.
46. R. Cavalli, M.R. Gasco, P. Chetoni, S. Burgalassi, M.F. Saettone, Solid lipid nanoparticles (SLN) as ocular delivery system for tobramycin, Int J Pharm, 2002. 238(1-2): p. 241-5.
47. Q.Y. Xiang, M.T. Wang, F. Chen, T. Gong, Y.L. Jian, Z.R. Zhang, Y. Huang, Lung-targeting delivery of dexamethasone acetate loaded solid lipid nanoparticles, Arch Pharm Res, 2007. 30(4): p. 519-25.
48. E. Souto, S.A. Wissing, C.M. Barbosa, R.H. Müller, Development of a controlled release formulation based on SLN and NLC for topical clotrimazole delivery, Int J Pharm, 2004. 278: p. 71–7.
49. V. Jenning, M. Schäfer-Korting, S. Gohla, Vitamin A-loaded solid lipid nanoparticles for topical use: drug release properties, J Control Release, 2000. 66(2-3): p. 115-26.
50. R.H. Müller, K. Mäder, S. Gohla, Solid lipid nanoparticles (SLN) for controlled drug delivery - A review of the state of art, Euro J Pharm Biopharm, 2000. 50: p. 161-77.
51. C. Santos Maia, W. Mehnert, M. Schaller, H.C. Korting, A. Gysler, A. Haberland, M. Schäfer-Korting, Drug targeting by solid lipid nanoparticles for dermal use, J Drug Target, 2002. 10(6): p. 489-95.
52. J. Stecova, W. Mehnert, T. Blaschke, B. Kleuser, R. Sivaramakrishnan, C.C. Zouboulis, H. Seltmann, H.C. Korting, K.D. Kramer, M. Schäfer-Korting, Cyproterone acetate loading to lipid nanoparticles for topical acne treatment: particle characterisation and skin uptake, Pharm Res, 2007. 24(5): p. 991-1000.
53. M. Joshi, V. Patravale, Nanostructured lipid carrier (NLC) based gel of celecoxib, Int J Pharm, 2008. 346(1-2): p. 124-32.
54. H. Chen, X. Chang, D. Du, W. Liu, J. Liu, T. Weng, Y. Yang, H. Xu, X. Yang, Podophyllotoxin-loaded solid lipid nanoparticles for epidermal targeting, J Control Release, 2006. 110(2): p. 296-306.
55. J. Liu, W. Hu, H. Chen, Q. Ni, H. Xu, X. Yang, Isotretinoin-loaded solid lipid nanoparticles with skin targeting for topical delivery, Int J Pharm, 2007. 328(2): p. 191-5.
56. K.A. Shah, A.A. Date, M.D. Joshi, V.B. Patravale, Solid lipid nanoparticles (SLN) of tretinoin: potential in topical delivery, Int J Pharm, 2007. 345(1-2): p. 163-71.
57. M. Joshi, V. Patravale, Formulation and evaluation of nanostructured lipid carrier (NLC)-based gel of valdecoxib, Drug Dev Ind Pharm, 2006. 32(8): p. 911-8.
58. H. Zhai, H.I. Maibach, Effects of skin occlusion on percutaneous absorption: an overview, Skin Pharmacol Appl Skin Physiol, 2001. 14(1): p. 1-10.

59. V. Jenning, A. Gysler, M. Schäfer-Korting, S.H. Gohla, Vitamin A loaded solid lipid nanoparticles for topical use: Occlusive properties and drug targeting to the upper skin, Euro J Pharm Biopharm, 1999. 49: p. 211-8.
60. V. Teeranachaideekul, R.H. Müller, V.B. Junyaprasert, Encapsulation of ascorbyl palmitate in nanostructured lipid carriers (NLC)--effects of formulation parameters on physicochemical stability, Int J Pharm, 2007. 340(1-2): p. 198-206.
61. V. Jenning, S.H. Gohla, Encapsulation of retinoids in solid lipid nanoparticles (SLN), J Microencapsul, 2001. 18(2): p. 149-58.
62. J.P. Jee, S.J. Lim, J.S. Park, C.K. Kim, Stabilization of all-trans retinol by loading lipophilic antioxidants in solid lipid nanoparticles, Eur J Pharm Biopharm, 2006. 63(2): p. 134-9.
63. R.H. Müller, A. Dingler, The next generation after liposomes: solid lipid nanoparticles (SLN, Lipopearls) as dermal carrier in cosmetics, Eurocosmetics, 1998. 7/8: p. 19-26.
64. J. Pardeike, R.H. Müller. Physical stability of nanostructured lipid carriers (NLC) in an o/w urea cream. in Annual Meeting of the Controlled Release Society (CRS). Long Beach, USA: Controlled Release Society, 7-11 July 2007, 2007. 2
65. P. Shahgaldian, L. Quattrocchi, J. Gualbert, A.W. Coleman, P. Goreloff, AFM imaging of calixarene based solid lipid nanoparticles in gel matrices, Eur J Pharm Biopharm, 2003. 55(1): p. 107-13.
66. E. Souto, S.A. Wissing, C.M. Barbosa, R.H. Müller, Evaluation of the physical stability of SLN and NLC before and after incorporation into hydrogel formulations, Euro J Pharm Biopharm, 2004. 58: p. 83-90.
67. A. Lippacher, R.H. Müller, K. Mäder, Preparation of semisolid drug carriers for topical application based on solid lipid nanoparticles, Int J Pharm, 2001. 214: p. 9–12.
68. M. Radtke, R.H. Müller, Nanostructured lipid drug carriers, Nanotechnology, 2001: p. 48-52.
69. M. Menschikowski, A. Hagelgans, G. Siegert, Secretory phospholipase A2 of group IIA: is it an offensive or a defensive player during atherosclerosis and other inflammatory diseases?, Prostaglandins Other Lipid Mediat, 2006. 79(1-2): p. 1-33.
70. B.L. Diaz, J.P. Arm, Phospholipase A(2), Prostaglandins Leukot Essent Fatty Acids, 2003. 69(2-3): p. 87-97.
71. R.K. Arni, R.J. Ward, Phospholipase A2--a structural review, Toxicon, 1996. 34(8): p. 827-41.
72. E.A. Dennis, History, classification, structure and function of phospholipase A2, in *Phospholipase A2 Basic and clinical aspects in inflammatory diseases*, W. Uhl, T.J. Nevalainen, M.W. Büchler, Editors. 1997, Karger: Basel. p. 1-7.
73. R.H. Schaloske, E.A. Dennis, The phospholipase A2 superfamily and its group numbering system, Biochim Biophys Acta, 2006. 1761(11): p. 1246-59.
74. D.A. Six, E.A. Dennis, The expanding superfamily of phospholipase A2 enzymes: classification and characterization, Biochemica et Biophysica Acta, 2000. 1488(2000): p. 1-19.
75. J. Balsinde, M.V. Winstead, E.A. Dennis, Phospholipase A2 regulation of arachidonic acid mobilization, FFBS Letters, 2002. 531(2002): p. 2-6.
76. J. Witkowski, The growing phospholipase A2 superfamily of signal transduction enzymes, TIBS, 1997. 22(22): p. 1-2.
77. W. Pruzanski, E. Stefanski, P. Vadas, N.S. Ramamurthy, Inhibition of extracellular release of proinflammatory secretory phospholipase A2 (sPLA2) by sulfasalazine: a novel mechanism of anti-inflammatory activity, Biochem Pharmacol, 1997. 53(12): p. 1901-7.
78. S. Yedgar, D. Lichtenberg, E. Schnitzer, Inhibition of phospholipase A(2) as a therapeutic target, Biochim Biophys Acta, 2000. 1488(1-2): p. 182-7.

79. S. Yedgar, Y. Cohen, D. Shoseyov, Control of phospholipase A2 activities for the treatment of inflammatory conditions, Biochim Biophys Acta, 2006. 1761(11): p. 1373-82.
80. F. Granata, B. Balestrieri, A. Petraroli, G. Giannattasio, G. Marone, M. Triggiani, Secretory phospholipases A2 as multivalent mediators of inflammatory and allergic disorders, Int Arch Allergy Immunol, 2003. 131(3): p. 153-63.
81. T.J. Nevalainen, Phospholipase A2 in acute pancreatitis: review, Am J Surg, 2007. 194(2007): p. 28-32.
82. H. Nakae, S. Endo, K. Inada, Y. Yaegashi, T. Takakuwa, Y. Yamada, N. Arakawa, T. Suzuki, S. Taniguchi, T. Shimamura, M. Ogawa, H. Teraoka, Nitrite/nitrate (NOX) and type II phospholipase A2, leukotriene B4, and platelet-activating factor levels in patients with septic shock, Res Commun Mol Pathol Pharmacol, 1996. 92(2): p. 131-9.
83. Y. Yamada, S. Endo, Y. Kamei, T. Minato, M. Yokoyama, S. Taniguchi, H. Nakae, K. Inada, M. Ogawa, Plasma levels of type II phospholipase A2 and nitrite/nitrate in patients with burns, Burns, 1998. 24(6): p. 513-7.
84. J.D. Winkler, L.A. Marshall, Phospholipase A2 in Arthritis, in *Phospholipase A2 Basic and Clinical Aspects in Inflammatory Diseases*, W. Uhl, T.J. Nevalainen, M.W. Büchler, Editors. 1997, Karger: Basel. p. 214-224.
85. S. Masuda, K. Murakami, K. Komiyama, M. Ishihara, Y. Ishikawa, T. Ishii, I. Kudo, Various secretory phospholipase A2 enzymes are expressed in rheumatoid arthritis and augment prostaglandin production in cultured synovial cells, FEBS J., 2005. 272(2005): p. 655-72.
86. L. Arbibe, D. Vial, L. Touqui, Phospholipase A2 and acute respiratory distress syndrome, in *Phospholipase A2 Basic and Clinical Aspects in Inflammatory Diseases*, W. Uhl, T.J. Nevalainen, M.W. Büchler, Editors. 1997, Karger: Basel. p. 79-87.
87. A. Ottlecz, J.J. Romero, L.M. Lichtenberger, Helicobacter infection and phospholipase A2 enzymes: effect of Helicobacter felis-infection on the expression and activity of sPLA2 enzymes in mouse stomach, Mol Cell Biochem, 2000. 221(2000): p. 71-7.
88. G.Y. Sun, J. Xu, M.D. Jensen, A. Simonyi, Phospholipase A2 in the central nervous system: implications for neurodegenerative diseases, J Lipid Res, 2003. 45: p. 205-13.
89. G.S.D. Moses, M.D. Jensen, L.F. Lue, D.G. Walker, A.Y. Sun, A. Simonyi, G.Y. Sun, Secretory PLA2-IIA: a new inflammatory factor for Alzheimer's disease, Journal of Neuroinflammation, 2006. 3(28): p. 1-11.
90. C.I. Svensson, K.K. Lucas, X.Y. Hua, H.C. Powell, E.A. Dennis, T.L. Yaksh, Spinal Phospholipase A2 in inflammatory hyperalgesia: Role of the small, secretory Phospholipase A2, Neuroscience, 2005. 133(2005): p. 543-53.
91. B. Johansen, S. Andersen, W. Sjursen, P. Gundersen, Phospholipase A2 in psoriasis. Phospholipase A2 Basic and clinical aspects in inflammatory diseases, ed. M.W. Büchler, E.H. Farthmann. Vol. 24. 1997: Karger. 250.
92. J. Oestvang, B. Johansen, PhospholipaseA2: A key regulator of inflammatory signalling and a connector to fibrosis development in atherosclerosis, Biochim Biophys Acta, 2006. 1761(2006): p. 1306-16.
93. A. Menter, A. Gottlieb, S.R. Feldman, A.S. Van Voorhees, C.L. Leonardi, K.B. Gordon, M. Lebwohl, J.Y. Koo, C.A. Elmets, N.J. Korman, K.R. Beutner, R. Bhushan, Guidelines of care for the management of psoriasis and psoriatic arthritis: Section 1. Overview of psoriasis and guidelines of care for the treatment of psoriasis with biologics, J Am Acad Dermatol, 2008. 58(5): p. 826-50.
94. J.D. Bos, M.A. de Rie, The pathogenesis of psoriasis: Immunological facts and speculations, Immunol Today, 1999. 20(1): p. 40-6.

95. K. Ikai, Psoriasis and the arachidonic acid cascade, J Dermatol Sci, 1999. 21(3): p. 135-46.
96. U. Haas, M. Podda, M. Behne, S. Gurrieri, A. Alonso, G. Furstenberger, J. Pfeilschifter, G. Lambeau, M.H. Gelb, M. Kaszkin, Characterization and differentiation-dependent regulation of secreted phospholipases A in human keratinocytes and in healthy and psoriatic human skin, J Invest Dermatol, 2005. 124(1): p. 204-11.
97. S. Andersen, W. Sjursen, A. Laegreid, G. Volden, B. Johansen, Elevated expression of human nonpancreatic phospholipase A2 in psoriatic tissue, Inflammation, 1994. 18(1): p. 1-12.
98. K.E. Rys-Sikora, R.L. Konger, J.W. Schoggins, R. Malaviya, A.P. Pentland, Coordinate expression of secretory phospholipase A(2) and cyclooxygenase-2 in activated human keratinocytes, Am J Physiol Cell Physiol, 2000. 278(4): p. C822-33.
99. D.S. Grass, R.H. Felkner, M.Y. Chiang, R.E. Wallace, T.J. Nevalainen, C.F. Bennett, M.E. Swanson, Expression of human group II PLA2 in transgenic mice results in epidermal hyperplasia in the absence of inflammatory infiltrate, J Clin Invest, 1996. 97(10): p. 2233-41.
100. W. Sjursen, O.L. Brekke, B. Johansen, Secretory and cytosolic phospholipase A(2)regulate the long-term cytokine-induced eicosanoid production in human keratinocytes, Cytokine, 2000. 12(8): p. 1189-94.
101. J. Balsinde, M.A. Balboa, P.A. Insel, E.A. Dennis, Regulation and inhibition of phospholipase A2, Annu Rev Pharmacol Toxicol, 1999. 39: p. 175-89.
102. K. Sonoki, M. Iwase, N. Sasaki, S. Ohdo, S. Higuchi, Y. Takata, M. Iida, Secretory PLA2 inhibitor indoxam suppresses LDL modification and associated inflammatory responses in TNFalpha-stimulated human endothelial cells, Br J Pharmacol, 2008. 153(7): p. 1399-408.
103. B.P. Smart, Y.H. Pan, A.K. Weeks, J.G. Bollinger, B.J. Bahnson, M.H. Gelb, Inhibition of the complete set of mammalian secreted phospholipases A(2) by indole analogues: a structure-guided study, Bioorg Med Chem, 2004. 12(7): p. 1737-49.
104. R.W. Schevitz, N.J. Bach, D.G. Carlson, N.Y. Chirgadze, D.K. Clawson, R.D. Dillard, S.E. Draheim, L.W. Hartley, N.D. Jones, E.D. Mihelich, Structure-based design of the first potent and selective inhibitor of human non-pancreatic secretory phospholipase A2, Nat Struct Biol, 1995. 2(6): p. 458-65.
105. R.C. Oslund, N. Cermak, M.H. Gelb, Highly specific and broadly potent inhibitors of mammalian secreted phospholipases A2, J Med Chem, 2008. 51(15): p. 4708-14.
106. M.C. Meyer, P. Rastogi, C.S. Beckett, J. McHowat, Phospholipase A2 inhibitors as potential anti-inflammatory agents, Curr Pharm Design, 2005. 11.
107. G. Faure, Natural inhibitors of toxic phospholipase A2, Biochemie, 2000. 82(2000): p. 833-840.
108. T. Wilson, D.L. Christie, Gravidin, an endogenous inhibitor of phospholipase A2 activity, is a secretory component of IgA, Biochem Biophys Res Commun, 1991. 176(1): p. 447-52.
109. R. Raghupathi, R.C. Franson, Inhibition of phospholipase A2 by cis-unsaturated fatty acids: evidence for the binding of fatty acid to enzyme, Biochim Biophys Acta, 1992. 1126(2): p. 206-14.
110. P.A. Krijnen, C. Meischl, R. Nijmeijer, C.A. Visser, C.E. Hack, H.W. Niessen, Inhibition of sPLA2-IIA, C-reactive protein or complement: new therapy for patients with acute myocardial infarction?, Cardiovasc Hematol Disord Drug Targets, 2006. 6(2): p. 113-23.

111. R.A. Deems, D. Lombardo, B.P. Morgan, E.D. Mihelich, E.A. Dennis, The inhibition of phospholipase A2 by manoalide and manoalide analogues, Biochim Biophys Acta, 1987. 917(2): p. 258-68.
112. Y. Park, Y. Kim, Xenorhabdus nematophilus inhibits p-bromophenacyl bromide (BPB)-sensitive PLA2 of Spodoptera exigua, Arch Insect Biochem Physiol, 2003. 54(3): p. 134-42.
113. F.F. Davidson, J. Hajdu, E.A. Dennis, 1-Stearyl,2-stearoylaminodeoxy phosphatidylcholine, a potent reversible inhibitor of phospholipase A2, Biochem Biophys Res Commun, 1986. 137(2): p. 587-92.
114. W. Pruzanski, R.A. Greenwald, I.P. Street, F. Laliberte, E. Stefanski, P. Vadas, Inhibition of enzymatic activity of phospholipases A2 by minocycline and doxycycline, Biochem Pharmacol, 1992. 44(6): p. 1165-70.
115. K. Tanaka, H. Arita, Secretory phospholipase A2 inhibitors. Possible new anti-inflammatory agents, Agents Actions Suppl, 1995. 46: p. 51-64.
116. R.C. Franson, R.M. Ottenbrite, Cytoprotective compounds, in United States. 1996, Virginia Commonwealth University, Richmond, VA: USA.
117. R.C. Franson, R.M. Ottenbrite, Cytoprotective fatty moiety compounds, in United States. 1997, Virginia Commonwealth University (Richmond, VA): USA.
118. R.C. Franson, R.M. Ottenbrite, Cytoprotective compounds, in United States. 1998, Virginia Commonwealth University (Richmond, VA): USA.
119. R.C. Franson, R.M. Ottenbrite, Cytoprotective compounds, in United States. 2000, Virginia Commonwealth University, Richmond, VA: USA.
120. R.C. Franson, R.M. Ottenbrite, Cytoprotective compounds, in United States. 2002, Virginia Commonwealth University, Richmond, VA: USA.
121. H. Saveyn, D. Mermuys, O. Thas, P. van der Merren, Determination of the refractive index of water-dispersible granules for use in laser diffraction experiments, Part. Part. Sayst. Charact., 2002. 19(2002): p. 426-32.
122. Malvern, Empirical methods for estimating refractive index values. 2007, Malvern Instruments Ltd.: Malvern. p. 4.
123. D. Giron, Thermal analysis and calorimetric methods in the characterisation of polymorphs and solvates, Thermochemica Acta, 1995. 248(1995): p. 1-59.
124. H. Budzikiewicz, R.D. Grigsby, Mass spectrometry and isotopes: A century of research and discussion, Mass Spectrom Rev, 2006. 25(1): p. 146-57.
125. K. Biemann, Mass Spectrometry, Annu Rev Biochem, 1963. 32: p. 755-80.
126. K.L. Chan, S.G. Kazarian, Detection of trace materials with Fourier transform infrared spectroscopy using a multi-channel detector, Analyst, 2006. 131(1): p. 126-31.
127. S.G. Kazarian, K.L. Chan, V. Maquet, A.R. Boccaccini, Characterisation of bioactive and resorbable polylactide/Bioglass composites by FTIR spectroscopic imaging, Biomaterials, 2004. 25(18): p. 3931-8.
128. K.L. Chan, S.G. Kazarian, A. Mavraki, D.R. Williams, Fourier transform infrared imaging of human hair with a high spatial resolution without the use of a synchrotron, Appl Spectrosc, 2005. 59(2): p. 149-55.
129. A. Burger, DTA und DSC: Grundlagen, Methodik und Auswertung, Pharmazie in unserer Zeit, 1982. 11(6): p. 177-89.
130. S.D. Clas, C.R. Dalton, B.C. Hancock, Differential scanning calorimetry: Applications in drug development, PSIT, 1999. 2(8): p. 311-20.
131. D.Q.M. Craig, A review of thermal methods for the analysis of the crystal form, solution thermodynamics and glass transition behaviour of polyethylene glycols, Thermochemica Acta, 1993. 248(1995): p. 189-203.
132. J.H. Flynn, Analysis of DSC results by integration, Thermochemica Acta, 1993. 217(1993): p. 129-149.

133. N.J. Coleman, D.Q.M. Craig, Modulated temperature differential scanning calorimetry: A novel approach to pharmaceutical thermal analysis, Int J Pharm, 1996. 136(1996): p. 13-29.
134. Malvern, Rapid refractive index determination for pharmaceutical actives, Malvern Instruments Ltd: Malvern. p. 4.
135. B. Rimez, H. Rahier, G. Van Assche, T. Artoos, M. Biesemans, B. Van Mele, The thermal degradation of poly(vinyl acetate) and poly(ethylene-co-vinyl acetate) Part I: Experimental study of degradation mechanism, Polym Degrad Stabil, 2008. 93(2008): p. 800-10.
136. M. Kuhnert-Brandstätter, R. Völlenklee, Thermische und IR-spektroskopische Untersuchungen an polymorphen Arzneistoffen: Acemetacin, Piroxicam, Propanololhydrochlorid und Urapidil, Anal Chem, 1985. 322(1985): p. 164-9.
137. H.A. Moynihan, I.P. O'Hare, Spectroscopic characterisation of the monoclinic and orthorhombic forms of paracetamol, Int J Pharm, 2002. 247(1-2): p. 179-85.
138. M. Wagner, Bestimmung der Adsorption/Desorption von Feuchtigkeit in pharmaceutischen Substanzen, UserCom, 2005. 1(2005): p. 9-11.
139. M. Kuhnert-Brandstätter, F. Pröll, Thermische Analyse von Hydraten organischer Verbindungen. I, Mikrochim Acta, 1983. II(1983): p. 463-76.
140. A. Grunenberg, [Polymorphism and thermal analysis of pharmaceutical agents], Pharm Unserer Zeit, 1997. 26(5): p. 224-31.
141. R. Noguerol-Cal, J.M. López-Vilarino, G. Fernández-Martínez, L. Barral-Losada, M.V. González-Rodríguez, High-performance liquid chromatography analysis of ten dayes for control of safety of commercial articles, J Chromatogr A, 2007. 1179(2008): p. 152-60.
142. H.G. Janssen, C. Swindells, P. Gunning, W. Wang, C. Grün, K. Mahabir, V.J. Maharaj, P.J. Apps, Quantification of appetite suppressing steroid glycosides from Hoodia gordonii in dried plant material, purified extracts and food products using HPLC-UV and HPLC-MS methods, Anal Chem Acta, 2008(2008).
143. P.S. Mukherjee, H.T. Karnes, Ultraviolet and fluorescence derivatization reagents for carboxylic acids suitable for high performance liquid chromatography: a review, Biomed Chromatogr, 1996. 10(5): p. 193-204.
144. K. Tsuji, W. Morozowich, GLC and HPLC determination of therapeutic agents: Part I. Chromatographic Science. Vol. 9. 1978, New York: Marcel Dekker. 415.
145. S. Cunha, J. Fernandes, M. Frerreira, HPLC/UV determination of organic acids in fruit juices and nectras, Euro Food Res Technol, 2002. 214(2002): p. 67-71.
146. S. Cunha, I.M.L.V.O. Ferreira, J. Fernandes, M.A. Faria, M. Beatriz, P.P. Oliveira, M.A. Ferreira, Determination of lactic, acetic, succinic and citric acids in table olives by HPLC/UV, J Liq Chromatogr R T, 2001. 24(7): p. 1029-38.
147. ICH, Validation of analytical procedures: Text and methodology. 2005, Ferderal Register. p. 11260.
148. A. Maltese, F. Maugeri, K.W. Ward, C. Bucolo, Development and validation of an RP-HPLC-UV method for the determination of BOL-303225-A, a new coumarin-based anti-inflammatory drug, in rat plasma, Biomed Chromatogr, 2007. 21(4): p. 351-5.
149. V.K. Venishetty, C. Durairaj, R. Sistla, M.R. Yamsani, P.V. Diwan, Development and validation of a reversed-phase HPLC method for determination of nitrendipine in rat plasma: application to pharmacokinetic studies, Biomed Chromatogr, 2007. 21(4): p. 363-8.
150. D.B. Pathare, A.S. Jadhav, M.S. Shingare, A validated stability indicating LC method for nateglinide, Drug Dev Ind Pharm, 2007. 33(5): p. 551-7.

151. K.P. Xiao, D. Chien, R. Markovich, A.M. Rustum, Development and validation of a stability-indicating reversed-phase high performance liquid chromatography method for assay of betamethylepoxide and estimation of its related compounds, J Chromatogr A, 2007. 1157(1-2): p. 207-16.
152. EHSLC, Guidelines for analysis of samples from pharmacokinetic studies - Method Validation. 2002, Guidelines of European Horserace Scientific Liaison Committee.
153. K.H. Bauer, K.H. Frömming, C. Führer, Lehrbuch der Pharmazeutischen Technologie. 6 ed. Vol. 6. 1999, Stuttgart: Wissenschaftliche Verlagsgesellschaft mbH Stuttgart. 472.
154. R. Voigt, Pharmazeutische Technologie - Für Studium und Beruf. 6 ed. Vol. 9. 2000, Stuttgart: Deutscher Apotheker Verlag Stuttgart. 687.
155. P.H. List, B.W. Müller, E. Nürnberg, Arzneiformenlehre - Ein Lehrbuch für Pharmazeuten. 3 ed. Vol. 3. 1982, Stuttgart: Wissenschaftliche Verlagsgesellschaft mbH Stuttgart. 605.
156. T. Young. in Proceedings of the Royal Society of London. London1805. 65
157. G. Buckton, Contact angle, adsorption and wettability - a review with respect to powders, Powder Technol, 1989. 61(1990): p. 237-49.
158. D. Li, Drop size dependence of contact angle and line tensions of solid-liquid systems, Colloids and Surfaces A: Physicochemical and Engineering Aspects, 1996. 116(1996): p. 1-23.
159. P. Fox, P. McSweeney, Influence of processing operations on the fat globule membrane. Dairy Chemistry and Biochemistry. 1998: Springer Verlag.
160. P. Paquin, Technological properties of high pressure homogenization: effect of fat globules, milk proteins, and polysaccarides, Int Dairy J, 1999. 9(3): p. 329-35.
161. L.C. Collins-Gold, R.T. Lyons, L.C. Bartholow, Parenteral emulsions for drug delivery, Adv Drug Deliv Rev, 1990. 5(1990): p. 189-208.
162. R. Barnadas-Rodriguez, M. Sabes, Factors involved in the production of liposomes with a high-pressure homogenizer, Int J Pharm, 2001. 213(1-2): p. 175-86.
163. W.J. Kelly, K.R. Muske, Optimal operation of high-pressure homogenization for intracellular product recovery, Bioprocess Biosyst Eng, 2004. 27(1): p. 25-37.
164. G. Kutz, S. Frieß, Moderne Verfahren zur Herstellung von halbfesten und flüssigen Emulsionen - eine aktuelle Übersicht, SÖFW, 1998. 124(1998): p. 308-13.
165. A.R. Kleinig, A.O.J. Middelberg, On the mechanism of microbial cell disruption in high-pressure homogenisation, Chem Eng Sci, 1997. 53(1998): p. 891-8.
166. R.H. Müller, K. Peters, Nanosuspension for the formulation of poorly soluble drugs 1. Preparation by a size-reduction technique, Int J Pharm, 1997. 160: p. 229-37.
167. W. Mehnert, K. Mäder, Solid lipid nanoparticles production, characterization and applications, Adv Drug Delivery Rev, 2001. 47: p. 165-96.
168. K.H. Mohr, High-pressure homogenization. Part II. The influence of cavitation on liquid-liquid dispersion in turbulence fields of high energy density, J Food Eng, 1086. 6(1987): p. 311-24.
169. K.H. Mohr, High-pressure homogenization. Part I. Liquid-liquid dispersion in turbulence field of high energy density, J Food Eng, 1986. 6(1987): p. 177-86.
170. J. Floury, A. Desrumaux, J. Lardières, Effect of high-pressure homogenization on droplet size distribution and rheological properties of model oil-in-water emulsion, Innovative Food Science & Emerging Technologies, 2000. 1(2000): p. 127-134.
171. R.H. Muller, C. Jacobs, O. Kayser, Nanosuspensions as particulate drug formulations in therapy. Rationale for development and what we can expect for the future, Adv Drug Deliv Rev, 2001. 47(1): p. 3-19.

172. J. Möschwitzer, G. Achleitner, H. Pomper, R.H. MÜller, Development of an intravenously injectable chemically stable aqueous omeprazole formulation using nanosuspension technology, Eur J Pharm Biopharm, 2004. 58(3): p. 615-9.
173. R.H. Müller, R. Schuhmann, Teilchengrößenmessung in der Laborpraxis, ed. APV. 1996: Wissenschaftliche Verlagsgesellschaft mbH Stuttgart.
174. Dynamic Light Scattering an Inroduction in 30 Minutes, Malvern Instruments: Malvern. p. 8.
175. M. Kaszuba, D. McKnight, M.T. Connah, F.K. McNeil-Watson, U. Nobbmann, Measuring sub nanometre sizes using dynamic light scattering, Journal of Nanoparticle Research, 2007. DOI 10.007/s11051-007-9317-4.
176. U. Kätzel, M. Stintz, S. Ripperger, Applicationsuntersuchungen zur Photonenkorrelationsspectroscopie im Rückstreubereich, Chemie Ingenieur Technik, 2003. 76(2004): p. 66-9.
177. K. Thode, R.H. Müller, M. Kresse, Two-time window and multiangle photon correlation spectroscopy size and zeta potential analysis - Highly sensitive rapid assay for dispersion stability, J Pharm Sci, 2000. 89: p. 1317-24.
178. A.R. Jones, Light scattering for particle characterization, Prog Energ Combust, 1999. 25(1999): p. 1-53.
179. C.M. Keck, R.H. Müller, Size analysis of submicron particles by laser diffractometry--90% of the published measurements are false, Int J Pharm, 2008. 355(1-2): p. 150-63.
180. R. Arnold. Theoretische Grundlagen des Dipolübergangsmoments. [cited 2008 11.06.].
181. R.H. Müller, Böhm, B. H. L., Grau, M. J., Nanosuspensionen - Formulierungen für schwerlösliche Arzneistoffe mit geringer Bioverfügbarkeit 1. Mitteilung: Herstellung und Eigenschaften, Die Pharmazeutische Industrie, 1999. 61: p. 74-78.
182. N. Hernandez-Kirstein, Development and characterisation of buparvaquone nanosuspensions for pulmonary delivery in the treatment of Pneumocystis pneumonia, in Biology, Chemistry and Pharmacy. 2006, Free University of Berlin: Berlin.
183. J. Möschwitzer, Drug nanocrystals preparation by high pressure homogenization - The universal formulation approach for poorly soluble drugs. 2005, Freie Universität Berlin: Berlin.
184. K.P. Krause, R.H. Müller, Production and characterisation of highly concentrated nanosuspensions by high pressure homogenisation, Int J Pharm, 2001. 214(1-2): p. 21-4.
185. C. Nyström, Dissolution properties of soluble drugs: theoretical background and possibilities to improve the dissulution behavior, in *Emusion and Nanosuspension for the Formulation of Poorly Soluble Drugs*, R.H. Müller, S. Benita, B. Böhm, Editors. 1998, Medpharm Scientific Publishers: Stuttgart. p. 143-7.
186. K. Arii, Y. Fukuta, T. Kai, Y. Kokuba, Preparation of fine emulsified fat particles without glycerol for intravenous nutrition, Eur J Pharm Sci, 1999. 9(1): p. 67-73.
187. M.J. Grau, O. Kayser, R.H. Müller, Nanosuspensions of poorly soluble drugs--reproducibility of small scale production, Int J Pharm, 2000. 196(2): p. 155-9.
188. K. Peters, Nanosuspensionen - Ein neues Formulierungsprinzip für schwerlösliche Arzneistoffe. 1999, Freie Universität Berlin: Berlin.
189. ICH, Stability testing of new drug substances and products Q1A(R2). 2003, ICH p. 18.
190. R.H. Müller, Zetapotential und Partikelladung in der Laborpraxis. APV paperback series. Vol. 37. 1996, Stuttgart: Wissenschaftliche Verlagsgesellschaft.
191. V. Teeranachaideekul, V.B. Junyaprasert, E.B. Souto, R.H. Müller, Development of ascorbyl palmitate nanocrystals applying the nanosuspension technology, Int J Pharm, 2008. 354(1-2): p. 227-34.

192. Malvern, Zeta Potential an Introduction in 30 Minutes, Malvern Instruments: Malvern. p. 6.
193. T.M. Riddick, Zeta-Meter Manual. 1968, Zeta-Meter Inc: New York.
194. P. Ney, Zetapotentiale und Flotierbarkeit von Mineralien. 1973, Wien - New York: Springer Verlag.
195. C. Jacobs, Neue Nanosuspensionsformulierungen für verschiedene Applikationsformen. 2003, Freie Universität Berlin: Berlin.
196. H.P. Latscha, H.A. Klein, Analytische Chemie. Chemie - Basiswisen III. Vol. 3. 1995, Berlin; Heidelberg: Springer Verlag.
197. D.J.W. Grant, H.G. Brittain, Solubility of pharmaceutical solids, in *Physical characterization of pharmaceutical solids*, H.G. Brittain, Editor. 1995, Marcel Dekker: New York. p. 321-386.
198. C. Nyström, M. Bisrat, Physicochemical aspects of drug release VIII. The relation between particle size and surface specific dissolution rate in agitated suspensions, Int. J. Pharm, 1988. 47: p. 223-31.
199. G. Torrado, S. Fraile, S. Torrado, S. Torrado, Process-indurced crystallite size and dissolution changes elucidated by a variety of analytical methods, Int J Pharm, 1998. 166: p. 65-73.
200. J.E. Kipp, The role of solid nanoparticle technology in the parenteral delivery of poorly water-soluble drugs, Int J Pharm, 2004. 284(1-2): p. 109-22.
201. M. Mosharraf, C. Nyström, The effect of particle size and shape on the szrface dissolution rate of micronized practically insoluble drugs, Int. J. Pharm, 1995. 122: p. 35-47.
202. E.K. Abnderberg, C. Nyström, M. Bisrat, Physicochemical aspects of drug release VII. The effect of surfactant concentration and drug particle size on solubility and dissolution rate of felodipine, a sparingly soluble drug, Int J Pharm, 1988. 47: p. 67-77.
203. M.T. Crisp, C.J. Tucker, T.L. Rogers, R.O. Williams, K.P. Johnston, Turbidimetric measurement and prediction of dissolution rates of poorly soluble drug nanocrystals, J Control Release, 2007. 117(3): p. 351-9.
204. J.K. Lee, D.B. Kim, J.I. Kim, P.Y. Kim, In vitro cytotoxicity tests on cultured human skin fibroblasts to predict skin irritation potential of surfactants, Toxicol In Vitro, 2000. 14(4): p. 345-9.
205. R. Osborne, M.A. Perkins, In vitro irritation testing with human skin cell cultures, Toxicol In Vitro, 1991. 5: p. 563-7.
206. L. Sanchez, M. Mitjans, M.R. Infante, M.P. Vinardell, Assessment of the potential skin irritation of lysine-derivative anionic surfactants using mouse fibroblasts and human keratinocytes as an alternative to animal testing, Pharm Res, 2004. 21(9): p. 1637-41.
207. T. Sun, S. Jackson, J.W. Haycock, S. MacNeil, Culture of skin cells in 3D rather than 2D improves their ability to survive exposure to cytotoxic agents, Journal of Biotechnology, 2006. 122: p. 372-81.
208. M. Pagé, N. Bejaoui, B. Cinq-Mars, P. Lemieux, Optimization of the tetrazolium-based colorimetric assay for the measurement of cell number and cytotoxicity, Int. J. Immunopharmacol, 1988. 10: p. 785-93.
209. B. Lindl. T., J., Zell- und Gewebekultur Einführung in die Grundlagen sowie ausgewählte Methoden und Anwendungen. 3 ed. Vol. 3. 1994, Stuttgart: Semper Bonis Artibus. 251.
210. K. Lange, Pharmakodynamische Differenzierung topischer Glucocorticoide in vitro. 1998, Freie Universität Berlin: Berlin.

211. E. Borenfreund, J.A. Puerner, Toxicity determination in vitro by morphological alterations and neutral red absorption, Toxicol Lett, 1985. 24: p. 119-24.
212. E. Borenfreund, The neutral red cytotoxicity assay. 1992, INVITOX. p. 7.
213. European Pharmacopeia. 6 ed. 2007.
214. Rote Liste. Arzneimittelverzeichnis für Deitschland (einschließlich EU-Zulassungen und bestimmter Medizinproducte). 2001, Frankfurt am Main: Rote Liste Service GmbH.
215. COLIPA, In vitro 3T3 NRU phototoxicity test. 1998, ZEBET/ ECVAM/ COLIPA Standard Operation Procedure. p. 18.
216. R.M. Rosa, J. do Nascimento Picada, J. Saffi, J.A. Henriques, Cytotoxic, genotoxic, and mutagenic effects of diphenyl diselenide in Chinese hamster lung fibroblasts, Mutat Res, 2007. 628(2): p. 87-98.
217. N. Dijoux, Y. Guingand, C. Bourgeois, S. Durand, C. Fromageot, C. Combe, P.J. Ferret, Assessment of the phototoxic hazard of some essential oils using modified 3T3 neutral red uptake assay, Toxicol In Vitro, 2006. 20(4): p. 480-9.
218. K. Maier, R. Schmitt-Landgraf, B. Siegmund, Development of an in vitro test system with human skin cells for evaluation of phototoxicity, Toxicol In Vitro, 1991. 5: p. 457-61.
219. H.C. Korting, S. Schindler, A. Hartinger, M. Kerscher, T. Angerpointner, H.I. Maibach, MTT-assay and neutral red release (NRR)-assay: relative role in the prediction of the irritancy potential of surfactants, Life Sci, 1994. 55(7): p. 533-40.
220. L. Benassi, G. Bertazzoni, S. Seidenari, In vitro testing of tensides employing monolayer cultures: a comparison with results of patch tests on human volunteers, Contact Dermatitis, 1999. 40(1): p. 38-44.
221. J.D. Harvell, K. Lammintausta, H.I. Maibach, Irritant contact dermatitis, in *Practical Contact Dermatitis*, J.D. Guin, Editor. 1995, McGraw-Hill: New York. p. 7-18.
222. J.H. Draize, G. Woodward, H.O. Calvery, Method for the study of irritation and toxicity of substances applied topically to the skin and mucous membranes, Journal of Pharmacology and Experimental Therapeutics, 1944. 82: p. 377-390.
223. OECD, Guideline for the testing of chemicals, No. 404: Acute dermal irritation/corrosion. 2002, OECD: Paris. p. 13.
224. M.P. Vinardell, M. Mitjans, Alternative methods for eye and skin irritation tests: An overview, J Pharm Sci, 2008. 97(1): p. 46-59.
225. G. Calvin, New approaches to the assessment of eye and skin irritation, Toxicol Lett, 1992. 64-65 Spec No: p. 157-64.
226. L. Phillips, M. Steinberg, H.I. Maibach, W.A. Akers, A comparison of rabbit and human skin response to certain irritants, Toxicol Appl Pharmacol, 1972. 21(3): p. 369-82.
227. M.K. Robinson, R. Osborne, M.A. Perkins, In vitro and human testing strategies for skin irritation, Ann N Y Acad Sci, 2000. 919: p. 192-204.
228. M. Liebsch, D. Traube, H. Kandarova, In vitro skin Irritation test: human skin model. 2004, BfR. p. 1-31.
229. F. Netzlaff, C.M. Lehr, P.W. Wertz, U.F. Schäfer, The human epidermis models EpiSkin, SkinEthic and EpiDerm: an evaluation of morphology and their suitability for testing phototoxicity, irritancy, corrosivity, and substance transport, Eur J Pharm Biopharm, 2005. 60(2): p. 167-78.
230. C. Faller, M. Bracher, N. Dami, R. Roguet, Predictive ability of reconstructed human epidermis equivalents for the assessment of skin irritation of cosmetics, Toxicol In Vitro, 2002. 16(5): p. 557-72.

231. R. Roguet, M. Régnier, C. Cohen, K.G. Dossou, A. Rougier, The use of in vitro reconstructed human skin in dermatoxicity testing, Toxicol In Vitro, 1994. 8(4): p. 635-9.
232. ECVAM, Performance Standards for Applying Human Skin Models to in vitro Skin Irritation Testing. 2007. p. 1-13.
233. E. Tinois, J. Tiollier, M. Gaucherand, H. Dumas, M. Tardy, J. Thivolet, In vitro and post-transplantation differentiation of human keratinocytes grown on the human type IV collagen film of a bilayered dermal substitute, Exp Cell Res, 1991. 193(2): p. 310-9.
234. R. Roguet, J. Cotovio, J. Fentem, P. Jones, C. Robles, Validation of the EPISKIN irritation test 42 houres assay for the prediction of acute skin irritation of chemicals. 2005, L'ORÉAL. p. 1-41.
235. D.A. Basketter, H.A. Griffiths, X.M. Wang, K.P. Wilhelm, J. McFadden, Individual, ethnic and seasonal variability in irritant susceptibility of skin: the implications for a predictive human patch test, Contact Dermatitis, 1996. 35(4): p. 208-13.
236. A. Gysler, U. Konigsmann, M. Schafer-Korting, Tridimensional skin models recording percutaneous absorption, Altex, 1999. 16(2): p. 67-72.
237. T. Welss, D.A. Basketter, K.R. Schroder, In vitro skin irritation: facts and future. State of the art review of mechanisms and models, Toxicol In Vitro, 2004. 18(3): p. 231-43.
238. C. Tornier, M. Rosdy, H.I. Maibach, In vitro skin irritation testing on reconstituted human epidermis: reproducibility for 50 chemicals tested with two protocols, Toxicol In Vitro, 2006. 20(4): p. 401-16.
239. T. Watanabe, T. Hasegawa, H. Takahashi, T. Ishibashi, H. Itagaki, K. Sugibayashi, Utility of MTT assay in three-dimensional cultured human skin model as an alternative for draize skin irritation test: approach using diffusion law of irritant in skin and toxicokinetics-toxicodynamics correlation, Pharm Res, 2002. 19(5): p. 669-75.
240. K. Sugibayashi, T. Watanabe, T. Hasegawa, H. Takahashi, T. Ishibashi, Kinetic analysis on the in vitro cytotoxicity using living skin equivalent for ranking the toxic potential of dermal irritants, Toxicol In Vitro, 2002. 16(6): p. 759-63.
241. R. Roguet, C. Cohen, C. Robles, P. Couretellemont, M. Tolle, J.P. Guillot, X. Pouradier Duteil, An interlaboratory study of the reproducibility and relevance of Episkin, a reconstructed human epidermis, in the assesment of cosmetic irritancy, Toxicol In Vitro, 1997. 12(1998): p. 295-304.
242. A. Chatterjee, R.J. Babu, M. Klausner, M. Singh, In vitro and in vivo comparison of dermal irritancy of jet fuel exposure using EpiDerm (EPI-200) cultured human skin and hairless rats, Toxicol Lett, 2006. 167(2): p. 85-94.
243. C.S. Weil, R.A. Scala, Study of intra- and interlaboratory variability in the results of rabbit eye and skin irritation tests, Toxicol Appl Pharmacol, 1971. 19(2): p. 276-360.
244. D.A. Basketter, M. Chamberlain, H.A. Griffiths, M. Rowson, E. Whittle, M. York, The classification of skin irritants by human patch test, Food Chem Toxicol, 1997. 35(8): p. 845-52.
245. ZEBET, The hen's egg-chorioallantoic membrane test (HET-CAM test) for the assessment of the eye irritation potential of chemical substances, Toxicology, 2001. 25: p. 1-7.
246. M. York, W. Steiling, A critical review of the assessment of eye irritation potential using the Draize rabbit eye test, J Appl Toxicol, 1998. 18(4): p. 233-40.
247. M. Balls, N. Berg, L.H. Bruner, R. Curren, O. de Suva, K.E. Earl, D.J. Esdaile, J.H. Fentem, M. Liebsch, Y. Ohno, M.K. Prinsen, S. H., A.P. Worth, Eye irritation testing: The way forward - The report and recommendation of ECVAM Workshop 34, ATLA, 1999. 27: p. 53-77.

248. M.K. Prinsen, An evaluation of the OECD proposal for the harmonised classification of eye irritants and corrosives. 1999, Nutrition and Food Research Institute, Division of Toxicology: Zeist. p. 72-77.
249. M. Liebsch, H. Spielman, Currently available in vitro methods used in the regulatory toxicology, Toxicol Lett, 2002. 127: p. 127-34.
250. N.P. Luepke, Hen's egg chorioallantoic membrane test for irritation potential, Food Chem Toxicol, 1985. 23(2): p. 287-91.
251. H. Spielmann, M. Liebsch, HET-CAM Test - Test protocol used in phase II of the German validation study for replacement of the Draize eye test (1990-1992), BGA-ZEBET, 1991: p. 1-8.
252. W. Steiling, The hen's egg test on the chorioallantoic membrane (HET-CAM) INCITTOX n°96. 1994, ECVAM DB-ALM. p. 18.
253. C. Lüring, T. Kalteis, K. Wild, L. Perlick, J. Grifka, Gewebetoxizität lokaler Anästhetika im HET-CAM Test, Der Schmerz, 2003. 3(17): p. 185-90.
254. P. Budai, L. Varnagy, In vitro ocular irritation toxicity study of some pesticides, Acta Vet Hung, 2000. 48(2): p. 221-8.
255. J.P. Hagino, S. Kinoshita, N. Tani, T. Nakumara, N. Ono, K. Konishi, H. Iimuara, H. Kojima, Y. Ohno, Interlaboratory validation of in vitro eye irritation tests for cosmetic ingredients (2) Chorioallantoic membrane (CAM) test, Toxicol In Vitro, 1999. 13: p. 99-113.
256. L. Gilleron, S. Coecke, M. Sysmans, E. Hansen, S. van Oproy, D. Marzin, H. van Cauteren, P. Vamparys, Evaluation of a modified HET-CAM assay as screening test for eye irritancy, Toxicol In Vitro, 1996. 10: p. 431-446.
257. M.P. Vinardell, M. Mitjans, The chorioallantonic membrane test as a model to predict the potential human eye irritation induced by commonly used laboratory solvents, Toxicol In Vitro, 2006. 20(2006): p. 1066-70.
258. J.E. Dahl, Potential of dental adhesives to induce mucosal irritation evaluated by the HET-CAM method, Acta Odontol Scand, 2007: p. 1-9.
259. P.U. Giacomoni, G. Rein, Factors of skin ageing share common mechanisms, Biogerontology, 2001. 2(4): p. 219-29.
260. P.U. Giacomoni, G. Rein, A mechanistic model for the aging of human skin, Micron, 2004. 35(3): p. 179-84.
261. R.J. Koch, An overview of facial wrinkles, West J Med, 1997. 167(6): p. 428.
262. S. Laube, Skin infections and ageing, Ageing Res Rev, 2004. 3(1): p. 69-89.
263. Y. Soroka, Z. Ma'or, Y. Leshem, L. Verochovsky, R. Neuman, F.M. Bregegere, Y. Milner, Aged keratinocyte phenotyping: morphology, biochemical markers and effects of Dead Sea minerals, Exp Gerontol, 2008. 43(10): p. 947-57.
264. K. De Paepe, A. Weerheim, E. Houben, D. Roseeuw, M. Ponec, V. Rogiers, Analysis of epidermal lipids of the healthy human skin: factors affecting the design of a control population, Skin Pharmacol Physiol, 2004. 17(1): p. 23-30.
265. J. Rogers, C. Harding, A. Mayo, J. Banks, A. Rawlings, Stratum corneum lipids: the effect of ageing and the seasons, Arch Dermatol Res, 1996. 288(12): p. 765-70.
266. G. Jenkins, Molecular mechanisms of skin ageing, Mech Ageing Dev, 2002. 123(7): p. 801-10.
267. E. Makrantonaki, C.C. Zouboulis, Skin alterations and diseases in advanced age, Drug Discov Today: Dis Mech, 2008. doic: 10.1016/j.ddmec.2008.05.08.
268. K. Sauermann, S. Jaspers, U. Koop, H. Wenck, Topically applied vitamin C increases the density of dermal papillae in aged human skin, BMC Dermatol, 2004. 4(1): p. 13.
269. V. Ravelojaona, L. Robert, A.M. Robert, Effect of cellular aging on collagen biosynthesis: II. Collagen synthesis and deposition by a human skin fibroblast strain over 25 passages, Arch Gerontol Geriatr, 2008. 47(3): p. 368-76.

270. J.Y. Lee, Y.K. Kim, J.Y. Seo, C.W. Choi, J.S. Hwang, B.G. Lee, I.S. Chang, J.H. Chang, Loss of elastic fibers causes skin wrinkles in sun-damaged human skin, J Dermatol Sci, 2007. 50(2008): p. 99-107.
271. M.J. Kent, N.D. Light, A.J. Bailey, Evidence for glucose-mediated covalent cross-linking of collagen after glycosylation in vitro, Biochem J, 1985. 225(3): p. 745-52.
272. J.H. Rabe, A.J. Mamelak, P.J. McElgunn, W.L. Morison, D.N. Sauder, Photoaging: mechanisms and repair, J Am Acad Dermatol, 2006. 55(1): p. 1-19.
273. R. Stern, H.I. Maibach, Hyaluronan in skin: aspects of aging and its pharmacologic modulation, Clin Dermatol, 2008. 26(2): p. 106-22.
274. T. Ryan, The ageing of the blood supply and the lymphatic drainage of the skin, Micron, 2004. 35(3): p. 161-71.
275. G. Heyn, Haut im Alter - Den Spuren der Zeit begegnen, Pharmazeutische Zeitung, 2007. 1/2007: p. 16-21.
276. Z.A. Medvedev, An attempt at a rational classification of theories of ageing, Biol Rev Camb Philos Soc, 1990. 65(3): p. 375-98.
277. L. Heyflick, The limited in vitro lifetime of human diploid cell strains, Exp. Cell Res., 1965. 37: p. 614-636.
278. M.G. Kosmadaki, B.A. Gilchrest, The role of telomeres in skin aging/photoaging, Micron, 2004. 35(3): p. 155-9.
279. M. Sugimoto, R. Yamashita, M. Ueda, Telomere length of the skin in association with chronological aging and photoaging, J Dermatol Sci, 2006. 43(1): p. 43-7.
280. V.M. Dilman, Age-associated elevation of hypothalamic, threshold to feedback control, and its role in development, ageine, and disease, Lancet, 1971. 1(7711): p. 1211-9.
281. L.R. Dean, Aging and the decline of instrumentality, J Gerontol, 1960. 15: p. 403-7.
282. L.R. Dean, Aging and the decline of affect, J Gerontol, 1962. 17: p. 440-6.
283. J. Bjorksten, A common molecular basis for the aging syndrome, J Am Geriatr Soc, 1958. 8(10): p. 740-8.
284. R.R. Kohn, H.B. Bensusan, L. Klein, Cross-linkages in collagen, Science, 1964. 145(3628): p. 186-8.
285. D. Harman, Aging: a theory based on free radical and radiation chemistry, J. Gerontol., 1956. 11: p. 298-300.
286. K.B. Beckman, B.N. Ames, The free radical theory of aging matures, Physiol Rev, 1998. 78(2): p. 547-81.
287. H. Corstjens, L. Declercq, L. Hellemans, I. Sente, D. Maes, Prevention of oxidative damage that contributes to the loss of bioenergetic capacity in ageing skin, Exp Gerontol, 2007. 42(9): p. 924-9.
288. A. Kowald, The mitochondrial theory of aging, Biol Signals Recept, 2001. 10(3-4): p. 162-75.
289. B. Chakravarti, D.N. Chakravarti, Oxidative modification of proteins: age-related changes, Gerontology, 2006. 53(3): p. 128-39.
290. R. Kohen, I. Gati, Skin low molecular weight antioxidants and their role in aging and in oxidative stress, Toxicology, 2000. 148(2-3): p. 149-57.
291. F.L. Carne, Discovery of ubiquinone (coenzyme Q) and an overview of function, Mitochondrion, 2007. 7S: p. 2-7.
292. L. Ernster, G. Dallner, Biochemical, physiological and medical aspects of ubiquinone function, Biochim Biophys Acta, 1995. 1271(1): p. 195-204.
293. M. Bentinger, K. Brismar, G. Dallner, The antioxidant role of coenzyme Q, Mitochondrion, 2007. 7 Suppl: p. S41-50.

294. P. Forsmark-Andree, L. Ernster, Evidence for a protective effect of endogenous ubiquinol against oxidative damage to mitochondrial protein and DNA during lipid peroxidation, Mol Aspects Med, 1994. 15 Suppl: p. s73-81.
295. R.E. Beyer, Inhibition by coenzyme Q of ethanol- and carbon tetrachloride-stimulated lipid peroxidation in vivo and catalyzed by microsomal and mitochondrial systems, Free Radic Biol Med, 1988. 5: p. 297-303.
296. A. Maroz, R.F. Anderson, R.A. Smith, M.P. Murphy, Reactivity of ubiquinone and ubiquinol with superoxide and the hydroperoxyl radical: implications for in vivo antioxidant activity, Free Radic Biol Med, 2008.
297. R.E. Beyer, The participation of coenzyme Q in free radical production and antioxidation, Free Radic Biol Med, 1990. 8(6): p. 545-65.
298. Y. Nakajima, Y. Inokuchi, M. Nishi, M. Shimazawa, K. Otsubo, H. Hara, Coenzyme Q10 protects retinal cells against oxidative stress in vitro and in vivo, Brain Res, 2008. 1226: p. 226-33.
299. S.L. Molyneux, C.M. Florkowski, P.M. George, A.P. Pilbrow, C.M. Frampton, M. Lever, A.M. Richards, Coenzyme q(10) an independent predictor of mortality in chronic heart failure, J Am Coll Cardiol, 2008. 52(18): p. 1435-41.
300. B. Frei, M.C. Kim, B.N. Ames, Ubiquinol-10 is an effective lipid-soluble antioxidant at physiological concentrations, Proc Natl Acad Sci U S A, 1990. 87(12): p. 4879-83.
301. R.E. Beyer, B.A. Burnett, K.J. Cartwright, D.W. Edington, M.J. Falzon, K.R. Kreitman, T.W. Kuhn, B.J. Ramp, S.Y. Rhee, M.J. Rosenwasser, Tissue coenzyme Q (ubiquinone) and protein concentrations over the life span of the laboratory rat, Mech Ageing Dev, 1985. 32(2-3): p. 267-81.
302. J. Hatanaka, Y. Kimura, Z. Lai-Fu, S. Onoue, S. Yamada, Physicochemical and pharmacokinetic characterization of water-soluble Coenzyme Q(10) formulations, Int J Pharm, 2008. 363(1-2): p. 112-7.
303. Y. Shindo, E. Witt, D. Han, W. Epstein, L. Packer, Enzymic and non-enzymic antioxidants in epidermis and dermis of human skin, J Invest Dermatol, 1994. 102(1): p. 122-4.
304. S. Liedtke, S.A. Wissing, R.H. Müller, K. Mäder, Influence of high pressure homogenisation equipment on nanodispersions charakteristics, Int J Pharm, 2000. 196: p. 183-5.
305. M.R. Gasco, for producing solid lipid microspheres having a norrow size distribution, in USA patent 188837. 1993.
306. M.R. Gasco, Solid lipid nanspheres from warm microemuslion, Pharm. Technol. Eur., 1997. 9: p. 32-42.
307. L. Priano, D. Esposti, R. Esposti, G. Castagna, C. De Medici, F. Fraschini, M.R. Gasco, A. Mauro, Solid lipid nanoparticles incorporating melatonin as new model for sustained oral and transdermal delivery systems, J. Nanosci. Nanotechnol., 2007. 7: p. 3596-601.
308. B. Sjöström, B. Bergenstahl, Preparation of submicron drug particles in lecithin-stabilized o/w emulsions I. Model studies of the precipitation of cholesteryl acetate, Int. J. Pharm., 1992. 88: p. 53-62.
309. F.Q. Hu, H. Yuan, H.H. Zhang, M. Fang, Preparation of solid lipid nanoparticles with clobetasol propionate by a novel solvent diffusion method in aqueous system and physicochemical characterization, Int J Pharm, 2002. 239(1-2): p. 121-8.
310. M. Trotta, F. Debernardi, O. Caputo, Preparation of solid lipid nanoparticles by a solvent emulsification-diffusion technique, Int J Pharm, 2003. 257(1-2): p. 153-60.
311. M.A. Schubert, C.C. Müller-Goymann, Solvent injection as a new approach for manufacturing lipid nanoparticles--evaluation of the method and process parameters, Eur J Pharm Biopharm, 2003. 55(1): p. 125-31.

312. B. Heurtault, P. Saulnier, B. Pech, J.E. Proust, J.P. Benoit, A novel phase inversion-based process for the preparation of lipid nanocarriers, Pharm Res, 2002. 19(6): p. 875-80.
313. M. Garcý-Fuentes, D. Torres, M. Alonso, Design of lipid nanoparticles for the oral delivery of hydrophilic macromolecules, Colloid. Surface. B., 2002. 27: p. 159-68.
314. J. Pietkiewicz, M. Sznitowska, The choice of lipids and surfactants for injectable extravenous microspheres, Pharmazie, 2004. 59: p. 325-6.
315. C. Puglia, P. Blasi, L. Rizza, A. Schoubben, F. Bonina, C. Rossi, M. Ricci, Lipid nanoparticles for prolonged topical delivery: an in vitro and in vivo investigation, Int J Pharm, 2008. 357(1-2): p. 295-304.
316. C. Charcosset, A. El-Harati, H. Fessi, Preparation of solid lipid nanoparticles using a membrane contactor, J Control Release, 2005. 108(1): p. 112-20.
317. A.A. El-Harati, C. Charcosset, H. Fessi, Influence of the formulation for solid lipid nanoparticles prepared with a membrane contactor, Pharm Dev Technol, 2006. 11(2): p. 153-7.
318. A.J. Almeida, S.A. Runge, R.H. Müller, Peptide-loaded solid lipid nanoparticle (SLN): Influence of production parameters, Int J Pharm, 1996. 136: p. 155-63.
319. Tego® Care 450 Emulsifier for the formulation of o/w creams and lotions. [http://www.chemiplast.hu/specik/TEGO%20CARE%20450.pdf] 1999 [cited 24. Octorber 2008].
320. A. Dingler, Feste Lipid-Nanopartikel als kolloidale Wirkstoffträgersysteme zur dermalen Applikation. 1998, Freie Universität Berlin: Berlin.
321. V. Teeranachaideekul, E.B. Souto, V.B. Junyaprasert, R.H. Müller, Cetyl palmitate-based NLC for topical delivery of Coenzyme Q(10) - development, physicochemical characterization and in vitro release studies, Eur J Pharm Biopharm, 2007. 67(1): p. 141-8.
322. V. Teeranachaideekul, Nanostructured lipid carriers (NLC) - Stability improvement and release modification of ascorbyl palmitate and coenzyme Q10. 2008, Mahidol University: Bankok.
323. M.L. Bondi, E.F. Craparo, G. Giammona, M. Cervello, A. Azzolina, P. Diana, A. Martorana, G. Cirrincione, Nanostructured lipid carriers-containing anticancer compounds: preparation, characterization, and cytotoxicity studies, Drug Deliv, 2007. 14(2): p. 61-7.
324. C. Song, S. Liu, A new healthy sunscreen system for human: solid lipid nanoparticles as carrier for 3,4,5-trimethoxybenzoylchitin and the improvement by adding Vitamin E, Int J Biol Macromol, 2005. 36(1-2): p. 116-9.
325. C. Santos Maia, W. Mehnert, M. Schäfer-Korting, Solid lipid nanoparticles as drug carriers for topical glucocorticoids, Int J Pharm, 2000. 196(2): p. 165-7.
326. A.A. Date, M.D. Joshi, V.B. Patravale, Parasitic diseases: Liposomes and polymeric nanoparticles versus lipid nanoparticles, Adv Drug Deliv Rev, 2007. 59(6): p. 505-21.
327. S. Hatziantoniou, G. Deli, Y. Nikas, C. Demetzos, G.T. Papaioannou, Scanning electron microscopy study on nanoemulsions and solid lipid nanoparticles containing high amounts of ceramides, Micron, 2007. 38(8): p. 819-23.
328. F. Castelli, C. Puglia, M.G. Sarpietro, L. Rizza, F. Bonina, Characterization of indomethacin-loaded lipid nanoparticles by differential scanning calorimetry, Int J Pharm, 2005. 304(1-2): p. 231-8.
329. S.J. Lim, C.K. Kim, Formulation parameters determining the physicochemical characteristics of solid lipid nanoparticles loaded with all-trans retinoic acid, Int J Pharm, 2002. 243(1-2): p. 135-46.

330. C. Freitas, R.H. Müller, Effect of light and temperature on zeta potential and physical stability in solid lipid nanoparticle (SLN) dispersion, Int. J. Pharm, 1998. 168: p. 221-229.
331. K. Westesen, H. Bunjes, M.H.J. Koch, Physicochemical characterization of lipid nanoparticles and evaluation of their drug loading capacity and sustained release potential, J Control Release, 1996. 48: p. 223-36.
332. A. Saupe, Pharmazeutisch-kosmetische Anwendungen Nanostrukturierter Lipidcarrier (NLC): Lichtschutz und Pflege. 2004, Freie Universität Berlin: Berlin.
333. M. Radtke, Grundlegende Untersuchungen zur Arzneistoffinkorporation, -freisetzung und Struktur von SLN und NLC. 2003, Freie Universität Berlin: Berlin.
334. A. Saupe, S.A. Wissing, A. Lenk, R.H. Müller, C. Schmidt, Solid lipid nanoparticles (SLN) and nanostructured lipid carriers (NLC) – Structural investigations on two different carrier systems, Bio-Medical Mater Eng, 2005. 15: p. 393–402.
335. H. Bunjes, T. Unruh, Characterization of lipid nanoparticles by differential scanning calorimetry, X-ray and neutron scattering, Adv Drug Deliv Rev, 2007. 59(6): p. 379-402.
336. Y. Matsuda, R. Masahara, Photostability of solid-state ubidecarenone at ordinary and elevated temperatures under exaggerated UV irradiation, J Pharm Sci, 1983. 72(10): p. 1198-203.
337. S.A. Wissing, A. Lippacher, R.H. Müller, Investigations on the occlusive properties of solid lipid nanoparticles (SLN), J Cosmet Sci, 2001. 52: p. 313-24.
338. S.A. Wissing, R.H. Müller, The influence of the crystallinity of lipid nanoparticles on their occlusive properties, Int J Pharm, 2002. 242: p. 377-9.
339. T. deVringer, Topical preparation containing a suspension of lipid particles. 1997, 5,667,8000.
340. T. deVringer, Topical preparation containing a suspension of solid lipid particles 1999, 5,904,932
341. V. Teeranachaideekul, P. Boonme, E.B. Souto, R.H. Müller, V.B. Junyaprasert, Influence of oil content on physicochemical properties and skin distribution of Nile red-loaded NLC, J Control Release, 2008. 128(2): p. 134-41.
342. R.H. Müller, R.D. Petersen, A. Hommoss, J. Pardeike, Nanostructured lipid carriers (NLC) in cosmetic dermal products, Adv Drug Deliv Rev, 2007. 59(2007): p. 522-30.
343. T. de Vringer, Topical preparation containing a suspension of solid lipid particles. 1992, EP 0 506 197 A1.
344. V. Jenning, Feste Lipid-Nanopartikel (SLN) als Trägersystem für die dermale Applikation von Retinol: Wirkstoffinkorporation, -freisetzung und Struktur. 1999, Freie Universität Berlin: Berlin.
345. S.A. Wissing, SLN als innovatives Formulierungskonzept für pflegende und protektive dermale Zubereitungen. 2002, Freie Universität Berlin: Berlin.
346. E. Berardesca, EEMCO guidance for the assessment of stratum corneum hydration: electronical methods, Skin Res Technol, 1997. 3(1997): p. 126-32.
347. S.D. Mandawgade, V.B. Patravale, Development of SLNs from natural lipids: Application to topical delivery of tretinoin, Int J Pharm, 2008. 363(1-2): p. 132-8.
348. G. Suresh, K. Manjunath, V. Venkateswarlu, V. Satyanarayana, Preparation, characterization, and in vitro and in vivo evaluation of lovastatin solid lipid nanoparticles, AAPS PharmSciTech, 2007. 8(1): p. 24.
349. M. Joshi, S. Pathak, S. Sharma, V. Patravale, Design and in vivo pharmacodynamic evaluation of nanostructured lipid carriers for parenteral delivery of artemether: Nanoject, Int J Pharm, 2008.
350. A.J. Almeida, E. Souto, Solid lipid nanoparticles as a drug delivery system for peptides and proteins, Adv Drug Deliv Rev, 2007. 59(6): p. 478-90.

351. A. zur Muhlen, C. Schwarz, W. Mehnert, Solid lipid nanoparticles (SLN) for controlled drug delivery--drug release and release mechanism, Eur J Pharm Biopharm, 1998. 45(2): p. 149-55.
352. S.A. Wissing, R.H. Müller, Solid lipid nanoparticles as carrier for sunscreens: in vitro release and in vivo skin penetration, J Control Release, 2002. 81: p. 225-33.
353. H. Yuan, L.L. Wang, Y.Z. Du, J. You, F.Q. Hu, S. Zeng, Preparation and characteristics of nanostructured lipid carriers for control-releasing progesterone by melt-emulsification, Colloids Surf B Biointerfaces, 2007. 60(2): p. 174-9.
354. V. Venkateswarlu, K. Manjunath, Preparation, characterization and in vitro release kinetics of clozapine solid lipid nanoparticles, J Control Release, 2004. 95(3): p. 627-38.
355. M.L. Bondi, G. Fontana, B. Carlisi, G. Giammona, Preparation and characterization of solid lipid nanoparticles containing cloricromene, Drug Deliv, 2003. 10(4): p. 245-50.
356. A. zur Mühlen, W. Mehnert, Drug release and release mechanism of prednisolone loaded solid lipid nanoparticles, Pharmazie, 1998. 53: p. 552.
357. I. Brinkmann, C.C. Müller-Goymann, Role of isopropyl myristate, isopropyl alcohol and a combination of both in hydrocortisone permeation across the human stratum corneum, Skin Pharmacol Appl Skin Physiol, 2003. 16: p. 393-404.
358. G. Potard, C. Laugel, H. Schaefer, J.-P. Marty, The stripping technique: In vitro absorption and penetration of five UV filters on excised fresh human skin, Skin Pharmacol Appl, 2000. 13: p. 336-44.
359. U. Jacobi, M. Kaiser, H. Richter, H. Audring, W. Sterry, J. Lademann, The number of stratum corneum cell layers correlates with the pseudo-absorption of the corneocytes, Skin Pharmacol Physiol, 2005. 18(4): p. 175-9.
360. U. Jacobi, J. Gautier, W. Sterry, J. Lademann, Gender-Related Differences in the Physiology of the Stratum Corneum, Dermatology, 2005. 211: p. 312–317.
361. L. Coderch, M. de Pera, N. Perez-Cullell, J. Estelrich, A. de la Maza, J.L. Parra, The effect of liposomes on skin barrier structure, Skin Pharmacol Appl Skin Physiol, 1999. 12(5): p. 235-46.
362. V.P. Shah, Guidance for industry - Topical dermatological drug product NDAs and ANDAs - In vivo bioavailability, bioequivalence, in vitro release, and associated studies. 1998, FDA: Rockville. p. 16.
363. Y.N. Kalia, I. Alberti, N. Sekkat, C. Curdy, A. Naik, R.H. Guy, Normalization of stratum corneum barrier function and transepidermal water loss in vivo, Pharm Res, 2000. 17(9): p. 1148-50.
364. U. Jacobi, H.J. Weigmann, J. Ulrich, W. Sterry, J. Lademann, Estimation of the relative stratum corneum amount removed by tape stripping, Skin Res Technol, 2005. 11(2): p. 91-6.
365. V.P. Shah, G.L. Flynn, A. Yacobi, H.I. Maibach, C. Bon, N.M. Fleischer, T.J. Franz, S.A. Kaplan, J. Kawamoto, L.J. Lesko, J.P. Marty, L.K. Pershing, H. Schaefer, J.A. Sequeira, S.P. Shrivastava, J. Wilkin, R.L. Williams, Bioequivalence of topical dermatological dosage forms--methods of evaluation of bioequivalence, Pharm Res, 1998. 15(2): p. 167-71.
366. M. Ricci, C. Puglia, F. Bonina, C. Di Giovanni, S. Giovagnoli, C. Rossi, Evaluation of indomethacin percutaneous absorption from nanostructured lipid carriers (NLC): In vitro and in vivo studies, J Pharm Sci, 2005. 94(5): p. 1149-59.
367. R. Sivaramakrishnan, C. Nakamura, W. Mehnert, H.C. Korting, K.D. Kramer, M. Schafer-Korting, Glucocorticoid entrapment into lipid carriers--characterisation by parelectric spectroscopy and influence on dermal uptake, J Control Release, 2004. 97(3): p. 493-502.

368. Lebensmittel- und Futtermittelgesetzbuch in der Fassung der Bekanntmachung vom 26. April 2006 (BGBl. I S. 945), zuletzt geändert durch Artikel 12 des Gesetzes vom 26. Februar 2008 (BGBl. I S. 215). 2005.
369. Kosmetik-Verordnung in der Fassung der Bekanntmachung vom 7. Oktober 1997 (BGBl. I S. 2410), zuletzt geändert durch Artikel 1 der Verordnung vom 4. Juli 2008 (BGBl. I S. 1226)". 1977.
370. H. Schott, Rheology, in *Pharmaceutical Sciences*, Remington, Editor. 1990, Mack Publishing Co: Easton. p. 310-26.
371. A. Lippacher, R.H. Müller, K. Mäder, Liquid and semisolid SLN dispersions for topical application: rheological characterization, Euro J Pharm Biopharm, 2004. 58: p. 561–7.
372. A.N. Martin, P. Bustamonte, A.H. Chun, Rheology, in *Physical Pharmacy*, A.N. Martin, Editor. 1993, Lippincott Williams & Wikins. p. 453-464.
373. L.E. Pena, B.L. Lee, J.F. Stearns, Secondary structural rheology of a model cream, J Soc Cosmet Chem, 1994. 45(2): p. 77-84.
374. Arzneimittelgesetz in der Fassung der Bekanntmachung vom 12. Dezember 2005 (BGBl. I S. 3394), zuletzt geändert durch Artikel 9 Abs. 1 des Gesetzes vom 23. November 2007 (BGBl. I S. 2631), 1976.
375. Bundesdatenschutzgesetz in der Fassung der Bekanntmachung vom 14. Januar 2003 (BGBl. I S. 66), zuletzt geändert durch Artikel 1 des Gesetzes vom 22. August 2006 (BGBl. I S. 1970). 1990.
376. J. Pardeike, R.H. Müller, Coenzyme Q10 loaded NLCs: preparation, occlusive properties and penetration enhancement, Pharm Tech Europe, 2007. 19(7): p. 46-9.
377. S.A. Wissing, R.H. Müller, The influence of solid lipid nanoparticles on skin hydration and viscoelasticity – in vivo study, Euro J Pharm Biopharm, 2003. 56: p. 67-72.

Publication list

Book chapters

1. Pardeike, J., Müller, R.H., HET-CAM Test, in: www.pharmazie-lehrbuch.de, accepted
2. Pardeike, J., Müller, R.H., Tape Stripping Test, in: www.pharmazie-lehrbuch.de, accepted
3. Pardeike, J., Müller, R.H., Bestimmung der Hautfeuchtigkeit, Hautelastizität und des Transepidermalen Wasserverlusts, in: www.pharmazie-lehrbuch.de, accepted

Papers

1. Pardeike, J., Müller, R.H., Coenzyme Q10 loaded NLCs: preparation, occlusive properties and penetration enhancement, Pharmaceutical Technology Europe, 2007, 19 (7), p. 46-49
2. Müller, R.H., Pardeike, J., Petersen, R., Hommoss, A., Nanolipid carriers (NLC): The new cosmetic carrier generation, SÖFW Journal, 2007 (5): p. 14-20
3. Müller, R.H., Hommoss A., Pardeike, J., Schmidt, C., Lipid nanoparticles (NLC) as novel carrier for cosmetics - Special features & state of commercialisation, SÖFW Journal, 2007, (9): p. 40-46
4. Müller, R.H., Petersen, R., Hommoss, A., Pardeike, J., Nanostructured lipid carriers (NLC) in cosmetic dermal products, Advanced Drug Delivery Reviews, 2007, 59 (6): p. 522-530
5. Pardeike, J., Hommoss, A., Müller, R.H., Lipid nanoparticles (SLN, NLC) in cosmetic and pharmaceutical dermal products, International Journal of Pharmaceutics; 2008, doi:10.1016/j.ijpharm.2008.10.003

Proceedings

1. Müller, R.H., Hommoss, A., Pardeike, J., Schmidt, C., Lipid nanoparticles (NLC) as novel carrier for cosmetics – Special features & state of commercialisation, in: Cosmetic Science Conference (CSC) at InCosmetics, Barcelona, Spain, April 5, 2006
2. Pardeike, J., Müller, R.H., Penetration enhancement and occlusion properties of coenzyme Q10 loaded NLC, in: 33rd Annual Meeting of the Controlled Release Society (CRS), Vienna, Austria, July 22-26, 2006

3. Pardeike, J., Müller, R.H., Penetration enhancement and occlusion properties of coenzyme Q10-loaded NLC, in: Socrates Intensive Program - Galenos Course "Skin Barrier Function: Pharmaceutic and Cosmetic Applications", Lyon, France, September 15-29, 2006
4. Müller, R.H., Pardeike, J., Hommoss, A., Nanoparticles in therapeutics: drug nanocrystals and lipid nanoparticles, in: Nanotrends, Potsdam, Germany, May 8-August 11, 2006
5. Pardeike, J., Müller, R.H., In vitro and in vivo occlusion properties of nanostructured lipid carriers (NLC), in: 34th Annual Meeting of the Controlled Release Society (CRS), Long Beach, USA, July 7-11, 2007
6. Pardeike, J., Müller, R.H., Physical stability of nanostructured lipid carriers (NLC) in an o/w urea cream, in: 34th Annual Meeting of the Controlled Release Society (CRS), Long Beach, USA, July 7-11, 2007
7. Pardeike, J., Müller, R.H., Phospholipase A_2-inhibitors - evaluation of the eye tolerability of PX-13 & PX-18 nanosuspensions by HET-CAM test, in: 6th World Meeting on Pharmaceutics, Biopharmaceutics and Pharmaceutical Technology, Barcelona, April 7-10, 2008
8. Pardeike, J., Müller, R.H., The use of reconstructed human epidermis for the evaluation of the skin irritation potential of PX-13 and PX-18 nanosuspension, in: 35th Annual Meeting of the Controlled Release Society (CRS), New York, USA, July 11-16, 2008
9. Pardeike, J., Müller, R.H., Tolerability evaluation of PX-13 and PX-18 in primary human fibroblasts and keratinocytes monolayer cell cultures, in: 35th Annual Meeting of the Controlled Release Society (CRS), New York, USA, July 11-16, 2008

Abstracts:

1. Pardeike, J., Müller, R.H., In vivo skin hydration properties of a coenzyme Q10 containing cream with nanostructured lipid carriers (NLC), in: Annual Meeting of the American Association of Pharmaceutical Scientists (AAPS), San Antonio, USA, October 29-November 2, 2006
2. Pardeike, J., Müller, R.H., Penetration enhancement and occlusion properties of coenzyme Q10 loaded NLC, in: Annual Meeting of the American Association of Pharmaceutical Scientists (AAPS), San Antonio, USA, October 29-November 2, 2006

3. Wang, Q., Sun, A.Y., Pardeike, J., Simonyi, A. Müller, R.H., Berney, R., Sun, G.Y., Neuroprotective effects of a nanoparticulate formulation of $sPLA_2$ inhibitor PX-18 in cerebral ichemia/reperfussion, in: International Society for Neurochemistry, Cancún, Mexico, 2007, Journal of Neurochemistry, 102 (Suppl. 1): p. 127
4. Pardeike, J., Schulz, K.H., Miller, T., Müller, R.H., Coenzyme Q10 loaded NLC: in vitro release and in vivo skin penetration, in: Annual Meeting of the American Association of Pharmaceutical Scientists (AAPS), San Diego, USA, November 11-15, 2007
5. Pardeike, J., Al-Samman, M., Müller, R. H., Stability evaluation of coenzyme Q10 loaded NLC, in: Annual Meeting of the American Association of Pharmaceutical Scientists (AAPS), San Diego, USA, November 11-15, 2007
6. Pardeike, J., Keck, C.M. Müller, R.H., Coenzyme Q10-loaded NLC - in vivo performance on skin, in Menopause Andropause Anti-Aging, Vienna, Austria, December 6-8, 2007
7. Bari, F., Zimmermann, A., Pardeike, J., Farkas, E., Domoki, F., Secretory phospholipase A2 is involved in hypoxic cerebrovascular injury in the newborn piglet, in International Stroke Conference, New Orleans, USA, February 19-22, 2008
8. Joshi, M., Pardeike, J., Nikolic, S., Müller, R.H., Nanostructured lipid carriers for dermal application: recent advances, in: 7th Conference and Workshop on Biological Barriers and Nanomedicine – Advanced Drug Delivery and Predictive non vivo Testing Technologies, Saarbrücken, Germany, Fabruary 20-29, 2008, p.45
9. Pardeike, J., Müller, R.H., Nanosuspensions of the poor water soluble phospholipase A_2-inhibitor PX-18, in: Annual Meeting of the American Association of Pharmaceutical Scientists (AAPS), Atlanta, Georgia, USA, November 16-20, 2008
10. Pardeike, J., Müller, R.H., Development and validation of a reverse-phase HPLC-UV method for the novel phospholipase A_2 inhibitor PX-18, in: Annual Meeting of the American Association of Pharmaceutical Scientists (AAPS), Atlanta, Georgia, USA, November 16-20, 2008

Oral Presentation

1. Pardeike, J., Müller, R.H., PX-13/18 – New phospholipase A_2-inhibitors for dermal application as nanoparticles, in: 7th European Workshop on Particulate Systems (EWPS), Berlin, Germany, May 30-31, 2008

Acknowledgements

I would like to express my gratitude to Prof. Dr. Rainer H. Müller for giving me the opportunity to work on this interesting topic, his scientific guidance and his support especially if it came to clearing the way to realize my ideas. I would like to thank him also for giving me the possibility to present the results of my work and gain helpful suggestions and new ideas on international congresses.

I would like to thank PharmaSol GmbH (Berlin, Germany) for providing some of the consumables used in this work, provision of analytical equipment and for sponsoring my participation in international congresses.

I would like to thank Mr. Richard Berney (Richard Berney Associates, LLC, USA) for enabling the project with the two phospholipase A_2 inhibitors and the arrangement of many fruitful co-operations with scientists from all over the world.

I would like to thank Prof. Dr. Monika Schäfer-Korting who gave me the possibility to perform the dermal and ocular safety tests in her laboratories at the Department of Pharmacology and Toxicology at the Freie Universität Berlin.

For the provided support with the chemistry, I would like to thank Dr. Marcel Špulák from the Department of Inorganic and Organic Chemistry at the Charles University, Czech Republic.

I would like to thank all my colleagues and friends at the Freie Universität Berlin for the good time I had during the last years. I would like to thank all of you for the warm atmosphere, brain storming, support and the important moments of fun and relaxation.

My special thanks go to Mr. Aiman Hommoss for his never-ending provided support no matter of which nature and his friendship.

I would like to thank Ms. Inge Volz who rendered every assistance possible during the HPLC method development and validation as well as during the qualitative analyzes of heaps of samples. Ms. Corinna Schmidt I would like to thank for her engagement and assistance every

time a small experiment turned into a mountain of work. I would like to thank Ms. Hannelore Gonska for the isolation and cultivation of the cells.

I would like to thank Mr. Kay Schwabe for the preparation of the creams used in the *in vivo* skin hydration study and Dr. Wolfgang Mehnert for his help with the statistical analyzes of the obtained data. My thanks go also to the volunteers who participated in the *in vivo* study.

My friends all over the world I would like to thank for understanding, encouraging and supporting me with a lot of patience during the last years.

I would like to thank my parents, my sister and my grandmother from all of my heart for their love, constant support and faith in me during all the years.